Newly Developed Conjugated Polymer Systems for Nitroexplosive Detection: Insights into the Mechanistic Investigations

A thesis submitted by

Arvin Sain Tanwar

Roll No. 126122039

to

Indian Institute of Technology Guwahati

for the award of the degree of

Doctor of Philosophy

Department of Chemistry
Indian Institute of Technology Guwahati
Guwahati - 781039
India

June-2018

Dedicated to My Parents

INDIAN INSTITUTE OF TECHNOLOGY GUWAHATI
Department of Chemistry

STATEMENT

I do hereby declare that the work contained in the thesis entitled **"Newly Developed Conjugated Polymer Systems for Nitroexplosive Detection: Insights into the Mechanistic Investigations"** is the result of investigations carried out by me in the Department of Chemistry, Indian Institute of Technology Guwahati, Guwahati, Assam India under the supervision of Prof. Parameswar Krishnan Iyer, Professor, Department of Chemistry, Indian Institute of Technology Guwahati, Guwahati, Assam, India. This work has not been submitted elsewhere for the award of any degree.

June, 2018 **Arvin Sain Tanwar**

IIT Guwahati

INDIAN INSTITUTE OF TECHNOLOGY GUWAHATI
Department of Chemistry

CERTIFICATE

This is to certify that the work contained in the thesis entitled **"Newly Developed Conjugated Polymer Systems for Nitroexplosive Detection: Insights into the Mechanistic Investigations"** by **Arvin Sain Tanwar**, a Ph.D. student of Department of Chemistry, Indian Institute of Technology Guwahati, for the award of degree of Doctor of Philosophy has been carried out under my supervision and this work has not been submitted elsewhere for any degree.

Prof. Parameswar Krishnan Iyer
Thesis Supervisor
Department of Chemistry
Indian Institute of Technology Guwahati
Guwahati – 781039
Assam, India.

Acknowledgements

First and foremost I would like to express my sincere gratitude to my supervisor, Prof. Parameswar Krishnan Iyer for giving me an opportunity to work under his expert supervision. Throughout my Ph.D. life, he has been a continuous source of encouragement and with his expert guidance, prudent suggestions, indefinite support, freedom to work and patience shown to me, made it possible for me to finish this work. I earnestly thank him for teaching me many lessons about research and life. I consider it my good fortune to have him as Teacher and advisor in my Ph.D. life. This thesis would not have been possible without his bounteous effort.

I am indebted to my doctoral committee members, Prof. Biplab Mondal (Chairman), Dr. Kingsuk Mahata and Dr. Vishal Trivedi for their ingenious advices, suggestions and evaluation of my Ph.D progress, which helped me a lot in the betterment of my thesis.

I am grateful to all faculty members of the Department of Chemistry, IIT Guwahati for their help and encouragement and also the non-teaching staff of the Department for their technical support. I am thankful to the Central Instrument Facility (CIF), IIT Guwahati for various characterization facilities.

I gratefully acknowledge all my teachers especially Dr. Pratibha Kumari, Dr. Usha Yadav, Miss. Savita Rawat, Mr. Rajiv Chadda Sir, Prof. S. P. Bhutani, Prof. Yudhvir Sharma, Prof. A. K. Prasad, Prof. D. S. Rawat for their excellent teaching and motivation to pursue higher studies and they have a great impact on my life.

I convey my special thanks to Dr. Sameer Hussain, Dr. Akhtar Hussain Malik, Mr. Mohammad Adil Afroz, Mr. Laxmi Raman Adil and Mr. Saurabh Patidar for their continuing encouragement, invaluable advice and assistance in my thesis work. My best regards with Ritesh, Rahul, Raman and Debasish for their unconditional love, respect, assistance and moral support.

It is a pleasure to express my deep sense of gratitude to all my dear labmates Atul Da, Muthu Da, Radha Bhaiya, Sameer Bhai, Bhim Bhaiya, Suresh Anna, Akhtar, Anamika Kalita, Anamika Dey, Gopi, Sayan, Ashish, Dipjyoti, Adil Bhai, Niranjan, Rahul, Raman, Maimur, Subrata, Indrani, Ramesh ji, Ritesh, Rabindra, Debasish, Nehal, Nasima, Retwik, Biki, Anwesha, Priyanka Di, Himani Di and Ekta Di for building a friendly environment in Laboratory and making my days memorable. I would also like to acknowledge all interns/project fellows; Debojit da, Paran, Nystha, Payel, Mannu,

Sridatri, Dehingia, Ahirwar, Ajay, Tejasvini, and Patidar, for their assistance, respect and love.

I take this opportunity to express gratitude to my dear friends and colleagues(but not limited to) Priyank, Chetan, Bhavna, Banpreet, Ankita, Rahul Shahni, Samarpita, Pooja, Parveen, Khusboo, Dimpy, Bhagat, JP, Anshu, Arpita, Sonashree, Abhishek, Imran, Manas, Wajid, Shaad, Ajaz bhai, Anushree, Shilaj, Sumit, Nayan for their timely suggestion, inspirations and moral support. I will especially miss the wonderful moments shared with Ramanna Ji, Chiru Sir ji, Shubo da, Mudit, Shailesh, Nayan, Parth, Ram ji, Dubey, Gaurav, Kuldeep, Sohum, Shyamu, Tushar, Meena, Rajat, Vivek and Vaibhav during my stay at Brahmaputra hostel IITG.

Finally, it's my family, whose limitless love, absolute support, tolerance and blessings steered my Ph.D. journey to an end. I would like to express my sincere gratitude with great honour to my family members who continue to give me lots of love, strength, kind support and prayers which made me to reach this stage. I am fortunate and blessed to have such a caring and supportive mother Mrs. Neeru Tanwar and I am sure my father Late Mr. Veer Sain Tanwar, who sacrificed and struggled to make my life smooth going, must be watching me from heaven and feeling proud for this big achievement. I am grateful to my elder brother Mr. Robin Sain, whose continuous encouragement; support and believing in me that pushed me achieve this level of work. I am grateful to my sister Mrs. Vijeta Singh, brother-in-law Lt Cdr Mr. Vikram Singh, Sister-in-law Mrs. Payal Sain for their eternal love, cooperation and emotional support which were immensely needed to complete this work.

Thank you very much, everyone for you endless support and encouragement.

Arvin Sain Tanwar

Synopsis

The content of this synopsis report entitled **"Newly Developed Conjugated Polymer Systems for Nitroexplosive Detection: Insights into the Mechanistic Investigations"** is divided into six chapters. Chapter 1 specifically describes the respective research area where the scope and significance of the subsequent chapters are discussed. Chapter 2 discusses about the synthesis and characterization of conjugated polymer (PFAM) and its application in the rapid and specific recognition of nitroexplosive-picric acid (PA) on solid support and in solution based on IFE/PET mechanism. Chapter 3 describes the synthesis of a new water-soluble non-fluorescent cationic conjugated polyelectrolyte PPPy, which selectively recognized nitroexplosive PA by fluorescence "turn-on" in the presence of closely related nitroexplosive compounds via fluorescence indicator displacement assay (IDA) technique in water at pH 7.0. Chapter 4 highlights the synthesis of cationic CP PFBT *via* oxidative polymerization and displayed dual state emission in DMSO as well as in water, a phenomenon very rarely observed, and tested for nitroexplosive analytes detection to observe a remarkable fluorescence quenching response for picric acid (PA) in the both solvents. Contact mode detection of PA was also accomplished using easy, economical and portable fluorescent test strips for on-site detection, which can detect upto 0.22 attogram level of PA. Vapor phase detection of PA was also established, which can detect up to 42.6 ppb level of PA vapors. Interestingly, the mechanism of sensing in DMSO solvent was attributed to strong inner filter effect (IFE) and photo induced electron transfer (PET), while in H_2O the sensing occurs via possible resonance energy transfer (RET) and photoinduced electron transfer (PET), which is exceptional and not reported earlier for a single probe. Chapter 5 discusses the synthesis of the neutral "receptor-free" highly fluorescent conjugated polymers (PF1 and PF2), which detects PA by a fluorescence turn-off response, and was found as a result of exclusive IFE and was further confirmed via IFE corrections. Chapter 6 summarizes the thesis overview and the importance of various sensing mechanisms that can probably exist for nitroexplosive detection but not limited to these chemical entities. Additionally, the design principle of probes that can result in efficient sensing of picric acid via these mechanisms was also studied and presented.

Chapter 1: Introduction

Conjugated polymers (CPs) are typically organic macromolecules consisting of a backbone chain with alternating single and multiple bonds. The research on conducting polymers began in 1970's, when films of polyacetylene were found to exhibit profound increase in electrical conductivity when exposed to halogen vapors. In the year 2000, three scientists Alan J. Heeger, Alan MacDiarmid and Hideki Shirakawa, founders of the conjugated conducting polymer chemistry, won the Noble prize in chemistry for their discovery. Recently CPs became an important class of materials, which have been used in various emerging area of research such as field-effect transistors (FETs), polymer solar cells, light-emitting electrochemical cells (LECs), flat panel displays using OLEDs and chemical and bio-sensors. These wide range of applications are due to their distinguished delocalised π-bonds throughout the polymeric backbone, which is the origin of their emissive as well as conductive property. CPs can be obtained with a variety of polymeric backbones like poly(para-phenylenes) (PPP), polypyrrole (PPy), polyfluorene (PF), poly(para-phenylene vinylene) (PPV), poly(para-phenylene ethynylene) (PPE) and polythiophene (PT) **(Figure 1).**

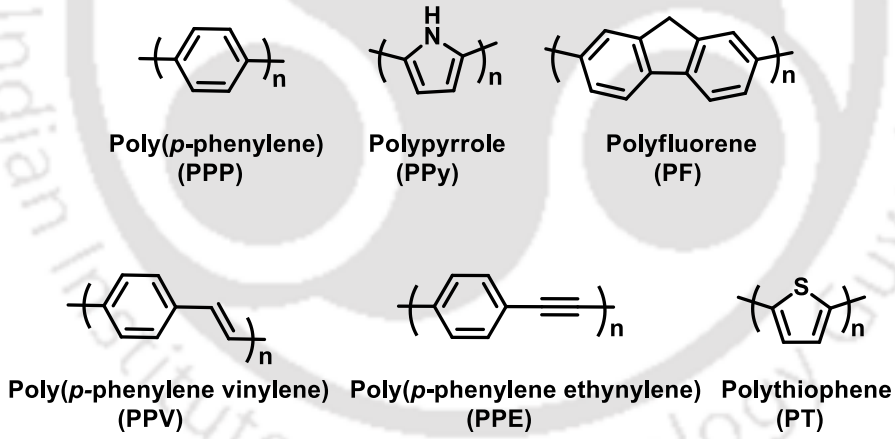

Figure 1. Structures of some well-known fluorescent conjugated polymer system.

Sensory signal amplification of CPs

CPs have more advantages than small molecular sensors because they are able to amplify the signal from a single binding event. The signal amplifying model of CPs was proposed by Swager group in 1995 and termed it as "molecular-wire effect" **(figure 2**). The conceptual basis of the signal amplification of the fluorescence sensory signal generated by CP is based upon binding with a target analyte. When an analyte binds locally to a receptor on a CP repeat unit the entire conjugated backbone is affected due to its 1-

dimensional wire-like property and the fluorescence of the entire polymer chain is altered. This results in an amplification of fluorescence when compared to small molecule sensors because a binding event on a small molecule only causes a single chromophore to change its fluorescence, whereas a CP binding event affects the fluorescence of an entire chain of chromophores by energy migration through the conducting polymer backbone. This amplification of signals provided by CPs is important for sensing applications because the molecules being analysed are often present in extremely dilute concentrations.

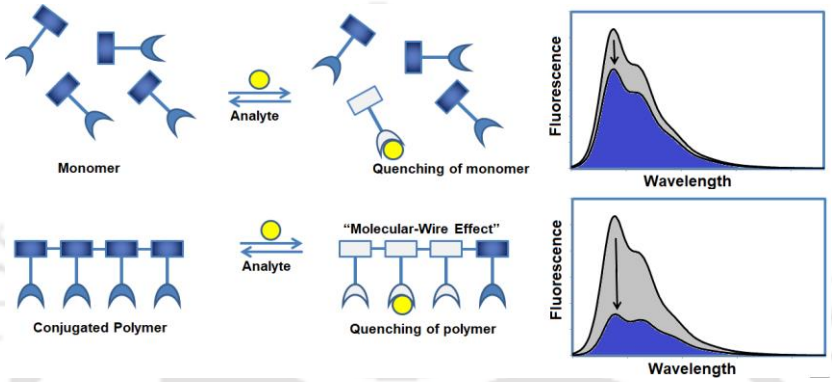

Figure 2. Pictorial representation of fluorescence quenching in monomer and polymer by analyte molecules.

Applications of conjugate polymeric systems in nitroexplosive sensing

CPs are one of the most promising class of materials for the recognition of nitroexplosives both in liquid phase as well as thin films owing to their high quantum efficiency, excellent molar absorptivity and high signal amplification via the "molecular wire effect". CPs provide unique optical properties and viability of distinguished receptor sites making them a desirable sensory candidate for detection of nitroexplosive at ultra-trace levels. Hence, in the recent year, researchers have designed various CPs and studied their potential application in detection of nitroexplosive-PA **(Figure 3)**, and explored distinguished mechanisms of sensing **(Figure 4)**.

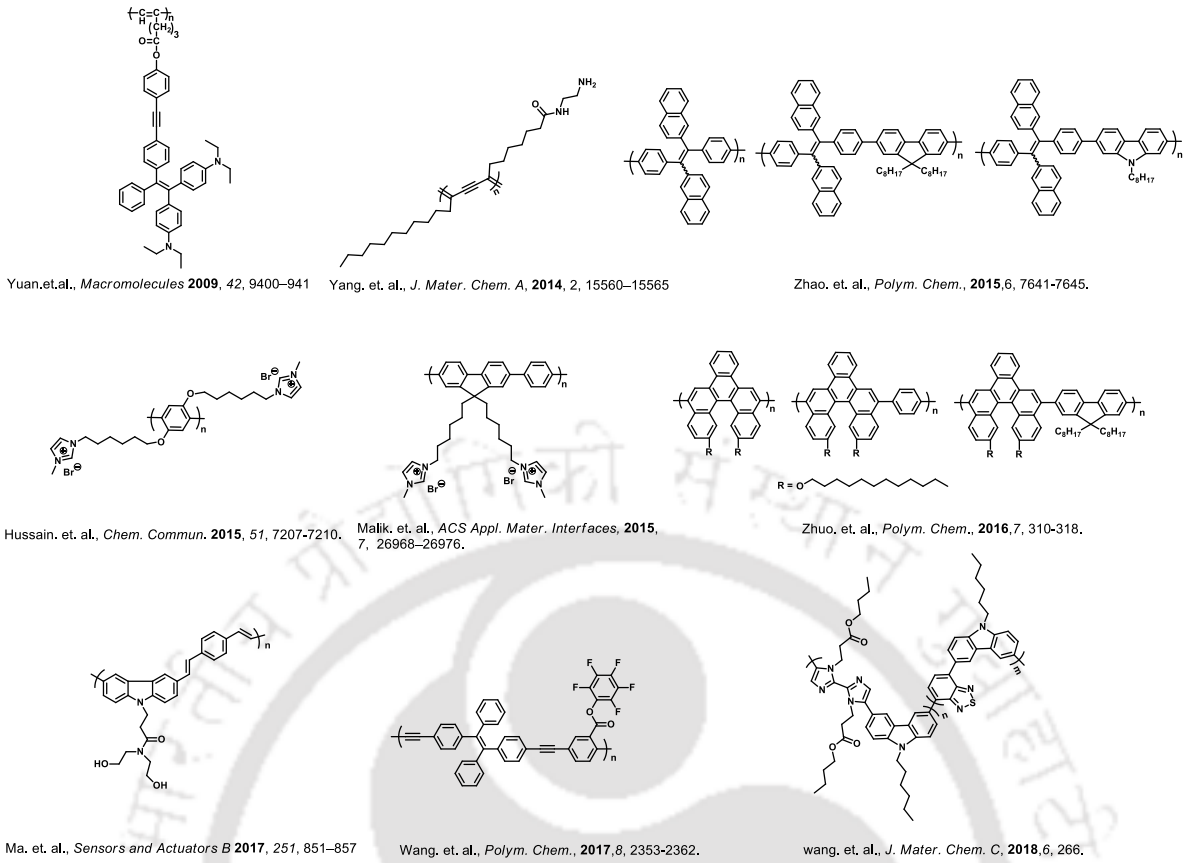

Figure 3. Structures of some conjugated polymer system used for PA detection.

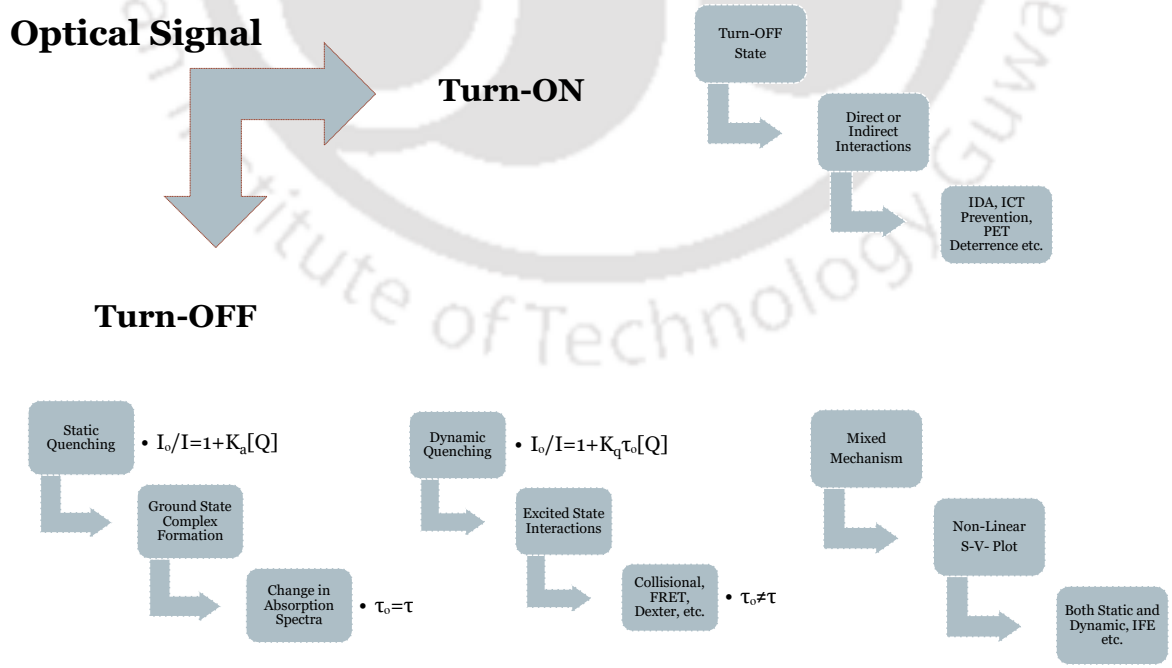

Figure 4. Flow chart representing various possible mechanism of sensing.

Chapter 2: Inner Filter Effect Based Selective Detection of Nitroexplosive-picric Acid in Aqueous Solution and Solid Support Using Conjugated Polymer

This chapter describes the synthesis of a new polyfluorene derivative, poly[4,4′-(((2-phenyl-9H-fluorene-9,9-diyl)bis(hexane-6,1-diyl))bis(oxy))-dianiline)] (PFAM) as shown in **Figure 5** *via* Suzuki coupling polymerization method in high yields for the rapid and specific recognition of nitroexplosive picric acid (PA) at 22.9 picogram level on solid support using paper strips and at 13.2 ppb level in aqueous solution. The polymer PFAM was well-characterized by means of NMR, UV−vis, fluorescence, time-resolved photoluminescence (TRPL) spectroscopy and cyclic voltammetry. The amplified signal response exclusively for PA was achieved via a strong inner filter effect (IFE), a phenomenon different from the widely reported ground-state charge transfer and/or Förster resonance energy transfer (FRET) based probes for nitroaromatics detection. Pendant amine groups attached on the side chains of PFAM provide enhanced sensitivity and exceptional selectivity via protonation assisted photoinduced electron transfer (PET) even in the presence of most common interfering nitroexplosives, as well as other analytes usually found in natural water. Thus, the PFAM based platform was demonstrated for monitoring traces of PA at very low levels even in competitive environment in solution as well as solid state **(Figure 6).**

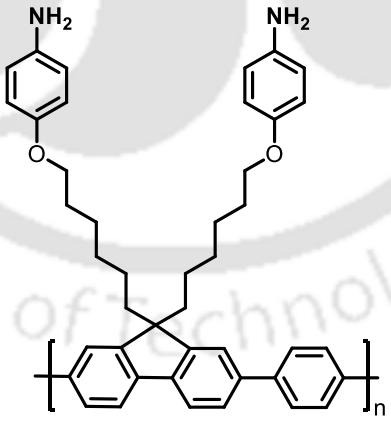

(PFAM)

Figure 5. Structure of poly[4,4′-(((2-phenyl-9H-fluorene-9,9-diyl)bis(hexane-6,1-diyl))bis(oxy))-dianiline)] (PFAM).

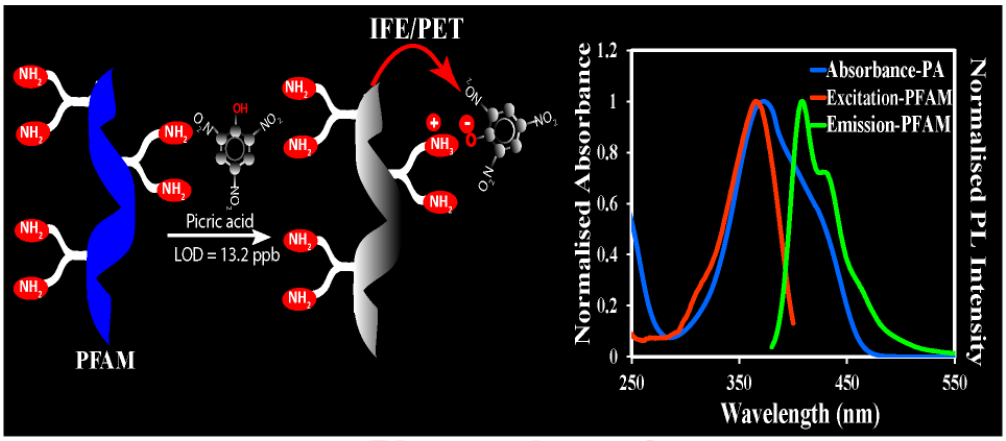

Figure 6. Schematic representation for the detection of picric acid by PFAM.

Chapter 3: Fluorescence "Turn-On" Indicator Displacement Assay Based Selective Detection of Nitroexplosive-picric Acid in Aqueous Media via a Cationic Conjugated Polyelectrolyte and Dye Complex

This chapter discusses about the synthesis of a new water-soluble nonfluorescent cationic conjugated polyelectrolyte poly(1,1′-((1,4-phenylenebis(oxy))bis-(propane-3,1-diyl))bis (pyridin-1-ium)bromide) (PPPy) (**Figure 7**) via an economical method of oxidative coupling polymerization in high yields. PPPy selectively recognized nitroexplosive picric acid (PA) by fluorescence "turn-on" in the presence of closely related nitroexplosive compounds, namely, 2,4,6-trinitrotoluene, 2,4-dinitrophenol, and 4-nitrophenol via fluorescence indicator displacement assay (IDA) technique in water at pH 7.0. The polymer PPPy was characterized by NMR spectroscopy, gel permeable chromatography, UV−vis spectroscopy. The polymer PPPy forms an electrostatic complex with uranine dye. This ensemble scheme was utilized to detect PA with a limit of detection (LOD) value of 295 nM (solution state) and 0.22 ppm (vapor state) through IDA, a phenomenon that is very different from the widely reported Förster resonance energy transfer, photoinduced electron transfer, ground-state charge transfer and inner filter effect based probes used for nitroexplosive PA detection (**Figure 8**).

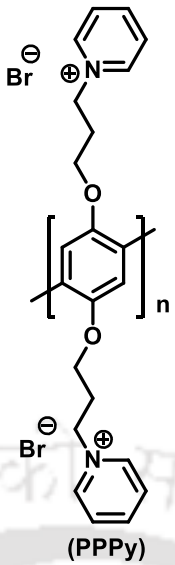

Figure 7. Structure of poly(1,1′-((1,4-phenylenebis(oxy))bis- (propane-3,1-diyl))bis(pyridin-1-ium)bromide) (PPPy)

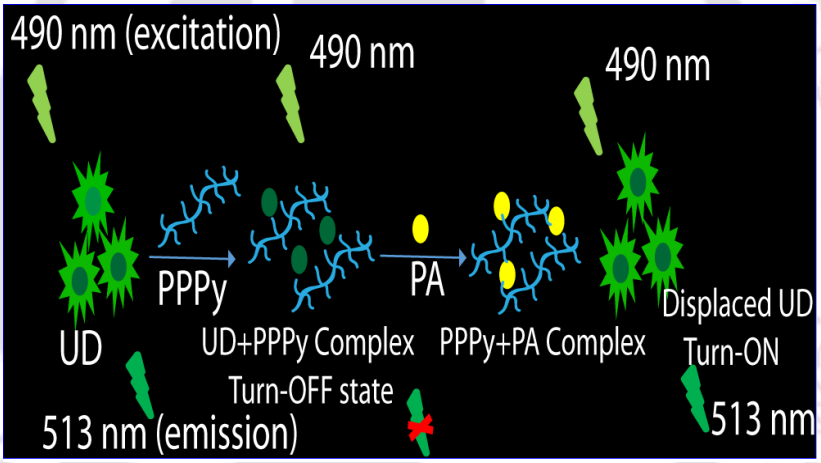

Figure 8. Schematic representation for the detection PA by IDA.

Chapter 4: Inner Filter Effect and Resonance Energy Transfer Based Attogram Level Detection of Nitroexplosive-Picric acid Using Dual Emitting Cationic conjugated Polyfluorene

In this chapter we have described the synthesis of a new a new cationic conjugated polyfluorene derivative, poly(3,3'-((9H-fluorene-9,9-diyl)bis(hexane-6,1-diyl))bis(1-methyl-1H-benzo[d][1,2,3]triazol-3-ium) bromide) (PFBT) (**Figure 9**) using a simple and inexpensive method of oxidative coupling polymerization. The polymer PFBT displayed dual state emission in DMSO as well as in water, a phenomenon very rarely observed, and tested for nitroexplosive analytes detection to observe a remarkable fluorescence quenching response for picric acid (PA) in both solvents. The polymer PFBT was found

to be highly sensitive and selective towards nitroexplosive PA in both the solvents (DMSO and H_2O) with exceptional quenching constant values of 2.69×10^4 M^{-1} and 2.18×10^5 M^{-1} and a very low detection limit of 92.7 nM (21.23 ppb) and 0.19 nM (43.53 ppt) in respective solvents. Furthermore, contact mode detection of PA was also accomplished using easy, economical and portable fluorescent test strips for on-site detection, which can detect upto 0.22 attogram level of PA. Vapor phase detection of PA was also established, which can detect up to 42.6 ppb level of PA vapors. Interestingly, the mechanism of sensing in DMSO solvent was attributed to strong inner filter effect (IFE) and photo induced electron transfer (PET), while in H_2O the sensing occurs via possible resonance energy transfer (RET) and photoinduced electron transfer (PET), which is exceptional and not reported earlier for a single probe (**Figure 10**).

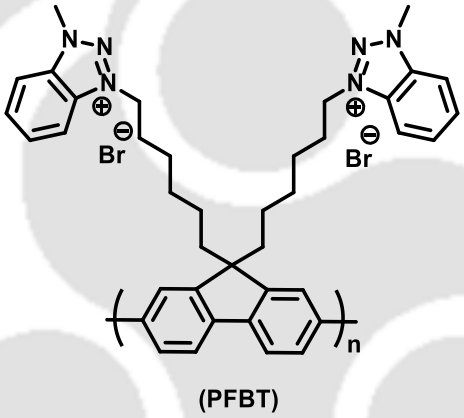

Figure 9. Structure of poly(3,3'-((9H-fluorene-9,9-diyl)bis(hexane-6,1-diyl))bis(1-methyl-1H-benzo[d][1,2,3]triazol-3-ium) bromide) (PFBT).

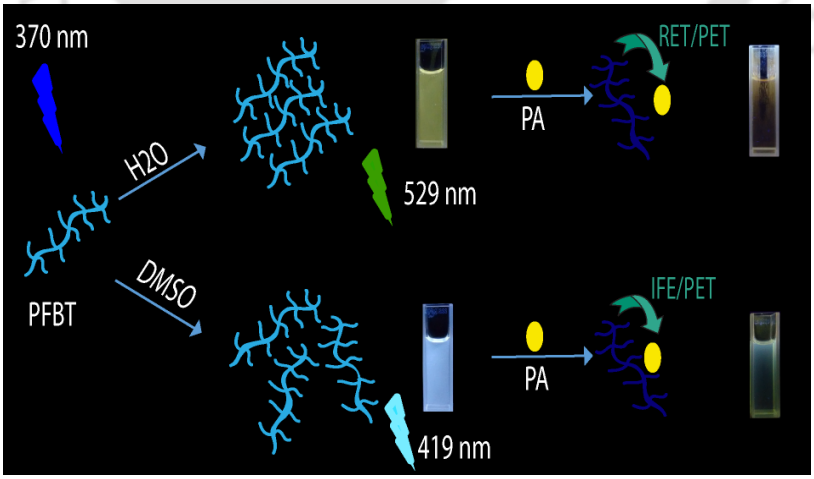

Figure 10. Schematic representation for the detection PA by PFBT.

Chapter 5: "Receptor Free" Inner Filter Effect Based Detection of Nitroexplosive-Picric Acid using two Polyfluorenes derivatives in solution and solid state and IFE corrections.

Previously inner filter effect (IFE) has been considered as an error in photoluminescence spectroscopy. Recently IFE has gained significance as one of the key cause of sensing mechanism in the area of chemical and biological sensing. IFE based sensing platforms provides simple and flexible sensing without any kind of interaction in between fluorophore and receptor. Therefore, it is quite challenging to design IFE based fluorophore and quencher combination. In this chapter, two "Receptor-free" fluorescent conjugated polymers of fluorene namely 9,9-bis(6-bromohexyl)-2-phenyl-9H-fluorene (PF1) and 9,9-bis(6-bromohexyl)-9H-fluorene (PF2) (**Figure 11**) were synthesized with slight modification in the main fluorescent backbone using Suzuki cross coupling polymerization and oxidative coupling polymerization methods with high yields respectively. The polymers were well characterized by gel permeable chromatography, NMR, UV-vis, fluorescence and time-resolved photoluminescence (TRPL) spectroscopies. The fluorescent polymers PF1 and PF2 explicitly recognize nitroexplosive picric acid (PA) among other nitroexplosive compounds used and displayed fluorescence quenching response in solution as well as on solid support via an IFE mechanism. The polymer, PF1 and PF2, were both found to be highly selective and sensitive towards the nitroexplosive PA with a high quenching constant value (K_{sv}) 5.1×10^4 M^{-1} and 5.0×10^4 M^{-1}, respectively and remarkably low LOD of 110 nM and 219 nM respectively. Contact mode detection of nitroexplosive PA was also performed using economical and transportable fluorescent paper test strips for on-site sensing, which can detect a minimum of 229.1 picogram level of PA. Earlier IFE mechanism for PA sensing has not been much explored in detailed and therefore we have studied it in detail and performed IFE correction for nitroexplosive PA and found ~ 77% suppression efficiency due to IFE (**Figure 12**).

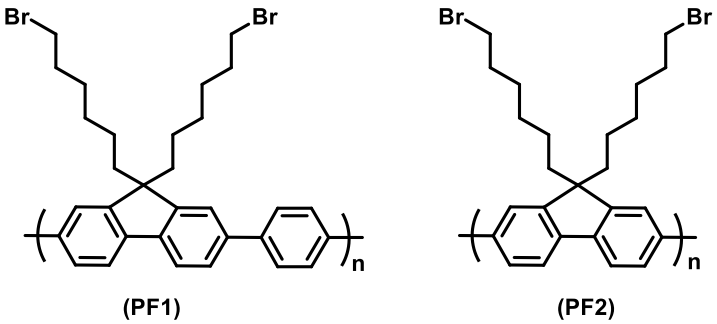

Figure 11. Structure of 9,9-bis(6-bromohexyl)-2-phenyl-9H-fluorene (PF1) and 9,9-bis(6-bromohexyl)-9H-fluorene (PF2)).

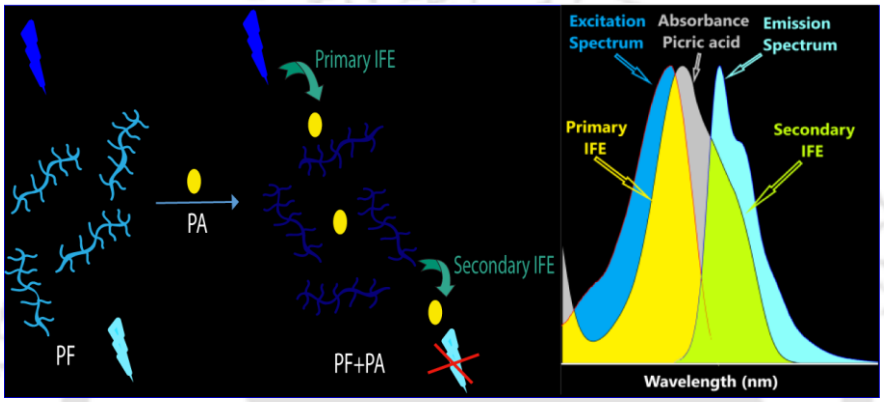

Figure 12. Schematic representation for the detection of PA by IFE mechanism.

Chapter 6

Thesis overview and Future Perspective

In summary, different types of conjugated polymeric systems have been designed, synthesized and utilized them in attaining simple, low cost and portable optical sensors capable of monitoring nitroexplosive-Picric acid (PA) at ultra-trace level. The mechanism of sensing for each of the CPs was studied in detail and explored. The conjugated polymer PFAM showed rapid and specific recognition toward PA on solid support and in solution based on IFE/PET mechanism. The non-fluorescent cationic conjugated polymer PPPy participates in indicator displacement assay resulting turn-on fluorescence selectively in presence of PA. The cationic conjugated polymer PFBT displayed substantial fluorescence quenching for PA in solution as well as solid state based on IFE and RET mechanism at attogram level of PA and utilised in making economical paper strips for on-site detection of nitroexplosive. The neutral "receptor-free" highly fluorescent conjugated polymers (PF1 and PF2) detect PA by a fluorescence turn-

off response which was found as a result of exclusive IFE and was further confirmed via IFE corrections. All the CPs systems were found to be highly sensitive and selective towards nitroexplosive-PA.

Additionally, this thesis includes chemo-sensors based on fluorescence turn-off, indicator displacement assay and "receptor-free" sensing. To date, there are only countable reports available for the PA detection based on CPs. There is still scope for designing and exploring new sensing mechanisms, in order to achieve an ideal sensory system for nitroexplosive detection.

Contents

Chapter 1

Introduction

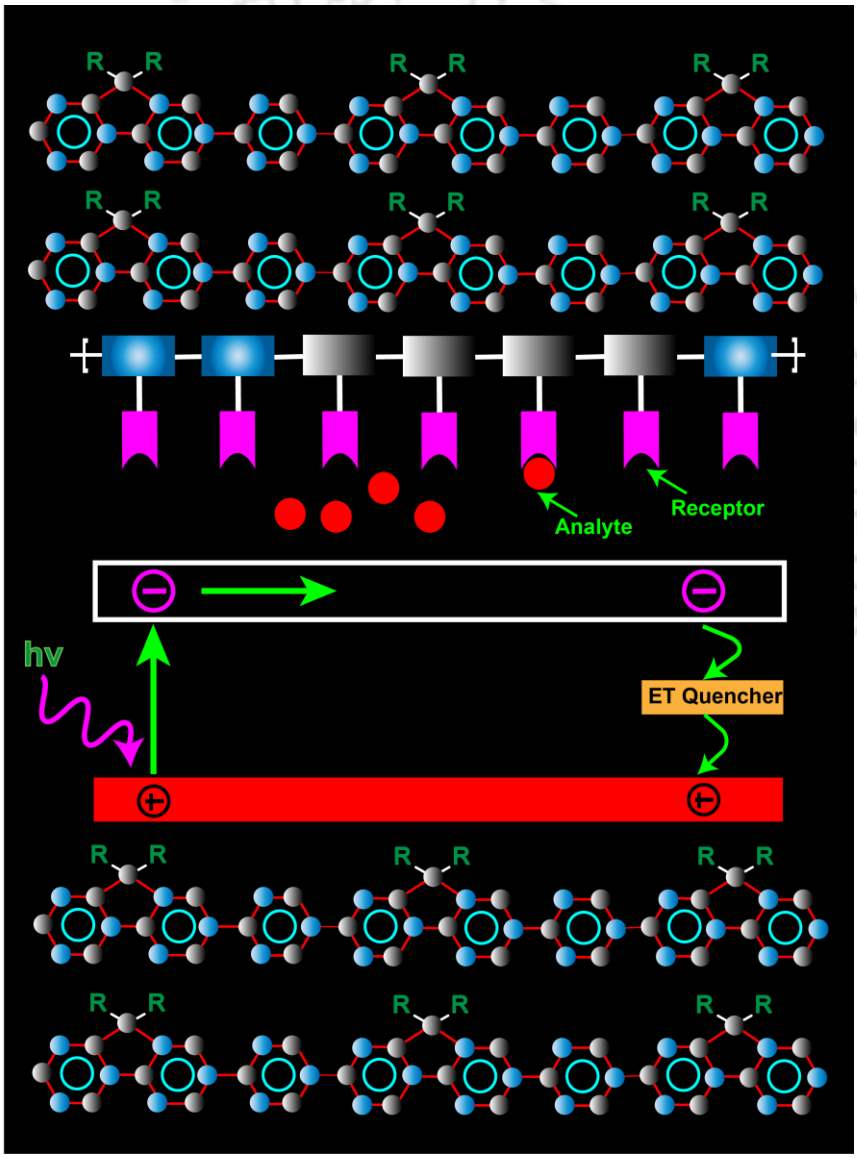

1.1 Introduction

Conjugated polymers (CPs) are typically organic macromolecules consisting of a backbone chain with alternating single and multiple bonds. The alternate σ and π bonds over the main backbone chain creates an electronic cloud throughout the chain, which is responsible for the delocalization of electrons, electrochemical properties and characteristic optical properties of CPs. The research on conducting polymers began in 1970's, when films of polyacetylene were found to exhibit profound increase in electrical conductivity on exposure to halogen vapours. In the year 2000, three scientists Alan J. Heeger, Alan MacDiarmid and Hideki Shirakawa, won the chemistry Noble prize for their discovery of conducting polymers. Recently CPs became an important class of materials, which have been explored in various emerging areas of research such as field-effect transistors (FETs),[1,2] polymer solar cells,[3] light-emitting diodes (LEDs),[4,5] and chemical and bio-sensors.[6,7] These wide range of applications are due to their distinguished delocalised π-bonds throughout the polymeric backbone, which is the origin of their emissive as well as conductive property.

CPs can be obtained with a variety of polymeric backbones like poly(para-phenylenes) (PPP),[8] polypyrrole (PPy),[9] polyfluorene (PF),[10] poly(para-phenylene vinylene) (PPV),[11] poly(para-phenylene ethynylene) (PPE)[12] and polythiophene (PT)[13] **(Figure 1.1).** One more benefit of using CPs is that the particular backbone can be functionalised with distinct receptors on the side chains, which can tune the photophysical properties of the CPs and enhance the selectivity and sensitivity of the CPs towards desired analytes.[7,14-18] Some of the CPs reported as a sensory material are shown in the **Figure 1.2**.

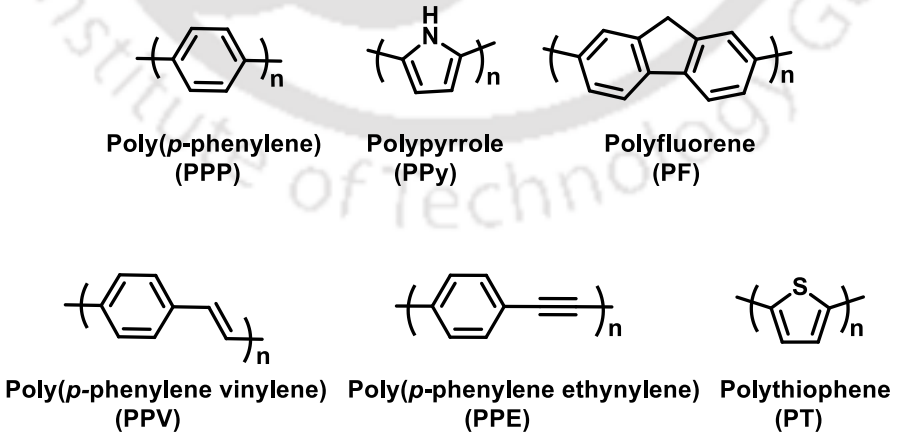

Figure 1.1 Structures of some common conjugated polymer backbone.

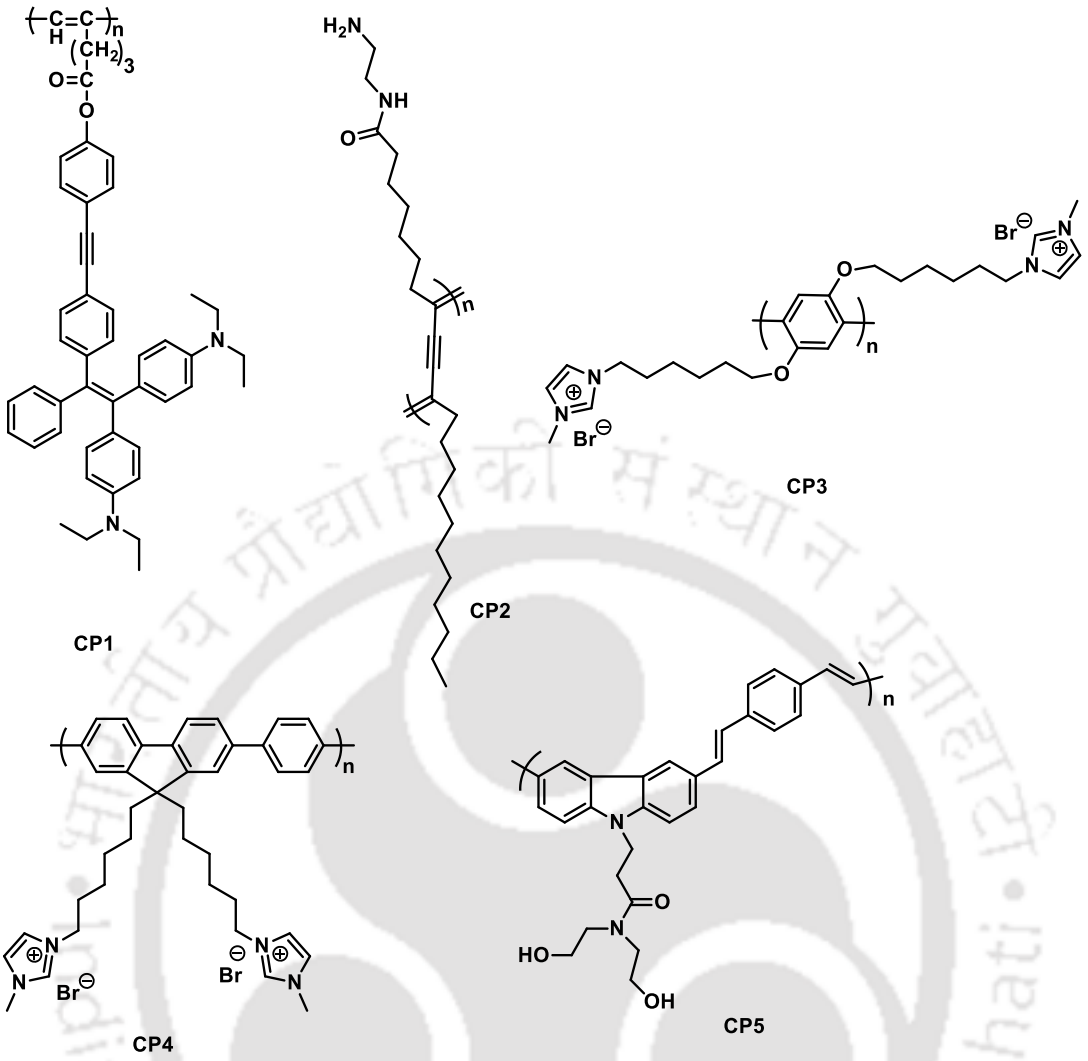

Figure 1.2 Structures of some conjugated polymers with a variety of side chain functionality used as sensory materials.

1.2 Advantages of using CPs as Sensory System

CPs have more advantages compare to various other small molecule sensors, because they are able to amplify the signal from a single binding event.[7,19] The signal amplifying model of CPs was proposed by Swager and co-workers in 1995 and termed as "molecular-wire effect" **(Figure 1.3)**.[19,20] The conceptual basis of the signal amplification of the fluorescence sensory signal generated by CP is based upon binding with a target analyte. When an analyte binds locally to a receptor attached to a CP, repeat unit the entire conjugation length on a backbone is affected due to its 1-dimensional wire-like property and the fluorescence of the entire polymer chain is altered. This results in an amplification of fluorescence response when compared to small molecule sensors because a binding event on a small molecule only causes a single chromophore to change its fluorescence, whereas a CP binding event affects the

fluorescence of an entire chain of chromophores by energy migration through the conducting polymer backbone. This amplification of signals provided by CPs is important for various sensing applications because the molecules being analysed are often present in extremely dilute concentrations.

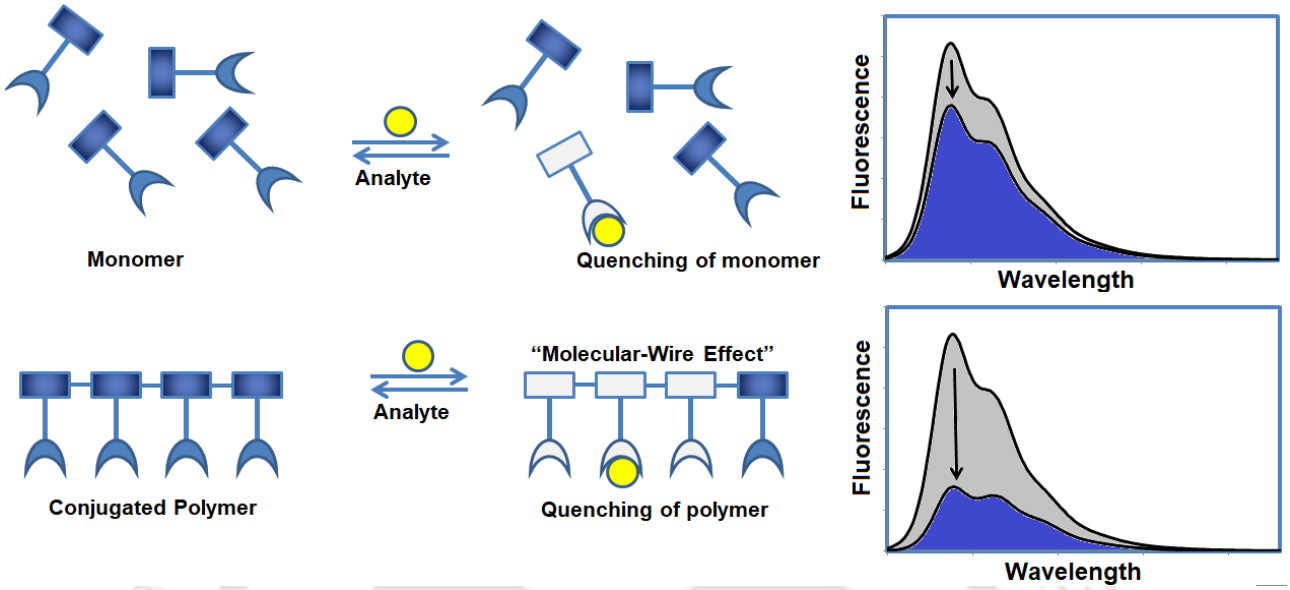

Figure 1.3 Pictorial representation of quenching of fluorescence in monomer and conjugated polymer by a particular analyte via "molecular wire effect".

1.3 Insights into the mechanistic investigation for fluorescence based nitroexplosive detection

It is because of the non-fluorescent nature of the explosive materials, fluorescence based detection of nitroexplosive emphasized the use of fluorescent probes which change their fluorescence in presence of explosives as an indicative test for explosive detection. There are many phenomenon which lead to change in emission intensity (turn-on or turn-off i.e. enhancement or quenching) and among all the previous reports chiefly using fluorescence method for explosive sensors, major of them are based on fluorescence quenching while a few reports are with fluorescence enhancement. On the basis of interaction between fluorophore and quencher, detection can be categorised into two categories (a) Interaction and (b) Interaction-free caused fluorescence detection.[21]

1.3.1 Fluorescence sensing based on interaction between fluorophore and explosive (quencher)

Interaction based detection of explosives is most common and in which fluorescence quenching method still dominates. There exists some interaction between fluorophore and explosive, which lead to several possible fluorescence quenching mechanism such as

resonance energy transfer (RET), photo-induced electron transfer (PET), intramolecular charge transfer (ICT) etc.[22] which results in the sensing of the nitroexplosive via a fluorescence turn-off signal.

1.3.1.1 Photo-induced electron transfer (PET)

Nitroexplosives possess electron withdrawing nitro groups, which makes them highly electron deficient that could easily bind to electron rich fluorescent sensory material via acceptor-donor (A-D) interactions.[23] In PET, a complex is formed between the electron donor and the electron acceptor species, where the excited fluorophore (donor) (D) donates an electron to the ground state of the acceptor (explosive compound) (A) yielding a complex [$D^+.A^-$], as shown in the **Figure 1.4.**[24] The charge transfer complex can return to the ground state via non-radiative transitions, but in some cases exciplex emission could be observed. Finally the extra electron on the acceptor is returned to the electron donor. In general, PET plays a major role in quenching of fluorescence and gives significant insights into the development of fluorescent nitroexplosive sensors.[21]

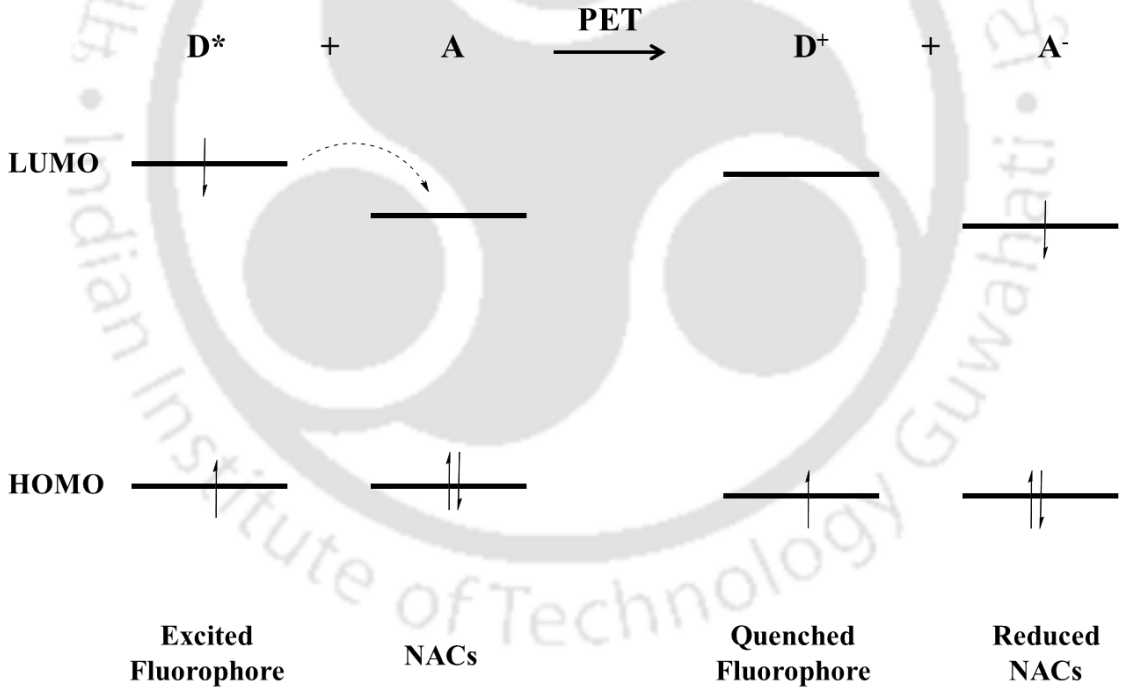

Figure 1.4 Molecular orbital schematic representation for PET.

1.3.1.2 Resonance energy transfer (RET)

A number of nitroexplosive sensors have been developed on the basis of energy transfer mechanism because it increases the sensitivity via enhancement in efficiency of fluorescence quenching. In RET, the excited donor molecule (D*) releases the energy while coming back to the ground state, which is absorbed by the acceptor molecule (A) and utilised by the

electron of acceptor to reach to the higher excited state (A*) as shown in the **Figure 1.5**. The rate of the energy transfer depends on three factors (1) relative orientation of the donor and acceptor dipoles, (2) extent of overlapping of the emission spectrum of donor and the absorption spectrum of acceptor and (3) distance between the donor and acceptor.[7,21] The probability of RET depends upon the extent of overlap between donor and acceptor. RET occurs due to the long range dipolar interactions though the D* and A. Therefore, RET is not sensitive to steric factors.[25,26]

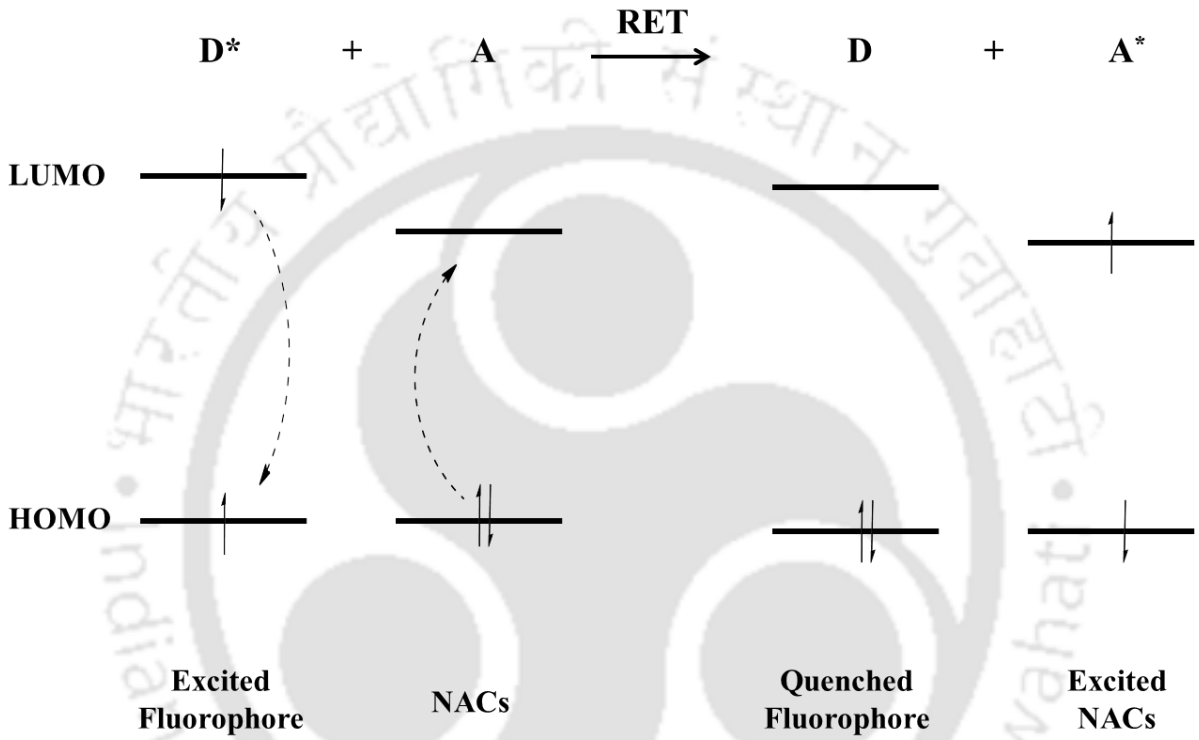

Figure 1.5 Molecular orbital schematic representation for RET.

1.3.1.3 Intramolecular charge transfer (ICT)

Involvement of ICT mechanism is quite known in the area of sensing and it has been already used in case of CP for fluoride detection.[27] However, its involvement in explosive detection is relatively new. Recently Xu *et al.* in 2013 developed a zwitterionic squarine dye based DNSA-SQ compound, which selectively detect PA via a ratiometric fluorescent method in the near IR region.[28] The change in fluorescence was ascribed to the ICT deterrence followed by the protonation of N atom of dimethylamine group by nitroexplosive PA. Through astute and coherent strategy of ICT fluorescent compounds, a ratiometric approach for nitroexplosive detection could be developed **(Figure 1.6)**.

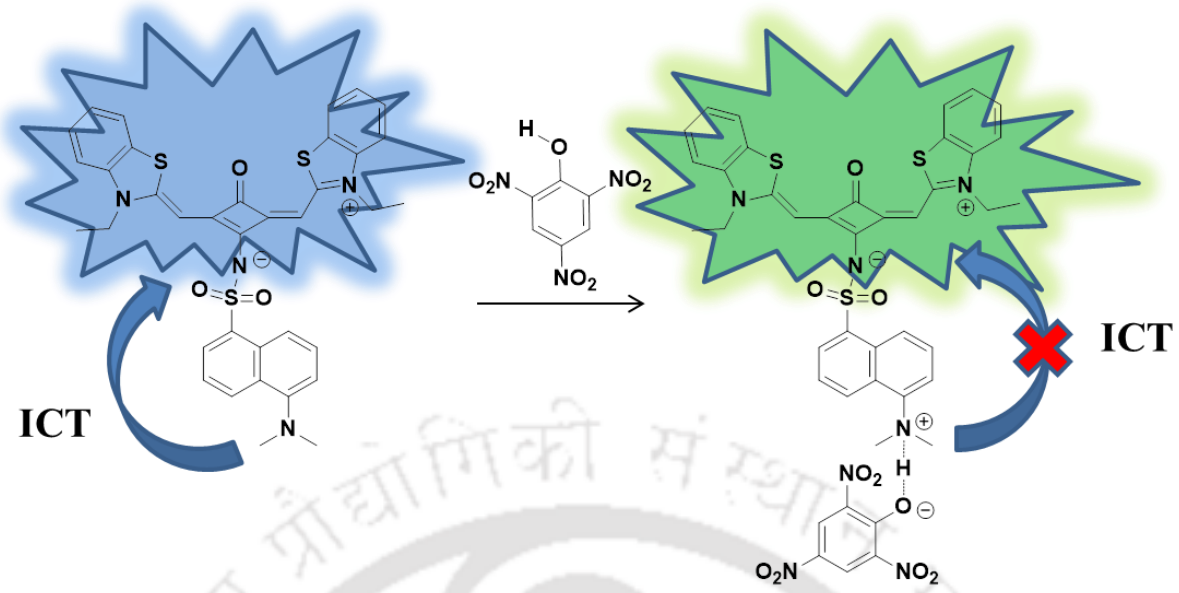

Figure 1.6 Schematic representation of ICT deterrence in the PA sensing.

1.3.2 Fluorescence sensing based on interaction-free between fluorophore and explosive (quencher)

So far a majority of developed sensors work on direct interaction between the fluorophore and the analyte (nitroexplosive).[7,21] Designing a sensor, which have no direct interaction with the analyte but they can sense the presence of a particular analyte, is highly challenging. The interaction-free detection of explosive is done by inner filter effect (IFE), which was previously considered as an error in fluorescence measurements but recently gained attention of distinguished researchers to develop various chemical and biological sensors based on this phenomenon.[29]

1.3.2.1 Inner filter effect (IFE)

IFE is an important phenomenon in spectrofluorometry based on the non-irradiation energy conversion model, which results from the absorption of the excitation and/or emission spectrum of fluorophore by the absorber (quencher or nitroexplosive) in the detection system, subsequently leading to an exponential quenching of fluorescence of fluorophore, which enhances sensitivity of the system and gives rise to low limit of detection in sensing.[22,29] IFE can be subdivided into two components primary IFE (pIFE), which arises from the absorption of the excitation radiation by the absorber, and secondary IFE (sIFE), which arises from the absorption of the emission radiation by the same absorber. IFE based systems work straight forward and doesn't require any interaction between fluorophore and quencher. It does

however just require the perfect combination of fluorophore and quencher, whose absorbance (quencher) overlap with excitation and/or emission of fluorophore **(Figure 1.7)**.[29]

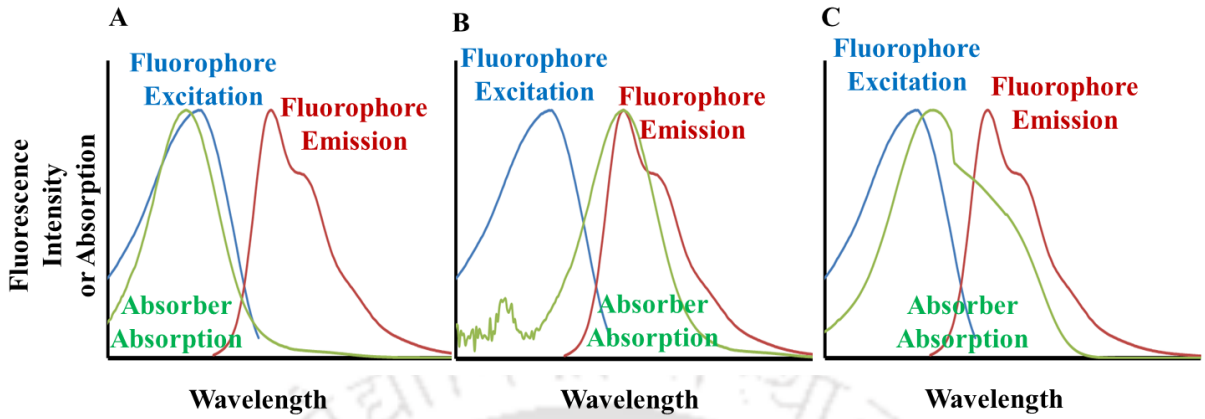

Figure 1.7 IFE conditions: overlapping of absorption spectrum of quencher with (A) excitation spectrum, (B) emission spectrum and (C) both excitation and emission spectrum of fluorophore.

1.4 Theory of fluorescence quenching

In a typical fluorescent molecule, quenching of fluorescence requires molecular contact between quencher and fluorophore. This contact can happen either with ground state fluorophore (X) or excited state fluorophore (X*) with quencher molecule (Q). The aforementioned quenching of fluorescence can occurs via two different mechanisms namely dynamic (collisional) quenching and static quenching. Quenching of fluorescence due to encounter or collision of excited state fluorophore with the quencher molecule is called as dynamic quenching as shown in equation 1.1. While quenching of fluorescence due to binding of the fluorophore in ground state to the quencher molecule is called as static quenching as shown in equation 1.2. The resultant complex is non-fluorescent in nature.

$$X^* + Q \xrightarrow{kq} X + Q \qquad 1.1$$

$$X + Q \underset{}{\overset{ka}{\rightleftharpoons}} [X, Q] \xrightarrow{h\nu} [X^*, Q] \longrightarrow X + Q \qquad 1.2$$

$$I_0/I = 1 + k_{sv}[Q] \qquad 1.3$$

These quenching routes can be distinguished by time-resolved measurements of fluorescence decay of fluorophore. In case of dynamic quenching, as it requires the molecular collision between excited fluorophores and the quencher thereby it is a diffusion controlled process. The quencher and fluorophore are unbound and quenching occurs as the excited fluorophore collides with the quencher. As a result the average fluorescence lifetime of the fluorophore

decreases with increase in the quencher concentration. Whereas in case of static quenching, fluorescence lifetime remains constant with increase in the concentration of quencher. As quenching occurs via the formation of ground-state complex between fluorophore and quencher, so any fluorophore not bound to the quencher will decay with its natural lifetime. So the change in fluorescence lifetime of fluorophore before and after addition of explosive quencher decides whether the quenching is dynamic or static process. Furthermore, from the Stern-Volmer plots as obtained from equation 1.3, it gives a linear I_0/I versus [Q] curve for both of the static and dynamic quenching as shown in Figure 1.8. Where I_0 and I denote the fluorescence emission of fluorophore in absence and presence of quencher [Q], respectively, and slope of the curve represents the Stern-Volmer constant (K_{sv}), which measures the sensitivity of the fluorophore toward the quencher. For dynamic quenching, $K_{sv} = k_q\tau_0$, where K_q is the bimolecular quenching constant and τ_0 denotes lifetime of the fluorophore [X*] in the absence of quencher [Q]. On the other hand for static quenching, $K_{sv} = k_a$, and the lifetime remains unchanged during the quenching process.

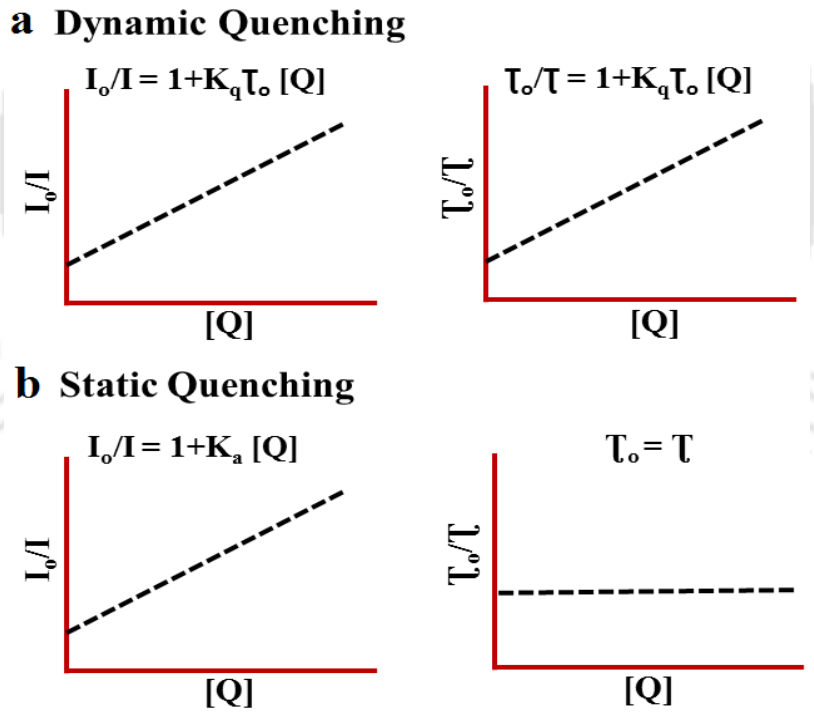

Figure 1.8 Plots obtained for (a) dynamic and (b) static quenching showing the effect of quencher concentration on fluorescence intensity and fluorescence lifetime of the fluorophore.

However, a non-linear (curved) nature of Stern-Volmer plot can be seen in most of the cases, due to involvement of various other complex processes like aggregation of chromophore,

change in association constant with change in quencher concentration, re-absorption processes and mixed quenching mechanism (dynamic and static quenching).[22]

1.4 Applications of CP systems in nitroexplosive sensing

During last few years, CPs have been widely used as biosensor and chemosensor material for various biological and chemical species, and recently became the most promising class of materials for the recognition of nitroexplosives in liquid phase as well as thin films owing to their high quantum efficiency, excellent molar absorptivity and high signal amplification via the "molecular wire effect". [6-7,16,30] CPs provide unique optical properties and viability of distinguished receptor sites making them a desirable sensory candidate for detection of nitroexplosive at ultra-trace levels. Hence, in years, researchers have designed various CPs and studied their potential application in detection of nitroexplosive-PA, which is of great current interest in both national security and environmental protection agency because it not only possesses explosive nature but also recognized as a hazardous pollutant.[31]

In 2009, Yuan *et al.*[32] synthesized luminogenic polyacetylenes and conjugated polyelectrolytes and used polyacetylene derivative (CP1) containing diethylamine functionalised tetraphenylethene (TPE) unit in the side chains for the superamplification fluorescence quenching by the explosives. Because of the AIE active TPE molecule, CP1 exhibits AIE property, which forms suspended nanoaggregates in 90% water/THF mixture and possess ~57 fold more emission as compared to its solution in THF. The emission of these nanoaggregates of CP1 is quenched by PA with a non-linear nature of stern-volmer plot having the quenching constant (K_{sv}) values 3.1×10^{4}, 1.7×10^{5} and 3.4×10^{5} M^{-1} obtained for the low, intermediate and high concentration of PA respectively. The selectivity studies of CP1 nanoaggregates with other nitroexplosive compounds were not reported and furthermore, quenching of the CP1 nanoaggregates can be seen with as low as 0.72 µM or 0.17 ppm of PA concentration. However, the detailed mechanism of sensing was not studied and the reason of the quenching was suggested to be penetration of PA molecule into 3-D network of CP1 nanoaggregates, which are suspended in the aqueous medium.

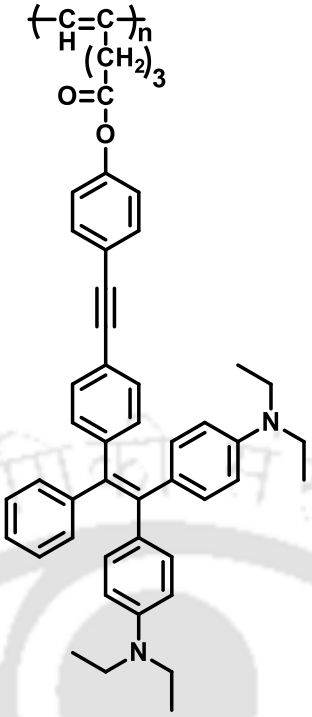

Figure 1.9 Structure of CP1.

Yang *et al.*[33] in 2014 developed a novel polydiacetylene (CP2) microtube for the selective and reproducible detection of PA in the aqueous media. Amine group present at the side chains of the PDA form the ion-pair with the PA and leading to a fluorescence turn-off signal in presence of PA. A linear nature of Stern-Volmer plot was observed for the emission intensity at 640 nm with a quenching constant (K_{sv}) of 1.3×10^4 M^{-1}. The limit of detection was calculated to be as low as 0.48 µM by using the equation 3σ/K, which is lower than the maximum acceptable level of PA i.e. 0.5 mg/mL in drinking water.

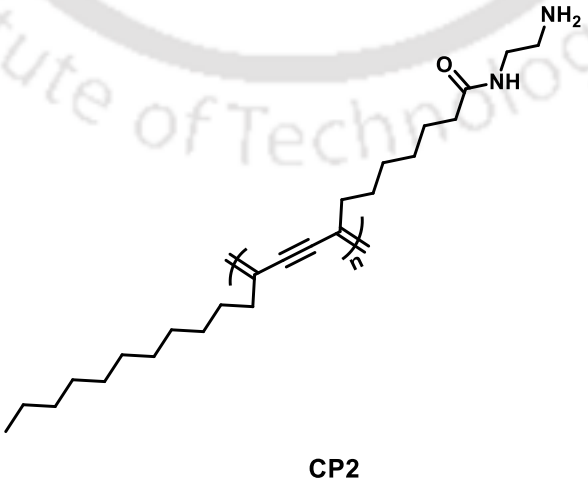

Figure 1.10 Structure of CP2.

In 2015, Gao *et al.*[34] synthesized three conjugated polymers based on di(naphthalene-2-yl)-1,2-diphenylethene unit, which is a new AIE active unit, making these polymers exhibit fascinating aggregation-enhanced emission and their application in nitroexplosive detection in aqueous media. The synthetic procedure involves Yamamoto coupling of 1,2-bis(4-bromophenyl)-1,2-di(naphthalen-2-yl) to get the homopolymer (CP3), and Suzuki coupling of 2,7-bis(4,4,5,5-tetramethyl-1,3,2-dioxaborolan-2-yl)-9,9-di-noctylfluorene and 2,7-bis(4,4,5,5-tetramethyl-1,3,2-dioxaborolan-2-yl)-9-n-octylcarbazole with 1,2-bis(4-bromophenyl)-1,2-di(naphthalen-2-yl) to get copolymers (CP4 and CP5) respectively. The polymers (CP3, CP4 and CP5) show close absorbance maxima i.e. 365, 369, and 371 nm, respectively and emit weak fluorescence at ~520 nm for P1, ~405-430 nm band with ~518 nm maxima for CP4 and CP5 in THF solution (excitation wavelength = 350 nm), which on increasing the water fraction blue-shifted to 515, 509 and 511 nm respectively. The Stern-Volmer plots of CP3, CP4 and CP5 showed a non-linear nature for PA, with quenching constant (K_{sv}) of 4204, 11830 and 6726 M^{-1}, respectively. The limit of detection using these polymers can reach up to ppm level. The mechanism of quenching was suggested to be excited state electron transfer from LUMO of polymers to LUMO of PA where the probable resonance energy transfer of the polymeric emission (donor) to the PA (acceptor) could be assumed.

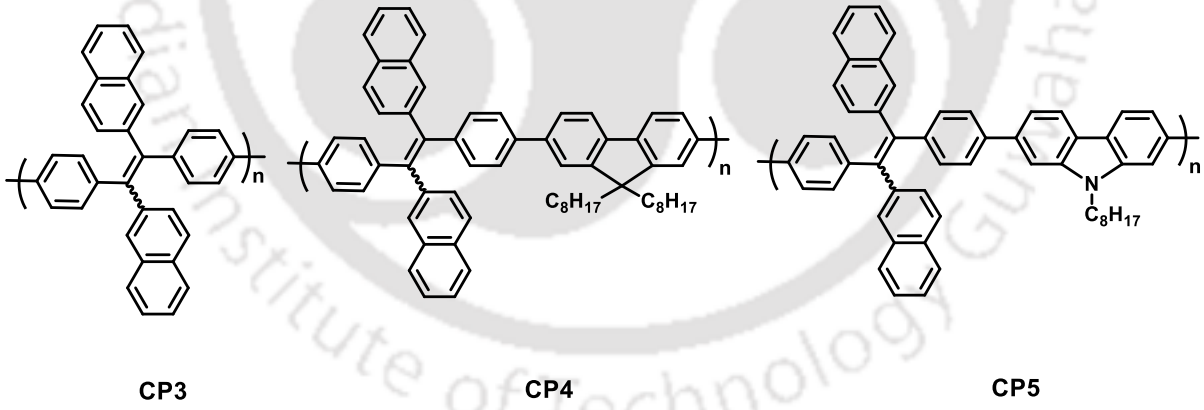

Figure 1.11 Structures of CP3, CP4 and CP5.

In 2015, Hussain *et al.*[35] synthesised a new cationic fluorescent conjugated polyelectrolyte (CP6) by introducing cationic methyl imidazolium unit onto the side chains of polyphenylene backbone, which makes the conjugated polymer solubilise in aqueous medium and also acts as a recognition site for the nitroexplosive PA. Since PA dissociates in aqueous media as anionic picrate, it forms strong electrostatic interaction with CP6 which favoured efficient charge transfer or energy transfer from the polyelectrolyte to the PA leading to amplification

in florescence quenching. Hence Stern-Volmer plot showed very high value of quenching constant (K_{sv}) of 1 $\times 10^7$ M^{-1} and a very low limit of detection value of 128 ppt obtained for this CP indicating the ultra-sensitivity toward PA. Also, polyelectrolyte can be used to make portable solid test strips made of paper and chitosan, both of them showing good utility of this method for on-site detection of PA.

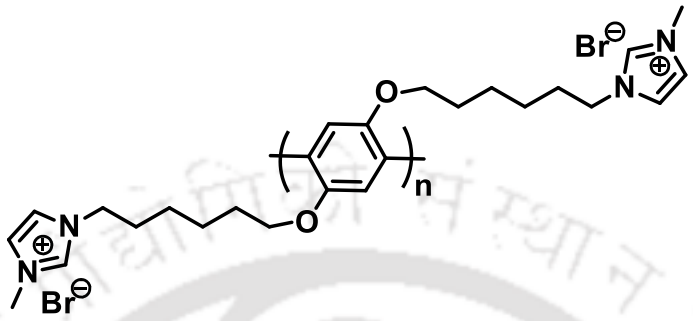

CP6

Figure 1.12 Structure of CP6.

Malik *et al.*[36] in 2015 developed cationic conjugated polymer nanoparticles or polymer dots of a polyfluorene derivative i.e. poly(3,3′-((2-phenyl-9H-fluorene-9,9-diyl)bis(hexane-6,1-diyl))bis(1-methyl-1H-imidazol-3-ium)bromide) (CP7), which can optically and electronically detect PA on various platforms like water, disposable films and electronic device. The synthesis of polymer involves Suzuki coupling polymerisation which was later functionalised with methyl imidazolium and using reprecipitation technique polymer nanoparticles were obtained. A highest value of quenching constant (K_{sv}) of 1.12 $\times 10^8$ M^{-1} was obtained from the Stern-Volmer plot and a very low limit of detection of 30.9 pM was obtained for detection of PA in water medium. For on-site detection purposes, polymer nanoparticles were dip coated over paper to attain simple, low cost and portable fluorescent test strips. Additionally, vapour phase detection of PA was achieved using polymer fabricated two terminal sensor device, which detect PA vapour under ambient conditions. The mechanism of sensing was attributed to the electrostatic interactions, photoinduced electron transfer (PET) and possible resonance energy transfer from polymer to PA.

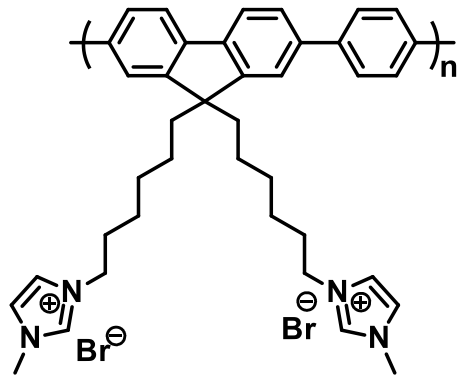

CP7

Figure 1.13 Structure of CP7.

In 2016, Zhou *et al.*[37] synthesised a series of CP (CP8, CP9 and CP10) based on benzo[5]helicene using Yamamoto homocoupling and Suzuki-Miyara cross coupling polymerisation method for the nitroexplosive sensing. The electron rich fluorescent CPs showed quenching response towards the electron deficient nitroaromatic compound in chloroform solution. Among all the electron deficient nitroexplosive compounds, these polymers showed highest value of Stern-Volmer quenching constant with an order of PA>TNT>DNT>NT, which is in accordance to their electron deficient nature in the chlorform. Additionally, for the on-site detection purposed, fluorescent film of polymer- P1 was prepared as it showed excellent fluorescent behaviour in solid state and when exposed to the vapour of various electron deficient compounds for 10 s, follows a quenching order of DNT>TNT>NT>PA. These results are based on the redox potential and vapour pressure of these analytes. The mechanism of sensing was suggested to be the strong charge-transfer complex formation between the electron rich polymer with the electron deficient nitroexplosives.

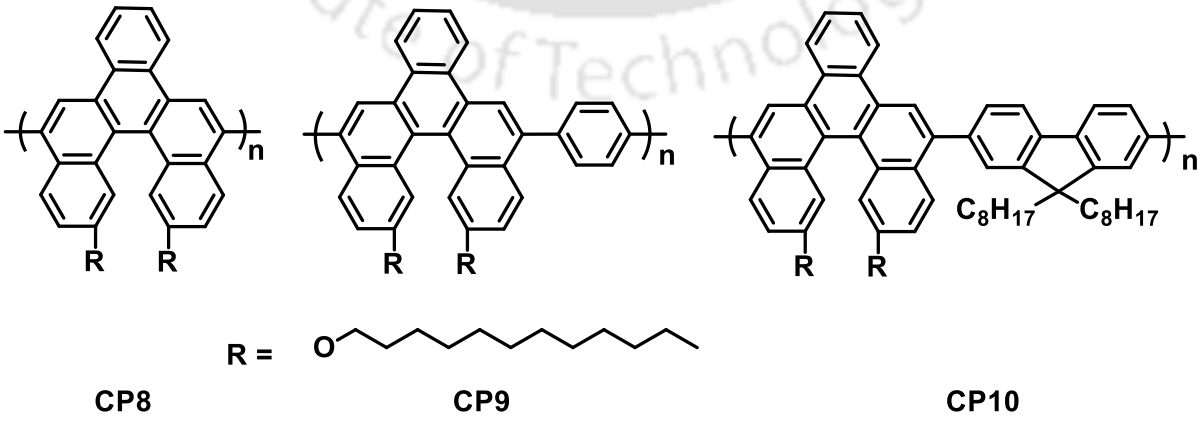

CP8 CP9 CP10

Figure 1.14 Structures of CP8, CP9 and CP10.

In 2017, Ma *et al.*[38] developed a fluorescent hydrophilic conjugated polymer (CP11) having hydroxyl group onto the side chain of main backbone. The polymer uniformly disperses in water and shows bright blue fluorescence. The hydroxyl groups attached onto the side chain are involved in making the hydrogen bonding with the nitroaromatic compounds, results an amplified fluorescence quenching in the aqueous medium. The CP11 shows absorbance maxima at 280 nm and emission maxima at 380 nm. The quenching efficiency of CP11 in water follows a particular order of TNT>DNT>NB>PA. The obtained results are depending on the exciton acceptance ability of CP11 and the electron withdrawing potency of the nitroaromatic compounds.

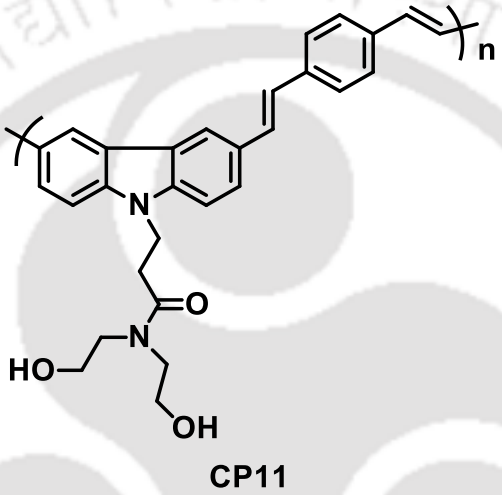

CP11

Figure 1.15 Structure of CP11.

In 2017, Wang *et al.*[39] synthesized three conjugated polymers with a common backbone of alternate tertraphenylethylene (TPE) and phenylene-ethylene unit via Sonogashira coupling polymerisation. Incorporation of TPE unit makes all of these polymers (CP12, CP13 and CP14) show AEE-active behaviour in THF/water mixtures, which was further utilized to develop these into fluorescent probes for nitroexplosive detection. The Stern-Volmer plots displayed a linear nature at the lower concentration of PA i.e. [PA] < 0.1 mM with a quenching constant (K_{sv}) of 37100, 56100 and 53700 M^{-1} for the P0, P1, and P2 respectively, and deviates from linearity at the higher concentration of PA i.e. [PA] > 0.2 mM. This non-linear nature of Stern-Volmer plot was ascribed to the "super-amplification effect" and the mechanism of fluorescence quenching was suggested to be photo-induced charge transfer from the polymer to the PA.

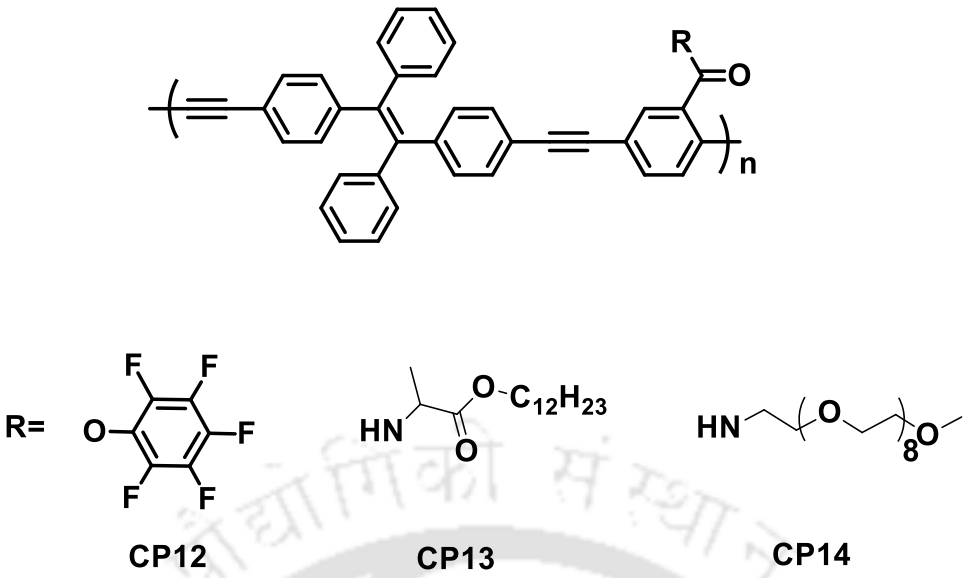

Figure 1.16 Structures of CP12, CP13 and CP14.

In 2018, Wang *et al.*[40] reported a fluorescent conjugated polymer (CP15) having donor-acceptor combination within the main backbone chain, which lead to aggregation enhanced FRET activity. The polymer shows absorbance maxima at 310 nm with a secondary weak peak at 450 nm in dioxane and similarly two emission peaks were seen at 416 nm and 560 nm. The emission peak at 560 nm is indicative of the intra and/or inter molecular FRET process from the carbazole-biimidazole emission to cabazole-benzoimidazole moiety. This polymer forms well dispersed fluorescent nanoparticles in water, which shows orangish-red emission (emission wavelength=572 nm, excitation wavelength = 333 nm) under UV illumination, which has been used for the detection of PA in aqueous medium. The Stern-Volmer plots show linear increment at lower concentration of PA i.e. [PA] < 100 µM with a quenching constant (K_{sv}) of 3.4 × 10^4 M^{-1} and deviates from linearity at the higher concentration of PA i.e. [PA] > 100 µM. The limit of detection of this polymer was calculated to be 0.51 µM and the mechanism of sensing was attributed to the photo-induced electron transfer from polymer nanoparticles to the PA.

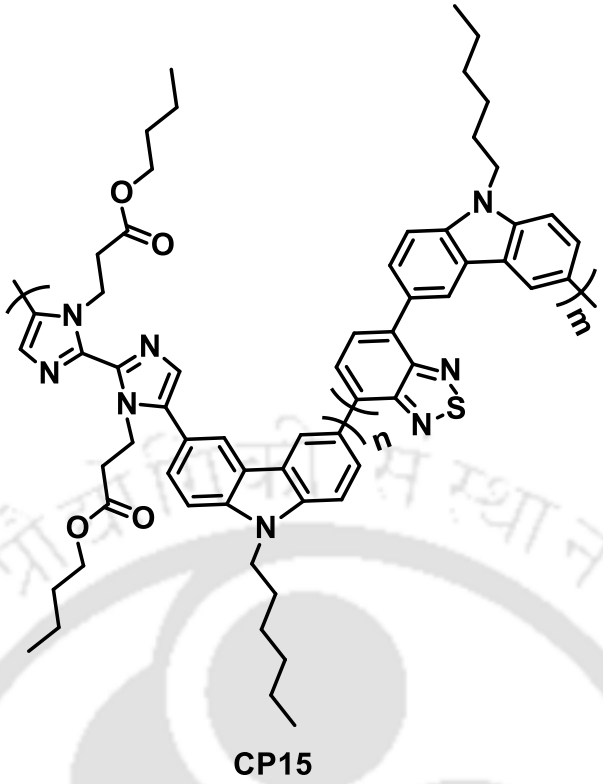

Figure 1.17 Structure of CP15.

1.5 Thesis overview and future perspective

The content of this thesis entitled **"Newly Developed Conjugated Polymer Systems for Nitroexplosive Detection: Insights into the Mechanistic Investigations"** is divided into six chapters.

- Chapter 1 discusses literature survey based on the latest trend in the sensing of nitroexplosive-PA by CPs and insights into their mechanistic details.
- Chapter 2 discusses about the synthesis and characterization of conjugated polymer (PFAM) and its application in the rapid and specific recognition of nitroexplosive-picric acid (PA) on solid support and in solution based on IFE/PET mechanism.
- Chapter 3 describes the synthesis of a new water-soluble non-fluorescent cationic conjugated polyelectrolyte PPPy, which selectively recognized nitroexplosive PA by fluorescence "turn-on" in the presence of closely related nitroexplosive compounds via fluorescence indicator displacement assay (IDA) technique in water at pH 7.0.
- Chapter 4 highlights the synthesis of cationic CP PFBT *via* oxidative polymerization and displayed dual state emission in DMSO as well as in water, a phenomenon very rarely observed, and tested for nitroexplosive analytes detection to observe a remarkable

fluorescence quenching response for picric acid (PA) in the both solvents. Contact mode detection of PA was also accomplished using easy, economical and portable fluorescent test strips for on-site detection. Interestingly, the mechanism of sensing in DMSO solvent was attributed to strong inner filter effect (IFE) and photo induced electron transfer (PET), while in H_2O the sensing occurs via possible resonance energy transfer (RET) and photoinduced electron transfer (PET), which is exceptional and not reported earlier for a single probe.

- Chapter 5 discusses the synthesis of the neutral "receptor-free" highly fluorescent conjugated polymers (PF1 and PF2), which detects PA by a fluorescence turn-off response, and was found as a result of exclusive IFE and was further confirmed via IFE corrections.
- Chapter 6 summarizes the thesis overview and the importance of various sensing mechanisms that can probably exist for nitroexplosive detection but not limited to these chemical entities. Additionally, the design principle of probes that can result in efficient sensing of picric acid via these mechanisms was also studied and presented.

References

(1) Torsi, L.; Dodabalapur, A.; Rothberg, L. J.; Fung, A. W. P.; Katz, H. E. *Science* **1996**, *272*, 1462.

(2) Sirringhaus, H. *Adv. Mater.* **2005**, *17*, 2411.

(3) Gunes, S.; Neugebauer, H.; Sariciftci, N. S. *Chem. Rev.* **2007**, *107*, 1324.

(4) Kraft, A.; Grimsdale, A. C.; Holmes, A. B. *Angew. Chem. Int. Ed.* **1998**, *37*, 402.

(5) Montali, A.; Smith, P.; Weder, C. *Synthetic Met.* **1998**, 97, 123.

(6) McQuade, D. T.; Pullen, A. E.; Swager, T. M. *Chem. Rev.* **2000**, *100*, 2537.

(7) Thomas, S. W.; Joly, G. D.; Swager, T. M. *Chem. Rev.* **2007**, *107*, 1339.

(8) Grimsdale, A. C.; Mullen, K. *In Emiss. Mater. Nanomater*. **2006**, *199*, 1.

(9) Patil, A. O.; Heeger, A. J.; Wudl, F. *Chem. Rev*. **1988**, *88*, 183.

(10) Scherf, U.; List, E. J. W. *Adv. Mater*. **2002**, *14*, 477.

(11) Kraft, A.; Grimsdale, A. C.; Holmes, A. B. *Angew. Chem. Int. Ed*. **1998**, *37*, 402.

(12) Bunz, U. H. F. *Chem. Rev*. **2000**, *100*, 1605.

(13) Perepichka, I. F.; Perepichka, D. F.; Meng, H.; Wudl, F. *Adv. Mater*. **2005**, *17*, 2281.

(14) Liu, B.; Bazan, G. C. *Chem. Mater*. **2004**, *16*, 4467.

(15) Liang, J.; Li, K.; Liu, B. *Chem. Sci*. **2013**, *4*, 1377.

(16) Zhu, C.; Liu, L.; Yang, Q.; Lv, F.; Wang, S. *Chem. Rev*. **2012**, *112*, 4687.

(17) Henson, Z. B.; Zhang, Y.; Nguyen, T. Q.; Seo, J. H.; Bazan, G. C. *J. Am. Chem. Soc.* **2013**, *135*, 4163.

(18) Jiang, H.; Taranekar, P.; Reynolds, J. R.; Schanze, K. S. *Angew. Chem. Int. Ed*. **2009**, *48*, 4300.

(19) Zhou, Q.; Swager, T. M. *J. Am. Chem. Soc.* **1995**, *117*, 12593.

(20) Zhou, Q.; Swager, T. M. *J. Am. Chem. Soc*. **1995**, *117*, 7017.

(21) Sun, X.; Wang, Y.; Lei, Y. *Chem. Soc. Rev.* **2015**, *44*, 8019.

(22) Lakowicz, J. R. *Principles of Fluorescence Spectroscopy*, Springer, Singapore, **2006**.

(23) Meaney, M. S.; McGuffin, V. L. *Anal. Chim. Acta*. **2008**, 610, 57.

(24) Valeur, B. *Molecular Fluorescence: Principles and Applications*, Wiley-VCH, **2002**.

(25) Zhang, Y.-Z.; Xiang, X.; Mei, P.; Dai, J.; Zhang, L.-L.; Liu, Y. *Spectrochim. Acta. Part A* **2009**, *72*, 907–914.

(26) Cantor, C. R. *Biophysical chemistry: Part II: Techniques for the study of biological structure and function*, Macmillan, **1980**.

(27) Tong, H.; Wang, L.; Jing. X.; Wang, F. *Macromolecules* **2003**, *36*, 2584.

(28) Xu, Y.; Li, B.; Li, W.; Zhao, J.; Sun. S.; Pang, Y. *Chem. Commun*. **2013**, *49*, 4764.

(29) Chen. S.; Yu. Y-L.; Wang. J-H. *Analytica Chimica Acta* **2018**, *999*, 13.

(30) Albert, K. J.; Lewis, N. S.; Schauer, C. L.; Sotzing, G. A.; Stitzel, S. E.; Vaid, T. P.; Walt, D. R. *Chem. Rev*. **2000**, *100*, 2595

(31) Tu, R. Y.; Liu, B. H.; Wang, Z. Y.; Gao, D. M.; Wang, F.; Fang, Q. L.; Zhang, Z. P. *Anal. Chem*. **2008**, *80*, 3458.

(32) Yuan. W. Z.; Zhao. H.; Shen. X. Y.; Mahtab. F.; Lam. J. W. Y.; Sun. J. Z.; Tang. B. Z. *Macromolecules* **2009**, *42*, 9400.

(33) Yang. G.; Hu. W.; Xia. H.; Zou. G.; Zhang. Q. *J. Mater. Chem. A* **2014**, *2*, 15560.

(34) Gao. M.; Wu. Y.; Chen. B.; He. B.; Nie. H.; Li. T.; Wu. F.; Zhou. W.; Zjou. J.; Zhao. Z. *Polym. Chem.*, **2015**, *6*, 7641.

(35) Hussain. S.; Malik. A. H.; Afroz. M. A.; Iyer. P. K. *Chem. Commun.* **2015**, *51*, 7207.

(36) Malik. A. H.; Hussain. S.; Kalita. A.; Iyer. P. K. *ACS Appl. Mater. Interfaces* **2015**, *7*, 26968.

(37) Zhou. L.; Li. M.; Lu. H.; Chen. C. *Polym. Chem.* **2016**, *7*, 310.

(38) Ma. X.; Wang. D.; Cui. Y.; Tao. F.; Wang. Y. *Sensors and Actuators B* **2017**, *251*, 851.

(39) Wang. X.; Wang. W.; Wang. Y.; Sun. J.; Tang. B. Z. *Polym. Chem.* **2017**, *8*, 2353.

(40) Wang. T.; Zhang. N.; Bai. R.; Bao. Y. *J. Mater. Chem. C* **2018**, *6*, 266.

Chapter 2

Inner Filter Effect Based Selective Detection of Nitroexplosive- Picric Acid in Solution and Solid Support Using Conjugated Polymer

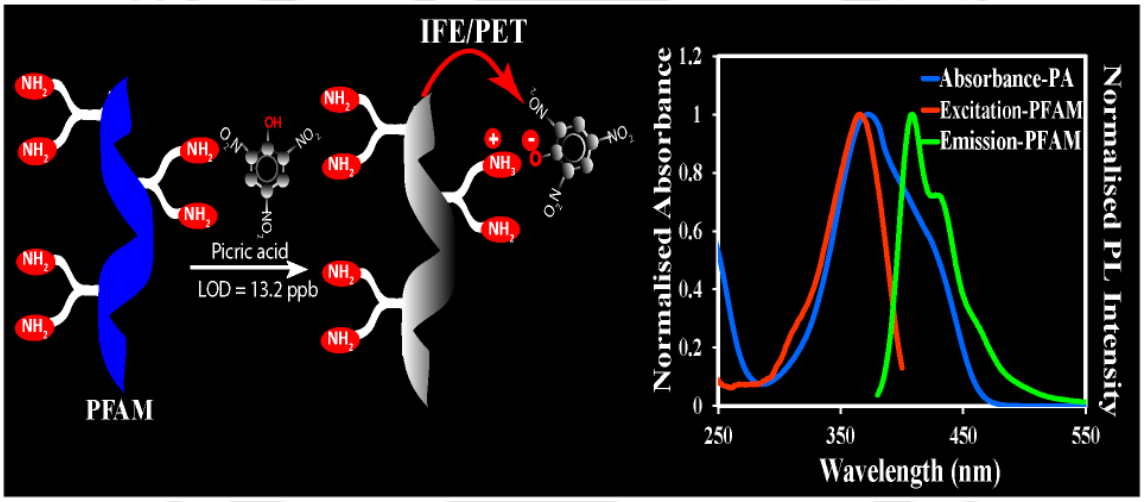

Tanwar, A. S.; Hussain, S.; Malik, A. H.; Afroz, M. A.; Iyer, P. K. *ACS Sens.* **2016**, 1, 1070–1077.

Abstract

A new polyfluorene derivative, poly[4,4′-(((2- phenyl-9H-fluorene-9,9-diyl)bis(hexane-6,1-diyl))bis(oxy))-dianiline)] (PFAM) was synthesized via the Suzuki coupling polymerization method in high yields for the rapid and specific recognition of nitroexplosive picric acid (PA) at 22.9 picogram level on solid support using paper strips and at 13.2 ppb level in aqueous solution. The polymer PFAM was well-characterized by means of NMR, UV−vis, fluorescence, time-resolved photoluminescence (TRPL) spectroscopy and cyclic voltammetry. The amplified signal response exclusively for PA was achieved via a strong inner filter effect (IFE), a phenomenon different from the widely reported ground-state charge transfer and/or Förster resonance energy transfer (FRET) based probes for nitroaromatics detection. Pendant amine groups attached on the side chains of PFAM provide enhanced sensitivity and exceptional selectivity via protonation assisted photoinduced electron transfer (PET) even in the presence of most common interfering nitroexplosives, as well as other analytes usually found in natural water. Thus, the PFAM based platform was demonstrated for monitoring traces of PA at very low levels even in competitive environment in solution as well as solid state

2.1 Introduction

Development of superior probes to monitor traces of nitroexplosives especially picric acid (PA), is of immense significance for homeland security, forensic investigations, as well as environmental protection.[1] Owing to the versatile applications of PA in dye, drugs, leather, fireworks, and matchbox industries, it pollutes natural water and has severe consequences on human health, viz., cancer, sycosis, damage to the liver and kidney as well as breathing organs.[2–4] Another critical problem associated with PA is its lower degradation in biosystems, thereby accounting for numerous chronic diseases.[5] Thus, there is an urgent need to develop highly sensitive and selective probes for determining traces of PA with respect to terrorist threats as well as environmental issues.

Several detection platforms have been established for monitoring nitroexplosives.[6] However, most of these methods suffer largely from issues of portability, selectivity, high operation cost, and on-field use. Owing to the notable sensitivity, rapid signal response time toward analytes, and ease of operation, the development of fluorescent-based probes is in huge demand.[7] With this in view, numerous fluorescent probes for nitroaromatics based on metal complexes, conjugated polymers (CPs), organic molecule dyes, nanoaggregates, and quantum dots have been reported.[8–23] Several of them suffer from the issues of discrimination, sensitivity, ease of handling, and on-site detection. Moreover, most of these probes are based on either Förster resonance energy transfer (FRET) or electron transfer processes that are distance dependent mechanisms and require close interaction between the sensor molecule and analyte to deliver a sensible signal response. The inner filter effect[24] (IFE) is another vital phenomenon of spectrofluorometry that does not require any link between the fluorophore and the quencher molecule, subsequently resulting in enhanced fluorescence quenching due to absorption of the excitation and/or emission by the absorbers (quencher). Recently, IFE has gained much attention in the field of sensors,[25–30] due to its simplicity, flexibility, and substantially enhanced sensitivity and selectivity. Zhang et al.[31] reported a fluorescent probe for the detection of TNT in a strong alkaline solution via IFE between absorptive Meisenheimer complex and fluorescent quantum dots. However, less attention has been paid in designing IFE based probes for sensing PA. Hence, development of an alternative method for PA detection that overcomes the existing limitations still remains a challenge for researchers due to the similar electron deficient nature of other nitroexplosives.

CPs are one of the most promising class of materials for the recognition of nitroexplosives both in liquid phase as well as thin films owing to their high quantum efficiency, excellent molar absorptivity, and high signal amplification via the "molecular wire effect".[1,32–44] In this regard, few probes based on CPs have been reported for monitoring PA, yet most of them are nonspecific due to the absence of specific binding sites or they lack sufficient sensitivity in various environments.[45–56] Hence, fluorescence amplifying detection of PA using CPs with suitable binding sites to achieve high selectivity and enhanced sensitivity for on-site detection remains highly appealing. Few amine substituted small molecules have also been explored as efficient materials for monitoring PA with high selectively via the formation of hydrogen bonding, protonation of amine groups, as well as electrostatic interaction.[9,12,33,57,58] This encouraged us to design a new CP PFAM incorporated with amine groups for the specific and amplifying detection of PA at very low concentration. The PA detection by PFAM is based on a strong inner filter effect (IFE) as well as favorable photoinduced electron transfer (PET) assisted by protonation, which further boosts the sensitivity of the probe. To the best of our knowledge, this is the first report based on CP for the selective detection of nitroexplosive picric acid via the inner filter effect, a phenomenon that is different from ground-state charge transfer and resonance energy transfer based sensors reported exhaustively.[11,47,57,59]

2.2 Experimental

2.2.1 Materials and measurements

Nitroexplosives viz., 2,4-dinitrotoluene (2,4-DNT), 2,6-dinitrotoluene (2,6-DNT), 4-nitrotoluene (4-NT), and 1,3-dinitrobenzene (1,3-DNB) were purchased from SigmaAldrich Chemicals. TNT and RDX were purchased from AccuStandard. PA was purchased from Loba Chemie Pvt. Ltd. All other chemicals and reagents were purchased from Alfa-Aesar and Merck, and were used as received without further purification. Milli-Q water was used for making stock solutions as well as experiment purposes. ^{1}H NMR (600 and 400 MHz) and ^{13}C NMR (150 and 100 MHz) spectra were obtained on Bruker Ascend 600 spectrometer and Varian-AS400 NMR spectrometer. UV/visible and photoluminescence spectra were recorded on a PerkinElmer Lambda-25 and Horiba Fluoromax-4 spectrofluorometer using 10 mm path length quartz cuvettes with a slit width of 3 nm at 298 K. Time-resolved fluorescence measurements were carried out in Edinburgh Instruments Life Spec II instrument. Cyclic voltammograms were recorded

using CH instruments model 700D series electrochemical workstation. Paper strip tests were performed using Whatman qualitative filter paper, grade 1. Gel permeable chromatography (GPC) was performed in THF using Agilent Technologies instrument with polystyrene as standard.

2.2.2 Synthetic Procedure

2.2.2a Synthesis of 2, 7-dibromo-9, 9-bis (6-bromohexyl)-9H-fluorene (M2):

Monomer (M2) was synthesized by using a previously established procedure from literature.[60] 2,7-dibromofluorene (1.0 g, 3.086 mmol) and catalytic amount of tetrabutyl ammonium iodide (TBAI) (0.24 g, 0.617 mmol) were taken in a 50 mL round bottom flask. 50% aqueous NaOH (50%, 12 mL) was added to the flask under inert condition. The flask was degassed using freeze-thaw cycles followed by addition of 1,6-dibromohexane (3.32 mL, 21.602 mmol). The reaction mixture was maintained at 70 °C and stirred for 4 h. Further, it was cooled to room temperature and extracted with dichloromethane (DCM). The DCM layer was washed with water thrice and dried over anhydrous sodium sulfate. The organic layer was concentrated using rotatory evaporator and crude compound obtained was purified via column chromatography over a silica gel pad using hexane (Yield = 1.8 g, 90 %). ^{1}H-NMR (400 MHz, $CDCl_3$, δ ppm): 7.53 (d, 2H), 7.45 (m, 4H), 3.29 (t, 4H), 1.92 (t, 4H), 1.68 (m, 4H), 1.18 (m, 4H), 1.08 (m, 4H), 0.58 (m, 4H).^{13}C NMR (100 MHz, $CDCl_3$, δ): 152.40, 139.31, 130.57, 126.33, 121.80, 121.45, 55.79, 40.26, 34.05, 32.83, 29.17, 27.97, 23.68.

2.2.2b Synthesis of Di-tert-butyl((((2,7-dibromo-9H-fluorene-9,9-diyl)bis(hexane-6,1-diyl))bis(oxy))bis(4,1-phenylene))-dicarbamate (M3):

A mixture of 2,7-dibromo-9,9-bis(6-bromohexyl)-9H-fluorene (M2) (0.100 g, 0.153 mmol), tert-butyl(4-hydroxyphenyl) carbamate (0.064 g, 0.307 mol) and potassium carbonate (0.127 g, 0.921 mmol) were heated at 70 °C in dry DMF for 24 h. The reaction was monitored by TLC using 10% EtOAc in hexane. After the completion of reaction, the mixture was cooled, filtered, and extracted multiple times using chloroform/water. The organic layer was collected, dried over anhydrous sodium sulfate, and evaporated to obtain crude product as a light brown colored product. Purification was performed by column chromatography (6% EtOAc:Hexane) (Yield = 0.102g, 73%). ^{1}H-NMR (600 MHz, $CDCl_3$, δ ppm) : 7.52 (d, 2H), 7.46 (d, 2H), 7.43 (s, 2H), 7.22 (d, 4H), 6.78 (d, 4H), 6.31 (s, 2H), 3.80 (t, 4H), 1.93 (m, 4H), 1.50 (s, 18H), 1.21 (m, 4H), 1.12 (m, 4H), 0.61 (m, 4H). ^{13}C NMR (100 MHz, $CDCl_3$, δ ppm): 155.07, 153.33, 152.34, 139.06, 131.36,

130.29, 126.11, 121.55, 121.27, 120.72, 114.80, 80.04, 68.08, 55.61, 40.05, 29.57, 29.13, 28.42, 25.65, 23.65. MS (ESI): calculated for $C_{47}H_{58}Br_2N_2O_6$ $[M + H]^+$: 907.2719; Found 907.2722. Elemental analysis: calculated for M3: C, 62.25; H, 6.45; N, 3.09; found: C, 62.42; H, 5.087; N, 3.27

2.2.2c Synthesis of Poly(di-tert-butyl((((2-phenyl-9H-fluorene-9,9-diyl)bis(hexane-6,1-diyl))bis(oxy))bis(4,1-phenylene))-dicarbamate) (P0):

A mixture of M3 (0.100 g, 0.11 mmol), tetrakistriphenylphosphine palladium(0) (0.0063 g, 0.005 mmol), benzene-1,4-bisboronic acid (0.018 g, 0.11 mmol), 3 mL of 2 M aq solution of K_2CO_3 and THF (9 mL) were taken in a flask fitted with a condenser. The reaction mixture was degassed thrice by freeze−thaw cycles followed by refluxing for 18 h under argon atmosphere. The reaction mixture was then cooled and extracted with chloroform/water thrice. The organic layer was then evaporated to dryness and purified by precipitation method in methanol twice. The product was obtained as grey color precipitate after drying in vacuum (Yield = 0.065 g, 71%). ^{1}H NMR (400 MHz, $CDCl_3$, δ ppm): 7.80(br), 7.701(br), 7.64(br), 7.53(br), 7.26(br), 6.80(br), 6.44(br), 3.83(br), 2.066(br), 1.62(br), 1.54(br), 1.30(br), 1.19(br), 0.90(br).^{13}C NMR (150 MHz, $CDCl_3$, δ ppm): 155.33, 153.36, 152.51, 151.07, 140.20, 139.99, 139.24, 131.43, 130.44, 129.01, 127.75, 127.35, 126.33, 126.30, 121.70, 121.48, 120.66, 120.39, 115.00, 80.32, 68.32, 55.64, 40.40, 29.86, 29.31, 28.55, 25.82, 23.80. GPC using polystyrene as standard in THF: $M_w = 1.03 \times 10^4$, PDI = 2.2.

2.2.2d Synthesis of Poly(4,4′-(((2-phenyl-9H-fluorene-9,9-diyl)bis-(hexane-6,1-diyl))bis(oxy))dianiline) (PFAM):

To the solution of polymer (P0), (0.05 g) in DCM, TFA (excess) was added and kept for stirring in inert atmosphere for 12 h at room temperature. The resulting viscous solution was washed repetitively with diethyl ether to obtain product as dry solid compound. Any unreacted polymer P0 was removed by dissolving the mixture again in dichloromethane, followed by decantation. The collected residue was dissolved in methanol and basified with TEA to obtain grey colored precipitate. This was then centrifuged, filtered, and washed with ether to get purified polymer PFAM (Yield = 0.035 g, 92%). ^{1}H NMR (400 MHz, $CDCl_3$, δ ppm): 7.78(br), 7.64(br), 7.48(br), 6.65(br), 6.58(br), 3.73(br), 3.34(br), 2.03(br), 1.55(br), 1.25(br), 1.15(br), 0.79(br).

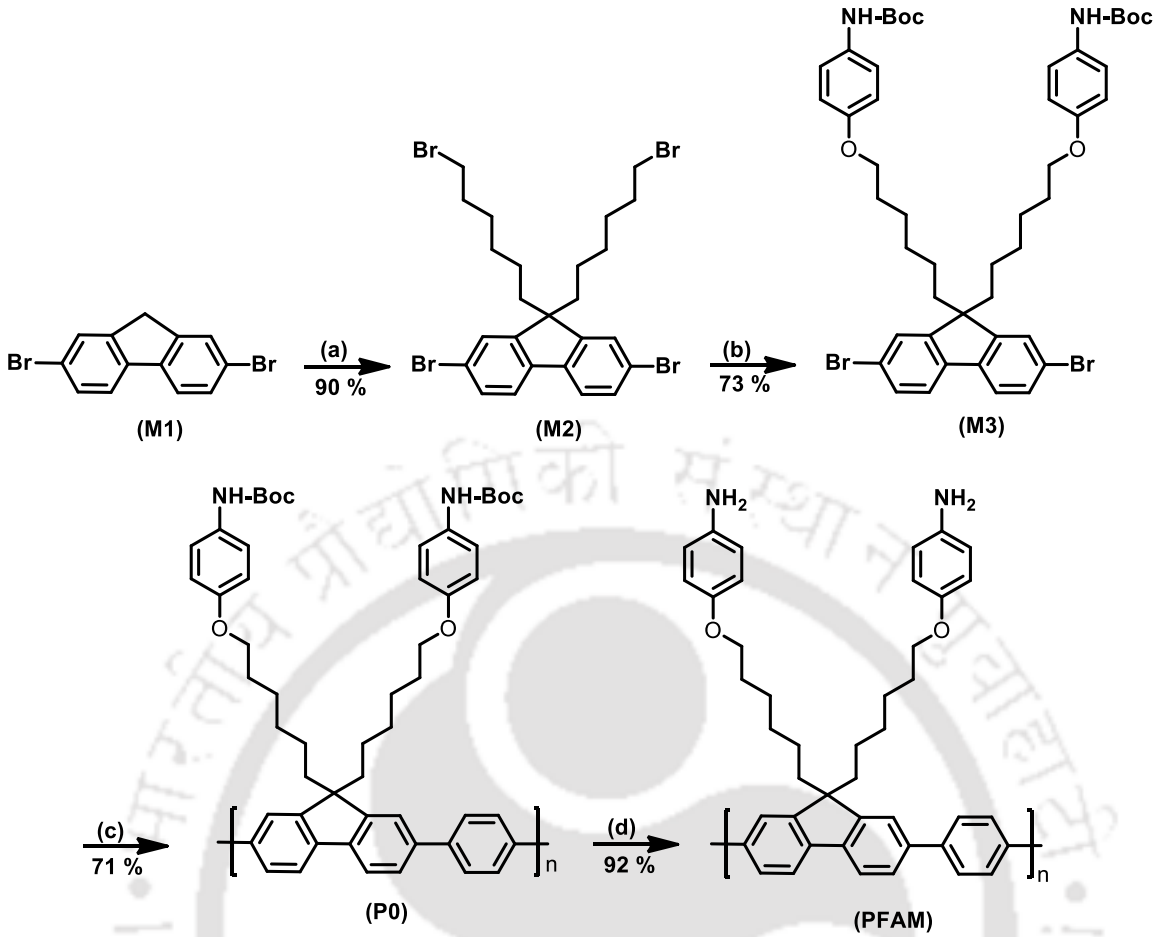

Scheme 2.1 Synthesis of the polymer-PFAM. (a) 1,6-Dibromohexane, 50% aq. NaOH, TBAI, 70 °C, 4 h; (b) tertbutyl(4-hydroxyphenyl)carbamate, DMF, K_2CO_3, reflux, 12 h; (c) tetrakistriphenylphosphine palladium(0), benzene-1,4-diboronic acid, 2 M aq. K_2CO_3, THF, reflux, 24 h; (d) TFA/CH_2Cl_2, rt, 12 h, followed by Et_3N in CH_3OH.

2.2.3 Preparation of stock solutions for sensing studies

Stock solution of polymer PFAM and explosives, viz., 2,6-dinitrotoluene, 2,4-dinitrotoluene, 4-nitrotoluene, and 1,3-dinitrobenzene, were prepared at concentrations of 10 mM in HPLC-grade THF. Stock solution (10 mM) of RDX and TNT was prepared in 1:1 CH_3CN:MeOH. Similarly, stock solution of other analytes, viz., PA, nitromethane (NM), nitrobenzene (NB), phenol, benzoic acid (BA), 4-nitrophenol (4-NP), and 2,4-dinitrophenol (2,4-DNP) were prepared in Milli-Q water at concentration of 10 mM. The absorption and fluorescence studies were performed after making different solutions of PFAM (1×10^{-6} M), each containing various concentrations of each analyte in 4:1/ THF:HEPES (pH = 7, 10 mM) in a quartz cuvette (1 cm × 1 cm). The spectra of each resultant mixture were recorded after mixing the solutions thoroughly at room temperature.

2.2.4 Calculations for photoluminescence quantum yield

The quantum yield of polymer PFAM was determined in THF using quinine sulfate (Φr = 0.54 in 0.1 M H_2SO_4) as reference material. The following equation[61,62] was employed for calculations

$$\Phi_s = \Phi_r (A_r F_s / A_s F_r)(\eta_s^2 / \eta_r^2)$$

where s and r represents the sample and reference, respectively, A denotes the absorbance, F is the relative integrated fluorescence intensity, and η is used for refractive index of the medium used.

2.2.5 Time-resolved decay measurements

Lifetime decay measurements of PFAM (1×10^{-6} M) in the presence and absence of PA (5×10^{-5} M) were carried out using pulse excitation of 375 nm and emission at 408 nm. The curves were fitted biexponentially and the average lifetime was considered for consistency in results. Lifetime of each component, amplitude, and average lifetime are shown in Table A2.1.

2.2.6 Preparation of paper strips

Fluorescence test strips were prepared by dipping the Whatman filter paper (70 mm diameter) in the solution of PFAM (10^{-4} M) in THF followed by drying of solvent in an air stream. The filter paper coated with PFAM was then cut into the desired number of pieces (1 cm × 1 cm) and used for the surface sensing purposes.

2.2.7 Calculating detection limit

Different solutions of PFAM (1×10^{-6} M), each containing PA (0 μM, 0.33 μM, 0.66 μM, 0.99 μM, 1.33 μM, 1.66 μM, and 1.99 μM) were prepared separately in 4:1 THF:HEPES buffer (pH 7.0, 10 mM) and the fluorescence spectrum was recorded for each sample. A calibration curve was then plotted between fluorescence intensity and concentration of PA to obtain the regression curve equation. The detection limit was calculated using the equation 3σ/k, where σ represents the standard deviation for the intensity of PFAM in the absence of PA and k denotes the slope.

2.2.8 Electrochemistry

The cyclic voltammogram for PFAM was recorded using three-electrode cell under inert atmosphere at room temperature. A glassy carbon electrode acts as a working electrode, while the saturated $Ag/AgNO_3$ electrode and platinum wire were employed as reference

and counter electrodes, respectively. $TBAPF_6$ (0.1 M) in acetonitrile was used as supporting electrolyte with Fc^+/Fc couple as an internal reference. A total of 5 μL of PFAM (1 mM) dissolved in THF was drop-cast on a working electrode over the area of 7 mm^2 to record cyclic voltammogram. Noticeable oxidation potential was observed for the polymer PFAM. From the onset method (E_{HOMO} = −[E(onset, ox vs Fc^+/ Fc) + 4.8] (eV)) the HOMO level of PFAM was calculated to be −5.65 eV. Using the band gap of 3.02 eV as determined from the onset of UV−vis spectrum of PFAM, the LUMO level of polymer PFAM was finally calculated to be −2.62 eV.

2.3 Results and Discussion

2.3.1 Synthesis and Characterization of Poly(4,4′-(((2-phenyl-9H-fluorene-9,9-diyl)bis(hexane-6,1-diyl))bis(oxy))- dianiline) (PFAM)

The synthetic scheme for polymer PFAM is presented in Scheme 2.1. The monomer (M2) was subjected to substitution by Boc protected aminophenol followed by the Suzuki polymerization reaction to obtain polymer P0 in high yields. The polymer P0 was then deprotected using TFA to obtain the final polymer PFAM with pendant amine groups. The products at each step were well characterized and purified before further use (Figures A2.1−A2.6). The molecular weight Mw of precursor polymer P0 as determined by GPC was found to be 1.03×10^4, PDI = 2.2, in THF using polystyrene as standard (Figure A2.7). The p-aminophenol group attached on the side chains of PFAM acts as a selective recognition site for PA and facilitates its sensing efficiency via photoinduced electron transfer. The CP PFAM exhibited good solubility in most organic solvents with fluorescence quantum yield (Φs) of 0.30 in THF. The absorption and emission maxima were observed at 370 and 408 nm (excitation at 366 nm), respectively, in THF solution.

2.3.2 Sensing and selectivity studies

Considering the critical environmental applications, sensing studies for PA were performed in 4:1/ THF:HEPES buffer (pH = 7.0, 10 mM). The PFAM displayed strong blue luminescence in dilute solutions under UV light illumination that was visible to the naked eye. Fluorescence quenching experiments were performed by varying the concentrations of nitro compounds in the solution of PFAM (1×10^{-6} M). It was observed that addition of only 3.3×10^{-6} M PA solution causes instant fluorescence quenching of ~25% which further reaches 95% at 5×10^{-5} M PA concentration (Figure 2.1a). The disappearance of the blue luminescence of PFAM in the presence of PA was clearly visible under UV light (Figure A2.8). Stern-Volmer plot was obtained via I_o/I vs [Q],

where I_o and I denote the fluorescence intensities before and after addition of quencher, [Q] represents the concentration of quencher added, and K_{sv} denotes the quenching constant (M^{-1}). The quenching constant value (K_{sv}) calculated through linear fitting of S-V plot was found to be 1.05×10^5 M^{-1} (inset of Figure 2.1a) indicating remarkable amplification quenching process for PA. The detection limit calculated using 3σ/k, was found to be 57.8 nM (13.2 ppb) (Figure A2.9), which is being reported for the first time using IFE assisted CP based detection of PA (Table A2.2).

To elucidate the selectivity, fluorescent titration experiments were performed by adding various common interfering analytes, viz., TNT, 2,4-DNT, 2,6-DNT, RDX, 1,3-DNB, 4-NT, BA, NB, NM, and phenol to the solution of PFAM (1×10^{-6} M) in 4:1/THF:HEPES buffer (Figure 2.1b and Figure A2.10). Interestingly, no significant change in the fluorescence of PFAM was observed after introducing these analytes. It can be seen from Figure 2.1c that at lower PA concentration, S−V plot follows a linear nature that further deviates from linearity and rises exponentially at higher concentration. However, all other nitroexplosives displayed only linear increment in S−V plot (Figure 2.1c). The exponential nature of S−V plot for CP indicates an amplified quenching and may be accountable for the efficient singlet exciton migration[63] within the polymer chains, additional energy transfer process, self-absorption,[1,64] or quencher-induced aggregation of the polymer chains.[65] The K_{sv} value obtained for PA was significantly high compared to other analytes indicating an amplified quenching and remarkable selectivity of PFAM toward PA. Furthermore, other metal ions (Hg^{2+}, Al^{3+}, Cd^{2+}, Zn^{2+}, Cu^{2+}, Ni^{2+}, Ca^{2+}, Co^{3+}, Cr^{2+}, Pb^{2+}, La^{3+}, Mn^{2+}) as well as anions (I^-, F^-, BH_4^-, NO_3^-, N_3^-, S^{2-}, BF_4^-, CN^-, $H_2PO_4^-$, HPO_4^{2-}, PO_4^{3-}, NO_2^-, AcO^-) usually found in natural water did not have any effect on the fluorescence of PFAM (Figures A2.11−A2.12) which confirms the exclusive selectivity of PFAM toward PA and suggesting the viability of this system for practical applications in natural water.

2.3.3 Sensing in competitive environment

For day-to-day application purposes, the detection of PA in competitive environment is highly desirable. To demonstrate this potential, various fluorescence titrations were performed in the presence of several other interfering analytes. In a typical experiment, a solution of TNT (5×10^{-5} M) was added initially to the solution of PFAM (1×10^{-6} M) to access most of the binding sites of the polymer, but no significant change in the fluorescence intensity was observed (Figure 2.1d). The solution of PA was then

introduced which resulted in significant fluorescence quenching. The same set of experiments were repeated with rest of the analytes and similar results were obtained with almost no change in quenching efficiency of PA (Figure 2.1d and Figures A2.13-A2.22). It is noteworthy to mention that most of the chemosensors developed for PA suffered from very large interference by several other electron deficient nitro aromatics that prevent the practical applicability of those systems. The present method provides a simple, reliable, rapid, and efficient platform for the specific detection of PA even in a competitive environment.

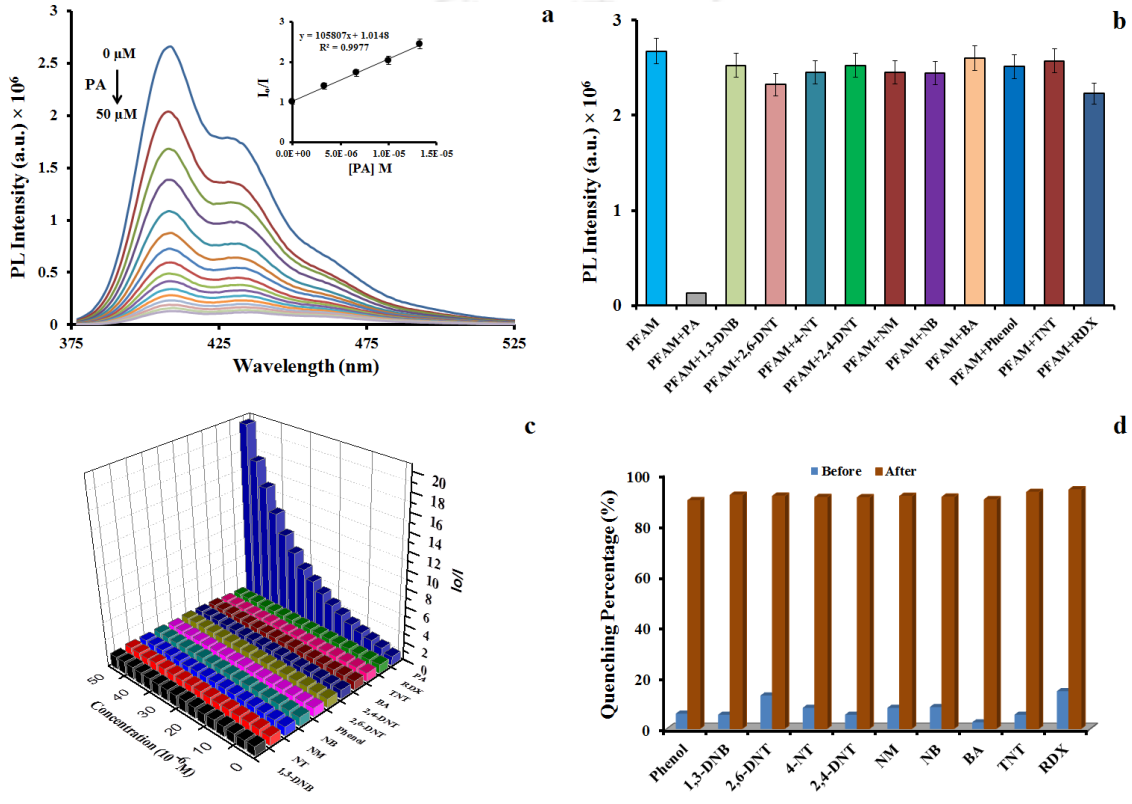

Figure 2.1 (a) Photoluminescence spectra of PFAM (1×10^{-6} M) with various concentrations of PA in 4:1/THF:HEPES buffer (pH = 7.0, 10 mM). Inset: Stern−Volmer plot for PA. (b) Bar diagram depicting the effect of various interfering analytes (5×10^{-5} M) on emission maximum of PFAM (1×10^{-6} M) (error bars = ±5%). (c) Stern−Volmer plots obtained for various interfering analytes in 4:1/THF:HEPES buffer (pH = 7.0, 10 mM). (d) Percentage of quenching by different interfering analytes (5×10^{-5} M) before and after addition of 5×10^{-5} M PA.

2.3.4 Mechanism of sensing

On the basis of these observations, there could be three possible mechanisms for PA sensing by PFAM. These are (a) FRET or IFE between PFAM and PA, (b) formation of a ground-state electrostatic complex, and (c) PET from PFAM to PA. To fulfill the

conditions of FRET or IFE, there should be significant spectral overlap between the absorption spectrum of quencher (PA) and emission spectrum of fluorophore (PFAM). Note that the absorption spectrum of PA has a wide range from 280 to 480 nm and showed significant spectral overlap with excitation and emission spectrum of polymer PFAM (Figure 2.2a). Hence, to ascertain the main reason for quenching, the lifetime decay of PFAM was monitored in the absence and presence of PA. It is evident from Figure 2.2b that the lifetime of PFAM (0.298 ns) does not display any significant change after adding PA (0.287 ns). This confirms that quenching occurred primarily via a static mechanism and ruled out the possibility of FRET in the quenching process. Hence, IFE could be the main mechanism responsible for fluorescence quenching of PFAM by PA. This can be explained via inefficient overlap between the absorption spectra of other nitroaromatics and excitation/emission spectrum of PFAM that subsequently results in poor IFE (Figure 2.2c). Furthermore, UV−visible spectra of PFAM with PA (Figure 2.2d) displayed a minor increment in the absorption intensity without causing any shift in the peak of PFAM. This excludes the possibility of aggregation of PFAM chains by PA and formation of any ground-state charge transfer complex between PFAM and PA. Hence, IFE is the most probable mechanism likely responsible for the high sensitivity and selectivity of PFAM toward PA.

To elucidate the role of electrostatic complex on quenching efficiency, control experiments were performed taking 2,4-DNP, 4-NP, and PA as model compounds since they all contain a single −OH group with a variable number of $-NO_2$ groups that control their acidity in the order PA > 2,4-DNP > 4-NP. Since PA is a stronger acid compared to 2,4-DNP and 4-NP, it has greater tendency to interact with PFAM via acid−base interaction to form a stable electrostatic complex.[9,12,57,58] Hence, the percentage of fluorescence quenching by these compounds was found in the order PA > 2,4-DNP > 4-NP (Figure 2.3). Nitro analytes that do not possess hydroxyl groups cannot interact strongly with the free basic amine sites of PFAM, and hence displayed negligible quenching efficiencies. Note that the spectral overlap region between absorption spectra of PA or DNP and excitation/emission spectra of PFAM is almost the same (Figure A2.23), yet the quenching efficiency is greater for PA. This can be explained via the ease of photoinduced electron transfer (PET) from polymer PFAM to PA induced by acid−base interaction. PET is a well-known phenomenon that exists in sensor systems when both the probe and the sensing analyte come at a particular distance via some favorable interactions. Since the acid−base interaction brings PFAM and PA into close

proximity, there is a strong possibility of PET from polymer PFAM to PA that subsequently enhances the sensitivity of the probe. To demonstrate this, cyclic voltammetry (CV) was carried out to calculate the highest occupied molecular orbital (HOMO) and lowest unoccupied molecular orbital (LUMO) levels of PFAM (Figure 4a). However, from CV only the oxidation process was observed, since the polymer PFAM is electron-rich and the HOMO level was calculated to be −5.65 eV. Considering an optical band gap of 3.02 eV via the onset of the UV−vis absorption band, the LUMO level was found to be −2.62 eV. These results demonstrate the possibility of photoinduced electron transfer from high-energy LUMO of PFAM (−2.62 eV) to low-energy LUMO of PA (−3.89 eV),[10] resulting in enhanced fluorescence quenching (Figure 2.4b).

Note that LUMO values[66] of 2,4-DNP (−2.82 eV) and 4-NP (−2.22 eV) are usually above that of PA, resulting in reduced quenching efficiency. Although PA has the lowest LUMO energy level compared to other analytes,[10] viz., DNT (−3.5 eV), NT (−3.2 eV), TNT (−3.7 eV), the quenching efficiency by other analytes does not follow this order. This is in agreement with the formation of an electrostatic complex and strong IFE between PFAM and PA, unlike in other nitroaromatics. Thus, it can be concluded that high selectivity and enhanced sensitivity of PFAM toward PA is due to strong IFE and a favorable PET process induced by formation of the electrostatic complex.

To investigate whether the protonation of PFAM by PA is the decisive factor behind the fluorescence quenching, a control experiment was performed using TFA, a stronger acid than PA. It was found that TFA has an insignificant effect on the emission of PFAM even at much higher concentrations than PA (Figure A2.24), suggesting that PA plays a key role in the quenching effect via PET rather than the sole acidity. In another control experiment, preprotonated PFAM was subjected to a PA salt solution. Significant fluorescence quenching was observed (Figure A2.25) with slightly greater sensitivity, i.e., 40 μM PA salt solution was employed instead of 50 μM. This can be attributed to the ease of electrostatic interaction between PA salt and preprotonated PFAM, resulting in enhanced quenching efficiency. To further confirm whether ion pairing followed by protonation is crucial for the proposed sensing and selectivity, TNT was introduced in the presence of TFA. Interestingly, no change in the emission of PFAM was observed (Figure A2.26) confirming that ionic pairing followed by protonation is essential for sensing purposes.

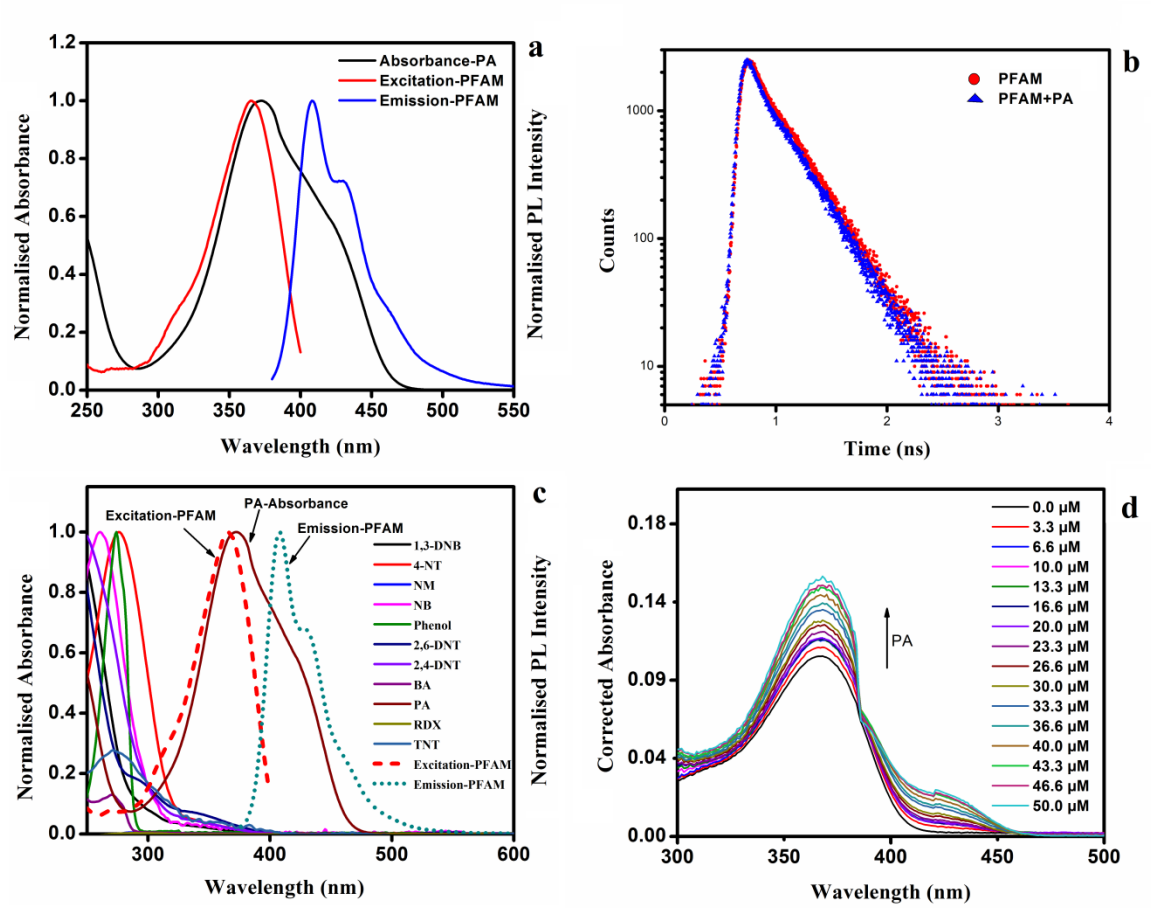

Figure 2.2 (a) Overlap between excitation/emission spectra of PFAM and absorption spectrum of PA in 4:1/THF:HEPES buffer (pH = 7.0,10 mM). (b) Lifetime decay of PFAM (1×10^{-6} M) before and after addition of PA (5×10^{-5} M). (c) Overlap between excitation/emission spectra of PFAM and absorption spectra of various nitroaromatics in 4:1/THF:HEPES buffer (pH = 7.0,10 mM). (d) UV−visible spectra of PFAM (1×10^{-6} M) with increasing concentration of PA.

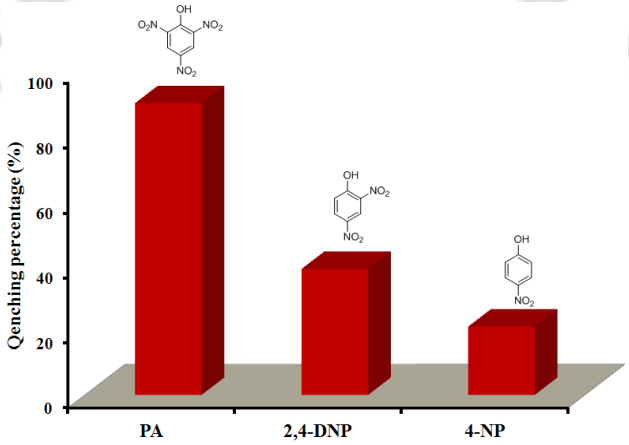

Figure 2.3 Comparison of fluorescence quenching of PFAM obtained for PA, 2,4-DNP, and 4-NP in 4:1/THF:water.

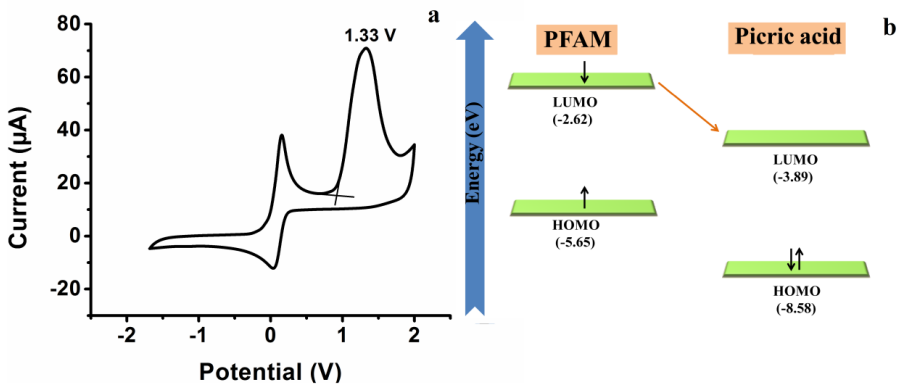

Figure 2.4 (a) Cyclic voltammogram of PFAM film on glassy carbon electrode using 0.1 M tetrabutylammonium hexafluorophosphate ($TBAPF_6$) as a supporting electrolyte in CH_3CN solution with a scan rate of 50 mV/s. (b) Pictorial representation of PET from LUMO of PFAM to the LUMO of PA.

2.3.5 Analysis of PA in natural water samples

Among all nitroexplosives, PA has maximum solubility in water due to the presence of the hydroxyl group. It can easily contaminate water bodies as an effluent from various sources. Hence, development of suitable probes that can monitor and estimate the traces of PA in natural water samples is highly significant. High selectivity of polymer PFAM for PA in competitive environments encouraged us to utilize it for detection in natural water samples. To accomplish this, natural water samples from the Brahmaputra river (near IITG campus and Serpentine Lake inside IITG campus) were collected independently, centrifuged at 5000 rpm for 30 min, and filtered using a 0.2 μm membrane. The samples were then spiked with known concentration of PA and used for sensing purposes by adding known volumes from each sample. The results obtained (Table 2.1) were compared with a standard calibration curve (Figure A2.27) which confirms the feasibility of the system to detect PA efficiently even under competitive environment and which is perceived to be very difficult.

Table 2.1 Determination of PA in Natural Water Samples

River Water Samples				Lake Water Samples			
Sample	Added (10^{-6} M)	Found (10^{-6} M)[a]	Recovery (%)	Sample	Added (10^{-6} M)	Found (10^{-6} M)[a]	Recovery (%)
RW1	3.00	2.83± 0.07	94.3	LW1	5.00	4.81± 0.23	96.2
RW2	6.00	5.63± 0.26	93.8	LW2	8.00	7.57± 0.24	94.6
RW3	9.00	8.82± 0.40	98.0	LW3	11.00	10.37± 0.48	94.2

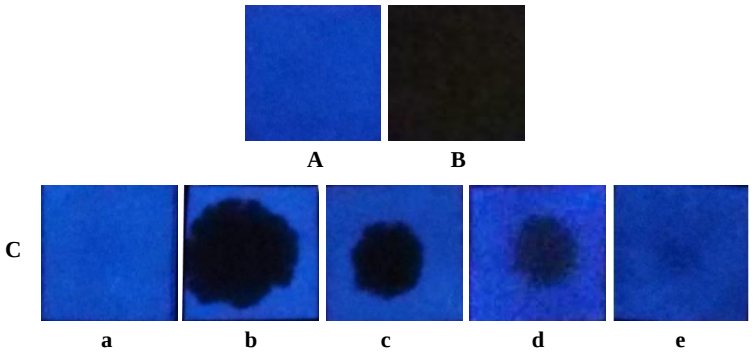

Figure 2.5 Photographs (under 365 nm UV-light) of fluorescent test strips. (A) before and (B) after dipping in PA (10^{-4} M) solution in water. (C) (a) Before and after ((b) 10^{-3} M, (c) 10^{-5} M, (d) 10^{-6} M, (e) 10^{-8} M) applying spots of different concentrations of PA solution.

2.3.6 Solid state studies for on-site detection

The human body, clothing, and other surroundings can be contaminated by traces of nitroexplosives during manufacture of fireworks, matches, rockets, and explosive devices. Therefore, detection of nitroexplosives in trace amounts is especially an appealing field of research with respect to forensic and analytical sciences. In this context, we performed the paper strip tests using Whatman filter paper. The desired sizes of paper strips were cut and dip-coated in the solution of PFAM (10^{-4} M) in THF followed by drying in air. PFAM coated paper strips (Figure 2.5A) displayed complete fluorescence quenching (Figure 2.5B) after dipping in solution of PA (10^{-4} M). The paper strip was then recycled by washing carefully with water and used thrice efficiently (Figure A2.28). To monitor the effect of various concentration of PA on PFAM coated paper strips, different concentrations of PA solution in water (10 μL each) were applied as small random spots and observed under UV-light (lamp excited at 365 nm). Dark spots of various paper strips displayed the regulation of quenching behavior by PA (Figure 2.5C). However, a paper strip with water (blank) did not show any noticeable change (Figure 2.5C(a)). The minimum amount of PA that can be detected by the naked eye was found to be as low as 10 μL of 10^{-8} M, thereby confirming the detection of 22.9 pg PA, which is among the best reported values.[12,59,67–70] Interestingly, other nitroaromatics did not cause any significant change in the emission of PFAM (Figure A2.29) confirming the selectivity of the probe in the solid state platform.

2.4 Conclusion

In conclusion, picric acid detection was achieved at incredibly low levels of 57.8 nM (13.2 ppb) using a newly synthesized amine functionalized conjugated polymer PFAM in solution state as well as on a solid-based platform using simple filter paper strips. The excellent signal response for PA was accomplished via a strong inner filter effect (IFE) and favorable photoinduced electron transfer (PET) between polymer PFAM and PA assisted by acid−base interactions. PFAM reports the first conjugated polymer based example of designing IFE based probes for sensing PA. The rapid and on-site detection applicability of this system in the competitive environment establishes the method as very effective and suitable for real sample analysis as demonstrated by analyzing natural sample.

References

(1) Salinas, Y.; Martínez-Máñez, R.; Marcos, M. D.; Sancenón, F.; Costero, A. M.; Parra, M.; Gil, S. *Chem. Soc. Rev*. **2012**, *41*, 1261.

(2) Akhavan, J. In Chemistry of Explosives, Royal Society of Chemistry, 2nd ed., 2004.

(3) Ashbrook, P. C.; Houts, T. A. *Chem. Health Safety*, **2003**, *10*, 27.

(4) Innovative Treatment Technologies: Annual Status Report, U.S. Environmental Protection Agency: Washington, D.C., 8th ed., **1996**.

(5) Shen, J.; Zhang, J.; Zuo, Y.; Wang, L.; Sun, X.; Li, J.; Han, W.; He, R. *J. Hazard. Mater*. **2009**, 163, 1199.

(6) Germain, M. E.; Knapp, M. J. *Chem. Soc. Rev*. **2009**, *38*, 2543.

(7) Martínez-Máñez, R.; Sancenón, F.; Hecht, M.; Biyical, M.; Rurack, K. *Anal. Bioanal. Chem*. **2011**, *399*, 55.

(8) Peng, Y.; Zhang, A.-J.; Dong, M.; Wang, Y.-W. *Chem. Commun*. **2011**, *47*, 4505.

(9) Dinda, D.; Gupta, A.; Shaw, B. K.; Sadhu, S.; Saha, S. K. *ACS Appl. Mater. Interfaces* **2014**, *6*, 10722.

(10) Bhalla, V.; Gupta, A.; Kumar, M.; Rao, D. S. S.; Prasad, S. K. *ACS Appl. Mater. Interfaces* **2013**, *5*, 672.

(11) Roy, B.; Bar, A. K.; Gole, B.; Mukherjee, P. S. *J. Org. Chem*. **2013**, *78*, 1306.

(12) Dey, N.; Samanta, S. K.; Bhattacharya, S. *ACS Appl. Mater. Interfaces* **2013**, *5*, 8394.

(13) Martinez, H. P.; Grant, C. D.; Reynolds, J. G.; Trogler, W. C. *J. Mater. Chem.* **2012**, *22*, 2908.

(14) Wang, X.; Guo, Y.; Li, D.; Chen, H.; Sun, R. *Chem. Commun*. **2012**, *48*, 5569.

(15) Li, D.; Liu, J.; Kwok, R. T. K.; Liang, Z.; Tang, B. Z.; Yu, J. *Chem. Commun.* **2012**, 48, 7167.

(16) Xu, Y.; Li, B.; Li, W.; Zhao, J.; Sun, S.; Pang, Y. *Chem. Commun.* **2013**, *49*, 4764.

(17) Li, X.-G.; Liao, Y.; Huang, M.-R.; Strong, V.; Kaner, R. B. *Chem. Sci.* **2013**, *4*, 1970.

(18) Béreau, V.; Duhayon, C.; Sutter, J.-P. *Chem. Commun*. **2014**, *50*, 12061.

(19) Zhang, Y.; Chen, G.; Lin, Y.; Zhao, L.; Yuan, W. Z.; Lu, P.; Jim, C. K. W.; Zhang, Y.; Tang, B. Z. *Polym. Chem.* **2015**, *6*, 97.

(20) Kaur, S.; Bhalla, V.; Vij, V.; Kumar, M. *J. Mater. Chem. C* **2014**, *2*, 3936.

(21) Kaur, S.; Gupta, A.; Bhalla, V.; Kumar, M. *J. Mater. Chem. C* **2014**, *2*, 7356.

(22) Ye, J.; Zhao, L.; Bogale, R. F.; Gao, Y.; Wang, X.; Qian, X.; Guo, S. Zhao, J.; Ning, G. *Chem. Eur. J.* **2015**, *21*, 2029.

(23) Gole, B; Bar, A. K.; Mukherjee, P. S. *Chem. Eur. J.* **2014**, *20*, 13321.

(24) Lakowicz, J. R. *In Principles of Florescence spectroscopy*, 3rd ed; Springer: Singapore, **2010**; pp. 443.

(25) Shang, L.; Dong, S. *Anal. Chem*. **2009**, *81*, 1465.

(26) Dutta, P.; Saikia, D.; Adhikary, N. C.; Sarma, N. S. *ACS Appl. Mater. Interfaces* **2015**, *7*, 24778.

(27) Li, G.; Fu, H.; Chen, X.; Gong, P.; Chen, G.; Xia, L.; H Wang, H.; You, J.; Wu, Y. *Anal. Chem.* **2016**, *88*, 2720.

(28) Rong, M.; Lin, L.; Song, X.; Zhao, T.; Zhong, Y.; Yan, J.; Wang, Y.; Chen, X. *Anal. Chem.* **2015**, *87*, 1288.

(29) Lin, M.; Zou, H. Y.; Yang, T.; Liu, Z. X.; Liu, H.; Huang, C. Z. *Nanoscale* **2016**, *8*, 2999.

(30) Kim, H.; Lee, B.; Byeon, S. *Chem. Commun.* **2015**, *51*, 725.

(31) Xiao, S. J.; Zhao, X. J.; Hu, P. P.; Chu, Z. C.; Huang, C. Z.; Zhang, L. *ACS Appl. Mater. Interfaces* **2016***, 8,* 8184.

(32) Zhu, C.; Liu, L.; Yang, Q.; Lv, F.; Wang, S. *Chem. Rev.* **2012**, *112,* 4687.

(33) Sohn, H.; Sailor, M. J.; Magde, D.; Trogler, W. C. *J. Am. Chem. Soc.* **2003**, *125*, 3821.

(34) Wang, Y.; La, A.; Brückner, C.; Lei, Y. *Chem. Commun.* **2012**, *48*, 9903.

(35) Gopalakrishnan, D.; Dichtel, W. R. *J. Am. Chem. Soc.* **2013**, *135*, 8357.

(36) Ghosh, K. R.; Saha, S. K.; Wang, Z. Y. *Polym. Chem.* **2014**, *5*, 5638.

(37) Toal, S. J.; Trogler, W. C. *J. Mater. Chem.* **2006**, *16*, 2871.

(38) Kim, H. N.; Guo, Z.; Zhu, W.; Yoon, J.; Tian, H. *Chem. Soc. Rev.* **2011**, *40*, 79.

(39) Thomas III, S. W.; Joly, G. D.; Swager, T. M. *Chem. Rev.* **2007**, *107*, 1339.

(40) McQuade, D. T.; Pullen, A. E.; Swager, T. M. *Chem. Rev.* **2000**, *100*, 2537.

(41) Rochat, S; Swager, T. M. *ACS Appl. Mater. Interfaces* **2013**, *5*, 4488.

(42) Liang, J.; Lia, K.; Liu, B. *Chem. Sci.* **2013**, *4*, 1377.

(43) Gutacker, A.; Lin, C.-Y.; Ying, L.; Nguyen, T.-Q.; Scherf, U.; Bazan, G. C. *Macromolecules* **2012**, *45*, 4441.

(44) Feng, X.; Lv, F.; Liu, L.; Tang, H.; Xing, C.; Yang, Q.; Wang, S. *ACS Appl. Mater. Interfaces* **2010**, *2*, 2429.

(45) Xu, B.; Wu, X.; Li, H.; Tong, H.; Wang, L. *Macromolecules* **2011**, *44*, 5089.

(46) Shaligram, S.; Wadgaonkar, P. P.; Kharul, U. K. *J. Mater. Chem. A* **2014**, *2*, 13983.

(47) Hussain, S.; Malik, A. H.; Afroz, M. A.; Iyer, P. K. *Chem. Commun*. **2015**, *51*, 7207.

(48) Li, H.; Wu, H.; Zhao, E.; Li, J.; Sun, J. Z.; Qin, A.; Tang, B. Z. *Macromolecules* **2013**, *46*, 3907.

(49) Liu, Y.; Gao, M.; Lam, J. W. Y.; Hu, R.; Tang, B. Z. *Macromolecules* **2014**, *47*, 4908.

(50) Zhou, H.; Li, J.; Chua, M. H.; Yan, H.; Tang, B. Z.; Xu, J. *Polym. Chem.* **2014**, *5*, 5628.

(51) Sang, N.; Zhan, C.; Cao, D. *J. Mater. Chem. A* **2015**, *3*, 92.

(52) Liu, J.; Zhong, Y.; Lu, P.; Hong, Y.; Lam, J. W. Y.; Faisal, M.; Yu, Y.; Wong, K. S.; Tang, B. Z. *Polym. Chem.* **2010**, *1*, 426.

(53) Hu, R.; Maldonado, J. L.; Rodriguez, M.; Deng, C; Jim, C. K. W.; Lam, J. W. Y.; Yuen, M. M. F.; Ramos-Ortiz, G.; Tang, B. Z. *J. Mater. Chem.* **2012**, *22*, 232.

(54) Wang, J.; Mei, J.; Yuan, W.; Lu, P.; Qin, A.; Sun, J.; Ma, Y.; Tang, B. Z. *J. Mater. Chem.* **2011**, *21*, 4056.

(55) Martinez, H. P.; Grant, C. D.; Reynolds, J. G.; Trogler, W. C. *J. Mater. Chem.* **2012**, *22*, 2908.

(56) Sanchez, J. C.; Trogler, W. C. *J. Mater. Chem.* **2008**, *18*, 3143.

(57) Mukherjee, P. S.; Acharyya, K. *Chem. Commun*. **2014**, *50*, 15788.

(58) Vij, V.; Bhalla, V.; Kumar, M. *ACS Appl. Mater. Interfaces* **2013**, *5*, 5373.

(59) Malik, A. H.; Hussain, S.; Kalita, A.; Iyer, P. K. *ACS Appl. Mater. Interfaces* **2015**, *7*, 26968.

(60) Saikia, G.; Iyer, P. K. *J. Org. Chem.* **2010**, *75*, 2714.

(61) Hussain, S.; Malik, A. H.; Iyer, P. K. *ACS Appl. Mater. Interfaces* **2015**, *7*, 3189.

(62) Hussain, S.; De, S.; Iyer, P. K. *ACS Appl. Mater. Interfaces*, **2013**, *5*, 2234.

(63) Tan, C.; Pinto, M. R.; Schanze, K. S. *Chem. Commun.* **2002**, 446.

(64) Zhao, D.; Swager, T. M. *Macromolecules* **2005**, *38*, 9377.

(65) Jiang, H.; Zhao, X.; Schanze, K. S. *Langmuir* **2006**, *22*, 5541.

(66) Sk, M.; Biswas, S. *Cryst. Eng. Comm.* **2016**, *18*, 3104.

(67) Bhalla, V.; Kaur, S.; Vij, V.; Kumar, M. *Inorg. Chem.* **2013**, *52*, 4860.

(68) Feng, H.-T.; Zheng, Y.-S. *Chem. –A Eur. J.* **2014**, *20*, 195.

(69) Venkatramaiah, N.; Kumar, S.; Patil, S. *Chem. Commun*. **2012**, *48*, 5007.

(70) Yuan, W. Z.; Zhao, H.; Shen, X. Y.; Mahtab, F.; Lam, J. W. Y.; Sun, J. Z.; Tang, B. Z. *Macromolecules* **2009**, *42*, 9400.

Appendix

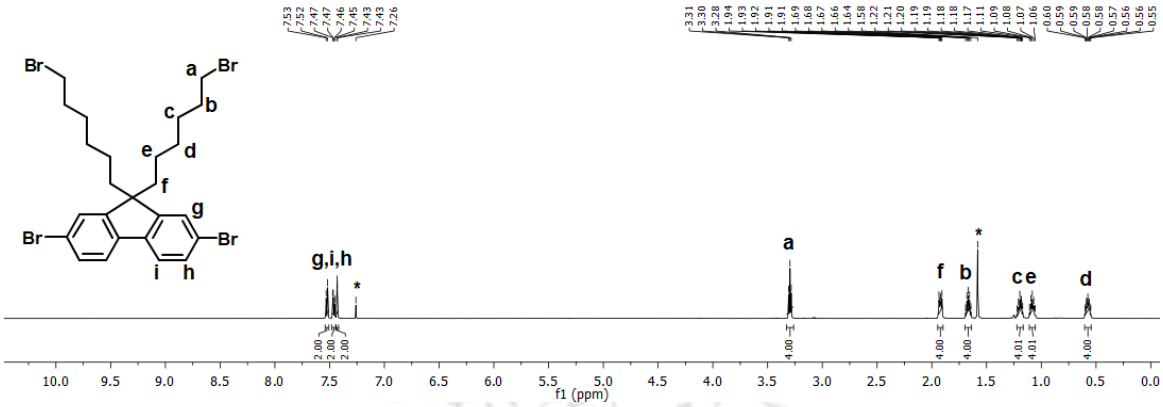

^{1}H-NMR of M2

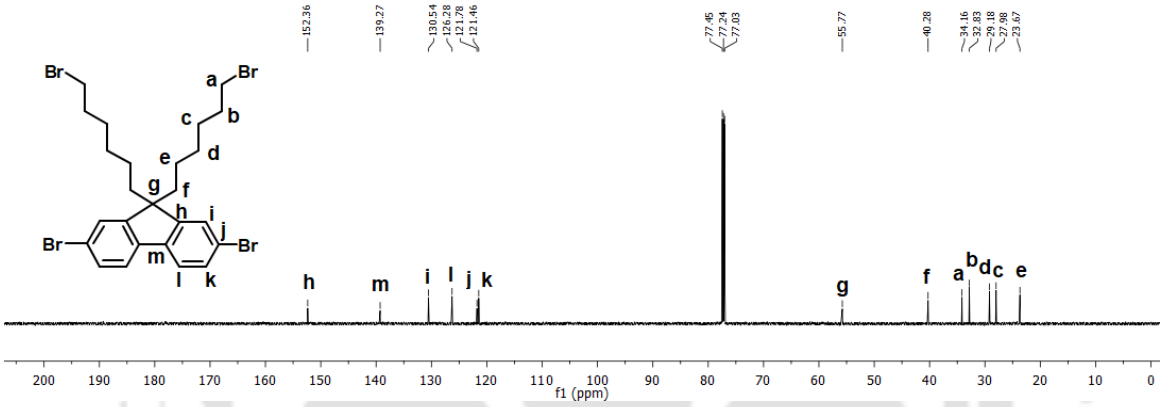

^{13}C-NMR of M2

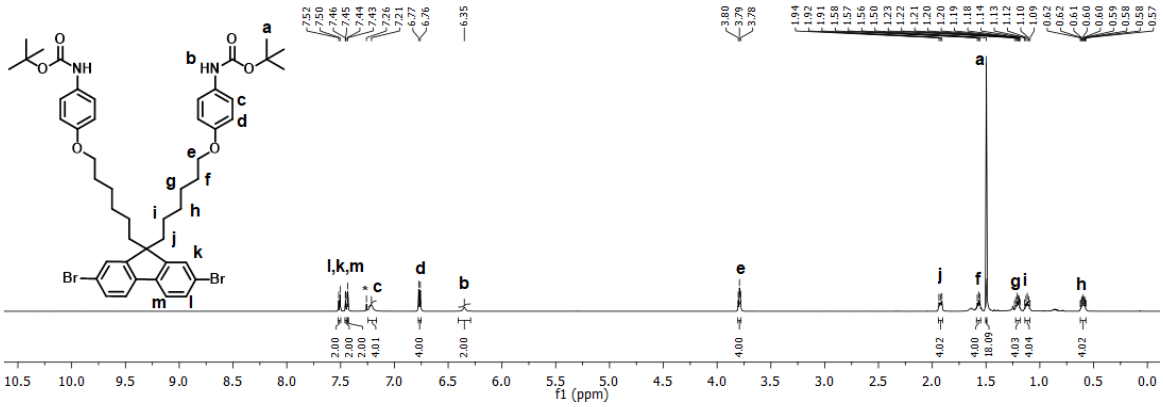

^{1}H-NMR of M3

Figure A2.1 ^{1}H-NMR and 13C-NMR spectra of monomer M2 and M3.

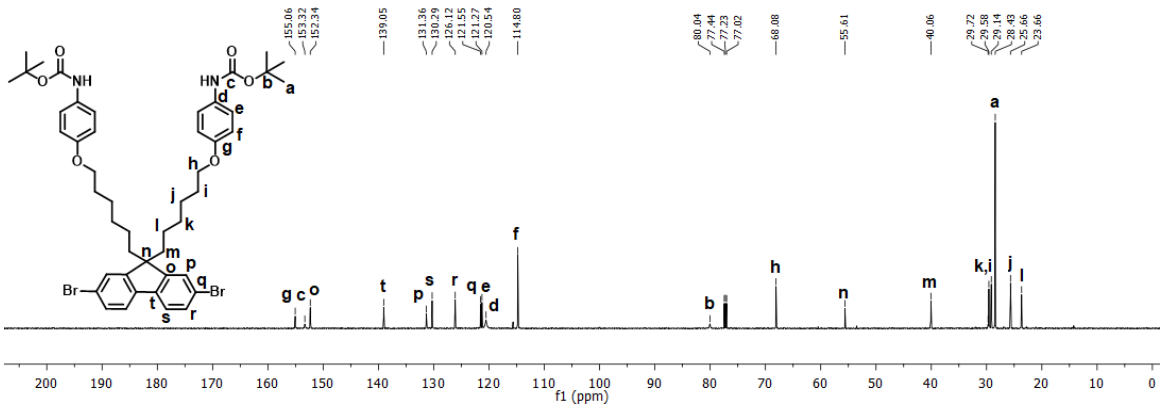

Figure A2.2 ^{13}C-NMR spectrum of monomer M3.

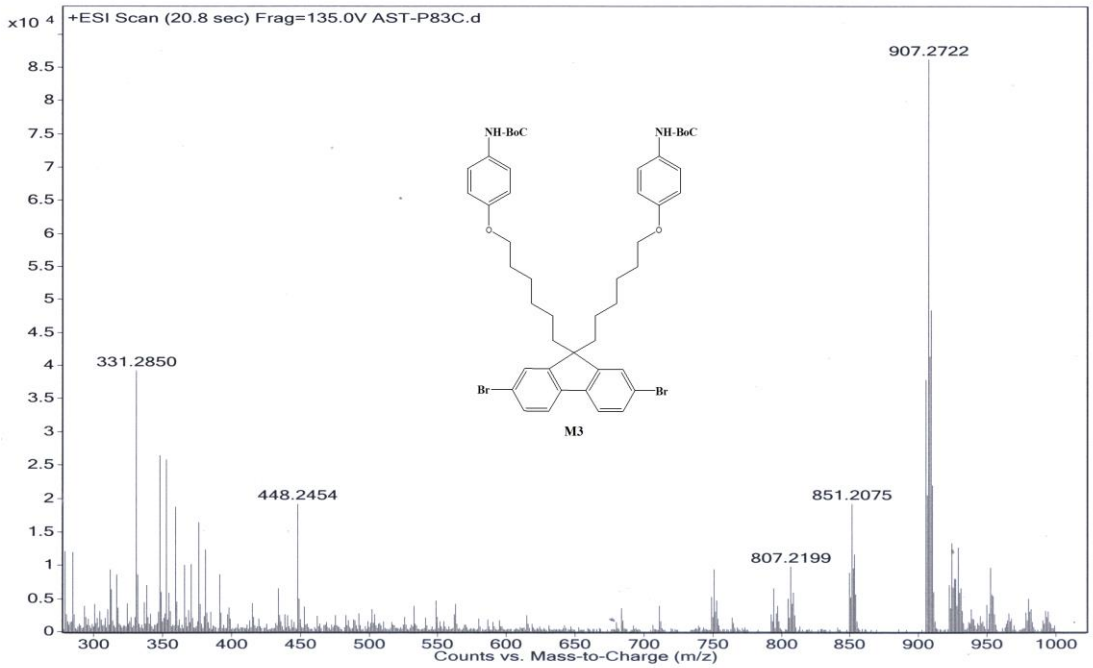

Figure A2.3 High resolution mass spectrum of monomer M3.

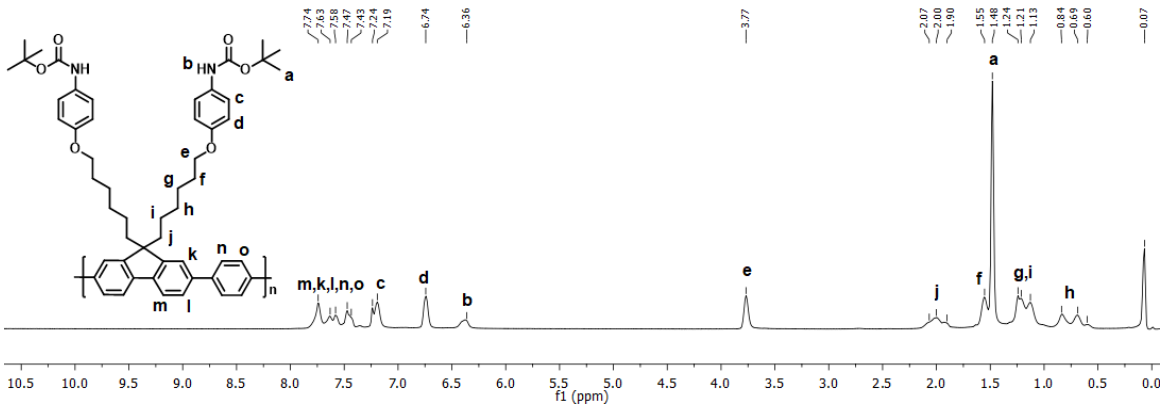

Figure A2.4 ^{1}H-NMR spectrum of polymer P0.

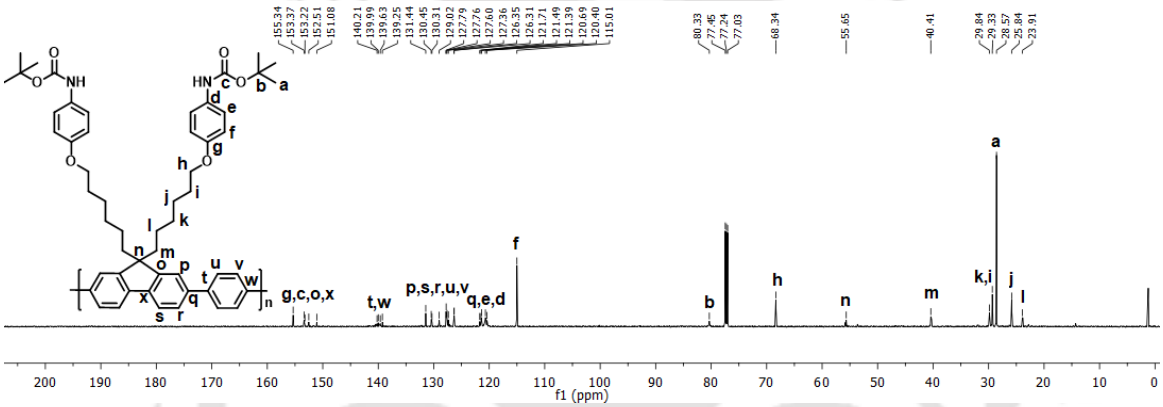

Figure A2.5 ^{13}C-NMR spectrum of polymer P0.

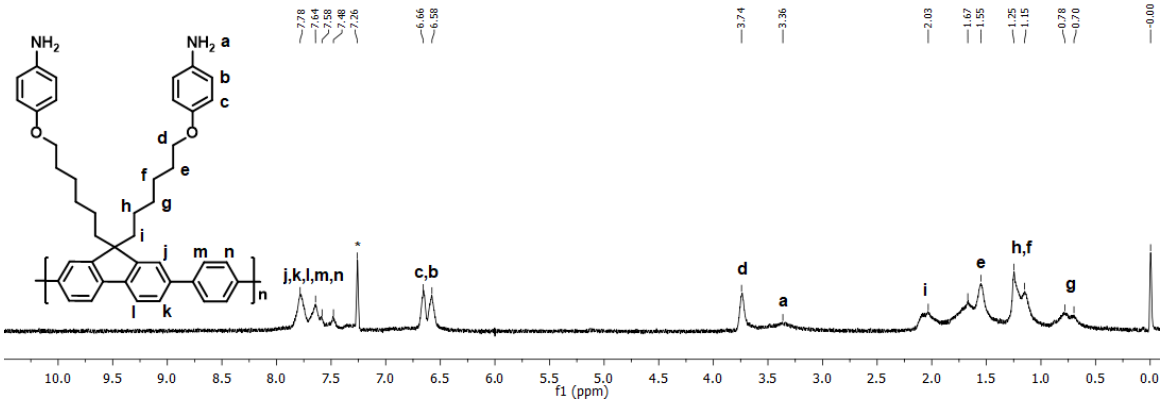

Figure A2.6 ^{1}H-NMR spectrum of polymer PFAM.

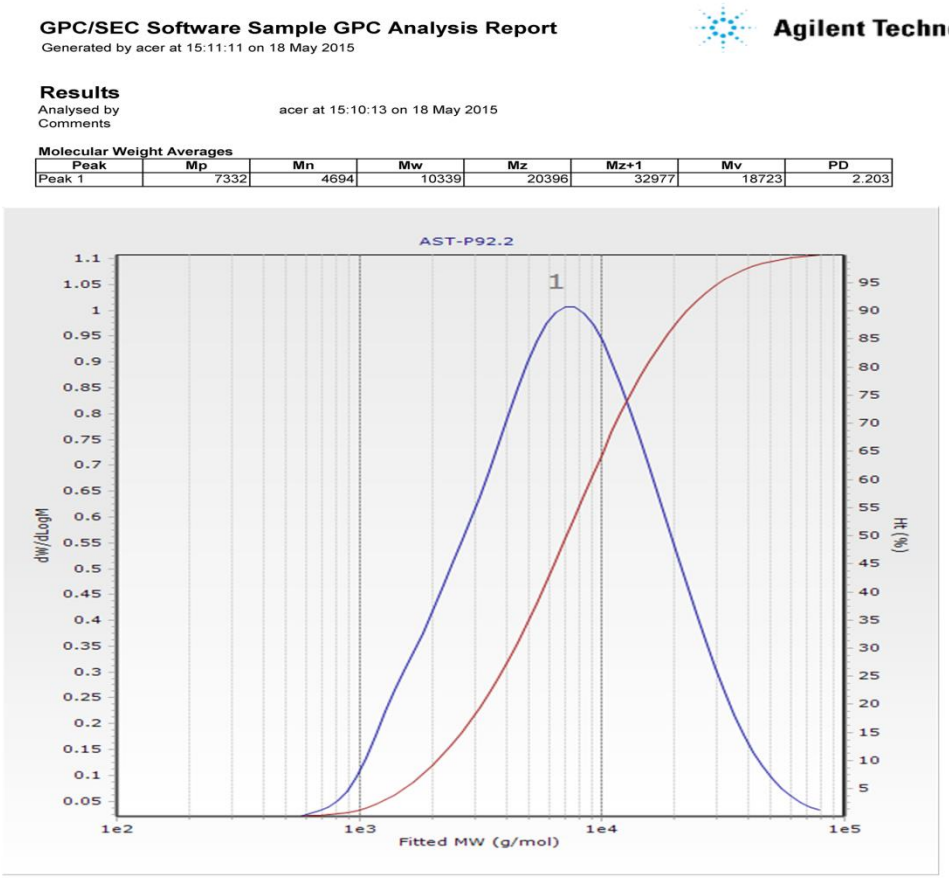

Figure A2.7 GPC chromatogram of polymer P0.

Figure A2.8 Image of PFAM under UV-light before and after addition of PA.

Table A2.1 Fluorescence lifetime decay of each component and their fractions.

Sample	τ_1 (ns)	%	τ_2 (ns)	%	χ^2	τ_{avg} (ns)
PFAM	0.068	3.040	0.306	96.96	1.086	0.298
PFAM-PA	0.060	4.863	0.299	95.14	1.048	0.287

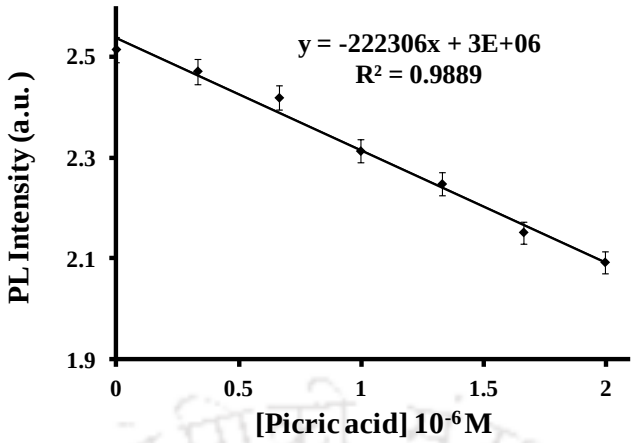

Figure A2.9 Fluorescence intensity of PFAM in 4:1/THF:HEPES buffer (pH=7, 10 mM) *vs* PA concentration.

LOD=3 × S.D./k

LOD = 3 × 4283.88/ (222306×10^6)

= 57.8 nM or 13.2 ppb

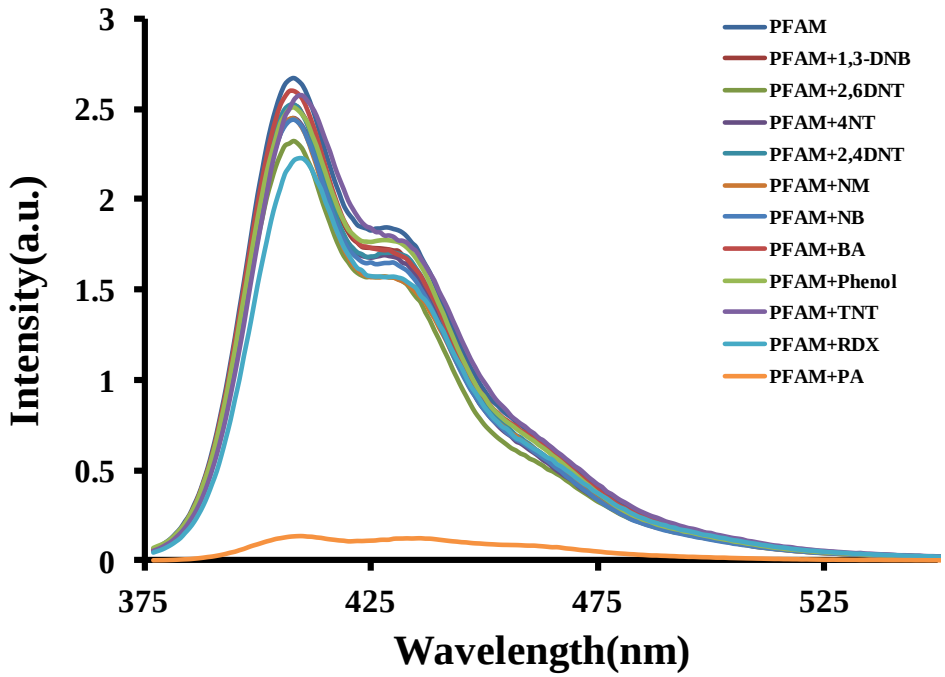

Figure A2.10 Photoluminescence spectra showing the effect of various nitro analytes (5 × 10^{-5} M) on the emission of PFAM (1 × 10^{-6} M) in 4:1/THF:HEPES buffer (pH=7.0,10 mM).

Table 2A.2 A comparative study of some conjugated polymers based reports for picric acid detection.

Publication	Stern-volmer Constant (M^{-1})	Detection Limit	Selectivity	Sensing Mechanism
Present Manuscript	***1.05 × 10^5***	***5.78 × 10^{-8} M (13.24 ppb)***	***Selective***	***Inner Filter Effect***
J. Am. Chem. Soc. **2003**, *125*, 3821-3830	In the range 10^3 - 10^4	Not reported	Not selective	Electron-transfer
Macromolecules **2009**, *42*, 9400-9411	3.5×10^5	0.17 ppm (0.72 µM)	Not studied	-
Macromol. Rapid Commun. **2010**, *31*, 834–839	8.4×10^3 6.36×10^4	Upto 1ppm	Not studied	-
Macromolecules **2011**, *44*, 5977–5986	8.48×10^5	Upto 1ppm	Not studied	Electron and/or energy transfer
Macromol. Rapid Commun. **2013**, *34*, 796−802	1.6×10^5	9×10^{-8} M	Not studied	Energy transfer
RSC Adv., **2013**, *3*, 8193–8196	2.33×10^5	1 ppm	Not studied	-
Macromolecules **2013**, *46*, 3907−3914	1.95×10^4 2.67×10^4	Upto 1µg/mL	Not studied	-
Macromolecules **2014**, *47*, 4908−4919	2.7×10^5	1µM	Not selective	Energy transfer
Polym. Chem., **2014**, *5*, 5628–5637	9.72×10^4 6.98×10^4 4.27×10^4	2.5 ppm	Not selective	Electron transfer
J. Mater. Chem. A, **2014**, *2*, 15560–15565	1.3×10^4	0.11 ppm (0.48µM)	Selective	Electron transfer
J. Mater. Chem. A, **2014**, *2*, 13983–13989	4.15×10^4 2.03×10^4	Not reported	Not selective	π–π interactions
Chem. Commun., **2015**, *51*, 7207–7210	1×10^7	0.128 ppb	Selective	Electron and/or energy transfer
J. Mater. Chem. A, **2015**, *3*, 92–96	2.6×10^5 8.3×10^4	About 1 ppm	Selective	Electron transfer

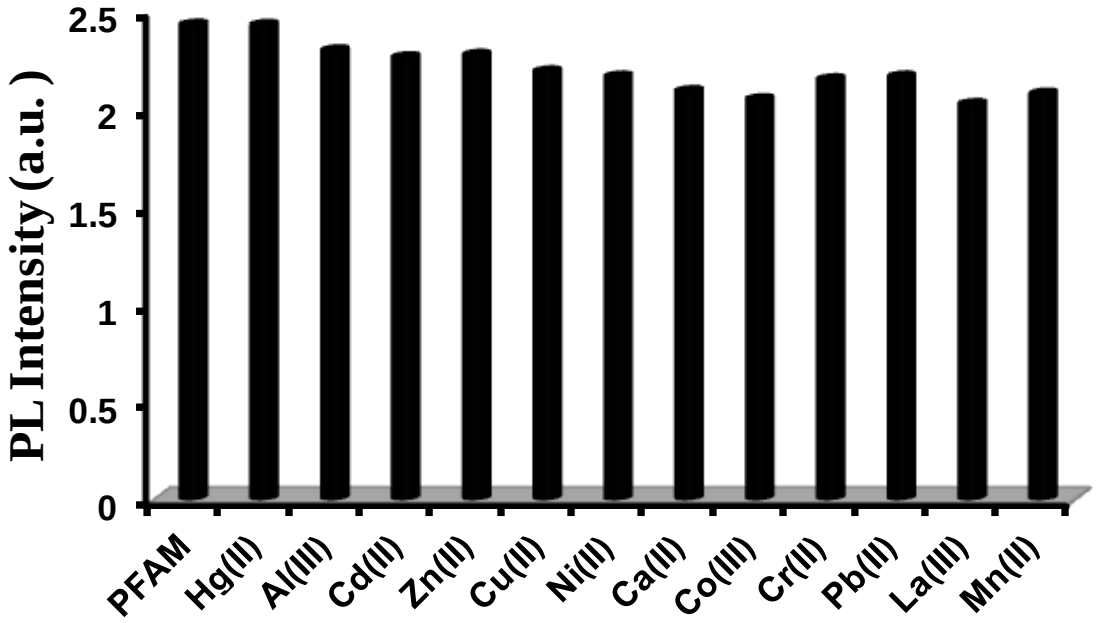

Figure A2.11 Bar diagram depicting effect of various metal ions (5×10^{-5} M) on the fluorescence intensity of PFAM (1×10^{-6} M).

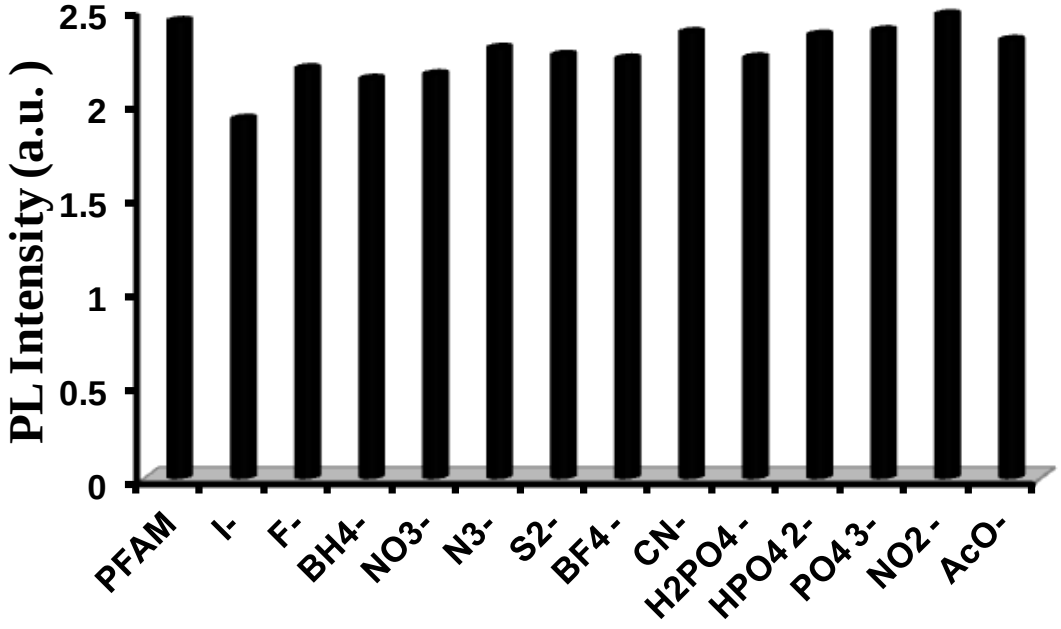

Figure A2.12 Bar diagram showing effect of various anions (5×10^{-5} M) on the fluorescence intensity of PFAM (1×10^{-6} M) in 4:1/THF:HEPES buffer (pH=7.0,10 mM).

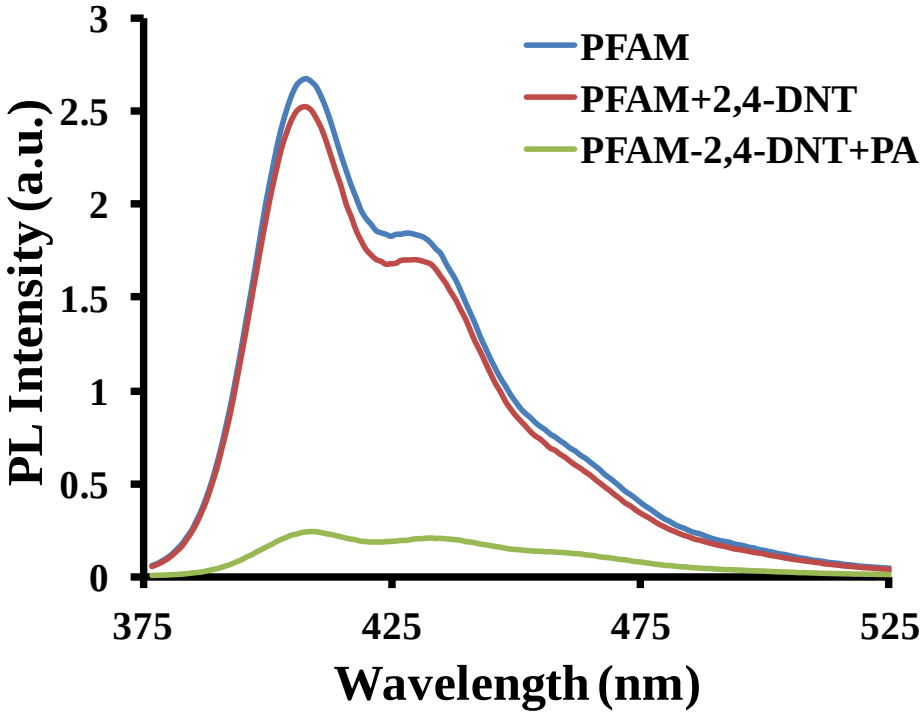

Figure A2.13. Emission spectra of PFAM (1× 10^{-6} M) with 2,4-DNT (5 × 10^{-5} M) followed by addition of PA (5 × 10^{-5} M) in 4:1/THF:HEPES buffer (pH=7.0,10 mM).

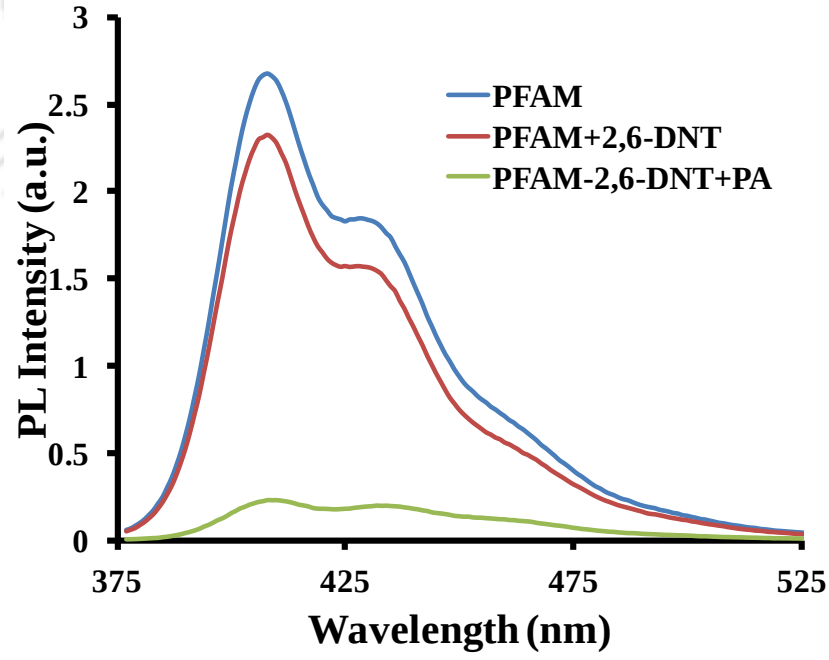

Figure A2.14. Emission spectra of PFAM (1 × 10^{-6} M) with 2,6-DNT (5 × 10^{-5} M) followed by addition of PA (5 × 10^{-5} M) in 4:1/THF:HEPES buffer (pH=7.0,10 mM).

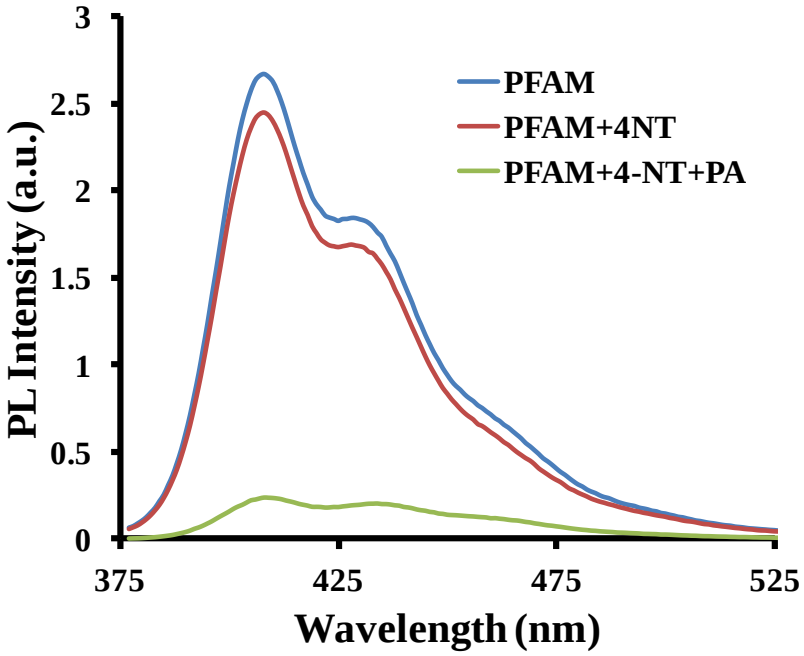

Figure A2.15. Emission spectra of PFAM (1×10^{-6} M) with 4-NT (5×10^{-5} M) followed by addition of PA (5×10^{-5} M) in 4:1/THF:HEPES buffer (pH=7.0,10 mM).

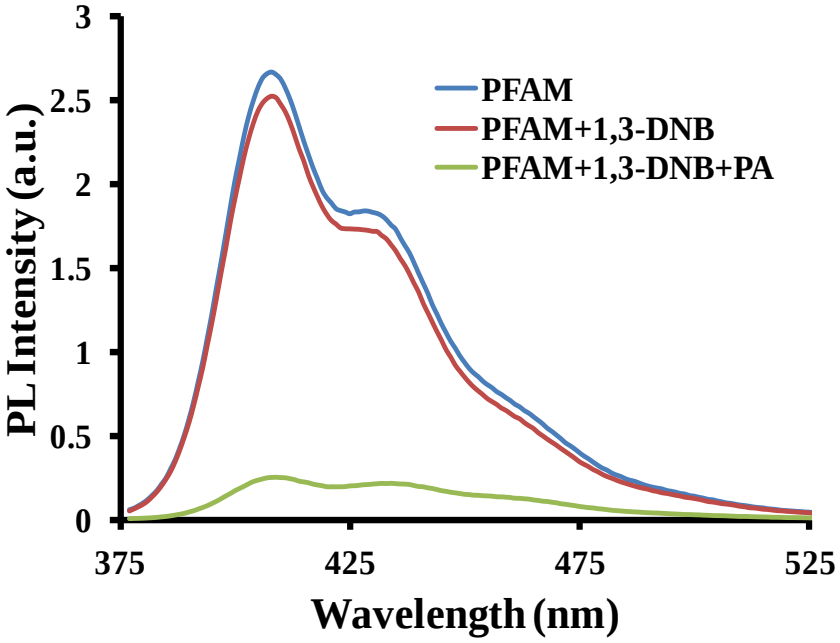

Figure A2.16. Emission spectra of PFAM (1×10^{-6} M) with 1,3-DNB (5×10^{-5} M) followed by addition of PA (5×10^{-5} M) in 4:1/THF:HEPES buffer (pH=7.0,10 mM).

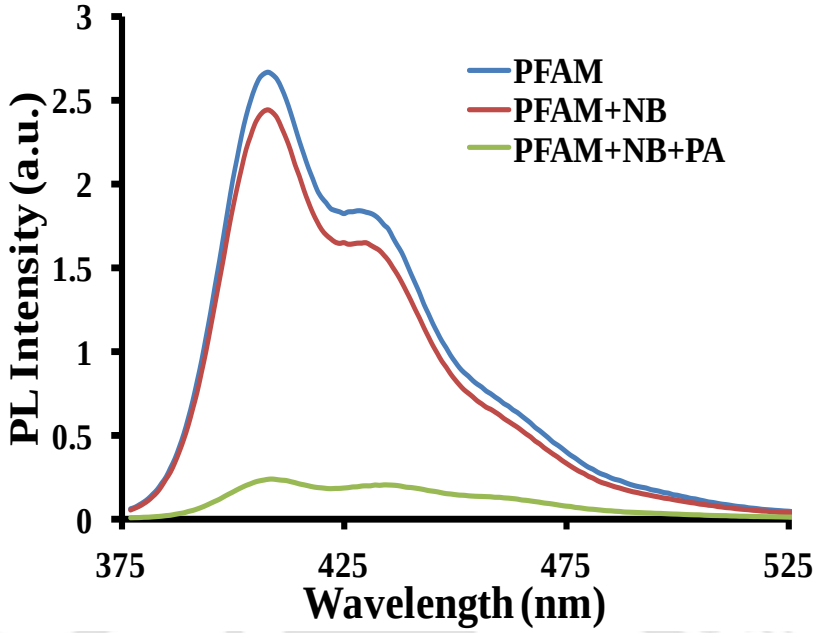

Figure A2.17. Emission spectra of PFAM (1×10^{-6} M) with NB (5×10^{-5} M) followed by addition of PA (5×10^{-5} M) in 4:1/THF:HEPES buffer (pH=7.0,10 mM).

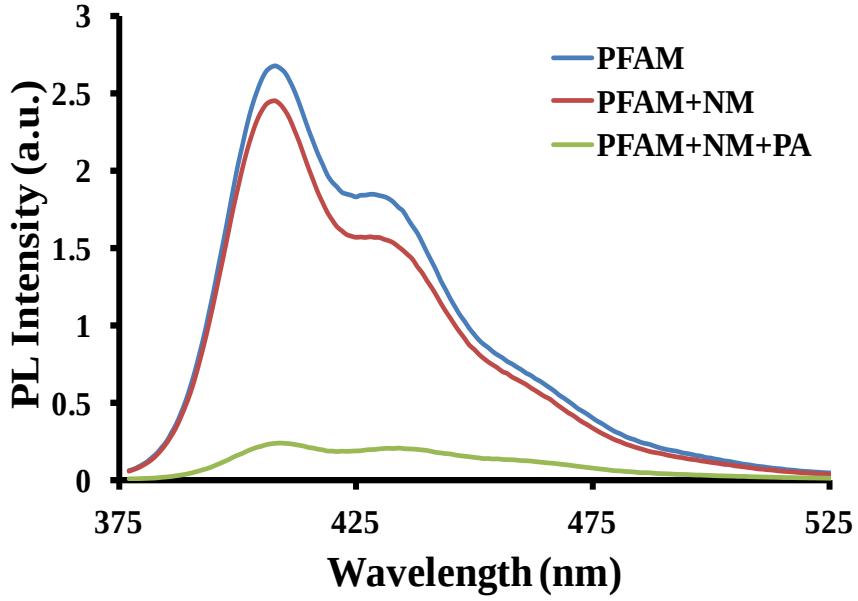

Figure A2.18. Emission spectra of PFAM (1×10^{-6} M) with NM (5×10^{-5} M) followed by addition of PA (5×10^{-5} M) in 4:1/THF:HEPES buffer (pH=7.0,10 mM).

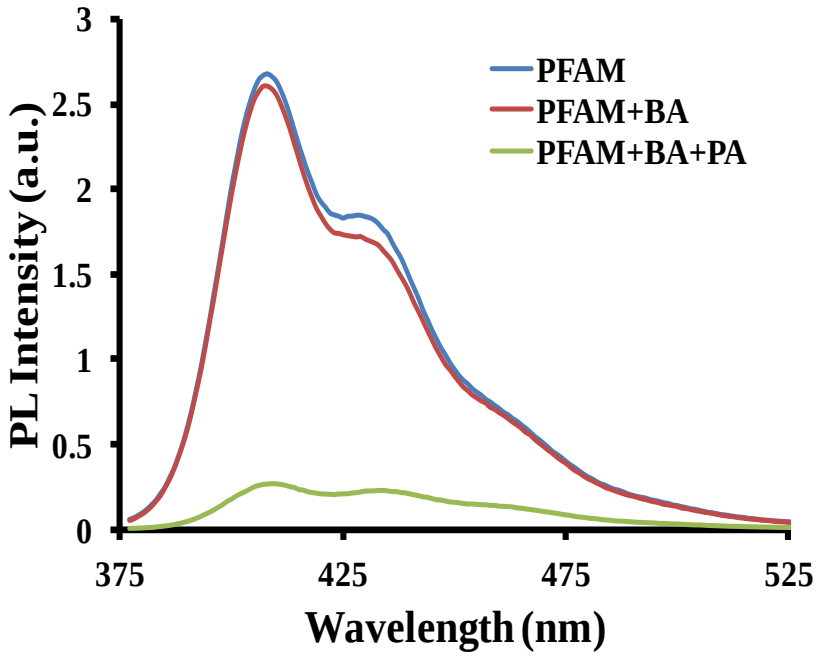

Figure A2.19. Emission spectra of PFAM (1×10^{-6} M) with BA (5×10^{-5} M) followed by addition of PA (5×10^{-5} M) in 4:1/THF:HEPES buffer (pH=7.0,10 mM).

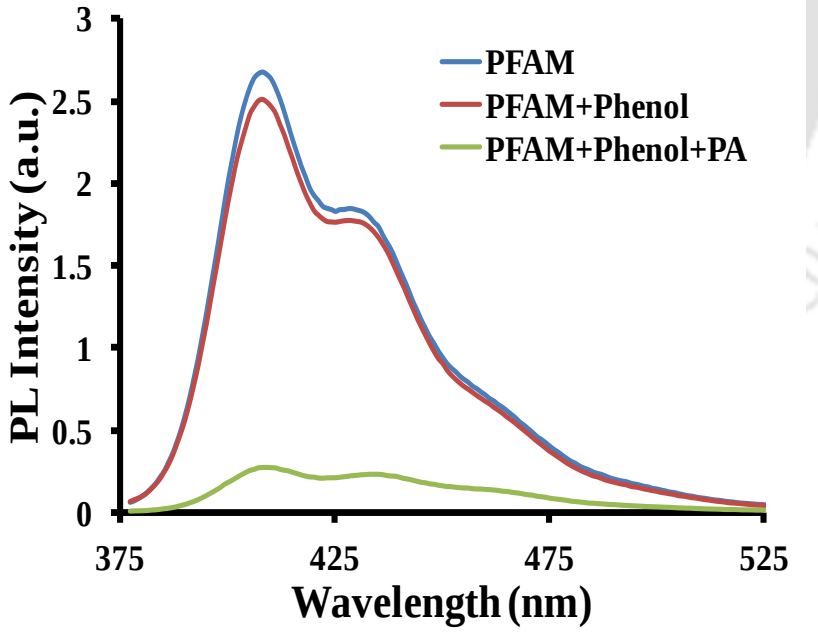

Figure A2.20. Emission spectra of PFAM (1×10^{-6} M) with Phenol (5×10^{-5} M) followed by addition of PA (5×10^{-5} M) in 4:1/THF:HEPES buffer (pH=7.0,10 mM).

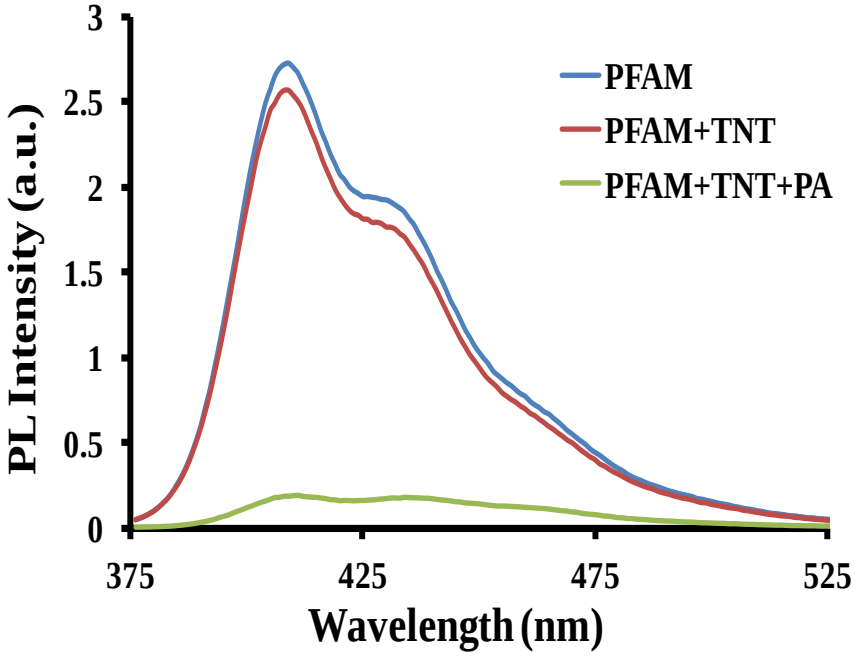

Figure A2.21. Emission spectra of PFAM (1× 10^{-6} M) with TNT (5 × 10^{-5} M) followed by addition of PA (5× 10^{-5} M) in 4:1/THF:HEPES buffer (pH=7.0,10 mM).

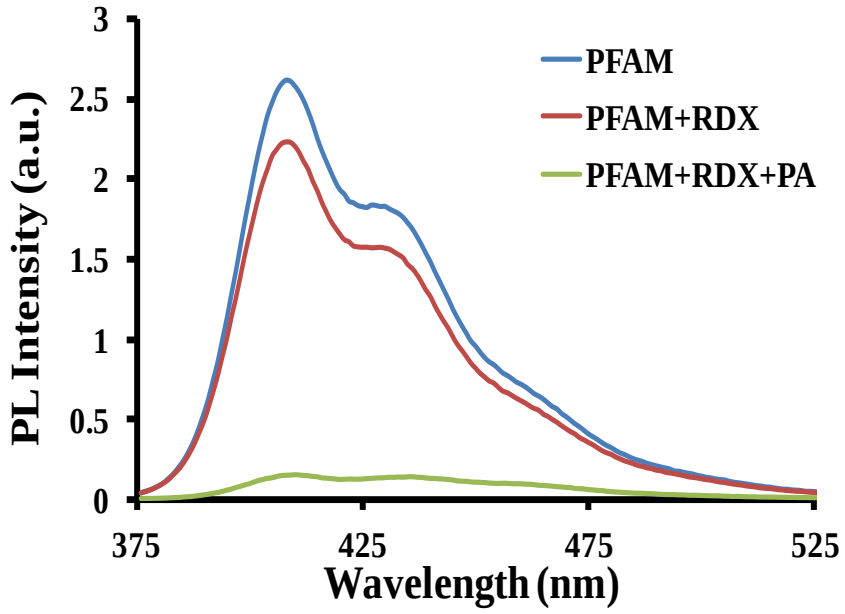

Figure A2.22. Emission spectra of PFAM (1× 10^{-6} M) with RDX (5 × 10^{-5} M) followed by addition of PA (5× 10^{-5} M) in 4:1/THF:HEPES buffer (pH=7.0,10 mM).

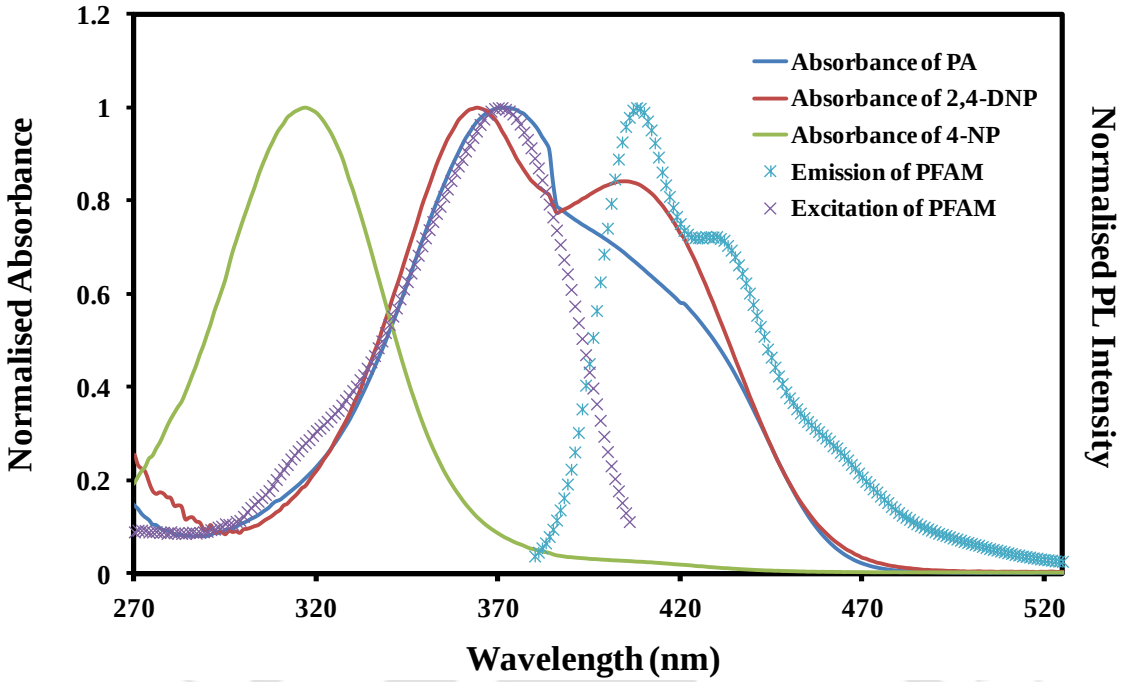

Figure A2.23. Overlap between excitation/emission spectra of PFAM and absorbance spectra of various nitrophenols.

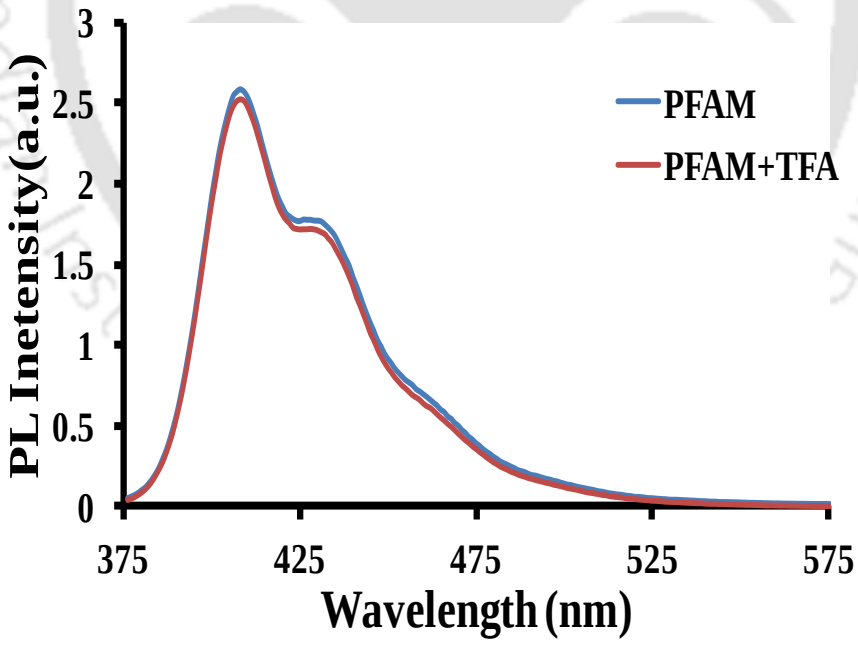

Figure A2.24. Emission spectra of PFAM (1×10^{-6} M) before and after adding TFA (1×10^{-4} M) in 4:1/THF:HEPES buffer (pH=7.0,10 mM).

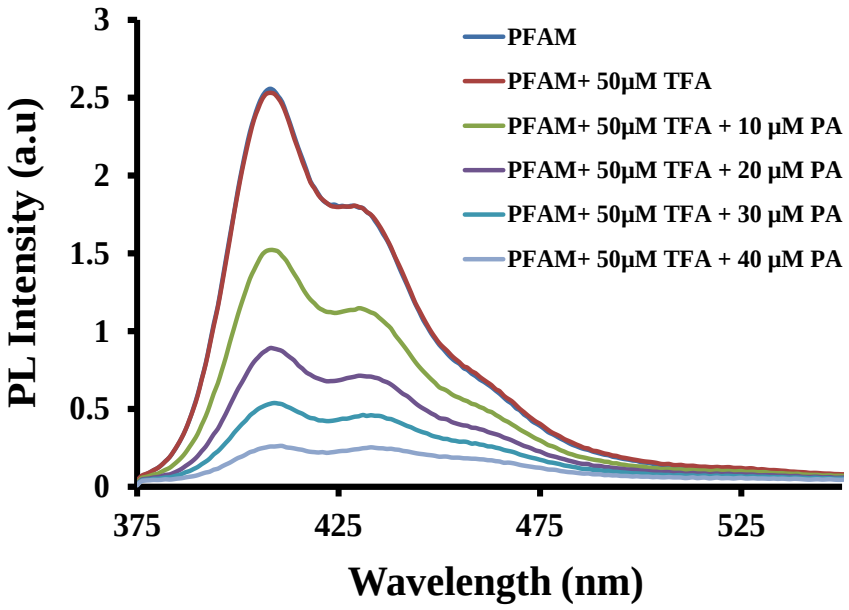

Figure A2.25. Emission spectra of PFAM/TFA (1 μM/50 μM) with different concentrations of PA salt solution in 4:1/THF:HEPES buffer (pH=7.0,10 mM).

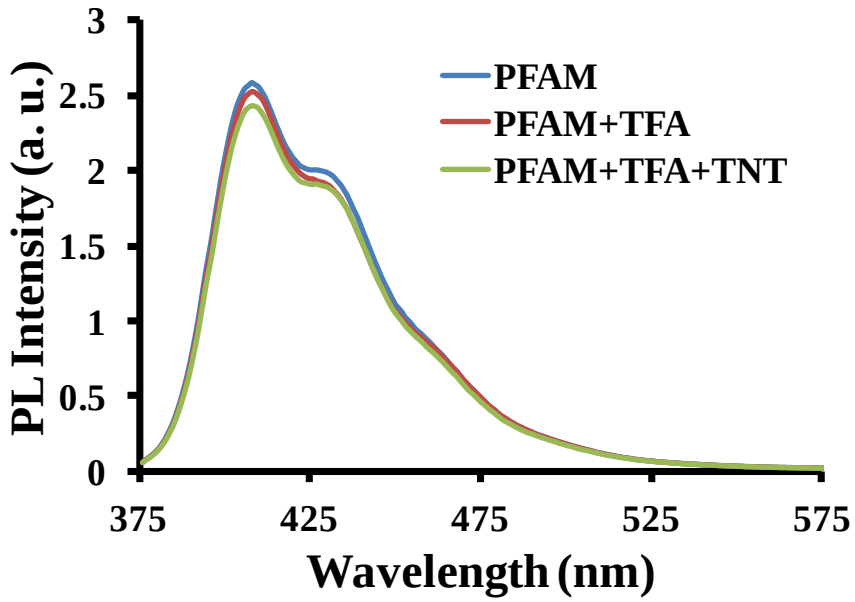

Figure A2.26. Change in emission spectra of PFAM (1×10^{-6} M) with TFA (1×10^{-4} M) followed by the addition of TNT (5×10^{-5} M) in 4:1/THF:HEPES buffer (pH=7.0,10 mM).

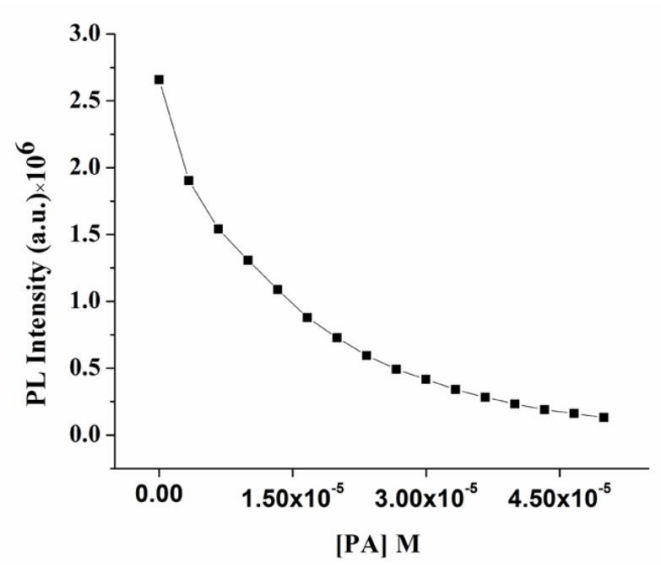

Figure A2.27. Calibration plot obtained for the estimation of PA.

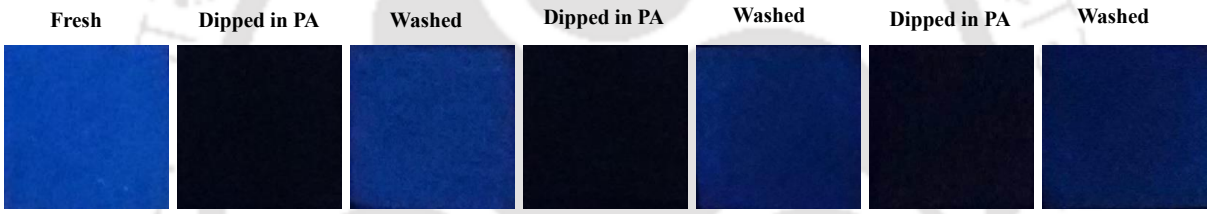

Figure A2.28. Recyclability test of PFAM coated paper strip.

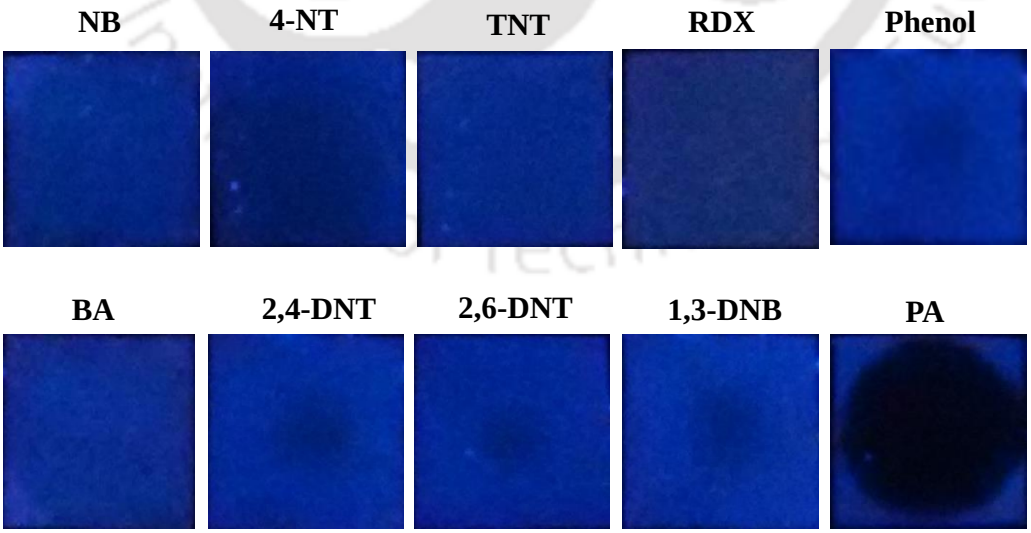

Figure A2.29. Colour of PFAM coated paper strips under UV light (lamp excitation-365 nm) after addition (10 μL) of 10^{-3} M solution of various analytes.

Chapter 3

Fluorescence "Turn-On" Indicator Displacement Assay-Based Sensing of Nitroexplosive Picric Acid in Aqueous Media via a Polyelectrolyte and Dye Complex

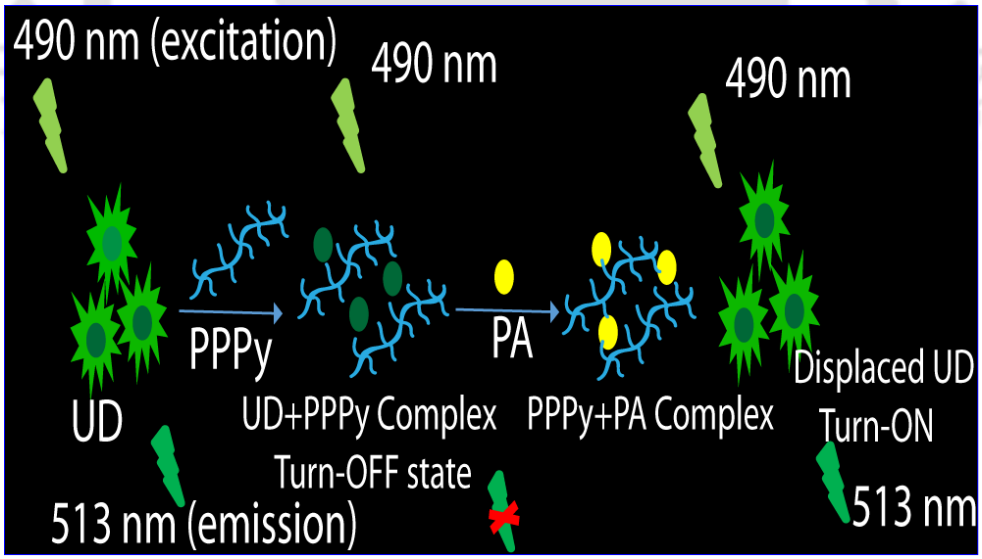

Tanwar, A. S.; Iyer, P. K. *ACS Omega* **2017**, 2, 4424–4430.

Abstract

A water-soluble non-fluorescent cationic conjugated polyelectrolyte poly(1,1′-((1,4-phenylenebis(oxy))bis- (propane-3,1-diyl))bis(pyridin-1-ium)bromide) (PPPy) was specifically synthesized via an economical method of oxidative coupling polymerization in high yields. PPPy selectively recognized nitroexplosive picric acid (PA) by fluorescence "turn-on" in the presence of closely related nitroexplosive compounds, namely, 2,4,6-trinitrotoluene, 2,4-dinitrophenol, and 4-nitrophenol via fluorescence indicator displacement assay (IDA) technique in water at pH 7.0. The polymer PPPy was characterized by NMR spectroscopy, gel permeable chromatography, UV−vis spectroscopy. The polymer PPPy forms an electrostatic complex with uranine dye. This ensemble scheme was utilized to detect PA with a limit of detection value of 295 nM (solution state) and 0.22 ppm (vapor state) through IDA, a phenomenon that is very different from the widely reported Förster resonance energy transfer, photoinduced electron transfer, ground-state charge transfer and inner filter effect based probes used for nitroexplosive PA detection.

3.1 Introduction

2,4,6-Trinitrophenol, commonly referred as picric acid (PA), has been categorized as a strong nitroexplosive compound. The potential explosive power of PA is remarkably superior than that of other competitive and interfering nitroexplosive 2,4,6-trinitrotoluene (TNT). Thus, its detection is of immense significance for homeland security and forensic investigation.[1,2] Owing to its high solubility in water and extensive use in dye, leather, drugs, matchbox, and firework industries, it can easily contaminate land and water resources.[3] PA is a well-known environmental pollutant that has lower degradation rate in biosystems and can cause severe health problems such as cancer, abnormal liver functions, sycosis, and damage to kidney as well as respiratory organs.[4,5] Furthermore, during metabolism, PA is transformed into picramic acid, which has even much higher mutagenic activity than PA.[6] Therefore, there is an urgent need to develop superior methods with high selectivity, rapid detection probes, and high sensitivity for PA detection with respect to environmental issues and terrorist threats.

Host/guest chemistry is a very active area of research in supramolecular chemistry.[7−11] The change in the response of host/dye complex property after the addition of particular analyte has been extensively investigated to build a selective and sensitive chemosensor.[12−23] Fluorescent dyes possess high affinity for macrocyclic host and significant change in fluorescence is observed after the host/dye complex formation in water medium.[9,15,22] When an analyte is introduced into the host/dye complex, it selectively displaces the dye from the host and forms a host/analyte complex with an initial fluorescence recovery. This phenomenon is generally termed as indicator displacement assay (IDA). There is competition between the analyte and the indicator for the selective binding of the host.[10,17] Several host/dye complex-based sensing with a variety of hosts used, such as calixarenes,[9,10,20,22] cyclodextrins,[15] cucurbiturils,[10,19,22] and pillararene,[21] have been reported. However, no report is available till date with a cationic conjugate polymer as a host. Notably, the IDA technique has been widely used for selective sensing of biological and environmental analytes such as basic amino acids,[19] adrafinil,[24] heparin,[25] carbohydrate,[26] citrate,[27,28] phosphate,[29−31] tartarate,[32,33] nitrate,[34] and so on.

Several literature methods are available for the sensitive detection of PA; however, most of them use organic media[35−41] and fluorescence “turn-off” and lack good selectivity toward PA,[37,42−44] with selected reports available based on fluorescence “turn-on” sensing.[45−51] The mechanisms of sensing involved in the previous reports are majorly photoinduced electron transfer and/or energy transfer process[52−54] and inner filter effect.[55] To the best of our

knowledge, there are no reports available for the sensitive PA (solution and vapor) detection based on fluorescence turn-on via IDA. In this work, we introduce a straightforward method to synthesize pyridinium receptor containing non-fluorescent cationic conjugated polymer poly- (1,1′-((1,4-phenylenebis(oxy))bis(propane-3,1-diyl))bis-(pyridin-1-ium)bromide (PPPy) (Scheme 3.1), which shows selective fluorescence turn-on sensing of PA over 2,4-dinitrophenol (2,4-DNP), 4-nitrophenol (4-NP), and TNT through the IDA technique in water at pH 7.0 for the first time (Scheme 3.1).

3.2 Experimental

3.2.1 Materials and methods

Nitroexplosives, namely, 4-NT, 1,3-DNB, 2,4-DNT, and 2,6-DNT, were purchased from Aldrich Chemicals. RDX and TNT were purchased from AccuStandard. PA was purchased from Loba Chemie Pvt. Ltd. HEPES buffer was purchased from Sigma-Aldrich Chemicals. Various other reagents and chemicals and were purchased from Merck and Alfa-Aesar and used without further purification. ^{1}H and ^{13}C NMR spectra were recorded at 400 and 100 MHz, respectively, using Varian-AS400 NMR spectrometer. Gel permeable chromatography (GPC) was performed in $CHCl_3$ using Shimadzu LC solution GPC instrument with polystyrene as the standard. All of the experimental titrations were done by using Milli-Q water. PerkinElmer Lambda-25 spectrophotometer was used to record the UV−vis absorption spectra. Horiba Fluoromax-4 spectrofluorometer was used to record the PL spectra by using quartz cuvettes of 10 mm path length and having a slit width of 1 nm at 298 K.

3.2.2 Synthetic procedure

3.2.2a Synthesis of 1,4-Bis(3-bromopropoxy)benzene (M1):

In a 50 mL round-bottom flask (RBF) fitted with water condenser, a mixture of potassium carbonate (12.5 g, 90.81 mmol) and hydroquinone (1.0 g, 9.08 mmol) in dry acetone (20 mL) was taken and degassed followed by stirring under inert atmosphere for 30 min. Subsequently, 1,3-dibromopropane (6.48 mL, 63.56 mmol) was added to the above mixture and refluxed for 24 h. After completion of the reaction, it was concentrated, chloroform was added and filtered. The chloroform layer was washed thrice with water, concentrated to get a crude product M1, which was further purified via column chromatography to obtain a white product (yield = 75%). ^{1}H NMR (400 MHz, $CDCl_3$, δ ppm): 2.29 (m, 4H), 3.60 (t, 4H), 4.05 (t, 4H), 6.84 (s, 4H). ^{13}C NMR (100 MHz, $CDCl_3$, δ ppm): 153.17, 115.67, 66.08, 32.62, 30.41.

3.2.2b Synthesis of Poly(1,4-bis(3-bromopropoxy)benzene) (PPBr):

In a three-necked RBF, ferric chloride (anhydrous) (1.84 g, 11.36 mmol) was solubilized in nitrobenzene (10 mL) under continuous nitrogen flow. Monomer M1 (1.0 g, 2.84 mmol) (solubilized in nitrobenzene (15 mL)) was added to flask dropwise. After that, the reaction mixture flask was kept for 36 h under stirring at rt, followed by precipitation in methanol. The solution was centrifuged and precipitates were washed with methanol (repeated thrice). The resulting precipitates were lastly dried under vacuum to obtain a brown polymer with 66% yield. The GPC using polystyrene as the standard in $CHCl_3$: M_w = 2.07 × 10^4; polydispersity index = 4.1. ^{1}H NMR (400 MHz, $CDCl_3$, δ ppm): 2.20 (br), 3.45 (br), 4.09 (br), 7.06 (br). ^{13}C NMR (100 MHz, $CDCl_3$, δ ppm): 150.01, 127.93, 117.08, 67.09, 32.64, 30.70.

3.2.2c Synthesis of PPPy:

Polymer PPBr (0.067 g) was dissolved in dry DMF (2 mL) and then pyridine (0.306 mL) was added to the reaction mixture under inert condition. Then, the reaction mixture was stirred for 24 h at 80 °C. The reaction mixture was then poured into excess of chloroform and stirred for 1 h to get a precipitate. The process was repeated thrice to remove excess pyridine, DMF, and PPBr. The solution was centrifuged and the precipitates were collected followed by drying under reduced pressure to get a dark brown sticky product with 70% yield. ^{1}H NMR (400 MHz, $CDCl_3$, δ ppm): 8.75 (br), 8.38 (br), 7.85 (br), 7.13 (br), 4.68 (br), 4.24 (br), 2.45(br).

3.2.2d Synthesis of (1,1′-((1,4-Phenylenebis(oxy))bis-(propane-3,1-diyl))bis(pyridin-1-ium)bromide) (M2’):

A mixture of pyridine (0.046 mL, 0.568 mmol) and 1,4-bis(3- bromopropoxy)benzene (M1) (0.100 g, 0.284 mmol) was dissolved in acetonitrile and refluxed overnight. On cooling, yellow crystals were obtained. These crystals were filtered and washed with chloroform to get pure shiny yellow crystal (yield = 85%). ^{1}H NMR (400 MHz, $CDCl_3$, δ ppm): 2.42 (m, 4H). 4.01 (t, 4H), 4.76 (t, 4H), 6.69 (s, 4H), 7.98 (t, 4H), 8.49 (t, 2H), 8.82 (d, 4H); ^{13}C NMR (100 MHz, $CDCl_3$, δ ppm): 29.63. 59.38, 65.07, 115.48, 128.05, 144.33, 145.61, 151.84; mass spectrometry (electrospray ionization): calculated for $C_{22}H_{26}N_2O_2^{2+}$ $[m/z]^{2+}$: 175.0997; found: 175.1118.

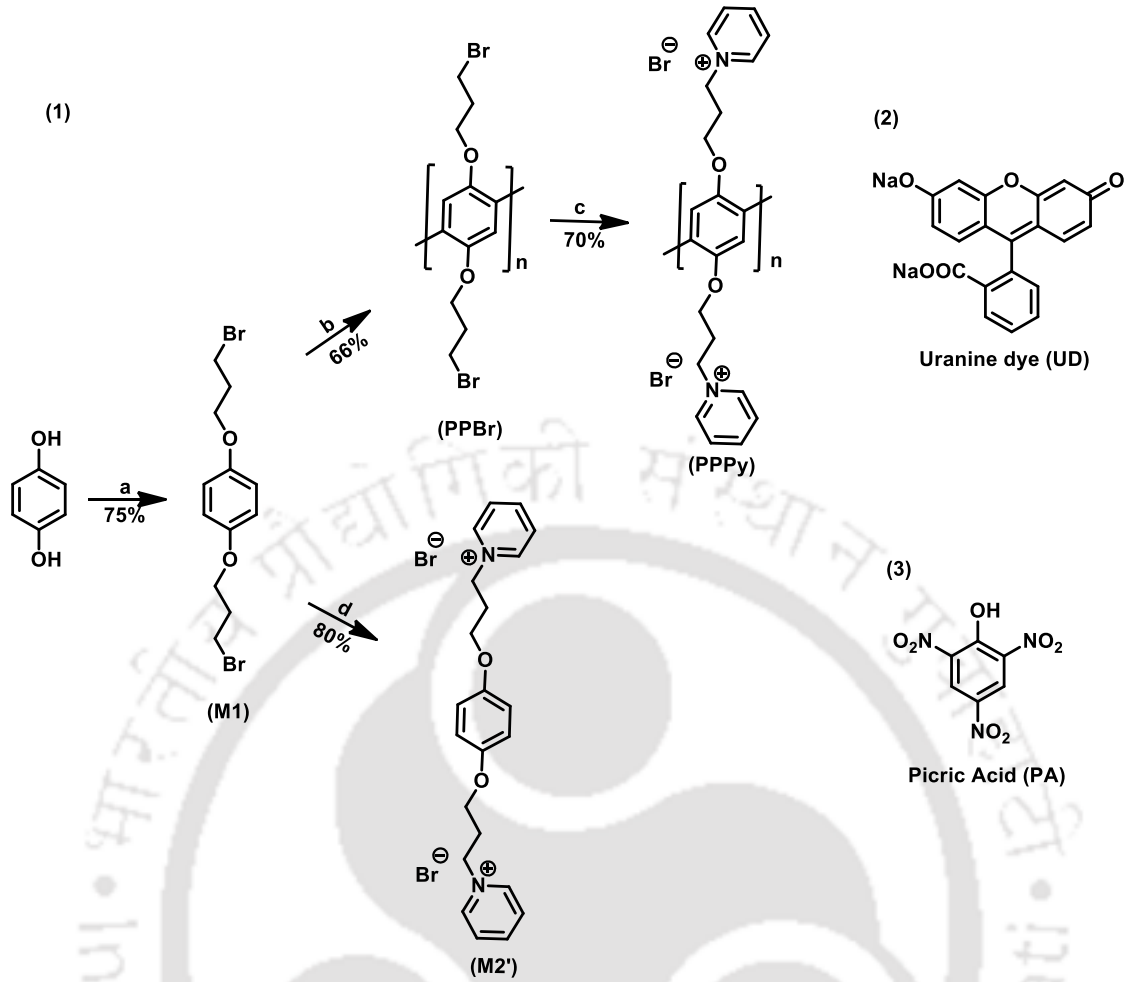

Scheme 3.1 (1) Synthesis of the Polymer PPPy and Monomer M2' and Chemical Structures of (2) Uranine Dye (UD) and (3) PA. (a) 1,3-Dibromopropane, dry acetone, K_2CO_3, reflux, 24 h. (b) $FeCl_3$, nitrobenzene (NB), room temperature (rt), 36 h, (c) pyridine, dimethylformamide (DMF), 70 °C, 24 h, and (d) pyridine, acetonitrile, reflux, overnight.

3.2.3 Sensing Studies in Aqueous Solution

The stock solutions of the polymer PPPy and other analytes, namely, NB, nitromethane, BA, 4-NP, phenol, and 2,4-DNP, were prepared in Milli-Q water at concentrations of 1×10^{-3} and 1×10^{-2} M, respectively. Stock solutions of other nitroaromatics, namely, 2,6- DNT, 2,4-DNT, 4-NT, and 1,3-DNB, were prepared at concentrations of 1×10^{-2} M in high-performance liquid chromatography grade tetrahydrofuran. Stock solutions of TNT and RDX were prepared at concentration of 1×10^{-2} M in 1:1 CH_3CN/MeOH. The absorption measurements and the PL titrations of UD (6.6×10^{-6} M) with different concentrations of the polymer PPPy were carried out by sequentially adding various concentrations of the polymer PPPy (1.6×10^{-6}, 3.3×10^{-6}, 5.0×10^{-6}, 6.66×10^{-6}, 8.3×10^{-6}, 10.0×10^{-6}, 11.6×10^{-6}, 13.3×10^{-6}, 15.0×10^{-6}, and 16.6×10^{-6} M) to a 3 mL water medium buffered with HEPES

(0.01 M, pH 7.0) containing 6.6×10^{-6} M of UD in a quartz cuvette of 10 mm path length. The resultant mixtures were mixed thoroughly before recording the spectra at rt.

3.2.4 Titration Conditions

All of the UV−vis and PL titrations were carried out in aqueous solutions buffered with HEPES (pH 7.0, 0.01 M). The concentration of the fluorophore-UD was kept constant at 6.6×10^{-6} M throughout the fluorescence titrations.

3.2.5 Calculation of Detection Limit

For calculating the detection limit, different solutions of the polymer PPPy (16.6×10^{-6} M) and UD (6.6×10^{-6} M) each containing PA (3.3×10^{-6}, 6.6×10^{-6}, 10.0×10^{-6}, 13.3×10^{-6}, 16.6×10^{-6}, and 20.0×10^{-6} M) were taken individually in HEPES buffer (pH 7.0, 0.01 M) and then the emission spectrum was obtained for individual sample by exciting at 490 nm. A calibration plot was obtained between the fluorescence intensity and the increasing concentration of PA to get a regression curve equation. From the calibration curve, the LOD was evaluated using the equation 3σ/ K, where σ denotes the standard deviation for the intensity of UD and PPPy in the absence of PA and K is the slope of the curve.

3.2.6 Vapor-Phase Detection

Hundred milligrams of dried PA was taken in an airtight flask and kept for 2 days at rt and maintained at 40 °C for 15 min before titration so that the air inside the flask gets completely saturated with PA vapors. The vapor pressure (P) of PA was calculated using the integrated form of Clausius−Clapeyron equation ($\log_{10} P = A - B/T$).[56,57] Here, A and B are the two conventionally used fitting parameters. Furthermore, the concentration of PA vapors was also calculated by the following equation: saturation concentration (ppm) = P (mmHg)/760 mmHg $\times 10^6$, where P represents the vapor pressure of PA.[53] For each titration, the concentration of PA vapors was kept constant (i.e., 0.018 ppm, 50 mL) and purged through cuvette using a leak-proof syringe.

3.3 Results and Discussion

3.3.1 Synthesis and characterization of PPPy

The cationic polymer PPPy was obtained via post-functionalization polymerization method (Scheme 3.1 and Figures A3.1−A3.8). Pyridinium group strapped along the side chains of the PPPy makes the polymer highly soluble in polar solvents such as methanol, water, and so on, and also provides specific recognition site for PA because of attractive electrostatic interactions. The cationic polymer PPPy shows an absorbance maximum at 319 nm and does

not emit any kind of fluorescence in water buffered with 4-(2-hydroxyethyl)piperazine-1-ethanesulfonic acid (HEPES, pH 7.0, 0.01 M). The indicator used in the IDA studies is UD (Scheme 3.1), which has the absorbance and fluorescence maxima at 490 and 513 nm (excitation 490 nm), respectively, in water buffered with HEPES (pH 7.0, 0.01 M). The concentration of UD for every titration experiment was fixed at 6.6×10^{-6} M. In the preliminary experiment, the fluorescence of UD (6.6×10^{-6} M) in water buffered with HEPES (pH 7.0, 0.01 M) was measured in the presence of various concentrations of PPPy (1.6×10^{-6}, 3.3×10^{-6}, 5.0×10^{-6}, 6.66×10^{-6}, 8.3×10^{-6}, 10.0×10^{-6}, 11.6×10^{-6}, 13.3×10^{-6}, 15.0×10^{-6}, and 16.6×10^{-6} M) (Figure 3.1a). The fluorescence intensity of UD gradually quenched on further addition of PPPy, and 86% of the quenching occurred after the addition of PPPy in 16.6×10^{-6} M concentration. It should be noted that the addition of monomer M2' (Scheme 3.1) to the solution of UD barely affected its fluorescence intensity (Figure A3.9). This proved the high affinity of PPPy toward UD. The UV−vis spectra of UD were studied after adding PPPy in varying concentrations (1.6×10^{-6}, 3.3×10^{-6}, 5.0×10^{-6}, 6.66×10^{-6}, 8.3×10^{-6}, 10.0×10^{-6}, 11.6×10^{-6}, 13.3×10^{-6}, 15.0×10^{-6}, and 16.6×10^{-6} M) (Figure 3.1b). The absorbance maxima of UD (490 nm) was red shifted by 12 nm to 502 nm. This new peak at 502 nm in the UV−vis spectrum was indicative of the host/dye complex, that is, the PPPy/UD complex.

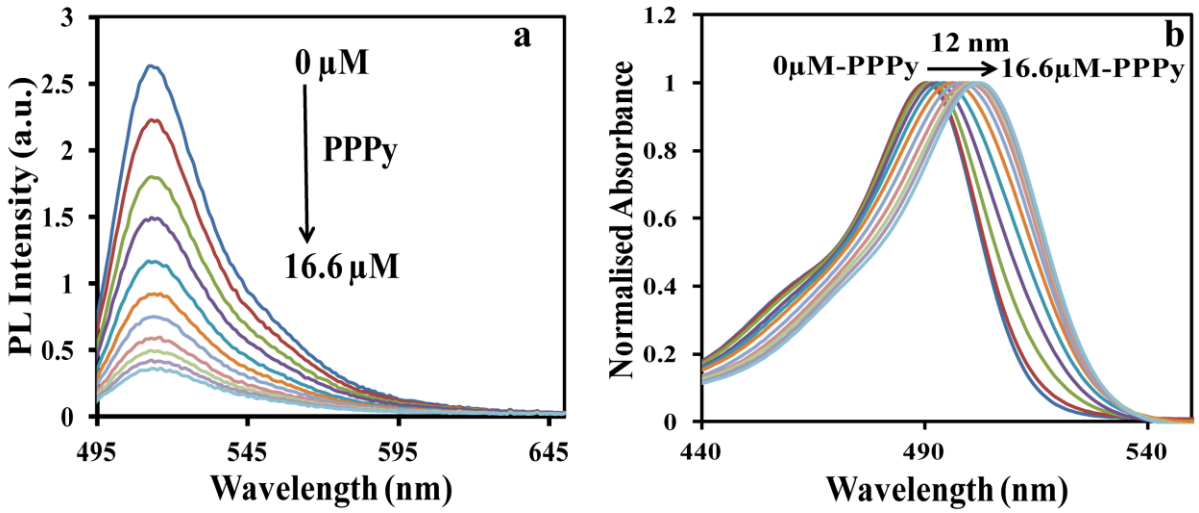

Figure 3.1 (a) Photoluminescence (PL) spectra of UD (6.6×10^{-6} M) with increasing concentrations of PPPy in water buffered with HEPES (0.01 M, pH 7.0). (b) UV−vis spectra of UD (6.6×10^{-6} M) with increasing concentrations of PPPy in water buffered with HEPES (0.01 M, pH 7.0).

To examine the displacement of the indicator, UD, from the cationic conjugated polymer PPPy, the IDA studies were done for PA, carried out in cuvettes, keeping the fixed concentration of resulting solution of PPPy (16.6×10^{-6} M)/UD (6.6×10^{-6} M) complex in water buffered with HEPES (pH 7.0, 0.01 M) by varying the concentration of PA. In typical IDA studies, fluorescence spectra of PPPy (16.6×10^{-6} M)/UD (6.6×10^{-6} M) complex were recorded at various concentrations of analyte PA (16.6×10^{-6}, 33.3×10^{-6}, 50.0×10^{-6}, 66.6×10^{-6}, 83.3×10^{-6}, 100.0×10^{-6}, 116.6×10^{-6}, 133.3×10^{-6}, 150.0×10^{-6}, and 166.6×10^{-6} M) (Figure 3.2a). The fluorescence intensity increased gradually with the addition of PA, and 86% dequenching occurred after the addition of PA in 166.6×10^{-6} M concentration. The UV−vis spectra of PPPy (16.6×10^{-6} M)/ UD(6.6×10^{-6} M) complex were recorded upon the addition of various concentrations of PA (16.6×10^{-6}, 33.3×10^{-6}, 50.0×10^{-6}, 66.6×10^{-6}, 83.3×10^{-6}, 100.0×10^{-6}, 116.6×10^{-6}, 133.3×10^{-6}, 150.0×10^{-6}, and 166.6×10^{-6} M) (Figure 3.2b). The absorbance maximum of UD/PPPy complex (502 nm) is blue shifted back to 490 nm, indicating the displacement of UD from the PPPy/UD complex.

In addition, the limit of detection (LOD) was calculated to be 295 nM based on the change inthe emission spectrum of the PPPy (16.6×10^{-6} M)/UD (6.6×10^{-6} M) complex at various concentrations of PA (3.3×10^{-6}, 6.6×10^{-6}, 10.0×10^{-6}, 13.3×10^{-6}, 16.6×10^{-6}, and 20.0×10^{-6} M) by using the equation 3σ/K (Figure A3.10), which is being reported for the first time

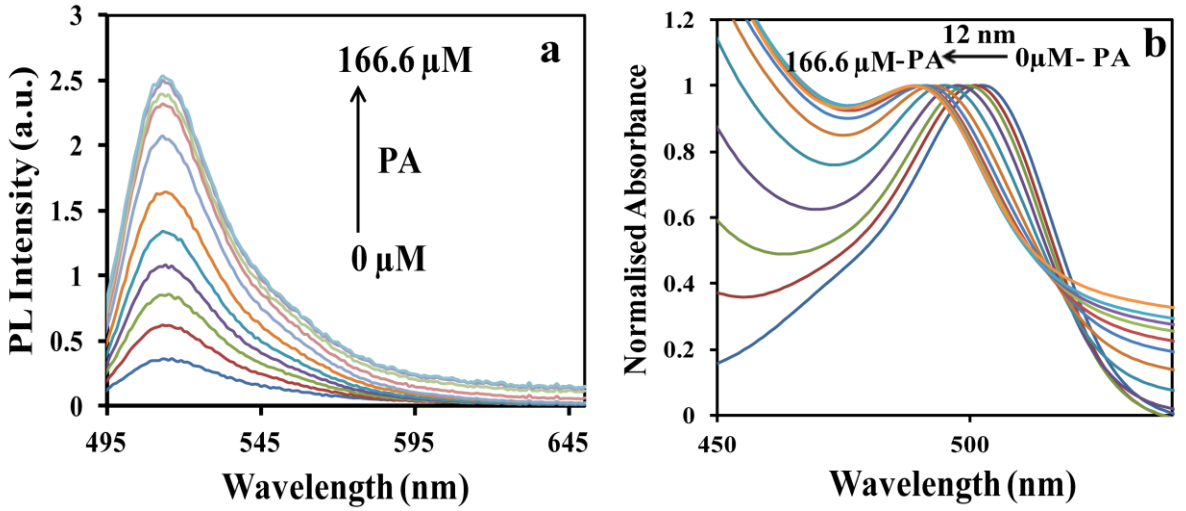

Figure 3.2 (a) PL spectrum of PPPy (16.6×10^{-6} M) and UD (6.6×10^{-6} M) complex with increasing concentrations of PA (166.6×10^{-6} M) in water buffered with HEPES (pH 7.0, 0.01 M). (b) UV−vis spectra of UD (6.6×10^{-6} M) and PPPy (16.6×10^{-6} M) complex with increasing concentrations of PA (166.6×10^{-6} M) in water buffered with HEPES (pH 7.0, 0.01 M).

by means of the IDA technique via a conjugated polymer−dye system (Table A3.1). The photograph of UD (6.6×10^{-6} M) solution (Figure 3.3a) in HEPES (pH 7.0, 0.01 M) was taken in natural light with successive additions of PPPy (16.6×10^{-6} M) (Figure 3.3b) and PA (166.6×10^{-6} M) (Figure 3.3c). Similarly, the photographs of vertical view of their respective solution were taken in the presence of 490 nm emission wavelength source using Horiba Fluoromax-4 spectrofluorometer (Figure 3.3).

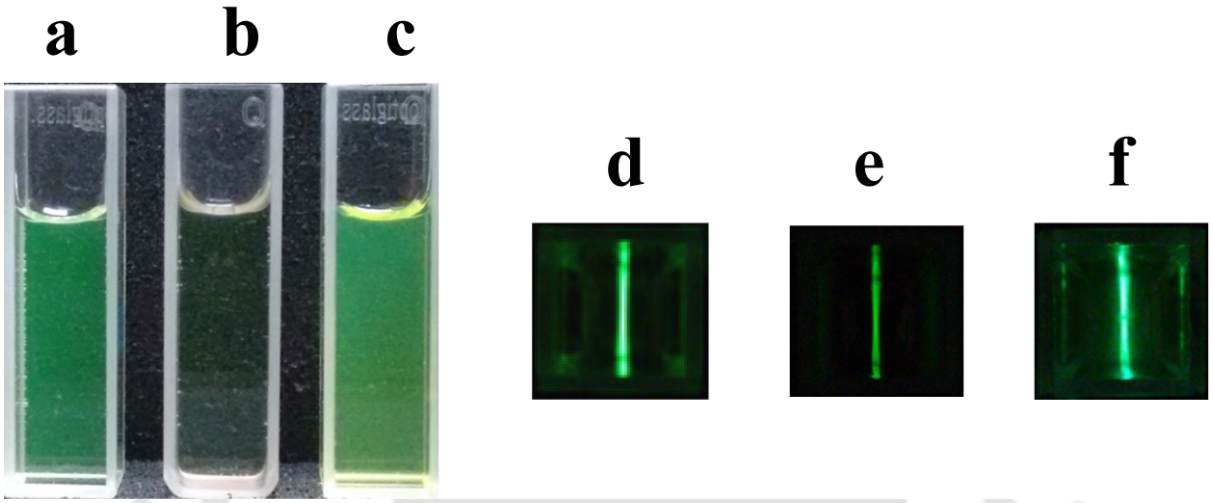

Figure 3.3 (a−c) Photographs of UD (6.6×10^{-6} M), UD (6.6×10^{-6} M)/PPPy (16.6×10^{-6} M) complex, and UD (6.6×10^{-6} M)/PPPy (16.6×10^{-6} M)/PA (166.6×10^{-6} M) in natural light, respectively. (d−f) Vertical view of cuvettes under 490 nm light source in Horiba Fluoromax-4 spectrofluorometer, respectively

3.3.2 Selectivity studies in competitive environment

To elucidate the selectivity, fluorescent IDA studies were performed by adding various common interfering analytes, namely, 2,4-DNP, 4-NP, TNT, research department explosive (RDX), 2,4-dinitrotoluene (2,4-DNT), 2,6-dinitrotoluene (2,6- DNT), 4-nitrotoluene (4-NT), 1,3-dinitrobenzene (1,3-DNB), benzoic acid (BA), NB, and phenol to the solution of PPPy (16.6×10^{-6} M)/UD (6.6×10^{-6} M) complex in water buffered with HEPES (pH 7.0, 0.01 M) (Figures 3.4a and A3.11). Interestingly, no significant change was seen in the PL spectra of PPPy/UD complex after the addition of these analytes. Furthermore, other metal ions (Fe^{3+}, Cd^{2+}, Zn^{2+}, Cu^{2+}, Co^{3+}, Cr^{2+}, Pb^{2+}, and Mn^{2+}) as well as anions ($H_2PO_4^-$, HPO_4^{2-}, PO_4^{3-}, I^-, Cl^-, F^-, NO_3^-, N_3^-, BF_4^-, and AcO^-) did not have any effect on the fluorescence of PPPy/UD complex (Figures 3.4b,3.4c, A3.12, and A3.13), which confirms the high selectivity of PPPy toward PA in the IDA studies. Sensing studies were also done in a competitive environment.

In a typical set of experiment, a solution of 2,4- DNP (166.6 × 10^{-6} M) was added initially to the solution of PPPy (16.6 × 10^{-6} M)/UD (6.6 × 10^{-6} M) complex in water buffered with HEPES (pH 7.0, 0.01 M), but no substantial change in the emission intensity was seen (Figure A3.14). The solution of PA (166.6 × 10^{-6} M) was then introduced to the same solution, which resulted in significant enhancement in fluorescence. The same sets of experiments were repeated with other nitroaromatic compounds and similar fluorescence turn-on response was obtained after the addition of PA (Figures A3.15− A3.24). It is worth mentioning that most of the existing chemosensor systems developed for the detection of PA suffered from a large interference by several other electron-deficient nitroaromatic compounds, particularly 2,4-DNP, 4-NP, and TNT. The present method provides a simple, rapid, reliable, and highly specific detection of PA even in a competitive environment.

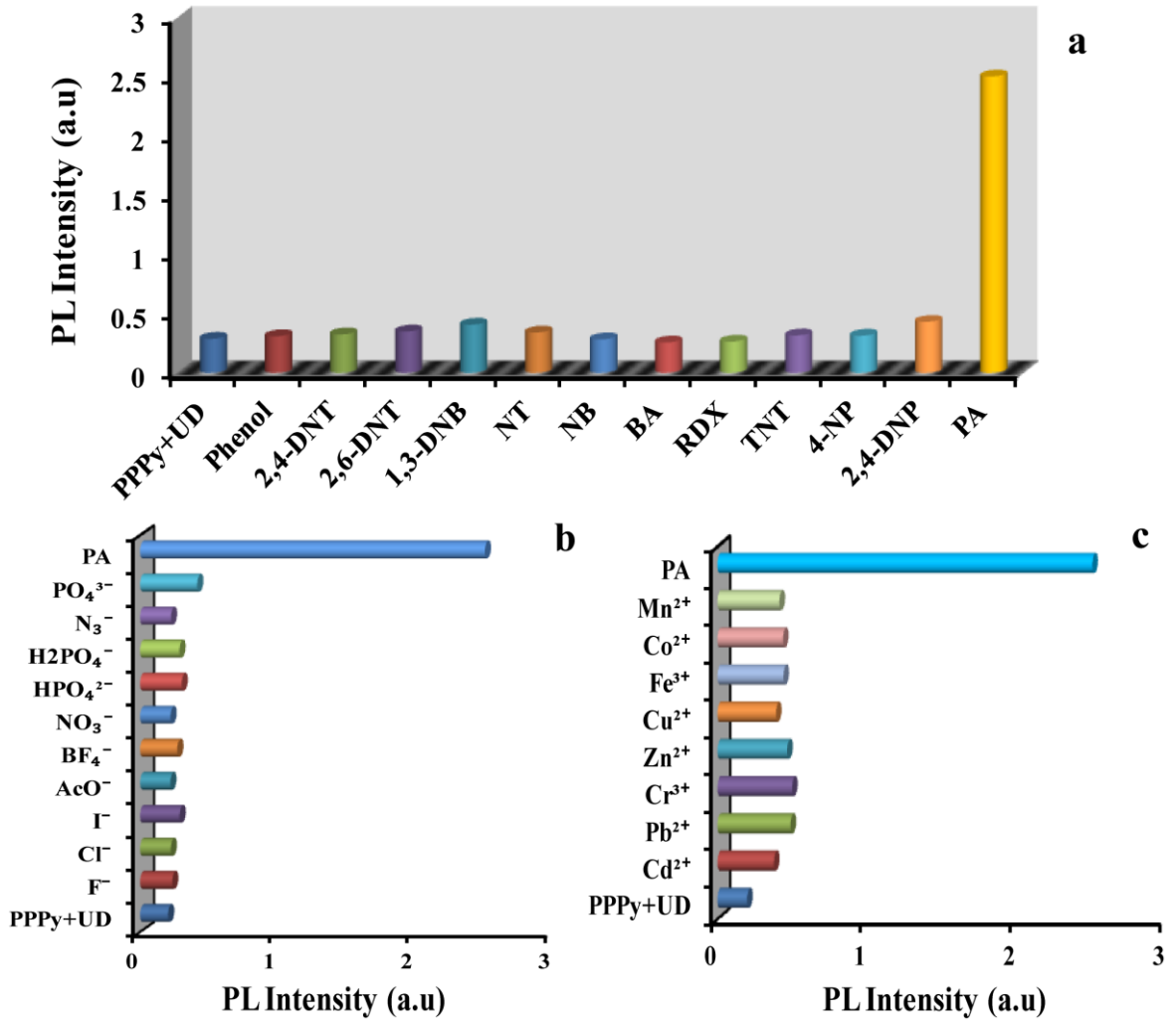

Figure 3.4 Bar diagrams depicting the effect of (a) various interfering analytes (166.6 × 10^{-6} M), (b) anions (166.6 × 10^{-6} M), and (c) metal ions (166.6 × 10^{-6} M) on the emission maximum of the PPPy (16.6 × 10^{-6} M)/UD (6.6 × 10^{-6} M) complex.

3.3.3 Vapor-phase detection

Vapor-phase detection of PA was also carried out by using PPPy. Fixed volumes of PA vapors of concentration (0.018 ppm, 50 mL) were purged through the UD/PPPy complex using a leak-proof syringe. The PL spectra were recorded after the purging of PA vapors in the cuvette and the increase in the emission maxima observed with each addition (Figures 3.5 and A3.25) were recorded. Furthermore, the LOD value was calculated to be 0.220 ppm based on the change in the emission spectrum of the PPPy (16.6×10^{-6} M)/UD (6.6×10^{-6} M) complex at various concentrations of PA vapors (0.316, 0.632, 0.948, 1.264, 1.580, and 1.896 ppm) using the equation 3σ/K (Figure A3.26). Thus, the present method established a rapid and specific detection of PA in the vapor phase as well, which remains a highly challenging and an exciting area of research.

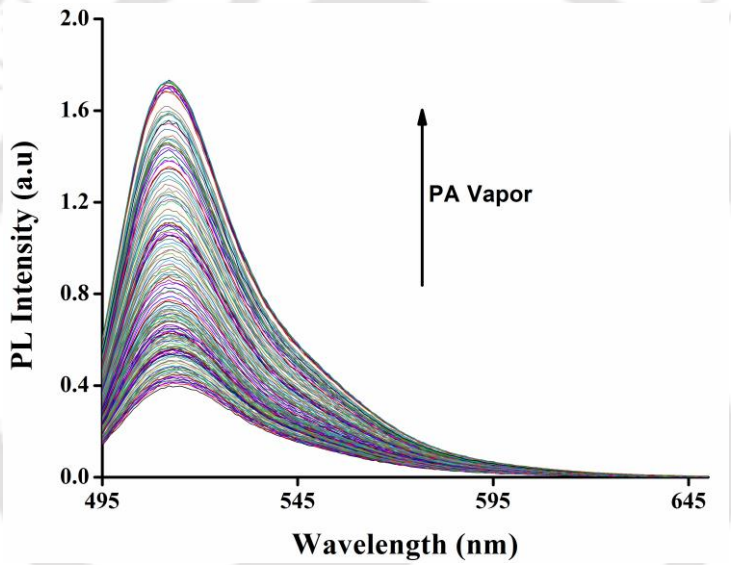

Figure 3.5 PL spectrum of PPPy (16.6×10^{-6} M) and UD (6.6×10^{-6} M) complex with increasing concentration of PA vapors in water buffered with HEPES (pH 7.0, 0.01 M).

3.4 Conclusion

In conclusion, a non-fluorescent cationic conjugated polymer was demonstrated to selectively detect PA among other closely related electron-deficient nitro aromatic compounds like 2,4-DNP, 4-NP, and TNT via fluorescent turn-on IDA using UD as the indicator for the first time. The ensemble system could be used to detect PA with a LOD of 295 nM in water buffered with HEPES (pH 7.0, 0.01 M) and 0.22 ppm in the vapor state. The addition of PA thus led to a quick fluorescence turn-on response of the PPPy/UD complex even at very low concentrations. This fluorescence turn-on based system avoids the erroneous false signals and significantly improves the detection sensitivity as compared with the assays that work on the fluorescence quenching methods.

References

(1) Sun, X.; Wang, Y.; Lei, Y. *Chem. Soc. Rev.* **2015**, *44*, 8019.

(2) Salinas, Y.; Martínez-Máñez, R.; Marcos, M. D.; Sancenón, F.; Costero, A. M.; Parra, M.; Gil, S. *Chem. Soc. Rev*. **2012**, *41*, 1261.

(3) Akhavan, J. In Chemistry of Explosives, Royal Society of Chemistry, 2nd ed. **2004**.

(4) Ashbrook, P. C.; Houts, T. A. *Chem. Health Safety* **2003**, *10*, 27.

(5) Innovative Treatment Technologies: Annual Status Report, U.S. Environmental Protection Agency: Washington, D.C., 8th ed., **1996**.

(6) Wollin, K. M.; Dieter, H. H. *Arch. Environ. Contam. Toxicol.* **2005**, *49*, 18.

(7) Wu, J.; Kwon, B.; Liu, W.; Anslyn, E. V.; Wang, P.; Kim, J. S. *Chem. Rev.* **2015**, *115*, 7893.

(8) Hof, F. *Chem. Commun.* **2016**, *52*, 10093.

(9) Norouzy, A.; Azizi, Z.; Nau, W. M. *Angew. Chem. Int. Ed*. **2015**, *54*, 792.

(10) Ghale, G.; Nau, W. M. *Acc. Chem. Res.* **2014**, *47*, 2150.

(11) Cakmak, S. E.; Leigh, D. A.; McTernan, C. T.; Nussbaumer, A. L. *Chem. Rev.* **2015**, *115*, 10081.

(12) Piatek, A. M.; Bomble, Y. J.; Wiskur, S. L.; Anslyn, E. V. *J. Am. Chem. Soc.* **2004**, *126*, 6072.

(13) Leontiev, A. V.; Rudkevich, D. M. *J. Am. Chem. Soc.* **2005**, *127*, 14126.

(14) Neelakandan, P. P.; Hariharan, M.; Ramaiah, D. *J. Am. Chem. Soc.* **2006**, *128*, 11334.

(15) Dsouza, R. N.; Pischel, U.; Nau, W. M. *Chem. Rev.* **2011**, *111*, 7941.

(16) Sokkalingam, P.; Kim, D. D.; Hwang, H.; Sessler, J. L.; Lee, C. H. *Chem. Sci.* **2012**, *3*, 1819.

(17) Kumar, V.; Ansyln, E. V. *J. Am. Chem. Soc.* **2013**, *135*, 6338.

(18) Liu, Y.; Bonizzoni, M. *J. Am. Chem. Soc.* **2014**, *136*, 14223.

(19) Minami, T.; Esipenko, N. A.; Zhang, B.; Isaacs, L.; Anzenbacher Jr. P. *Chem. Commun.* **2014**, *50*, 61.

(20) Yang, L.; Zhao, H.; Li, Y.; Ran, X.; Deng, G.; Zhang, Y.; Ye, H.; Zhao, G.; Li, C. *Analyst*, **2016**, *141*, 270.

(21) Hua, B.; Shao, L.; Yu, G.; Huang, F. *Chem. Commun.* **2016**, *52*, 10016.

(22) You, L.; Zha, D.; Anslyn, E. V. *Chem. Rev.* **2015**, *115*, 7840.

(23) Liu, Y.; Perez, L.; Mettry, M.; Easley, C. J.; Hooley, R. J.; Zhong, W. *J. Am. Chem. Soc.* **2016**, *138*, 10746.

(24) Caglayan, M. G.; Sheykhi, S.; Mosca, L.; Anzenbacher Jr. P. *Chem. Commun.* **2016**, *52*, 8279.

(25) Francoia, J. P.; Pascal, R.; Vial, L. *Chem. Commun.* **2015**, *51*, 1953.

(26) Janowski, V.; Severin, K. *Chem. Commun.* **2011**, *47*, 8521.

(27) Metzger, A.; Anslyn, E. V. *Angew. Chem. Int. Ed.* **1998**, *37*, 649.

(28) Fabbrizzi, L.; Foti, F.; Taglietti, A. *Org. Lett*. **2005**, *7*, 2603.

(29) Tobey, S. L.; Anslyn, E. V. *Org. Lett*. **2003**, *5*, 2029.

(30) Tobey, S. L.; Jones, B. D.; Anslyn, E. V. *J. Am. Chem. Soc.* **2003**, *125*, 4026.

(31) Tobey, S. L; Anslyn, E. V. *J. Am. Chem. Soc.* **2003**, *125*, 14807.

(32) Lavigne, J. J.; Anslyn, E. V. *Angew. Chem. Int. Ed.* **1999**, *38*, 3666.

(33) Nguyen, B. T.; Wiskur, S. L.; Anslyn, E. V. *Org. Lett.* **2004**, *6*, 2499.

(34) Niikura, K.; Bisson, A. P.; Anslyn, E. V. *J. Chem. Soc. Perkin Trans.* **1999**, *2*, 1111.

(35) Bereau, V.; Duhayon, C.; Sutter, J. P. *Chem. Commun.* **2014**, *50*, 12061.

(36) Acharyya, K.; Mukherjee, P. S. *Chem. Commun.* **2014**, *50*, 15788.

(37) Shaligram, S.; Wadgaonkar P. P.; Kharul, U. K. *J. Mater. Chem. A* **2014**, *2*, 13983.

(38) Sang, N.; Zhan, C.; Cao, D. *J. Mater. Chem. A* **2015**, *3*, 92.

(39) Swamy, C. A.; Thilagar, P. *Chem. Eur. J.* **2015**, *21*, 8874.

(40) Chowdhury, A.; Mukherjee, P. S. *J. Org. Chem.* **2015**, *80*, 4064.

(41) Shi, Z. Q.; Guo, Z. J.; Zheng, H. G. *Chem. Commun.* **2015**, *51*, 8300.

(42) Sohn, H.; Sailor, M. J.; Magde, D.; Trogler, W. C. *J. Am. Chem. Soc.* **2003**, *125*, 3821.

(43) Liu, Y.; Gao, M.; Lam, J. W. Y.; Hu, R.; Tang, B. Z. *Macromolecules* **2014**, *47*, 4908.

(44) Zhou, H.; Li, J.; Chua, M. H.; Yan, H.; Tang, B. Z.; Xu, J. *Polym. Chem.* **2014**, *5*, 5628.

(45) Xu, Y.; Li, B.; Li, W.; Zhao, J.; Sun, S.; Pang, Y. *Chem. Commun.* **2013**, *49*, 4764.

(46) Sivaraman, G.; Vidya, B.; Chellappa, D. *RSC Adv.* **2014**, *4*, 30828.

(47) Madhu, S.; Bandele, A.; Ravikanth, M. *RSC Adv.* **2014**, *4*, 7120.

(48) Chopra, R.; Bhalla, V.; Kumar, M.; Kaur, S. *RSC Adv.* **2015**, *5*, 24336.

(49) Gogoi, B.; Sarma, N. S. *ACS Appl. Mater. Interfaces* **2015**, *7*, 11195.

(50) Erande, Y.; Chemate, S.; More, A.; Sekar, N. *RSC Adv.* **2015**, *5*, 89482.

(51) Chemate, S.; Erande, Y.; Mohbiya, D.; Sekar, N. *RSC Adv.* **2016**, *6*, 84319.

(52) Hussain, S.; Malik, A. H.; Afroz, M. A.; Iyer, P. K. *Chem. Commun.* **2015,** *51*, 7207.

(53) Malik, A. H.; Hussain, S.; Kalita, A.; Iyer, P. K. *ACS Appl. Mater. Interfaces* **2015**, *7*, 26968.

(54) Kalita, A.; Hussain, S.; Malik, A. H.; Barman, U.; Goswami, N.; Iyer, P. K. *ACS Appl. Mater. Interfaces* **2016**, *8*, 25326.

(55) Tanwar, A. S.; Hussain, S.; Malik, A. H.; Afroz, M. A.; Iyer, P. K. *ACS Sens.* **2016**, *1*, 1070.

(56) Robert, G. E.; Melanie, J. W.; David, A. A.; Jay, W. G.; Peter, J. H. TrAC, *Trends Anal. Chem*. **2013**, *42*, 35.

(56) Cundall, R. B.; Palmer, T. F.; Wood, C. E. C. *J. Chem. Soc.,Faraday Trans. I,* **1981**, *77*, 711.

Appendix

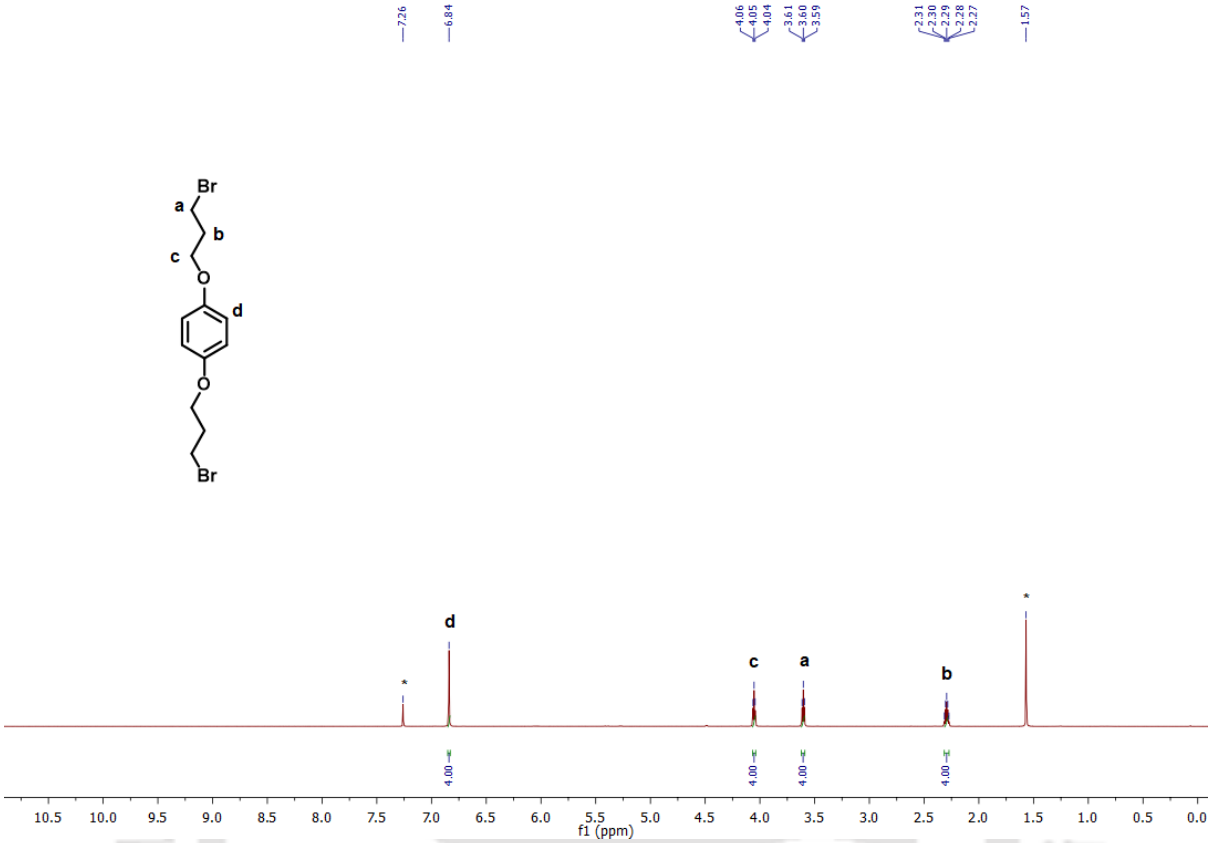

Figure A3.1 ^{1}H-NMR spectra of M1.

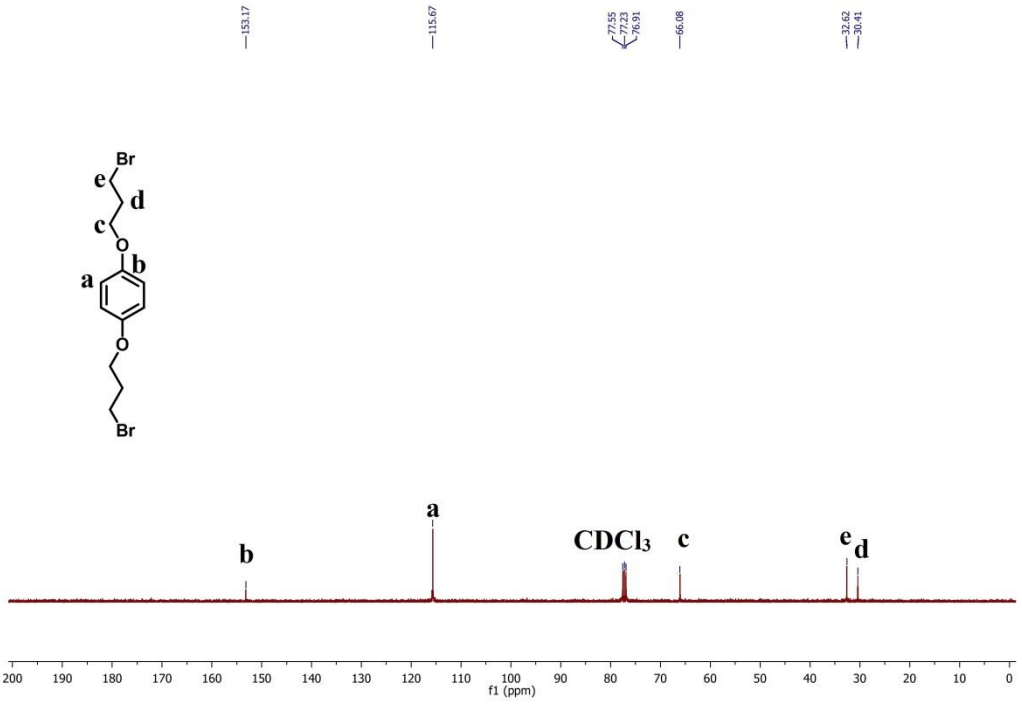

Figure A3.2 ^{13}C-NMR spectra of M1.

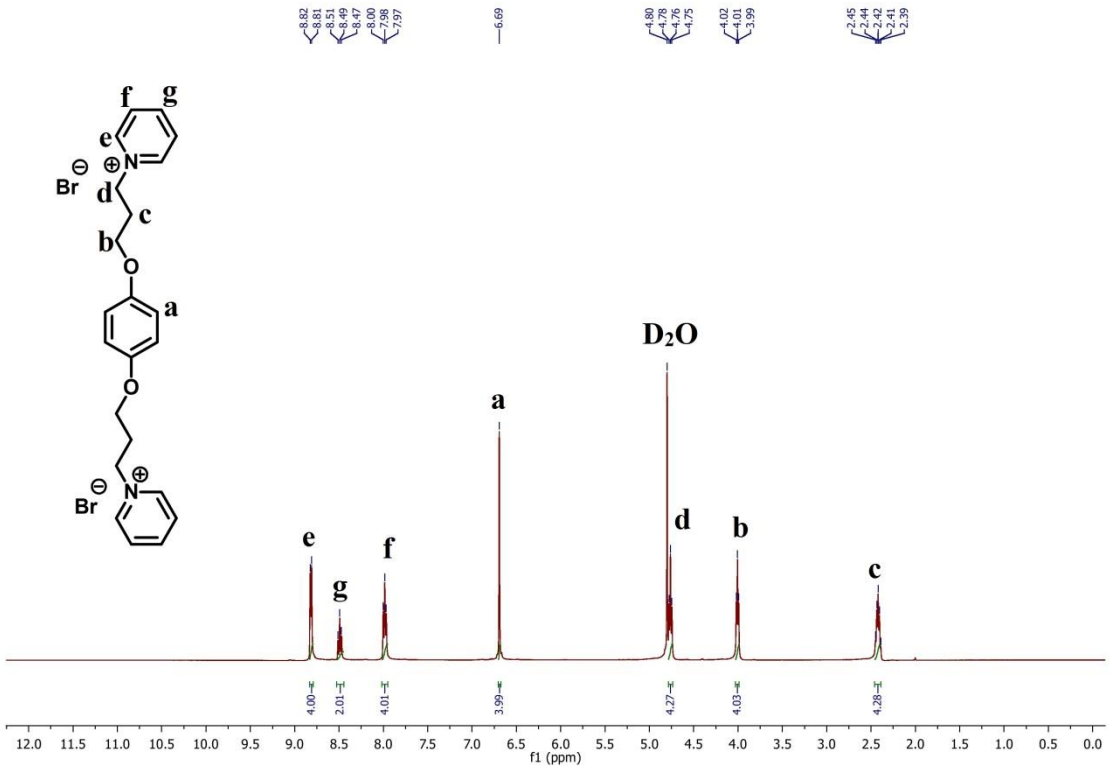

Figure A3.3 ^{1}H-NMR spectra of M2'.

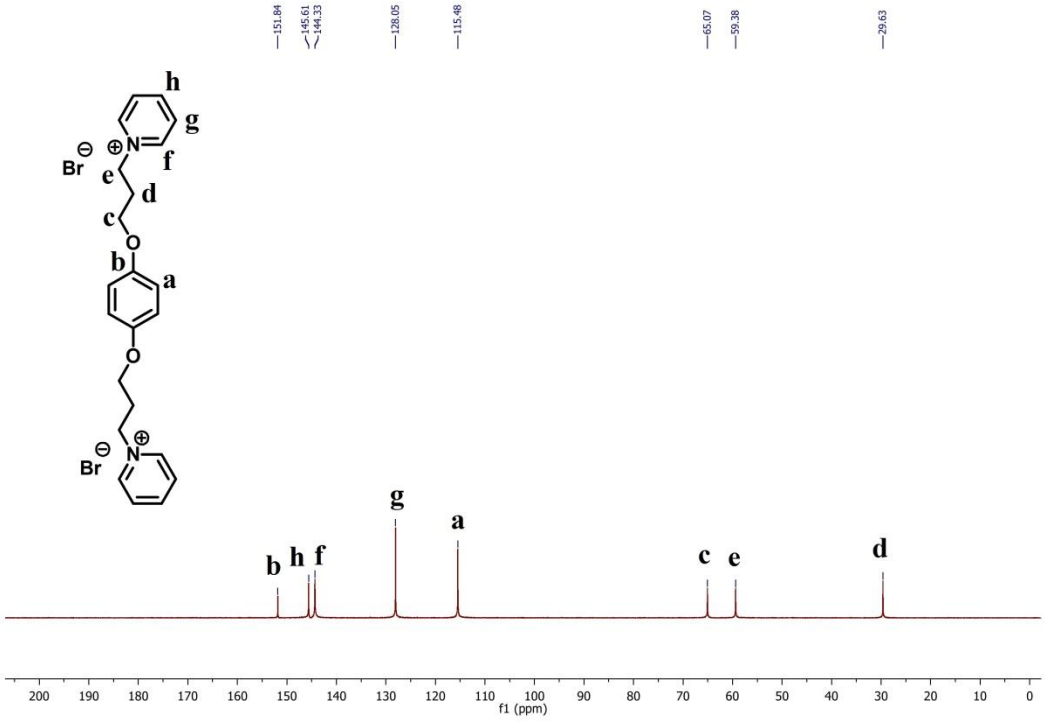

Figure A3.4 ^{13}C-NMR spectra of M2'.

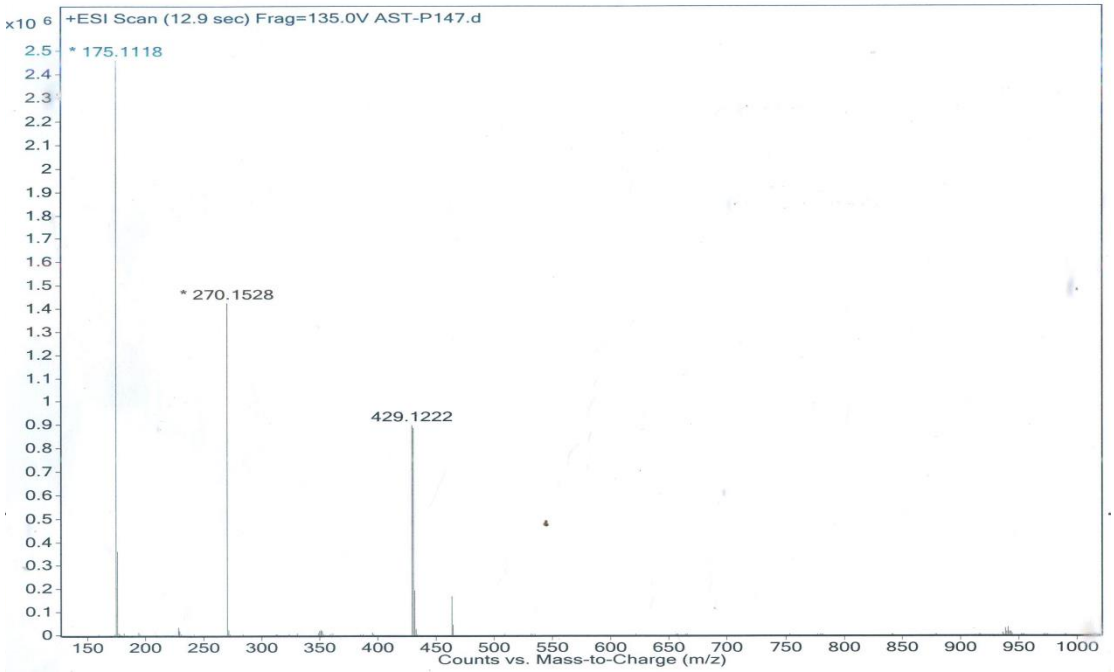

Figure A3.5 High resolution mass spectrum of monomer M2'.

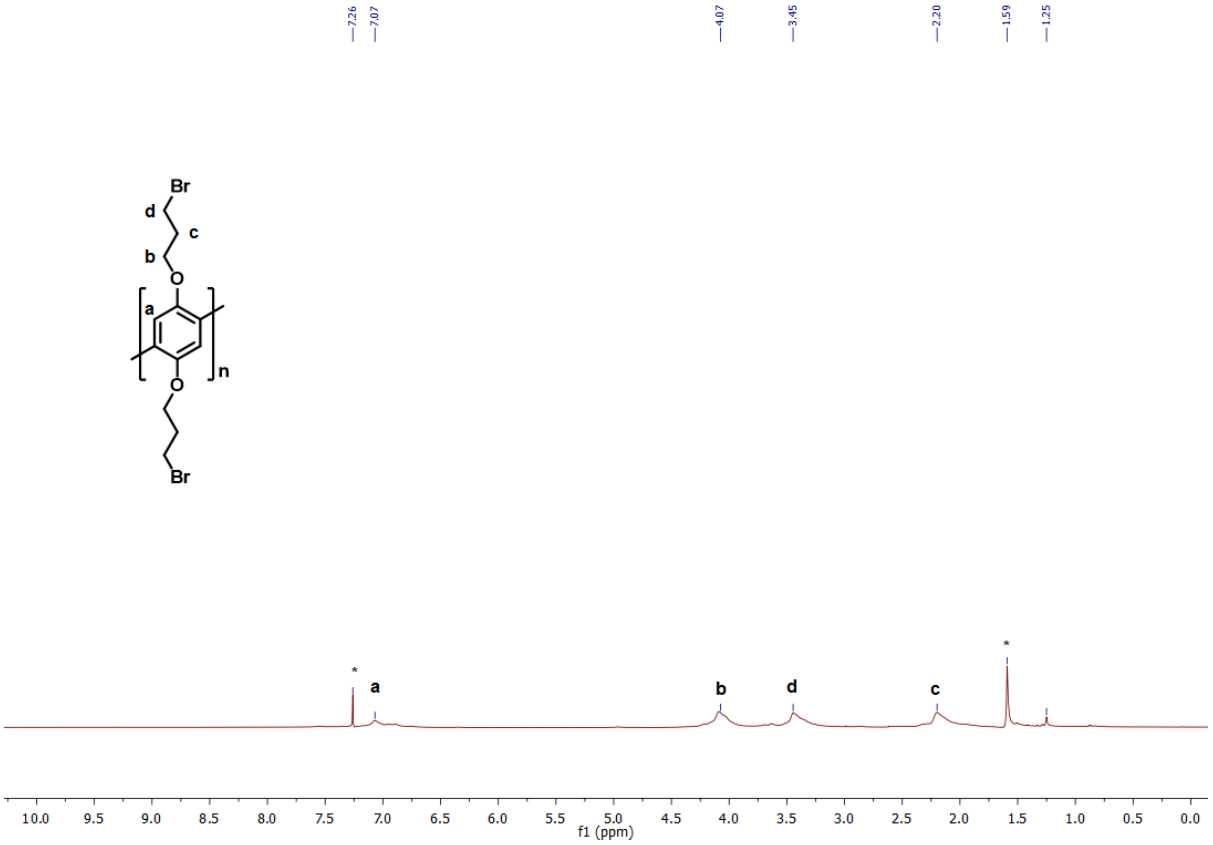

Figure A3.6 ^{1}H NMR spectra of PPBr.

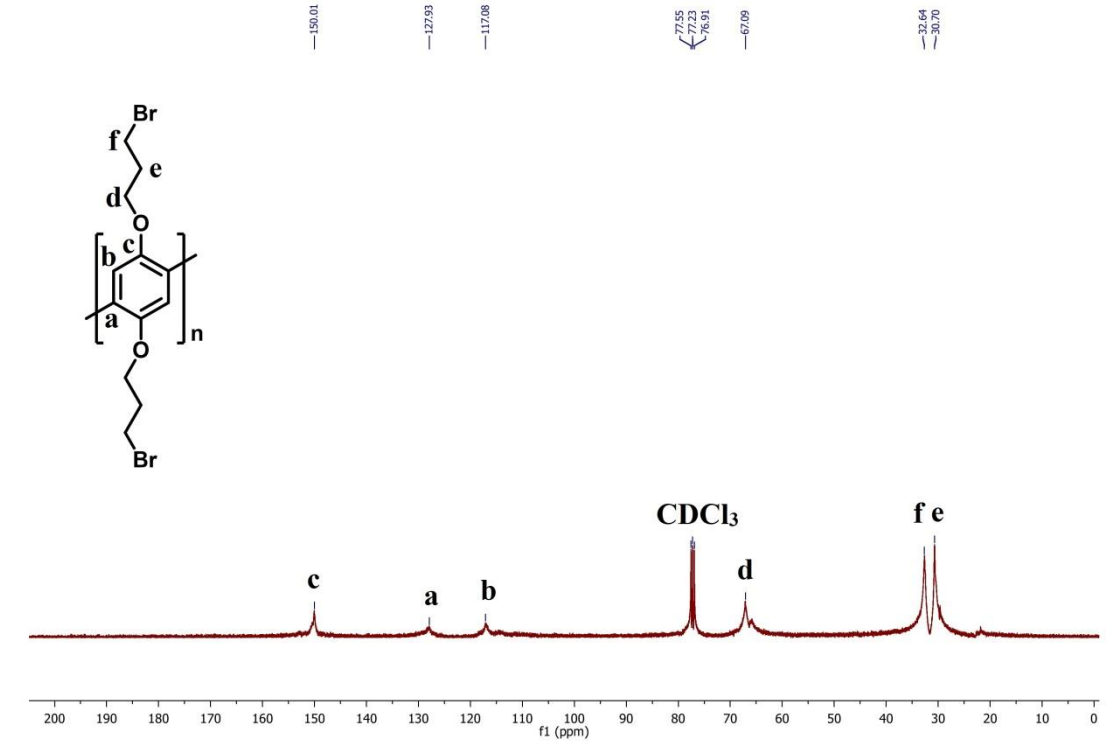

Figure A3.7 ^{13}C NMR spectra of PPBr.

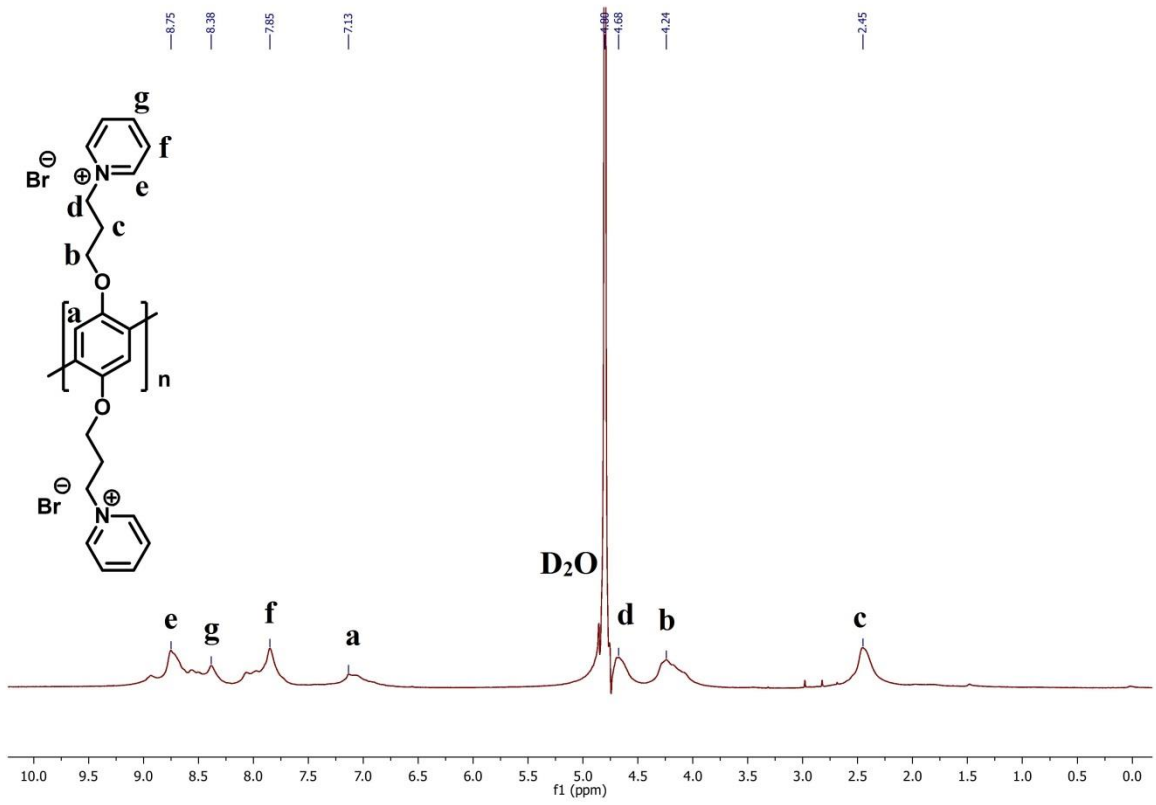

Figure A3.8 ^{1}H NMR spectra of PPPy.

Table 3A.1 A comparative study of various turn on chemosensor reported for PA detection.

Publication	Material used	Detection Limit	Medium Used	Sensing mechanism	Phase of Detection
Present Manuscript	***Conjugated polyelectrolyte and dye complex***	***295 nM***	***H_2O***	***IDA***	***Solution and Vapor phase***
45	Zwitterionic squaraine dye	70 nM	$CH_3CN:H_2O$ (9 : 1, v/v)	ICT Prevention	Solution
46	Rhodamine based derivative	45 nM	H_2O	Picrate adduct	Solution
47	3,5-bis(acetal) BODIPY	162 ppb	$CH_3CN:H_2O$ (9 : 1; v/v)	chemodosimeter PET deterrence	Solution
48	Rhodamine based derivative	35 nM	CH_3OH	spirocyclic ring opening	Solution
49	Curcumin−Tryptophan Conjugate	13.5 nM	H_2O (pH=4)	AIE	Solution
50	BODIPY derivative	0.65 ppb	Ethanol	PET deterrence	Solution
51	Acridine derivative	2.4×10^{-6} M	CH_3OH	PET deterrence	Solution

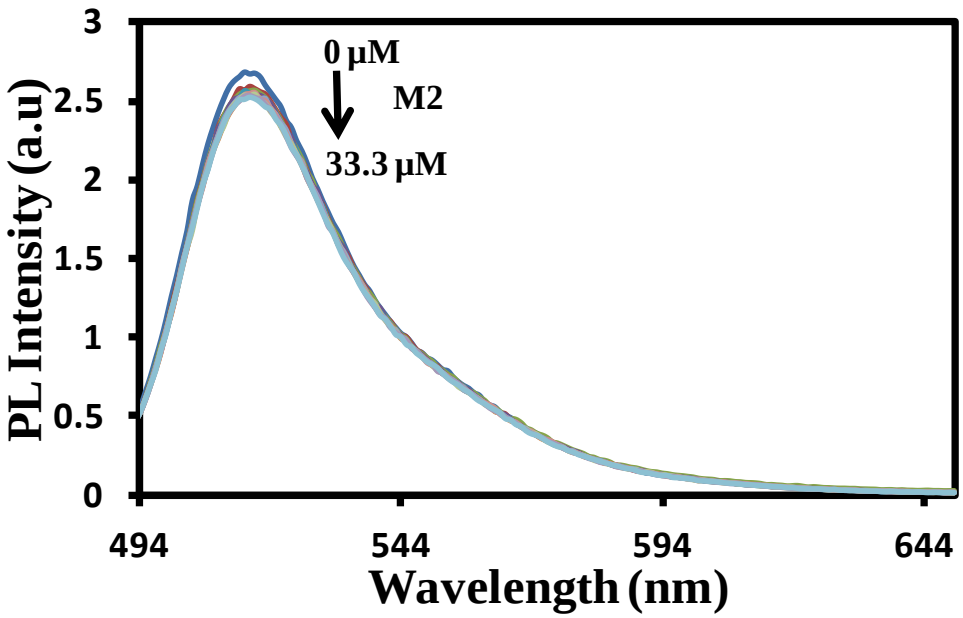

Figure A3.9 Photoluminescence spectra of UD (6.6×10^{-6} M) with increasing concentration of M2' in water buffered with HEPES (pH=7.0, 10mM).

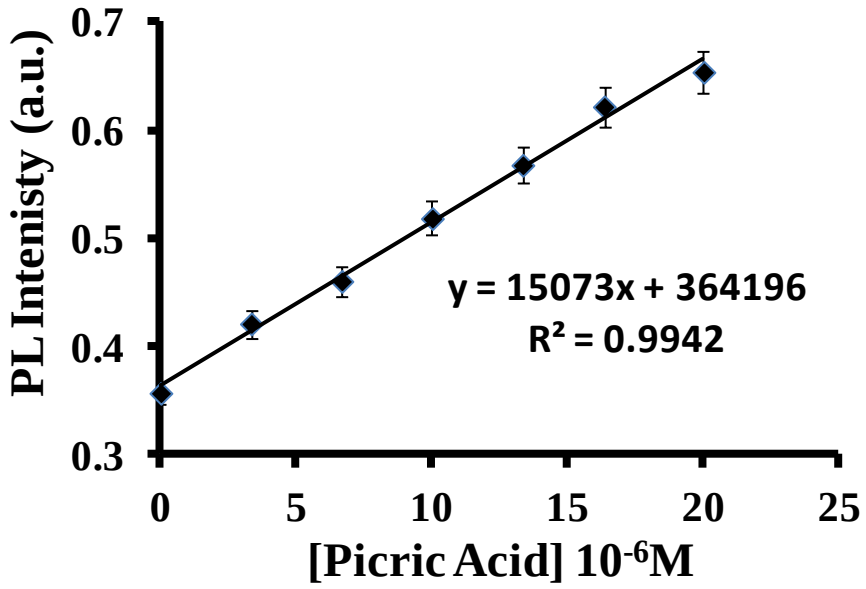

Figure A3.10 Fluorescence intensity of PPPy (16.6 µM) and UD (6.6 µM) in HEPES buffer (pH= 7.0, 10 mM) with increasing concentration of PA.

LOD=3 × S.D./k

LOD = 3 × 1485.21 / (15073× 10^6)

LOD= 295 nM

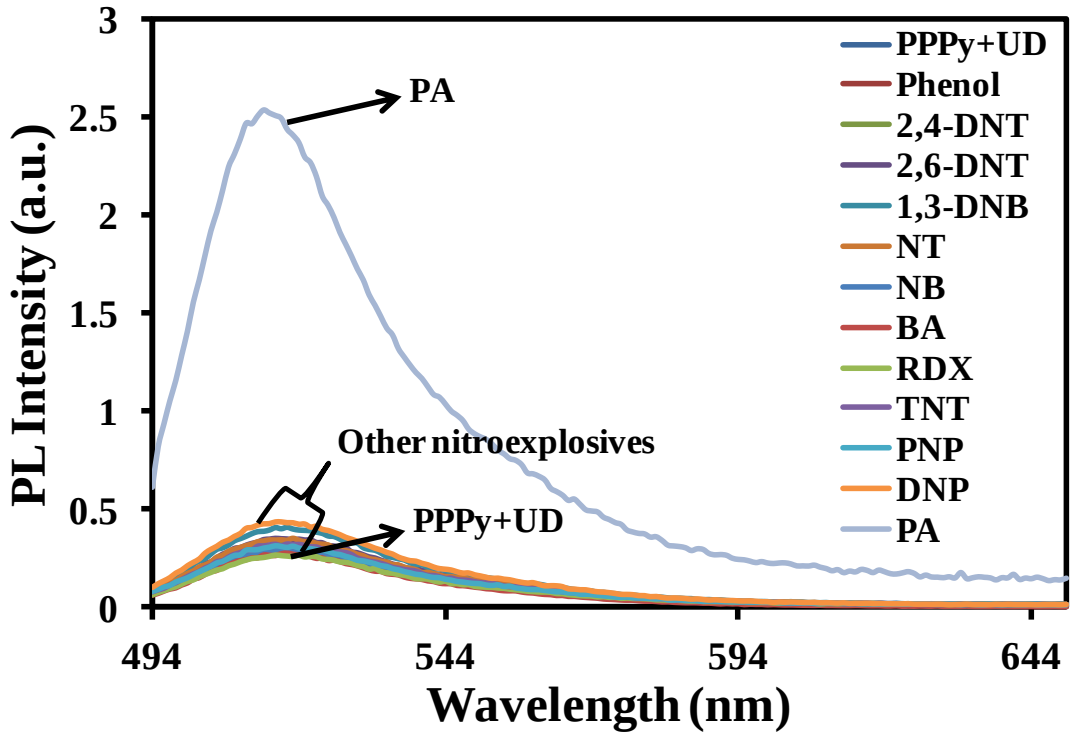

Figure A3.11. Change in Photoluminescence spectrum of UD (6.6 µM) and PPPy (16.6 µM) in the presence of various nitroexplosive compounds (166.6 µM) in Hepes buffer (pH-7.0, 10 mM).

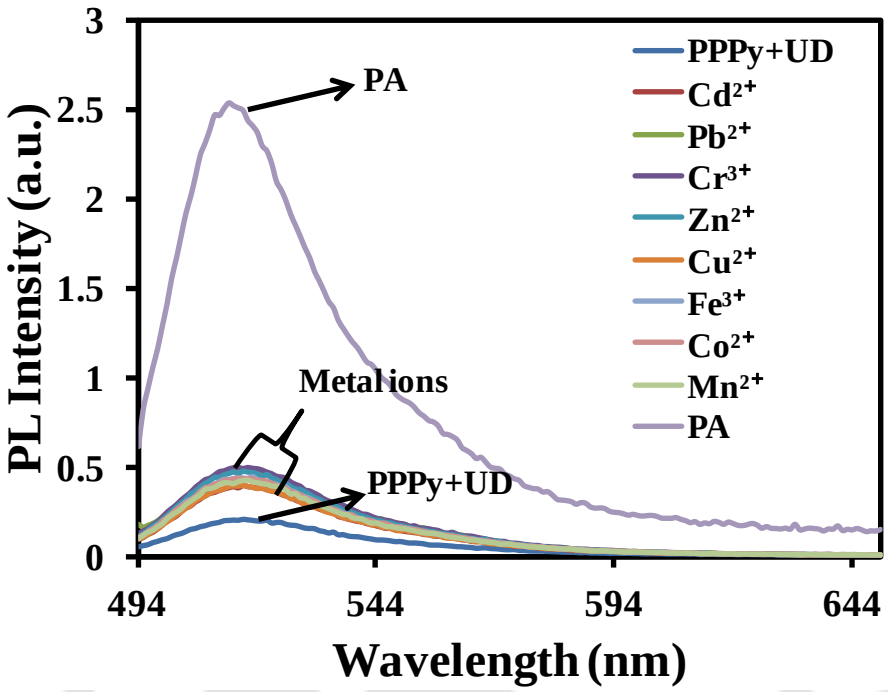

Figure A3.12. Change in Photoluminescence spectrum of UD (6.6 µM) and PPPy (16.6 µM) in the presence of various metal ions (166.6 µM) in HEPES buffer (10 mM, pH-7.0).

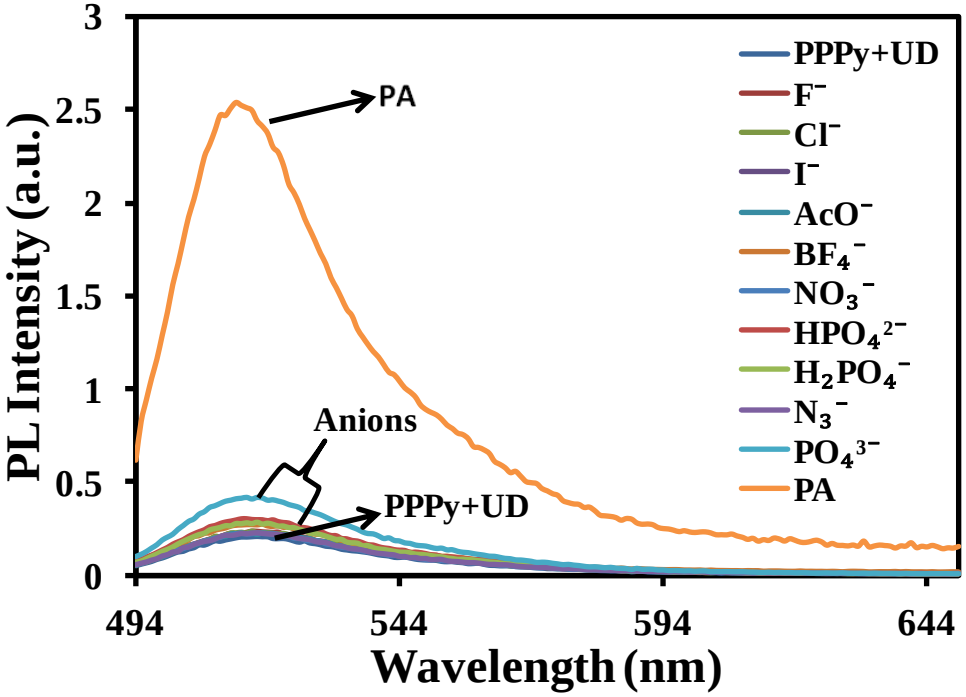

Figure A3.13. Change in Photoluminescence spectrum of UD (6.6 µM) and PPPy (16.6 µM) in the presence of various anions (166.6 µM) in HEPES buffer (10 mM, pH-7.0).

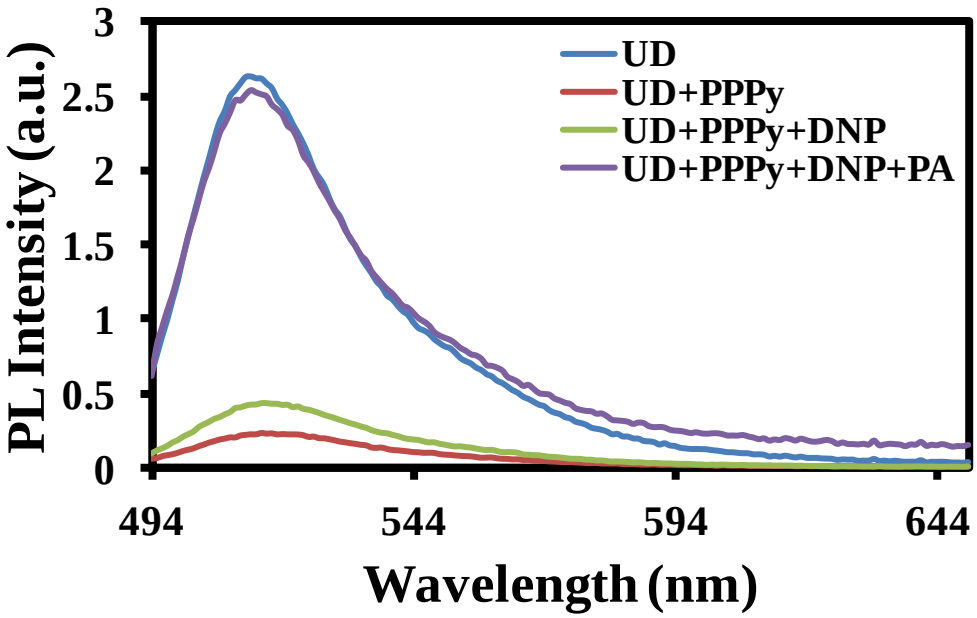

Figure A3.14. Emission spectra of UD (6.6 μM) with PPPy (16.6 μM) followed by addition of 2,4-DNP (166.6 μM) and PA (166.6 μM) in HEPES buffer (pH-7.0, 10 mM).

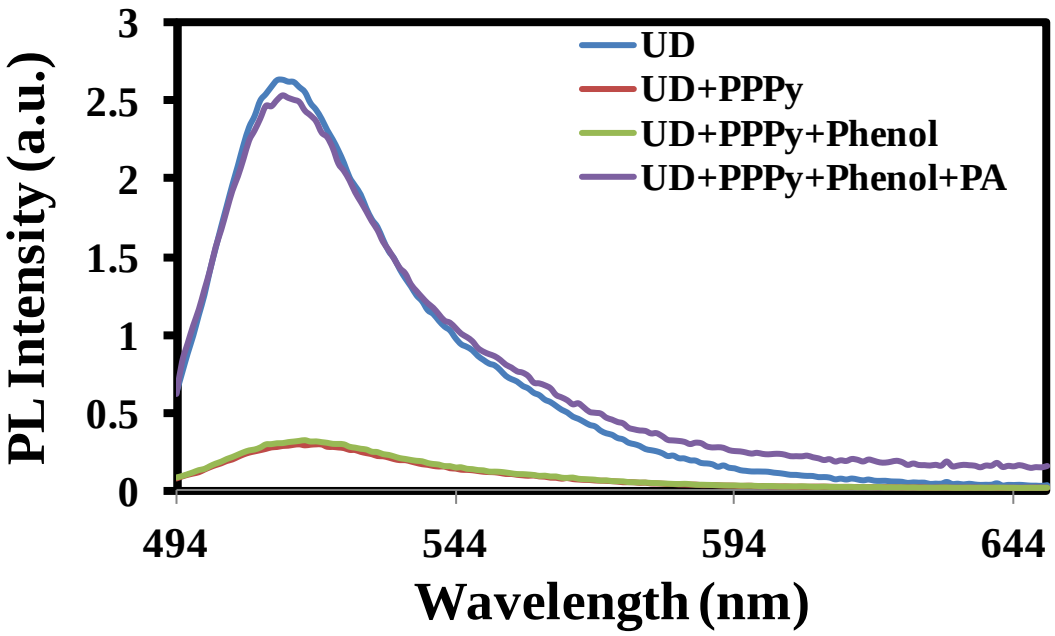

Figure A3.15. Emission spectra of UD (6.6 μM) with PPPy (16.6 μM) followed by addition of phenol (166.6 μM) and PA (166.6 μM) in HEPES buffer (pH-7.0, 10 mM).

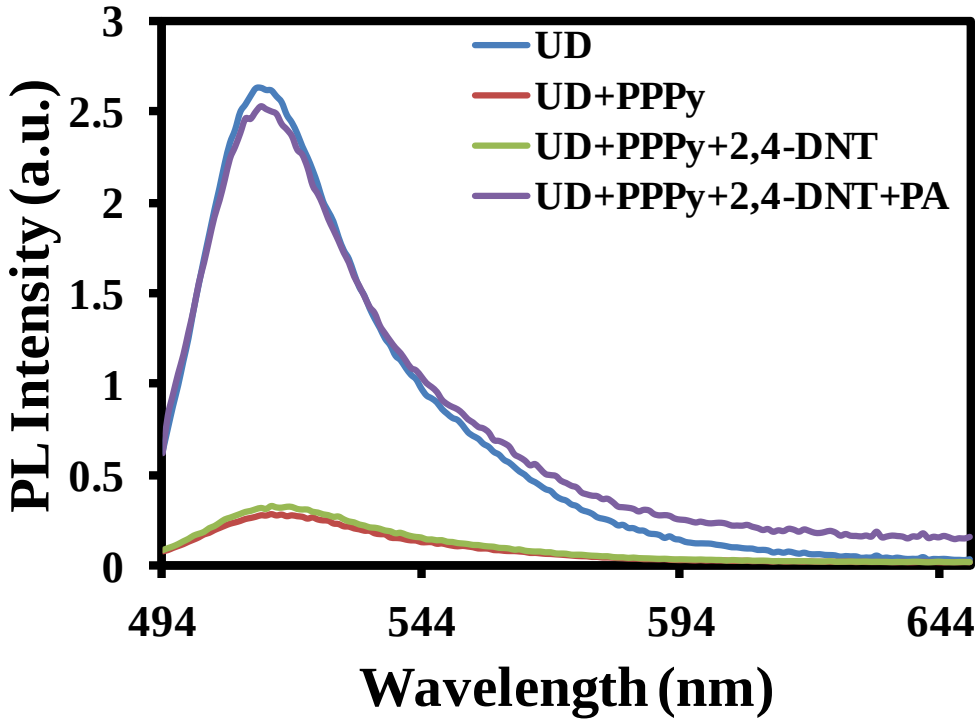

Figure A3.16. Emission spectra of UD (6.6 µM) with PPPy (16.6 µM) followed by addition of 2, 4- DNT (166.6 µM) and PA (166.6 µM) in HEPES buffer (pH-7.0, 10 mM).

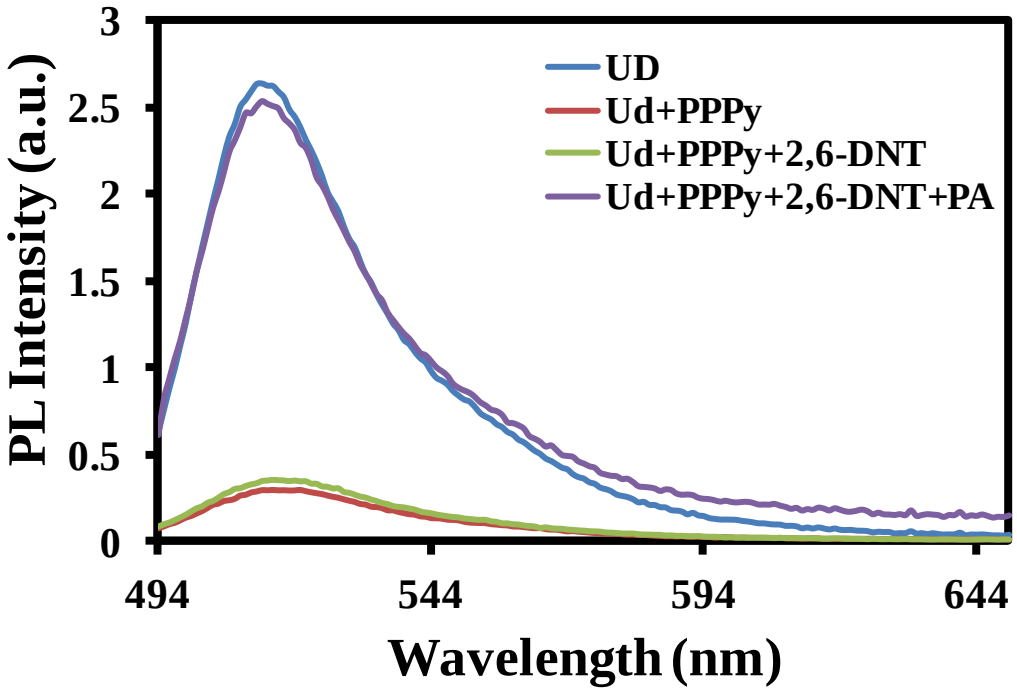

Figure A3.17. Emission spectra of UD (6.6 µM) with PPPy (16.6 µM) followed by addition of 2, 6- DNT (166.6 µM) and PA (166.6 µM) in HEPES buffer (pH-7.0, 10 mM).

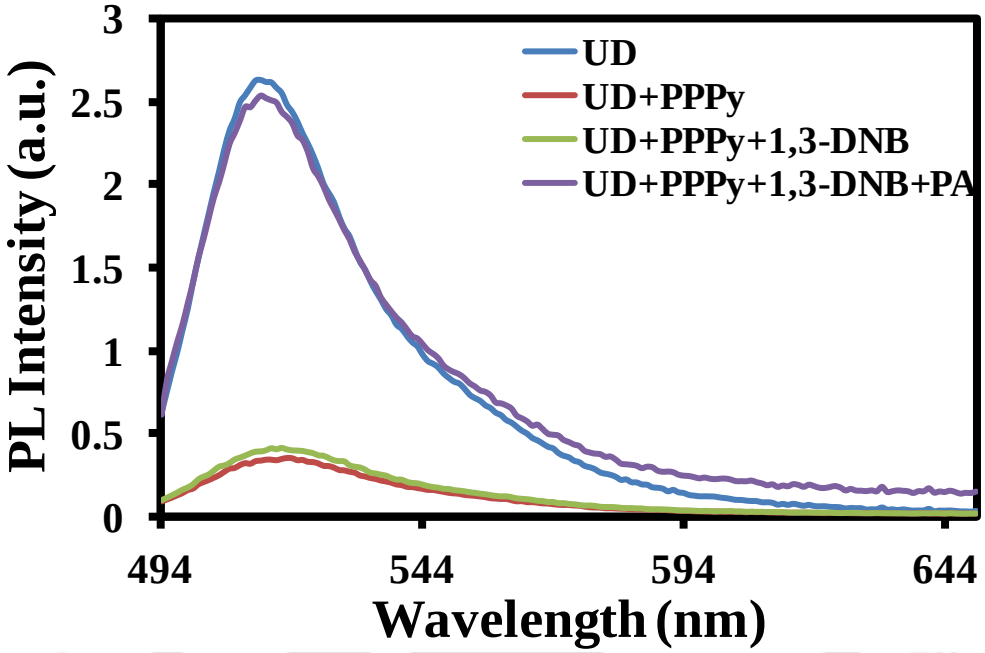

Figure A3.18. Emission spectra of UD (6.6 μM) with PPPy (16.6 μM) followed by addition of 1,3- DNB (166.6 μM) and PA (166.6 μM) in HEPES buffer (pH-7.0, 10 mM).

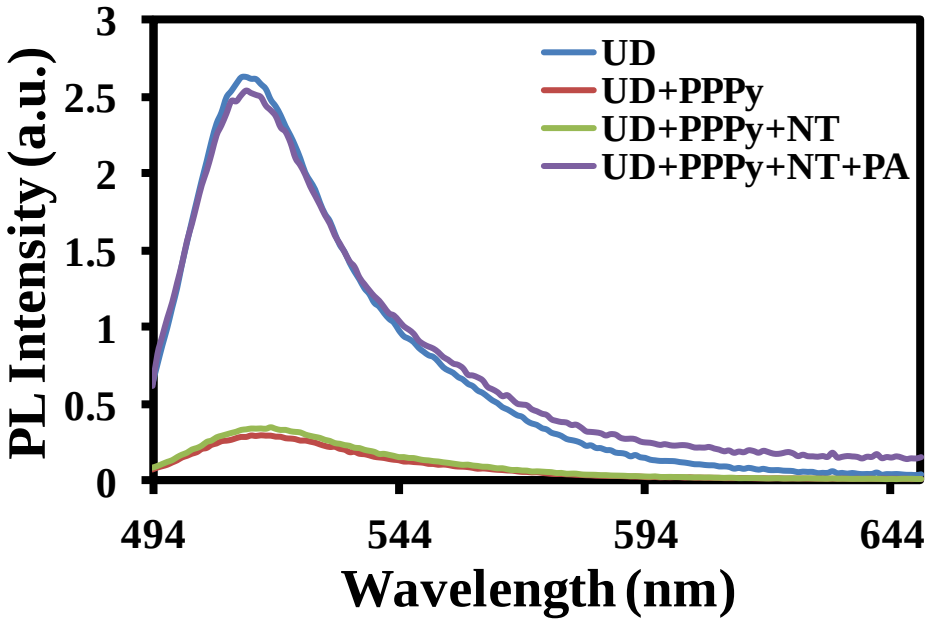

Figure A3.19. Emission spectra of UD (6.6 μM) with PPPy (16.6 μM) followed by addition of NT (166.6 μM) and PA (166.6 μM) in HEPES buffer (pH-7.0, 10 mM).

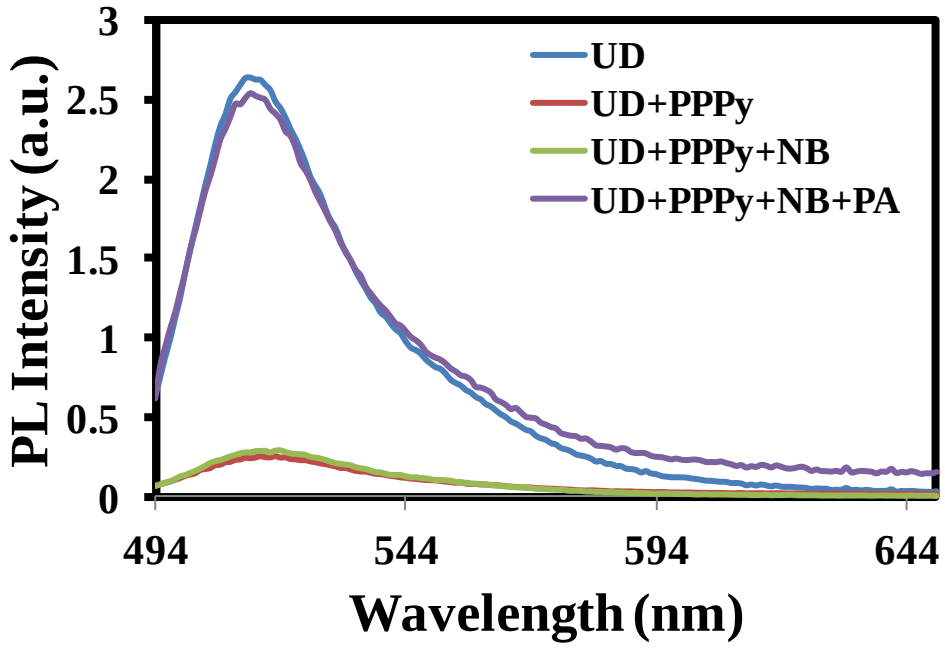

Figure A3.20. Emission spectra of UD (6.6 µM) with PPPy (16.6 µM) followed by addition of NB (166.6 µM) and PA (166.6 µM) in HEPES buffer (pH-7.0, 10 mM).

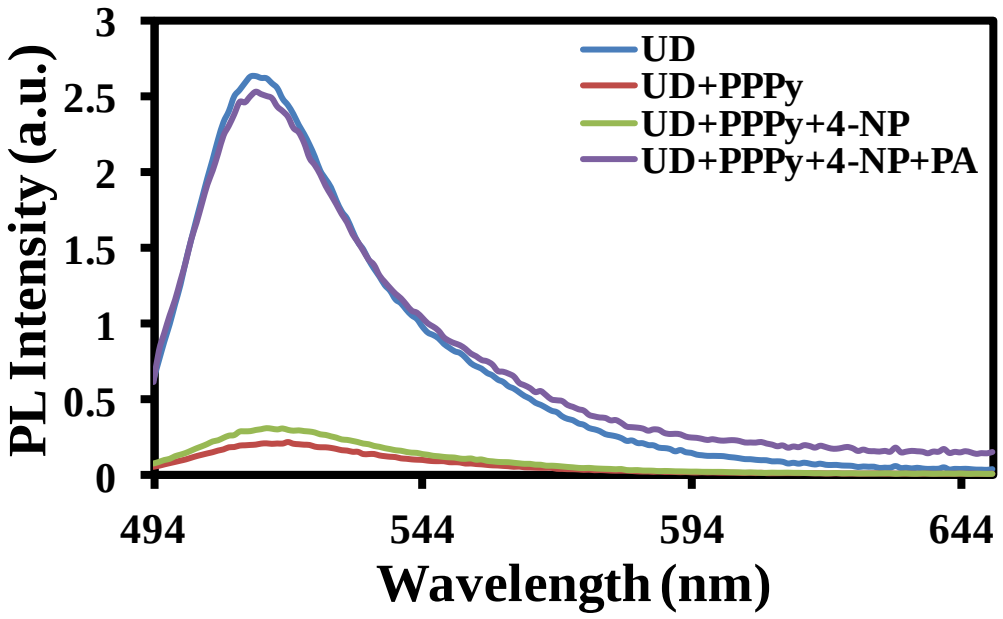

Figure A3.21. Emission spectra of UD (6.6 µM) with PPPy (16.6 µM) followed by addition of 4-NP (166.6 µM) and PA (166.6 µM) in HEPES buffer (pH-7.0, 10 mM).

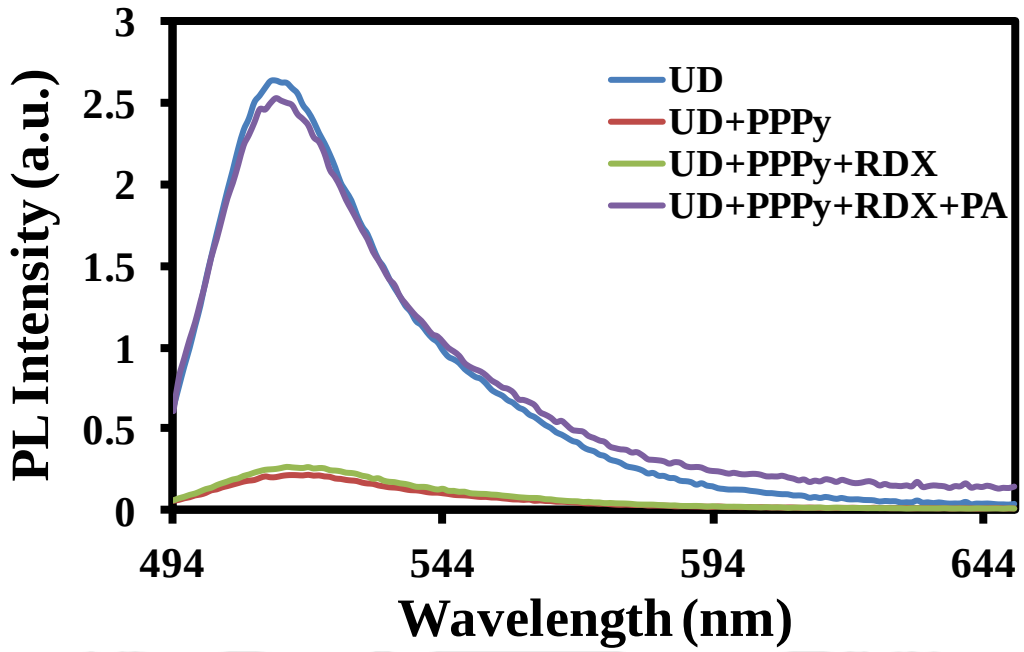

Figure A3.22. Emission spectra of UD (6.6 μM) with PPPy (16.6 μM) followed by addition of RDX (166.6 μM) and PA (166.6 μM) in HEPES buffer (pH-7.0, 10 mM).

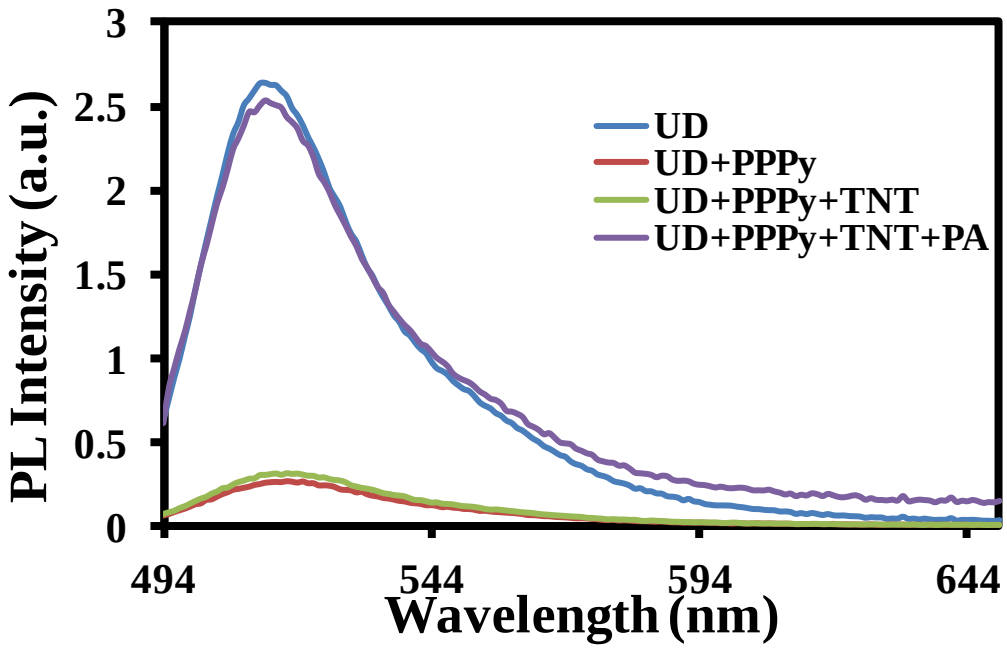

Figure A3.23. Emission spectra of UD (6.6 μM) with PPPy (16.6 μM) followed by addition of TNT (166.6 μM) and PA (166.6 μM) in HEPES buffer (pH-7.0, 10 mM).

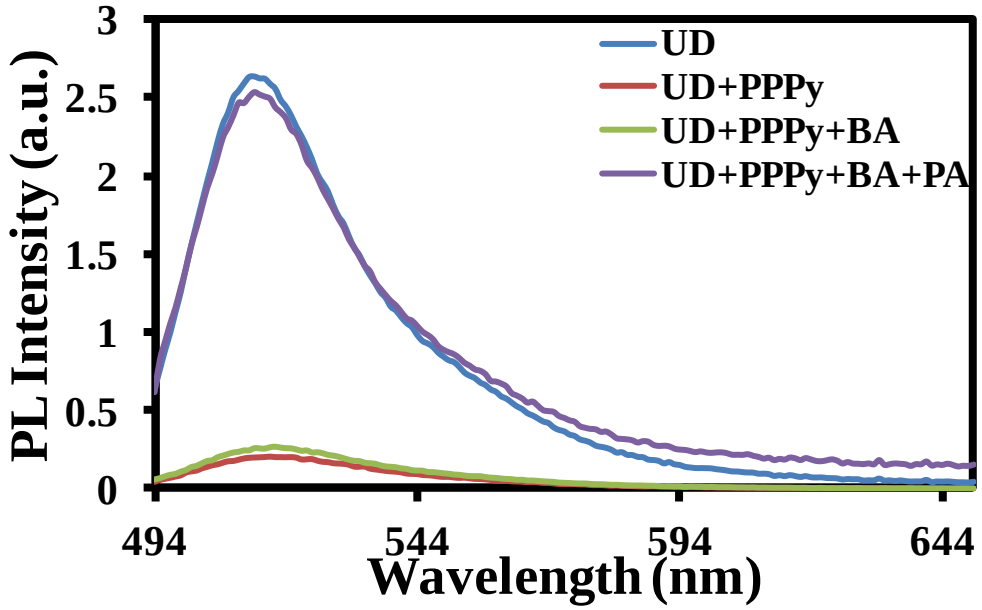

Figure A3.24. Emission spectra of UD (6.6 μM) with PPPy (16.6 μM) followed by addition of BA (166.6 μM) and PA (166.6 μM) in HEPES buffer (pH-7.0, 10 mM).

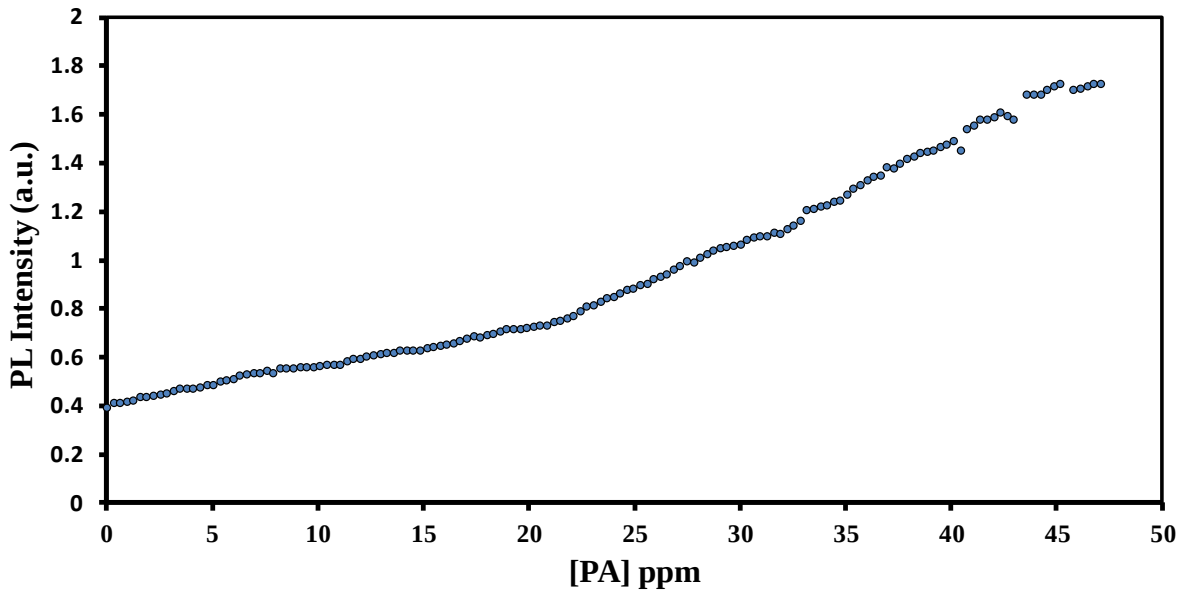

Figure A3.25. Fluorescence intensity of PPPy (16.6×10^{-6} M) and UD (6.6×10^{-6} M) complex at 513 nm with increasing concentration of PA vapors in water buffered with HEPES (pH=7.0, 0.01 M).

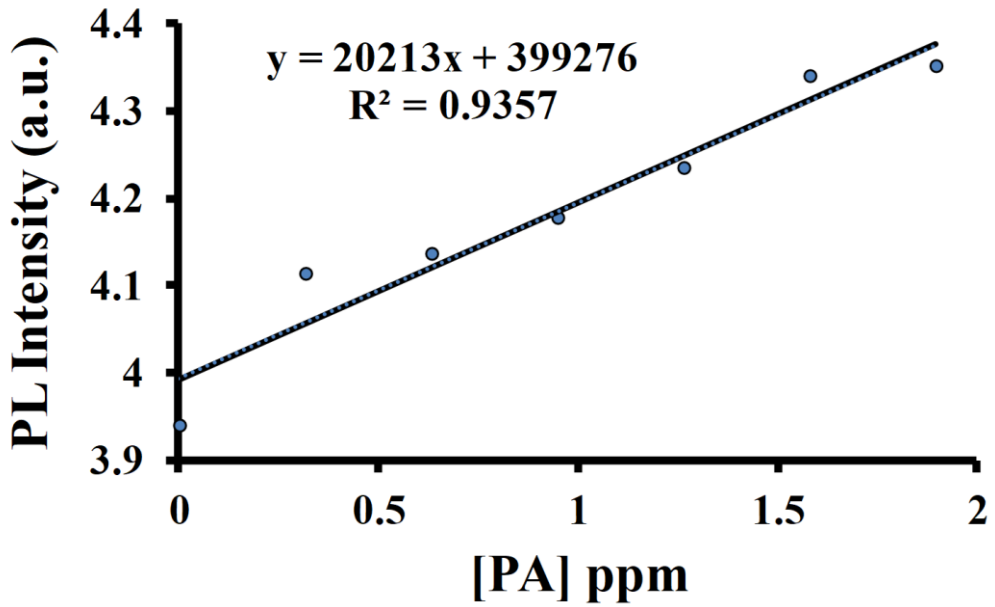

Figure A3.26. Fluorescence intensity of PPPy (16.6 μM) and UD (6.6 μM) in HEPES buffer (pH= 7.0, 10 mM) with increasing concentration of PA vapors.

LOD=3 × S.D./k

LOD = 3 × 1485.21 / (20213)

LOD= 0.22 ppm

Chapter 4

Inner Filter Effect and Resonance Energy Transfer Based Attogram Level Detection of Nitroexplosive-Picric Acid Using Dual Emitting Cationic Conjugated Polyfluorene

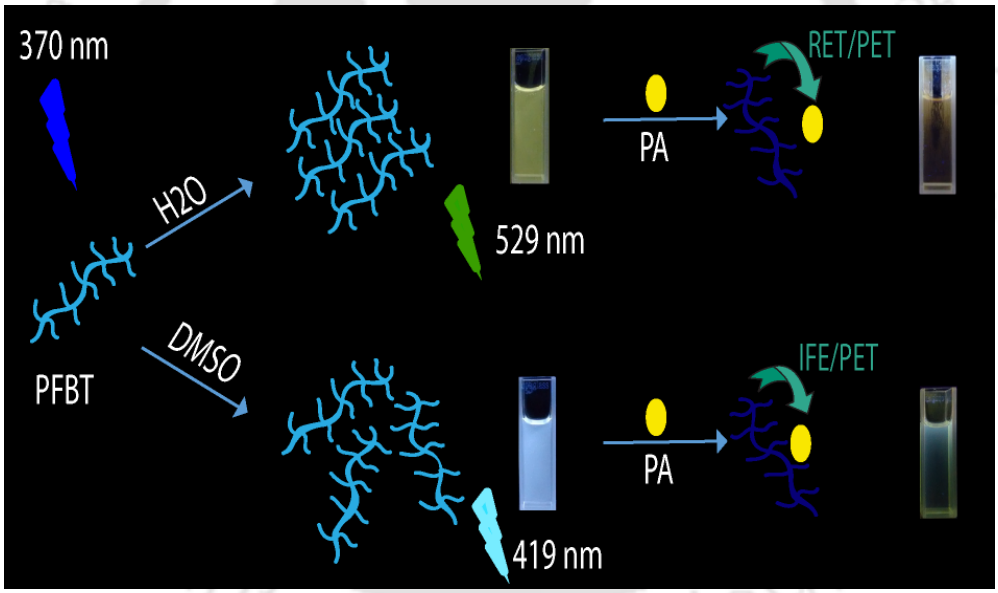

Tanwar, A. S.; Adil, L. R.; Afroz, M. A.; Iyer, P. K. *ACS Sensors* **2018**, *3*, 1451-1461.

Abstract

A new cationic conjugated polyfluorene derivative, poly(3,3'-((9H-fluorene-9,9-diyl)bis(hexane-6,1-diyl))bis(1-methyl-1H-benzo[d][1,2,3]triazol-3-ium)bromide)(PFBT) was synthesized using a simple and inexpensive method of oxidative coupling polymerization. The polymer PFBT displayed dual state emission in DMSO as well as in water, a characteristic phenomenon of polyfluorene homopolymers, and tested for nitroexplosive analytes detection to observe a remarkable fluorescence quenching response for picric acid (PA) in both solvents. The polymer PFBT was found to be highly sensitive and selective towards nitroexplosive PA in both the solvents (DMSO and H_2O) with exceptional quenching constant values of 2.69×10^4 M^{-1} and 2.18×10^5 M^{-1} and a very low detection limit of 92.7 nM (21.23 ppb) and 0.19 nM (43.53 ppt) in respective solvents. Furthermore, contact mode detection of PA was also accomplished using easy, economical and portable fluorescent test strips for on-site detection, which can detect upto 0.22 attogram level of PA. Vapor phase detection of PA was also established, which can detect up to 42.6 ppb level of PA vapors. Interestingly, the mechanism of sensing in DMSO solvent was attributed to strong inner filter effect (IFE) and photo induced electron transfer (PET), while in H_2O the sensing occurs via possible resonance energy transfer (RET) and photoinduced electron transfer (PET), which is exceptional and not reported earlier for a single probe.

4.1 Introduction

The development of high energy nitroexplosive sensing probes are in huge demand.[1-3] Picric acid (PA) is a well-known nitroaromatic explosive since world war I and possesses high energy content even superior to that of 2,4,6-trinitrotoluene (TNT).[4] Due to the high solubility of PA in water and its extensive application in the dye industries, pharmaceuticals, fireworks, chemical laboratories, and match box industries, it contaminates soil and natural water and therefore causes several serious health hazards like sycosis, cancer, damage to respiratory organs, abnormal liver functions and kidney failure.[5-7] Moreover, PA is converted to picramic acid during metabolism, which possess very high mutagenic activity in higher proportions than PA itself.[8] Additionally, because of the similar electron deficient nature of other nitroexplosives, especially TNT, it often interferes in the selective sensing of PA in presence of other competing nitroexplosive. Therefore, it turns out to be very vital and a challenging task to develop a method for highly sensitive and selective detection of PA with respect to homeland security and environment pollution.

There are many reports available on nitroexplosive detection based on various analytical techniques viz. high performance liquid chromatography,[9] surface enhance raman spectroscopy,[10] dynamic light scattering,[11] solid phase microextraction-ion mobility spectroscopy,[12] enzyme linked immunosorbent assay,[13] and electrochemical methods etc.[14] but these techniques have some disadvantages such as most of them are expensive, time consuming and less sensitive, complex to handle for on-site detection and thus unsuitable for hands-on use. In contrast, fluorescent probes based nitroexplosive sensing has attracted remarkable attention due to its simplicity, swift response time, noteworthy sensitivity, and capability of sensing in both solution as well as in solid state.[2,15] Therefore, researchers have created various fluorescence based probes such as quantum dots, organic molecule dyes, metal complexes, metal organic frameworks, nanoaggregates and conjugated polymers (CPs) for the nitroexplosive detection.[16-33] Nevertheless, these fluorescent probes have some limitations like poor sensitivity and selectivity, difficult to use for on-site detection purposes, vapor phase and utilization of organic medium for sensing. In addition, mechanism of fluorescence quenching for nitroexplosive detection has been reported earlier majorly based on either resonance energy transfer (RET) and/or electron transfer processes, ground state complex formation, inner filter effect (IFE) and indicator displacement assay (IDA).[32,34-37] However, less

attention has been paid for designing a probe with likely multiple sensing mechanisms and their elucidation. Hence, development of an efficient probe for PA detection with high selectivity and ultra-sensitivity in an aqueous, organic and solid state as well as in vapor phase is highly desirable and challenging.

CPs are forefront among various materials used in the area of sensing.[38-42] They possess excellent light harvesting properties and due to the 'molecular wire effect' an amplified fluorescence signal response is achieved making them highly sensitive toward analytes.[40] Recently, few reports appeared for nitroexplosive detection based on CP probes, yet sensitivity, selectivity and applicability in water can be improved by choosing an efficient receptor.[21,43-52] Hence, signal amplifying nature of CP sensors for the detection of nitroaromatic explosives with desirable receptor units, which offer high selectivity and extraordinary sensitivity to the CPs remains challenging. Previously, two cationic CPs for the sensitive detection of PA based on ground state charge transfer complexation and RET mechanisms were reported.[34,35] To further advance the overall sensing parameters it is necessary to explore new and alternate possible fluorescence mechanisms by designing better sensor probes. To realize this, methylbenzotriazolium appended cationic CP PFBT [poly(3,3'-((9H-fluorene-9,9-diyl)bis(hexane-6,1-diyl))bis(1-methyl-1H-benzo[d][1,2,3] triazol-3-ium)bromide)] for the specific and fluorescence amplifying detection of PA at ultra-low level was synthesized. Interestingly, the detection of PA in DMSO solvent is based on strong inner filter effect (IFE) assisted by PET while in water buffered with HEPES (pH-7.0, 10 mM) it is based on RET assisted by PET. To the best of our knowledge, no previous reports exist where a single probe detects PA based on both RET and IFE mechanisms, acting independently, in different solvents with high sensitivity and on multiple platforms, making PBFT a very unique probe for PA detection at such low levels. Moreover, detection of PA in very low levels in vapor phase was also possible with this probe.

4.2 Experimental

4.2.1 Materials and Measurements

PA was obtained from Loba Chemie Pvt. Ltd. Nitroaromatic compounds namely, 4-nitrotoluene (4-NT), 2,4-dinitrotoluene (2,4-DNT), 2,6-dinitrotoluene (2,6-DNT), 1,3-dinitrobenzene (1,3-DNB) and HEPES buffer were obtained from Sigma-Aldrich Chemicals. Research department explosive (RDX) and TNT were purchased from AccuStandard and used as received. Other compounds were obtained from Alfa-Aesar or

Merck and used without extra purification. All the sensing experiments and aqueous stock solution were prepared using Milli-Q water. ^{1}H NMR (600 and 400 MHz) and ^{13}C NMR (150 and 100 MHz) spectra were recorded on Varian-AS400 NMR spectrometer and Bruker Ascend 600 spectrometer respectively. Absorption spectra were obtained from Perkin Elmer Lambda-25 spectrophotometer. Photoluminescence spectra were obtained from Horiba Fluoromax-4 spectrofluorometer using quartz cuvettes of 10 mm path length keeping 3 nm of slit width at 298 K. Edinburg Life Spec II instrument was utilized for execution of time-resolved fluorescence studies. Gel Permeable Chromatography was carried out in THF using polystyrene as standard. Cyclic voltammogram was obtained by means of CH instruments Model 700D series Electrocchemical workstation. Whatman qualitative filter paper grade 1 was used to prepare portable fluorescent test strips.

4.2.2 Synthetic Procedure

4.2.2a Synthesis of 1-methyl-1H-benzo[d][1,2,3]triazole:

To a solution of benzotriazole (357 mg, 3 mmol) in DMF (10 mL), fine powder of NaOH (480 mg, 12 mmol) and methyl iodide (187 µL, 3 mmol) were added and mixed for 1 h at room temperature. After that it was decanted into water and extracted with chloroform. The chloroform layer was washed with water and dried over sodium sulfate (anhydrous). The crude product was obtained after concentrating the chloroform, which was purified by column chromatography over silica gel (Ethyl acetate: Hexane 1:9). (Yield = 60%). ^{1}H NMR ($CDCl_3$, 400 MHz, δ ppm): 8.07 (d, 1H), 7.52 (q, 2H), 7.40 (m, 1H), 4.31 (s, 3H). ^{13}C NMR ($CDCl_3$, 100 MHz, δ ppm): 145.83, 133.42, 127.24, 123.80, 119.70, 109.20, 34.16. MS (ESI): calculated for $C_7H_7N_3$ $[M+H]^+$: 134.0718; Found 134.0737.

4.2.2b Synthesis of 9,9-bis(6-bromohexyl)-9H-fluorene (M2):

Synthesis of monomer (M2) was carried out by previously established method.[53] In a 50 mL RBF, fluorene (1 g, 6.016 mmol), aqueous NaOH (50%) and tertabutyl ammonium iodide (TBAI) (0.476 g, 1.203 mmol) were taken. The flask was purged with argon gas and degassed using freeze-thaw cycles followed by addition of 1,6-dibromohexane (6.47 mL, 42.112 mmol). It was kept under stirring for 4 h at 70 °C. After completion of reaction, temperature was lowered to 25 °C and then extracted with chloroform followed by washing with water thrice. Thereafter, it was dried via sodium sulfate (anhydrous) and concentrated under low pressure to get crude product. Further purification of crude product was done over a silica gel pad via column chromatography technique taking hexane as eluent to yield the desired product. (Yield = 82 %, 2.4 g). ^{1}H NMR (400MHz,

$CDCl_3$, δ ppm): 7.32 (m, 6H), 7.71 (d, 2H), 3.27 (t, 4H), 1.63 (m, 4H), 1.97 (t, 4H), 1.06 (m, 4H), 1.16 (m, 4H), 0.60 (m, 4H). ^{13}C NMR (150MHz, CDCl3, δ ppm): 150.45, 141.28, 127.27, 127.01, 122.92, 119.89, 55.07, 40.40, 34.12, 32.81, 29.23, 27.93, 23.68.

4.2.2c Synthesis of poly(9,9-bis(6-bromohexyl)-9H-fluorene) (PF):

To a three necked round bottom flask, containing dissolved anhydrous ferric chloride (1.4 g, 8.124 mmol) in 15 mL of nitrobenzene fitted with argon inlet. A solution of 9,9-bis(6-bromohexyl)-9H-fluorene (1 g, 2.031 mmol) in 10 mL of nitrobenzene was then added slowly to the above round bottom flask using a syringe. The reaction mixture was kept under stirring for 36 h at room temperature followed by precipitation with methanol. The precipitates were dissolved in chloroform, reprecipitated from methanol, centrifuged and filtered (repeated thrice). Finally, it was dried under low pressure to obtain brown colored polymer. (Yield = 50 %, 49 mg). ^1H NMR (400 MHz, CDCl3, δ ppm): 7.70 (br), 7.86 (br), 7.33 (br), 2.08 (br), 3.30 (br), 1.69 (br), 1.18 (br), 1.27 (br), 0.73 (br). GPC using polystyrene as standard in THF: Mw =2.41 × 10^4, PDI=3.6.

4.2.2d Synthesis of poly(3,3'-((9H-fluorene-9,9-diyl)bis(hexane-6,1-diyl))bis(1-methyl-1H-benzo[d][1,2,3]triazol-3-ium) bromide) (PFBT):

Polymer PF (40 mg, 8.124 mmol) and 1-methyl-1H-benzo[d][1,2,3]triazole (108 mg, 81.24 mmol) was solubilized in 5 mL of dry DMF and 2 mL of dry THF. The reaction mixture was stirred for 24 h at 70 °C under inert atmosphere and then decanted into excess diethyl ether and stirred further to obtain precipitates. The precipitates were further washed thrice with chloroform filtered out and dried under vacuum to obtain brown polymer (PFBT). (Yield = 75%, 46 mg). ^1H NMR (600MHz, DMSO-d6, δ ppm): 8.32 (br), 8.14 (br), 7.97 (br), 7.87 (br), 7.79 (br), 7.48 (br), 7.36 (br), 4.54 (br), 3.95 (br), 2.89 (br), 2.08 (br), 1.37 (br), 1.10 (br), 0.66 (br).

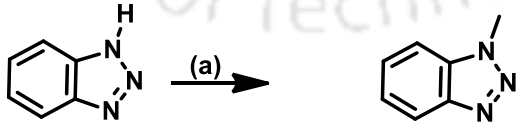

1-methyl-1*H*-benzo[*d*][1,2,3]triazole

Scheme 4.1 Synthesis of the 1-methyl-1H-benzo[d][1,2,3]triazole. (a) MeI, NaOH, DMF, rt, 1 h.

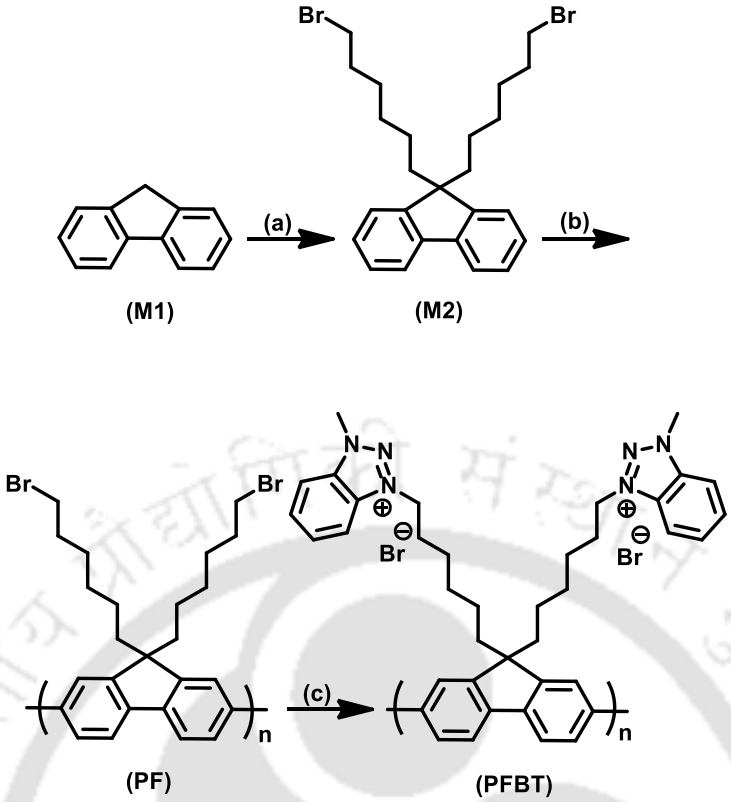

Scheme 4.2 Synthesis of the polymer-PFBT. (a) 50% NaOH(aq.), 1,6-dibromohexane, TBAI, 70°C, 4h. (b) $FeCl_3$, nitrobenzene, rt, 36 hr (c) 1-methyl-1H-benzo[d][1,2,3]triazole, DMF, THF, 70 °C, 24 h

4.2.3 Stock solutions for sensing studies

Stock solution of the polymer PFBT was prepared in DMSO solvent at a concentration of 1×10^{-3} M. Stock solution of various nitroaromatic compounds, namely, phenol, nitromethane (NM), nitrobenzene (NB), 4-nitrophenol (4-NP), 2,4-dinitrophenol (2,4-DNP) were prepared at concentrations of 1×10^{-3} M in MilliQ water. Stock solution of other nitroaromatics viz. 1,3-DNB, 2,4-DNT, 4-NT, 2,6-DNT were prepared in HPLC grade THF at concentrations of 1×10^{-2} M. RDX and TNT solutions were prepared in 1:1 MeOH:CH_3CN at concentration of 1×10^{-2} M. The absorption and fluorescence spectra of the Polymer PFBT with different nitroaromatic compounds were carried out in 3 mL of DMSO and water buffered with HEPES (10 mM, pH-7.0) having 3.3×10^{-6} M of PFBT in a 10 mm path length quartz cuvette.

4.2.4 UV-vis absorption spectrum of PFBT in DMSO:H_2O ratio

The UV-vis spectra of PFBT was studied under two different DMSO:H2O ratios. The isolated polymer-PFBT absorption band at 370 nm in DMSO:H2O (100:0) ratio is red shifted by 8 nm up to 378 nm in DMSO:H2O (0:100) ratio (Figure A4.1). This red shift

in the UV-vis absorption band can be interpreted as a result of J-type aggregation by non-covalent interactions between intermolecular polymer chains.[54-55]

4.2.5 Time-resolved decay measurements

Lifetime decay measurements of PFBT (3.3×10^{-6} M) in the presence and absence of PA (93.3×10^{-5} M) were carried out using pulse excitation of 375 nm and emission at 419 nm in DMSO. Similarly, Lifetime decay measurements of PFBT (3.3×10^{-6} M) in the presence and absence of PA (26.6×10^{-5} M) were carried out using pulse excitation of 375 nm and emission at 529 nm in aqueous medium buffered with HEPES (pH- 7.0, 10 mM). The curves were fitted bi-exponentially and average lifetime was considered for consistency in results (Table A4.1-A4.2).

4.2.6 Preparation of paper strips

Whatman filter paper (70 mm diameter) was taken and dipped into the solution of PFBT (3.3×10^{-6} M) in DMSO and dried to get fluorescent paper strip. The PFBT coated filter paper was then cut into desired number of pieces and size (1 cm × 1 cm) and used for portable surface sensing purposes.

4.2.7 Photoluminescence quantum yield

Quantum yields were measured using absolute fluorescent quantum yield via the integrating sphere method using an Edinburgh FLS980 fluorescence spectrometer.

4.2.8 Method used for detection limit calculation

For calculating detection limit in DMSO solvent, various samples of polymer PFBT (3.3×10^{-6} M) each having PA (0.33×10^{-6} M, 0.66×10^{-6} M, 1.0×10^{-6} M, 1.33×10^{-6} M, 1.66×10^{-6} M, 2.0×10^{-6} M) were taken separately and later photoluminescence spectrum was obtained for respective solution keeping the same excitation wavelength i.e. 370 nm. A regression equation was obtained from the calibration curve between emission maxima and concentration of PA. Limit of detection (LOD) was then calculated from the calibration plot using the equation $3\sigma/k$, where σ denotes standard deviation (SD) for the emission intensity of PFBT solution in the absence of PA and K denotes the slope of calibration curve. In a similar manner, LOD was determined in water medium, where different samples of PFBT (3.3×10^{-6} M) having different concentration of PA (0.0 M, 0.3×10^{-9} M, 0.6×10^{-9} M, 1.0×10^{-9} M, 1.3×10^{-9} M) were utilized to get the calibration curve between emission intensity and PA concentration. Using the equation $3\sigma/k$, LOD

was calculated for aqueous medium where σ designates standard deviation for PFBT solution intensity in the absence of PA and K denotes slope of the calibration curve.

4.2.9 Cyclic voltammetry studies

The cyclic voltammogram for PFBT was recorded using three-electrode cell with a saturated $Ag/AgNO_3$ electrode as a reference electrode platinum wire as a counter electrode and glassy carbon as working electrode. All these measurements were done under inert atmosphere at room temperature. Tertabutylammoniumhexafluorophosphate ($TBAPF_6$) (0.1 M) in CH_3CN was taken as supporting electrolyte and Fc^+/Fc couple was employed as internal reference. HOMO level of PFBT was calculated to be - 5.56 eV via onset method [E_{HOMO} = -(E(onset,ox vs F_c^+/F_c) + 4.8) (eV)]. Band gap of PFBT was determined from the onset of UV-vis spectrum of PFBT and finally LUMO level of PFBT was calculated to be - 2.65 eV.

4.2.10 Overlap integral value and Förster distance calculations

Overlap integral value determines the extent of energy transfer between the PFBT and PA. It was calculated by the using the below equation[35]

$$J(\lambda) = \int_0^\infty F_D(\lambda)\,\varepsilon_A(\lambda)\lambda^4 d\lambda$$

Where, J(λ) represents the overlap integral value, FD (λ) denotes corrected fluorescence intensity of PFBT from λ to Δλ with total intensity normalized to unity, ε_A denotes molar absorptivity of the acceptor (PA) at λ in $M^{-1}cm^{-1}$.Förster distance (R_0) was calculated by using the equation given below:

$$R_0 = 0.211[(J)Q(\eta^{-4})(k^2)]^{1/6}$$

where, J denotes the extent of spectral overlap between the emission spectrum of donor (PFBT) and absorption spectrum of acceptor (PA), Q represents the photoluminescence quantum yield of PFBT (donor), η denotes refractive index of the medium and k^2 signifies dipole orientation factor (generally considered as 0.667).

4.2.11 Calculations of inner filter effect correction

The role of IFE in the suppression of the fluorescence of PFBT can be calculated by using the below equation for a 1 cm size of cuvette.[56]

$$I_{corr}/I_{obs} = 10^{(Aex+Aem)/2}$$

Where, I_{corr} and I_{obs} are the fluorescence intensity before and after the IFE correction. A_{em} and A_{ex} are the UV-vis absorption value of the fluorophore (PFBT) having analytes (PA) at emission maxima and excitation wavelengths.

4.2.12 Vapor phase sensing

100 mg of the anhydrous PA was taken in an airtight flask, kept for two days at room temperature, maintained at 30 °C for 30 minutes before each titration so that the air inside the flask reached complete saturation level with the PA vapors. The integrated form of Clausius-Clayperon equation ($\log_{10} P = A-B/T$) was used to calculate the vapor pressure (P) of PA. Here, P represents the vapor pressure of PA, A and B are two conventionally used fitting parameters, and T corresponds to temperature. Furthermore, amount of PA vapors in ppm was calculated using the following equation: saturation concentration (ppm) = P (mmHg) / 760 mmHg × 10^6, where P denotes the vapor pressure of PA. The amount of PA vapors was maintained constant (101.64 ppb, 2.5 mL) for purging through fluorescence cuvette using an air-tight syringe.

4.3 Result and Discussion

4.3.1 Synthesis and characterization of PFBT

Synthetic pathway to precursor polymer poly(9,9-bis(6-bromohexyl)-9H-fluorene) (PF) and target polymer poly(3,3'-((9H-fluorene-9,9-diyl)bis(hexane-6,1-diyl))bis(1-methyl-1H-benzo[d][1,2,3] triazol-3-ium) bromide) (PFBT) are shown in Scheme 4.2. The monomer and polymers at each step were well characterized and purified before further use (Scheme 4.1, Figures A4.2-A4.8). The molecular weight of the precursor polymer PF was found to be 2.41 × 10^4, PDI= 3.6 in THF using polystyrene as standard. N-methyl benzotriazolium groups attached on to the side chains of PFBT act as specific recognition sites for PA and enhanced their sensing efficiency via electrostatic interactions. The CP PFBT exhibited high solubility in DMSO with a photoluminescence quantum yield (Φs) of 0.81 in DMSO and 0.19 in H_2O. The absorption maxima were observed at 370 nm in DMSO and at 378 nm in H_2O buffered with HEPES (pH= 7.0, 10 mM) (Figure A4.1).

The emission spectra were observed at 419 nm in DMSO and 529 nm in H_2O buffered with HEPES (pH= 7.0, 10 mM), when excited at 370 nm (excitation wavelength). To investigate this unique shift of 110 nm in the emission spectrum from 419 nm to 529 nm in 100% DMSO to 100% H_2O, the fluorescence spectra in various DMSO and water fraction ratios were recorded keeping the fixed concentration of PFBT (3.3 × 10^{-6} M).

When water ratios were increased to 30%, the emission intensity at 419 nm decreases and with further increment in water ratio the peak completely shifts to 529 nm, (Figure A4.9). The emission of new peak at 529 nm in water is due to the spontaneously formed polymer nanoaggregates via fluorene-fluorene non-covalent interaction and leading to aggregation caused quenching (ACQ) red-shifted effect, a unique phenomenon associated with polyfluorene homopolymers.[54,55] This unusual orange emission (huge 110 nm of stokes shift) has been attributed to intermolecular self-assembly behavior or due to J-type of aggregation as evident from UV-Visible spectrum of PFBT and as well as due to the formation of nano objects in aqueous environment.[54,55]

Fluorescence quenching experiments of PFBT were investigated in both mediums i.e. DMSO and water for various nitroexplosives viz. TNT, PA, 2,4-DNT, 2,6-DNT, 1,3-DNB, 4-NT, Phenol, NB, NM and RDX. Interestingly only PA showed significant fluorescence quenching in both these solvents. The concentration of PFBT (3.3×10^{-6} M) was kept constant in both solvents (DMSO and water) and then the quenching experiments were initiated by addition of various nitroexplosives.

4.3.2 Sensing Studies in DMSO

The polymer PFBT showed blue luminescence (419 nm) in dilute solution (3.3×10^{-6} M) under UV light illumination that was visible clearly by naked eyes (Figure A4.10). It was noticed that addition of first 3.3×10^{-6} M PA solution causes immediate fluorescence quenching ~10 %, which further reaches to 92 % on total addition of 93.3×10^{-6} M PA concentration (Figure 4.1a). Fading of blue fluorescence of PFBT in presence of PA under UV light illumination was also clearly visible by naked eyes (Figure A4.11). In order to calculate quenching efficiency of the PFBT in response to the PA concentration in solution, Stern-Volmer (S-V) plot was obtained using the equation ($I_0/I = 1 + K_{sv}[Q]$), where Io represents initial emission intensity devoid of any quencher; I represents the emission intensity after addition of quencher of concentration [Q]; and K_{sv} denotes the Stern-Volmer constant (M^{-1}). The K_{sv} determined through linear fitting of S-V plot was found to be 2.69×10^4 M^{-1} (inset of Figure 4.1a) signifying high sensitivity of PFBT for PA. LOD value for PA was calculated using standard method reported,[34] and found to be 92.7 nM (Figure A4.12).

4.3.3 Selectivity studies in DMSO

To investigate the selectivity of PFBT towards PA, various interfering analytes viz. TNT, RDX, 2,4-DNT, 2,6-DNT, 1,3-DNB, 4-NT, NM, NB and phenol were tested under the

same experimental conditions. As shown in Figure 4.1b, no substantial changes in the fluorescence quenching of PFBT was witnessed in presence of these interfering analytes. The Stern-Volmer plots for all these nitroexplosives were also obtained (Figure 4.1c). It could be observed clearly that at lower concentration of PA, S-V plot follows a linear nature, however, at higher concentration the curve rises exponentially. This non-linear nature of S-V curve signifies the amplified quenching in case of CP and may be liable for the singlet exciton migration within the polymer chains, self-absorption, or an additional energy transfer process. On the other hand, S-V plot remains linear for all other analytes confirming the absence of above phenomenon. Significantly higher value of K_{sv} was found for PA as compared to other nitroexplosives, indicating amplified quenching and remarkable selectivity. Furthermore, other inorganic ions (Cr^{3+} ,Cu^{2+}, Cd^{2+}, Hg^{2+}, Fe^{3+}, Co^{3+}, Zn^{2+}, Ag^{+}, Pb^{2+}, Mn^{2+}, Al^{3+}, Ni^{2+}, HCO_3^-, SO_4^{2-}, NO_3^-, S^{2-}, BF_4^-, CN^-, CO_3^{2-} ,I^-, F^-, Cl^- , PO_4^{3-}, $H_2PO_4^-$) that may be present in natural water samples did not show any interference with the fluorescence of PFBT (Figure A4.13), suggesting exclusive selectivity of PFBT towards PA and feasibility of this system for practical application in natural contaminated water.

4.3.4 Sensing in Competitive Environment

The specific recognition of PA in the occurrence with different nitroaromatic compounds is highly desirable for realistic application of this platform. All other nitroaromatic compounds possess similar electron deficient nature like PA and their presence may affect the sensitivity of PFBT and compete with PA, hence detection of PA in presence of different nitroexplosives remains challenging. To validate the selectivity of PFBT system, various photoluminescence titration experiments were conducted in the presence of these interfering nitroaromatic compounds. Initially, fluorescence spectrum of PFBT (3.3×10^{-6} M) was recorded and to the above, a solution of TNT (93.3×10^{-6} M) was added initially so that TNT molecules could attain maximum binding sites of the polymer, however addition of TNT resulted in no significant change in fluorescence intensity (Figure A4.14). After that, solution of PA (93.3×10^{-6} M) was added to the above mixture i.e. (PFBT+TNT), which resulted in significant quenching of fluorescence. Similar experiments were repeated with other analytes and the results obtained were quite similar to above case with almost no change in the quenching efficiency of PA (Figure 4.1d and Figure A4.15-A4.22).

4.3.5 Sensing Studies in Aqueous Medium

The polymer PFBT emits orange fluorescence (529 nm) in dilute solution (3.3×10^{-6} M) under UV light illumination that was visible clearly by naked eyes (Figure A4.10). It was also noticed that cationic CP PFBT is very sensitive to the PA in aqueous medium as compared in DMSO solvent. Initial addition of just 3.3×10^{-6} M PA solution causes immediate fluorescence quenching ~48 %, which further reaches 86 % on total addition of 26.6×10^{-6} M PA concentration (Figure 4.2a). The orange color is vanished in presence of PA and clearly visible under UV light illumination (Figure A4.11). In the same manner as observed with DMSO solvent, quenching efficiency of PFBT in water (pH-7.0, 10 mM, HEPES buffer) showed identical responses to the PA concentration as seen from the slope of S-V plot. The K_{sv} value determined through the linear fitting of S-V plot was found to be 2.18×10^{5} M^{-1} indicating very high sensitivity of PFBT for PA in water (inset of Figure 4.2a). The limit of detection (LOD) value for PA in aqueous medium was calculated using standard method reported, and found to be 0.19 nM (43.53 ppt) (Figure A4.23).

4.3.6 Selectivity studies in Aqueous Medium

To examine the selectivity of PFBT towards PA, various interfering analytes viz. TNT, RDX, 2,4-DNT, 2,6-DNT, 1,3-DNB, 4-NT, NB, phenol and NM were tested under the same experimental conditions. As shown in Figure 4.2b, no substantial change in fluorescence quenching was observed in presence of these interfering analytes. S-V plots for all other nitroexplosive were also obtained in water buffered with HEPES (pH- 7.0, 10 mM) and showed linear nature (Figure 4.2c). This linear nature of S-V curve in aqueous medium indicated the possibility of either static or dynamic type of quenching is happening. Significantly high value of K_{sv} was obtained for PA as compared to other nitroexplosives, indicating remarkable selectivity towards PA. Further, other inorganic ions (Cr^{3+} ,Cu^{2+}, Cd^{2+}, Hg^{2+}, Fe^{3+}, Co^{3+}, Zn^{2+}, Ag^{+}, Pb^{2+}, Mn^{2+}, Al^{3+}, Ni^{2+}, HCO_3^{-}, SO_4^{2-}, NO_3^{-}, S^{2-}, BF_4^{-}, CN^{-}, CO_3^{2-} ,I^{-}, F^{-}, Cl^{-} , PO_4^{3-}, H_2PO^{4-}) that can be present in natural water samples did not show any interference with the fluorescence of PFBT in water (pH-7.0, 10 mM, HEPES buffer) (Figure A4.24), suggesting exclusive selectivity of PFBT toward PA and motivated us to test the feasibility of this system for practical application in natural contaminated water.

4.3.7 Sensing in Competitive Environment

As mentioned in case of DMSO solvent, selectivity of PFBT system was also tested in water (pH-7.0, 10 mM, HEPES buffer) in a competitive environment with other

nitroaromatic compounds. In this case, first PL spectrum of PFBT (3.3×10^{-6} M) was recorded and to this a solution of TNT (26.6×10^{-6} M) was added so that TNT molecules could attain maximum binding sites of polymer. However, no substantial change in PL spectrum was observed after addition of TNT (Figure A4.25). To the same mixture i.e. (PFBT+ TNT), a solution of PA (26.6×10^{-6} M) was added which resulted in significant fluorescence quenching indicating superior recognition of PA by PFBT in presence of interfering analyte like TNT. Similar types of experiments were repeated with other analytes and no variation in results were obtained (Figure 4.2d and Figure A4.26-A4.33) as compared to most other chemosensor systems developed previously for the PA detection that suffer from huge interference. In sight of these studies, PFBT system provides a rapid, reliable and effective platform for PA detection in a competitive environment and irrespective of the solvent medium, which is exceptional.

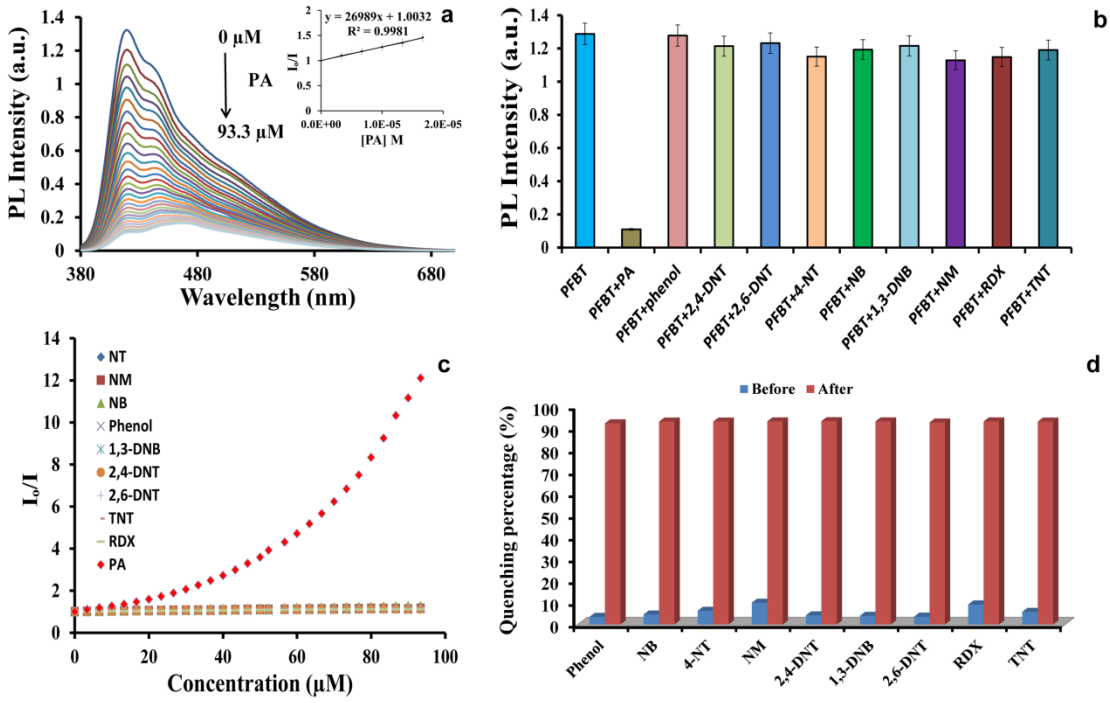

Figure 4.1 (a) PL spectra of PFBT (3.3×10^{-6} M) with various concentrations of PA in DMSO (inset: Stern-Volmer plot for PA). (b) Bar diagram showing effect of other nitroexplosives (93.3×10^{-6} M) on PL intensity of PFBT (3.3×10^{-6} M) (error bars = ±5%). (c) Stern-Volmer plots obtained for various interfering analytes in DMSO. (d) Percentage of quenching by different interfering analytes (93.3×10^{-6} M) before and after addition of 93.3×10^{-6} M PA.

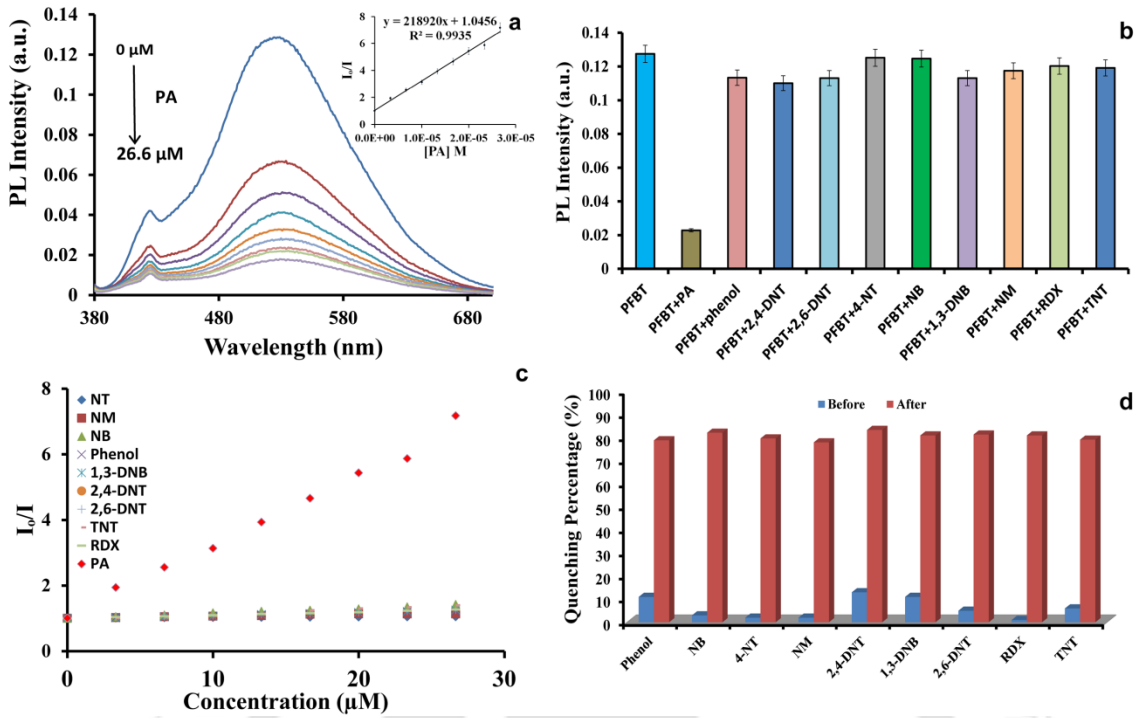

Figure 4.2 (a) PL spectra of PFBT (3.3×10^{-6} M) with various concentrations of PA in water buffered with HEPES (10 mM, pH- 7.0) (inset: Stern-Volmer plot for PA). (b) Bar diagram showing effect of other nitroexplosives (26.6×10^{-6} M) on PL intensity of PFBT (3.3×10^{-6} M) (error bars=±5%). (c) Stern-Volmer plots obtained for various interfering analytes in water buffered with HEPES (10 mM, pH- 7.0). (d) Percentage of quenching by different interfering analytes (26.6×10^{-6} M) before and after addition of 26.6×10^{-6} M PA.

4.3.4 Mechanism of sensing

There can be many reasons for quenching of fluorescence as reported in literature. However, based on the above observations, there could be majorly three possible mechanisms of sensing for PA detection by PFBT. These are (a) Inner filter effect (IFE) or Resonance energy transfer (RET) between PA and PFBT, (b) ground state charge transfer complex between PA and PFBT and (c) a favored PET from PFBT to PA. PA has a wide UV-vis absorbance spectrum from 280-480 nm and in the present PFBT system involving both the solvents i.e. (DMSO and water), PA shows a huge overlap with both excitation and emission spectrum of polymer PFBT (Figure 4.3a and 4.4a) which is the prerequisite for IFE and RET to take place. Ideally IFE occurs whenever there is a substantial spectral overlap of absorption spectra of quencher (PA) with excitation and/or

emission spectra of fluorophore (PFBT) while in case of RET, the spectral overlap happens exclusively between emission spectrum of fluorophore (PFBT) and absorption spectrum of quencher (PA). Hence, to determine key cause of quenching, fluorescence decay time of PFBT was examined in absence and presence of PA for both the solvents. Interestingly, there was no significant change in the fluorescence decay time of PFBT (0.464 ns) after the addition of PA (0.455 ns) in DMSO (Figure 4.3b). This consistency in the fluorescence decay time after the addition of PA confirms that the quenching is of static type in DMSO solvent and also rules out the possibility of any RET, which falls under the category of dynamic fluorescence quenching. Therefore, IFE could be the key cause for fluorescence quenching of PFBT rather than RET in DMSO. While in the case of aqueous medium, there was a significant change in the fluorescence decay time of PFBT (2.011 ns) after the addition of PA (0.692 ns) (Figure 4.4b). This significant change in decay time of PFBT in water medium confirms the dynamic fluorescence quenching mechanism and indicates RET is happening in water medium. These observations can be further clarified by the ineffective overlapping of spectrum between excitation/emission spectra of PFBT and the absorption spectra of other nitroaromatic compounds in DMSO and water which consequently resulted in poor IFE and RET in respective solvent (Figure 3c and 4c). This was further confirmed by calculation of IFE corrections and RET parameters in both the solvents. In case of water solvent, RET plays a major role in quenching with ~52% of RET efficiency (Table A4.3), while IFE contribution was very insignificant when quenching in water i.e. 11%, whereas the rest of the quenching efficiency came from PET mechanism (Figure A4.34 and Table A4.5). In case of DMSO solvent, RET contributed less than 2% of the quenching efficiency while the major quenching occurred via strong inner filter effect (IFE) i.e. ~69% and the rest came from PET mechanism (Figure A4.34 and Table A4.4) as discussed below. Furthermore, to check the possibility of ground state charge transfer complexation, UV-vis absorbance spectra of PFBT was obtained in presence of different PA concentrations. In both solvent cases, there was just an increase in the absorbance value but no new peak appeared (Figure 4.3d and 4.4d). These results eliminate the possibility of creation of any ground state complexation between PFBT and PA in DMSO as well as in water. Hence, on the basis of above observation it can be stated that IFE is the most probable mechanism in case of DMSO solvent and eventually accountable for high sensitivity and selectivity of PFBT for PA. Meanwhile, RET plays a major role in fluorescence quenching mechanism

in case of aqueous medium and resulting in very high sensitivity and selectivity of PFBT for PA.

Further, to investigate the interaction between PFBT and PA, we performed control competitive experiments using model compounds i.e. 2,4-DNP and 4-NP which are similar to PA. The only difference in the chemical structure of the above compounds is the quantity of $–NO_2$ groups linked to benzene ring, which makes the phenols acidic in a particular order of PA>2,4-DNP>4-NP. Moreover, PL quenching response obtained for these analytes followed the same order (Figure A4.35). Since, the number of electron deficient nitro groups attached to the phenolic ring is directly proportional to its acidity and so is the dissociation of phenol. This facilitates a favorable electrostatic interaction between cationic PFBT and the dissociated phenol. PA can undergo more dissociation than 2,4-DNP and 4-NP therefore resulting in more electrostatic interaction between PFBT and PA than 2,4-DNP and 4-NP subsequently highest fluorescence quenching.,

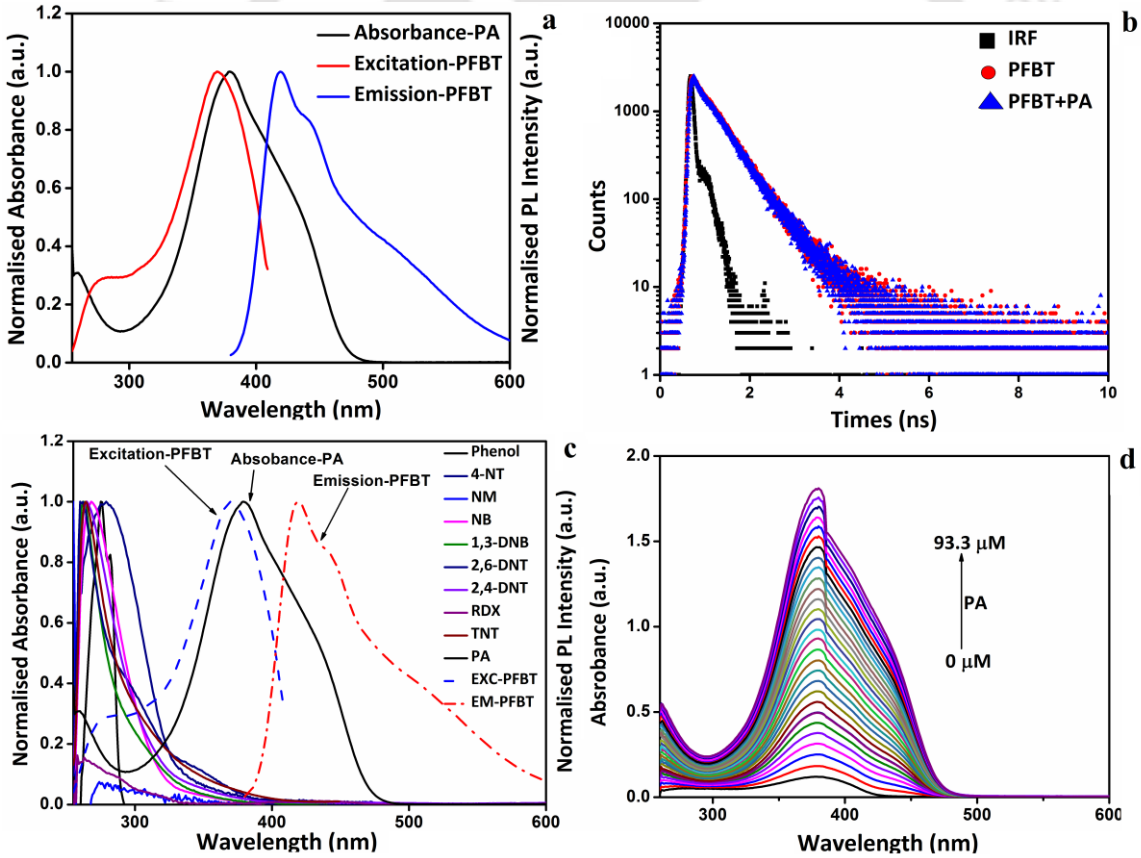

Figure 4.3 (a) Overlap between excitation/emission spectra of PFBT and absorption spectrum of PA in DMSO. (b) Lifetime decay of PFBT (3.3×10^{-6} M) before and after adding PA (93.3×10^{-6} M). (c) Overlap between emission/excitation spectra of PFAM and absorption spectra of different nitroaromatics in DMSO. (d) UV-visible spectra of PFBT (3.3×10^{-6} M) with increasing concentration of PA

Other analytes that are devoid of –OH functional groups can seldom interact effectively with PFBT and therefore showed negligible fluorescence quenching response. Moreover addition of an acid like trifluoroacetic acid (TFA), which is stronger acid than PA, did not influence fluorescence of PFBT (Figure A4.36). This can be justified via ease of PET from PFBT to PA. This electrostatic interaction promotes the PET or energy transfer mechanism for the highly selective response of PBFT toward PA. To further confirm the role of electrostatic interactions, sensing experiment was carried out in high ionic strengths solution by using NaCl solution (1M).[57] It was observed that the quenching efficiency of the polymer-PFBT decreases (13%) in high ionic strength solution, which indicates the reduction of electrostatic interactions between PFBT and PA in high ionic strength solutions leading to lessening in RET/PET mechanism (Figure A4.37).[57] To validate this, highest occupied molecular orbital (HOMO) level and lowest unoccupied

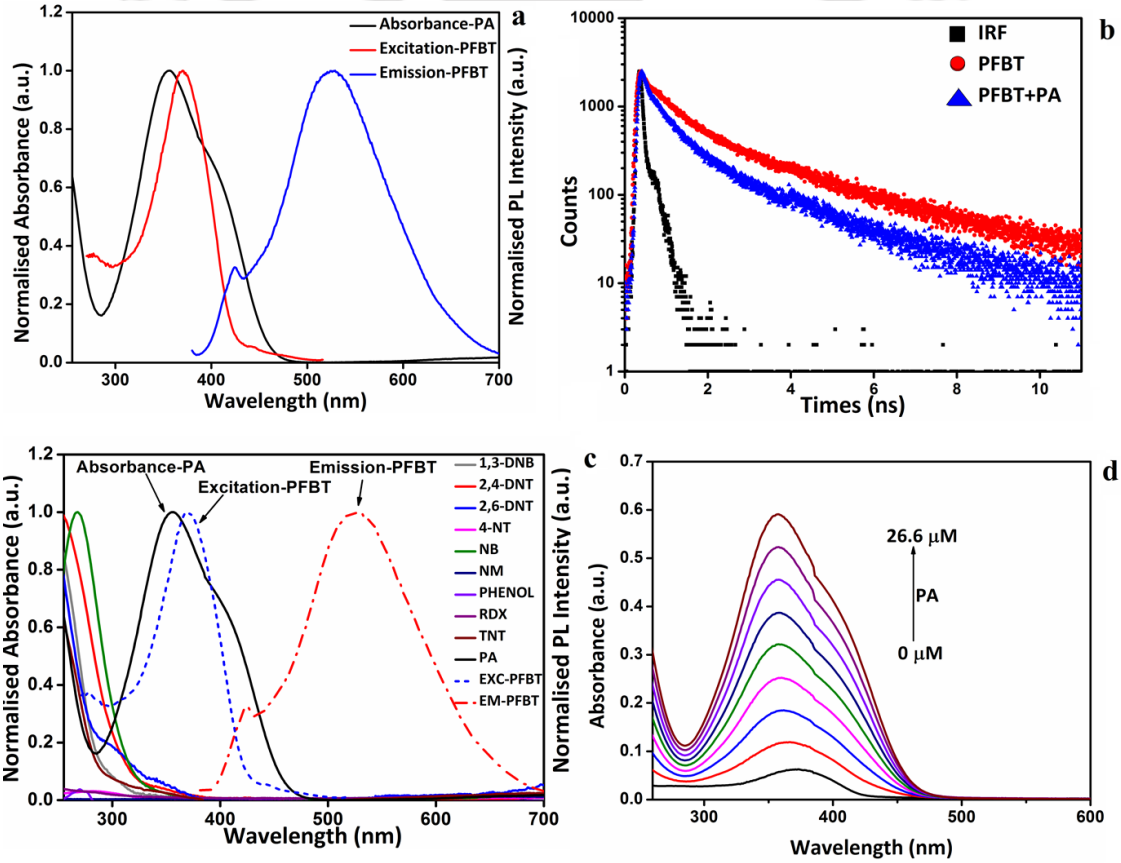

Figure 4.4 (a) Overlap between excitation/emission spectra of PFBT and absorption spectrum of PA in water buffered with HEPES (pH=7.0,10 mM). (b) Lifetime decay of PFBT (3.3×10^{-6} M) before and after addition of PA (26.6×10^{-6} M). (c) Overlap between excitation/emission spectra of PFBT and absorption spectra of various nitroaromatics in water buffered with HEPES (pH=7.0,10 mM). (d) UV-visible spectra of PFBT (3.3×10^{-6} M) with increasing concentration of PA.

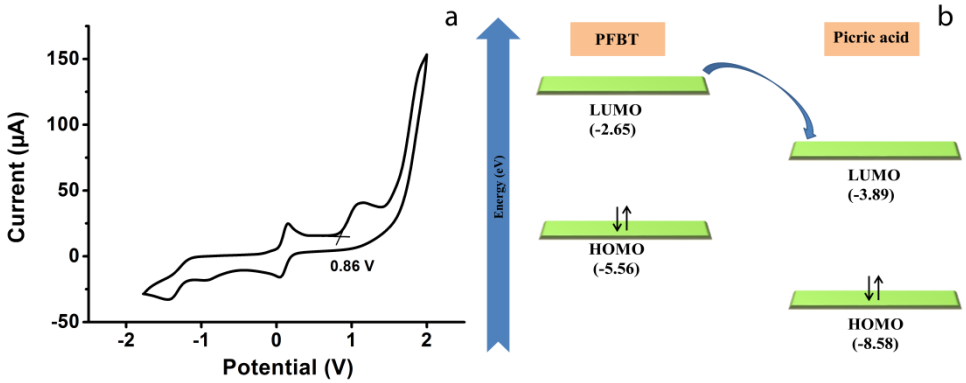

Figure 4.5 (a) Cyclic voltammogram of PFBT film on glassy carbon electrode with a scan rate of 50 mV/s. (b) Pictorial representation of photo induced electron transfer from LUMO of PFBT to the LUMO of PA

molecular orbital (LUMO) level of PFBT was obtained through cyclic voltammetry studies (Figure 4.5a). It was observed that there is a possibility of PET from LUMO of PFBT (-2.65 eV) to the LUMO of PA (-3.89 eV) resulting in superior quenching (Figure 4.5b). Note that, LUMO levels of 4-NP (-2.22 eV) and 2,4-DNP (-2.82 eV) are usually higher than LUMO of PA, resulting in reduced fluorescence quenching efficiency. PA has the lowest LUMO energy compared to other nitroexplosives, namely TNT (-3.7 eV), NT (-3.2 eV), DNT (-3.5 eV) etc., but the quenching efficiency was quite insignificant for them. This is in agreement with the electrostatic interaction enhanced PET and is valid in both solvents. Therefore, it can be concluded that PFBT possessed remarkable selectivity and enhanced sensitivity for PA due to strong IFE and possible PET in DMSO and RET and favorable PET in aqueous medium.

4.3.5 Analysis of PA in natural water samples

To verify the feasibility of the PFBT based method, it is highly important to recognize the presence of PA in natural water samples. Water samples were collected from the Brahmaputra river (near IITG campus) and sea water sample from Bay of Bengal. These

Table 4.1 Determination of PA in Natural Water Samples

Sample	Added (10^{-6} M)	Found (10^{-6} M)	Recovery (%)	RSD (%, n=3)
River	1.0	0.92	92.0	2.12
	2.5	2.34	93.6	6.06
	3.5	3.49	99.7	1.07
Sea	4.0	3.98	99.5	9.31
	6.0	5.99	99.8	1.71
	10.0	9.76	97.6	6.82

samples were centrifuged and filtered using 0.2 μm membrane filter. The recoveries were carried out by using samples spiked with known concentrations of PA (Table 4.1). As shown in Table 1, recoveries for PA in the Brahmaputra river water samples and sea water varied from 90% to 99% and RSD was found to be lower than 10 %. Therefore, PFBT showed excellent feasibility for detection of PA in real samples.

4.3.6 Sensing on Solid Support

For rapid and low cost on-site detection of PA, test strips were developed by dipping the Whatman filter paper in PFBT solution (10^{-4} M) followed by drying in air. 10 μL of various concentration of PA in water was applied on each paper strip. A dark spot was observed under UV lamp (365 nm), and this darkness appeared light at lower concentration of PA indicating quenching of PFBT (Figure 4.6). It can be seen from the naked eyes that the paper strips can detect minimum amount of 10 μL PA (10^{-16} M) solution that is equivalent to 0.22 attogram level, which is among the best reported literature values (Table A4.6). Furthermore, we checked the selectivity studies of PFBT on portable and readily usable paper strips. For this purpose, we applied 10 μL of other nitroaromatic compounds (10^{-3} M) and compared them with the PA spot to confirm that the paper strips were selective only for PA (Figure A4.38).

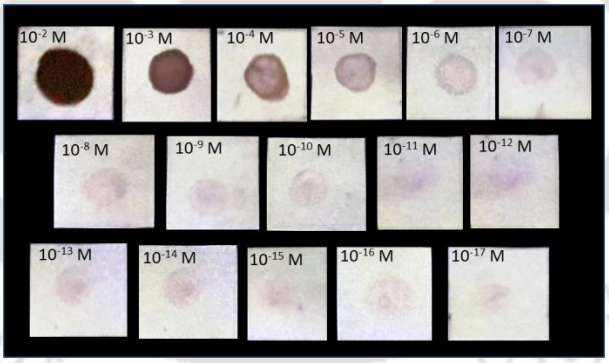

Figure 4.6 Photographs of fluorescent test strips after addition of 10 μL of PA solution of various concentrations [under UV-light (365 nm)]. A dark spot can be seen after the addition of PA.

4.3.7 Vapor-phase detection

As an advanced ability of the PFBT probe, PA was also detected in the vapor phase by using the PFBT in water medium. Fixed volumes of PA vapors (101.64 ppb, 2.5 mL) were passed through the PFBT solution in water via an air-tight syringe, thereafter the PL spectra were recorded and quenching in the fluorescence maxima was detected with each

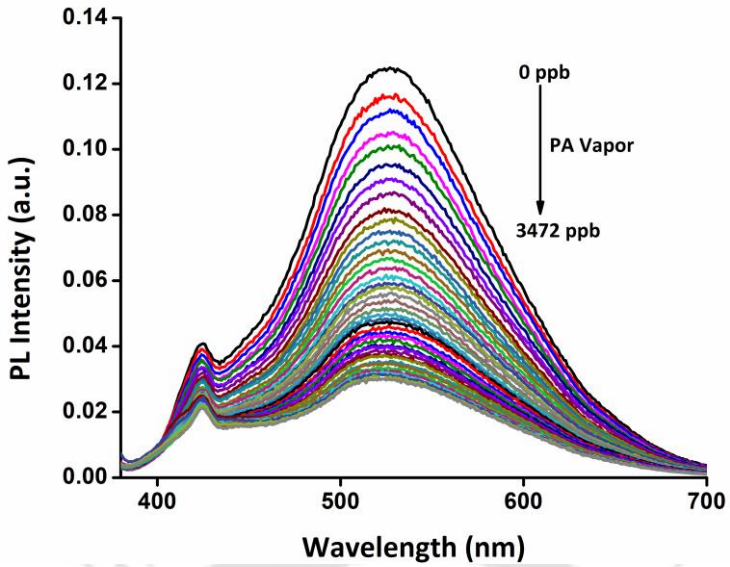

Figure 4.7 PL spectrum of PFBT (3.3×10^{-6} M) with increasing concentration of PA vapors in water buffered with HEPES (pH=7.0,10 mM).

addition (Figure 4.7 and A4.39). Furthermore, LOD of the PFBT polymer was calculated to be 42.6 ppb based on the change in the fluorescence maxima of PFBT in water at different amounts of PA vapors (84.7, 169.4, 254.1, 338.8, 423.5, 508.2 ppb) using the equation 3σ/K (Figure A4.40). Thus, the present system established a fast and selective detection of PA in the solution as well as vapor phase, which remains an exciting and highly challenging area of research.

4.4 Conclusion

In summary, a new cationic conjugated polymer PBFT was synthesized using simple and economic method of oxidative polymerization for PA sensing in solution and solid state. The polymer PFBT displayed dual emission in DMSO and aqueous medium. It was found that polymer PFBT senses PA in solution as well as on solid platform like normal filter paper strips for onsite portability purposes and an extremely low detection limits 92.7 nm and 0.19 nm were obtained in DMSO and water respectively while minimum of 0.22 attogram of PA can be detected using portable paper strips. This system can also detect PA in vapor phase with a very low limit of detection of 42.6 ppb. The fluorescence of the PFBT gets quenched by strong inner filter effect (IFE) and PET mechanisms between polymer and PA in DMSO. Whereas in case of aqueous medium, resonance energy transfer (RET) and PET mechanism are responsible of fluorescence quenching. This method is very simple and provides excellent selectivity and high sensitivity even in competing environment, therefore can be used for analyzing natural water samples.

References

(1) Salinas, Y.; Martinez-Manez, R.; Marcos, M. D.; Sancenon, F.; Costero, A. M.; Parra, M.; Gil, S. *Chem. Soc. Rev.* **2012**, *41*, 1261.

(2) Sun, X.; Wang, Y.; Lei, Y. *Chem. Soc. Rev.* **2015**, *44*, 8019.

(3) Shanmugaraju, S.; Mukherjee, P. S. *Chem. Commun.* **2015**, *51*, 16014.

(4) Ma, Y.; Li, H.; Peng, S.; Wang, L. *Anal. Chem.* **2012**, *84*, 8415.

(5) Akhavan, J. *Chemistry of Explosives*, 2nd ed.; Royal Society of Chemistry, **2004**

(6) Ashbrook, P. C.; Houts, T. A. *Chem. Health Saf.* **2003**, *10*, 27.

(7) Innovative Treatment Technologies. In Annual Status Report, 8th ed.; U.S. Enrionmental Protection Agency: Washington, DC, **1996**.

(8) Wollin, K.-M.; Dieter, H. H. *Arch. Environ. Con. Tox.* **2005**, *49*, 18.

(9) Moore, D. S. *Rev. Sci. Instrum.* **2004**, *75*, 2499.

(10) Yang, L.; Ma, L.; Chen, G.; Liu, J.; Tian, Z.-Q. *Chem. Eur. J.* **2010**, *16*, 12683.

(11) Dasary, S. S. R.; Senapati, D.; Singh, A. K.; Anjaneyulu, Y.; Yu, H.; Ray, P. C. *ACS Appl. Mater. Inter.* **2010**, *2*, 3455.

(12) Du, Y.; Wang, W.; Li, H. *Anal. Chem.* **2012**, *84*, 1725.

(13) Sapsford, K. E.; Charles, P. T.; Patterson, C. H.; Ligler, F. S. *Anal. Chem.* **2002**, *74*, 1061.

(14) Chen, X.; Cheng, X.; Gooding, J. J. *Anal. Chem.* **2012**, *84*, 8557.

(15) Hu, Z.; Deibert, B. J.; Li, J. *Chem. Soc. Rev.* **2014**, *43*, 5815.

(16) Peng, Y.; Zhang, A.-J.; Dong, M.; Wang, Y.-W. *Chem. Commun.* **2011**, *47*, 4505.

(17) Dinda, D.; Gupta, A.; Shaw, B. K.; Sadhu, S.; Saha, S. K. *ACS Appl. Mater. Inter.* **2014**, *6*, 10722.

(18) Bhalla, V.; Gupta, A.; Kumar, M.; Rao, D. S. S.; Prasad, S. K. *ACS Appl. Mater. Inter.* **2013**, *5*, 672.

(19) Roy, B.; Bar, A. K.; Gole, B.; Mukherjee, P. S. *J. Org. Chem.* **2013**, *78*, 1306.

(20) Dey, N.; Samanta, S. K.; Bhattacharya, S. *ACS Appl. Mater. Inter.* **2013**, *5*, 8394.

(21) Martinez, H. P.; Grant, C. D.; Reynolds, J. G.; Trogler, W. C. *J. Mater. Chem.* **2012**, *22*, 2908.

(22) Wang, X.; Guo, Y.; Li, D.; Chen, H.; Sun, R. *Chem. Commun.* **2012**, *48*, 5569.

(23) Li, D.; Liu, J.; Kwok, R. T. K.; Liang, Z.; Tang, B. Z.; Yu, J. *Chem. Commun.* **2012**, *48*, 7167.

(24) Xu, Y. Q.; Li, B. H.; Li, W. W.; Zhao, J.; Sun, S. G.; Pang, Y. *Chem. Commun.* **2013**, *49*, 4764.

(25) Li, X.-G.; Liao, Y.; Huang, M.-R.; Strong, V.; Kaner, R. B. *Chem. Sci.* **2013**, *4*, 1970.

(26) Zhang, Y. R.; Chen, G.; Lin, Y. L.; Zhao, L. F.; Yuan, W. Z.; Lu, P.; Jim, C. K. W.; Zhang, Y. M.; Tang, B. Z. *Polym. Chem.* **2015,** *6*, 97.

(27) Kaur, S.; Bhalla, V.; Vij, V.; Kumar, M. *J. Mater. Chem. C* **2014**, *2*, 3936.

(28) Gole, B.; Bar, A. K.; Mukherjee, P. S. *Chem. Eur. J.* **2014,** *20*, 13321.

(29) Ye, J.; Zhao, L.; Bogale, R. F.; Gao, Y.; Wang, X.; Qian, X.; Guo, S.; Zhao, J.; Ning, G. *Chem. Eur. J.* **2015**, *21*, 2029.

(30) Kaur, S.; Gupta, A.; Bhalla, V.; Kumar, M. *J. Mater. Chem. C* **2014**, *2*, 7356.

(31) Bereau, V.; Duhayon, C.; Sutter, J. P. *Chem. Commun.* **2014**, *50*, 12061.

(32) Tanwar, A. S.; Iyer, P. K. *ACS Omega* **2017**, *2*, 4424.

(33) Meher, N.; Iyer, P. K. *Nanoscale* **2017**, *9*, 7674.

(34) Hussain, S.; Malik, A. H.; Afroz, M. A.; Iyer, P. K. *Chem. Commun.* **2015**, *51*, 7207.

(35) Malik, A. H.; Hussain, S.; Kalita, A.; Iyer, P. K. *ACS Appl. Mater. Inter.* **2015**, *7*, 26968.

(36) Tanwar, A. S.; Hussain, S.; Malik, A. H.; Afroz, M. A.; Iyer, P. K. *ACS Sensors* **2016**, *1*, 1070.

(37) Kalita, A.; Hussain, S.; Malik, A. H.; Barman, U.; Goswami, N.; Iyer, P. K. *ACS Appl. Mater. Inter.* **2016**, *8*, 25326.

(38) Kim, H. N.; Guo, Z.; Zhu, W.; Yoon, J.; Tian, H. *Chem. Soc. Rev.* **2011**, *40*, 79.

(39) Lee, K.; Povlich, L. K.; Kim, J. *Analyst* **2010**, *135*, 2179.

(40) Thomas, S. W.; Joly, G. D.; Swager, T. M. *Chem. Rev.* **2007**, *107*, 1339.

(41) McQuade, D. T.; Pullen, A. E.; Swager, T. M. *Chem. Rev.* **2000**, *100*, 2537.

(42) Zhu, C.; Liu, L.; Yang, Q.; Lv, F.; Wang, S. *Chem. Rev.* **2012**, *112*, 4687.

(43) Sanchez, J. C.; Trogler, W. C. *J. Mater. Chem.* **2008**, *18*, 3143.

(44) Wang, J.; Mei, J.; Yuan, W.; Lu, P.; Qin, A.; Sun, J.; Ma, Y.; Tang, B. Z.. *J. Mater. Chem.* **2011**, *21*, 4056.

(45) Hu, R.; Maldonado, J. L.; Rodriguez, M.; Deng, C.; Jim, C. K. W.; Lam, J. W. Y.; Yuen, M. M. F.; Ramos-Ortiz, G.; Tang, B. Z. *J. Mater. Chem.* **2012**, *22*, 232.

(46) Liu, J.; Zhong, Y.; Lu, P.; Hong, Y.; Lam, J. W. Y.; Faisal, M.; Yu, Y.; Wong, K. S.; Tang, B. Z. *Polym. Chem.* **2010,** *1*, 426.

(47) Sang, N.; Zhan, C.; Cao, D. *J. Mater. Chem. A* **2015**, *3*, 92.

(48) Zhou, H.; Li, J.; Chua, M. H.; Yan, H.; Tang, B. Z.; Xu, J. *Polym. Chem.* **2014**, *5*, 5628.

(49) Liu, Y.; Gao, M.; Lam, J. W. Y.; Hu, R.; Tang, B. Z. *Macromolecules* **2014,** *47*, 4908.

(50) Li, H.; Wu, H.; Zhao, E.; Li, J.; Sun, J. Z.; Qin, A.; Tang, B. Z. *Macromolecules* **2013**, *46*, 3907.

(51) Shaligram, S.; Wadgaonkar, P. P.; Kharul, U. K. *J. Mater. Chem. A* **2014**, *2*, 13983-13989.

(52) Xu, B. W.; Wu, X. F.; Li, H. B.; Tong, H.; Wang, L. X. *Macromolecules* **2011**, *44*, 5089.

(53) Saikia, G.; Iyer, P. K. *J. Org. Chem.* **2010,** *75*, 2714.

(54) Muthuraj, B.; Mukherjee, S.; Patra, C. R.; Iyer, P. K. *ACS Appl. Mater. Inter.* **2016**, *8*, 32220.

(55) Chowdhury, S. R.; Mukherjee, S.; Das, S.; Patra, C.; Iyer, P. K. *Chem. Sci.* **2017**, 8, 7566.

(56) Lakowicz, J. R. In Principles of Fluorescence spectrosopy, 3rd ed; Springer: Singapore, **2010**.

(57) Sandanaraj. B. S.; Bayrakatar, H.; Krishnamoorthy, K.; Knapp, M. J.; Thayumanavan, S. *Langmuir*, **2007**, *23*, 3891.

Appendix

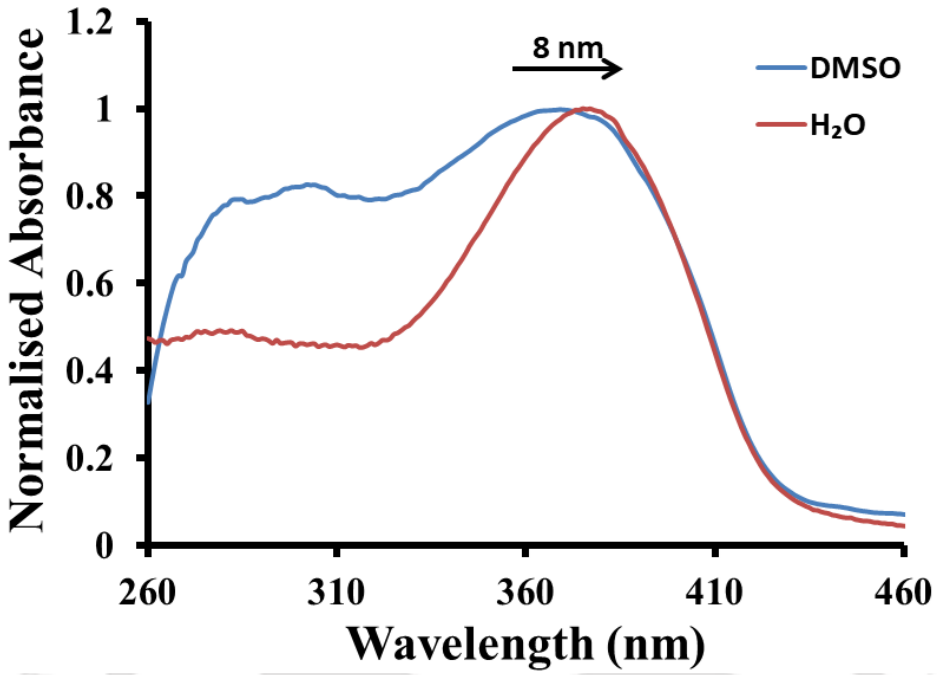

Figure A4.1 Normalised absorbance of PFBT (3.3×10^{-6} M) in DMSO and Water.

Table A4.1: Fluorescence lifetime decay of each component and their fractions in DMSO.

Sample	τ_1 (ns)	%	τ_2 (ns)	%	χ^2	τ_{avg} (ns)
PFBT	0.136	21.14	0.552	78.86	1.091	0.464
PFBT-PA	0.133	24.33	0.559	75.67	1.088	0.455

Table A4.2: Fluorescence lifetime decay of each component and their fractions in water.

Sample	τ_1 (ns)	%	τ_2 (ns)	%	χ^2	τ_{avg} (ns)
PFBT	0.668	46.60	3.183	53.40	1.125	2.011
PFBT-PA	0.452	59.37	2.482	40.63	1.128	0.692

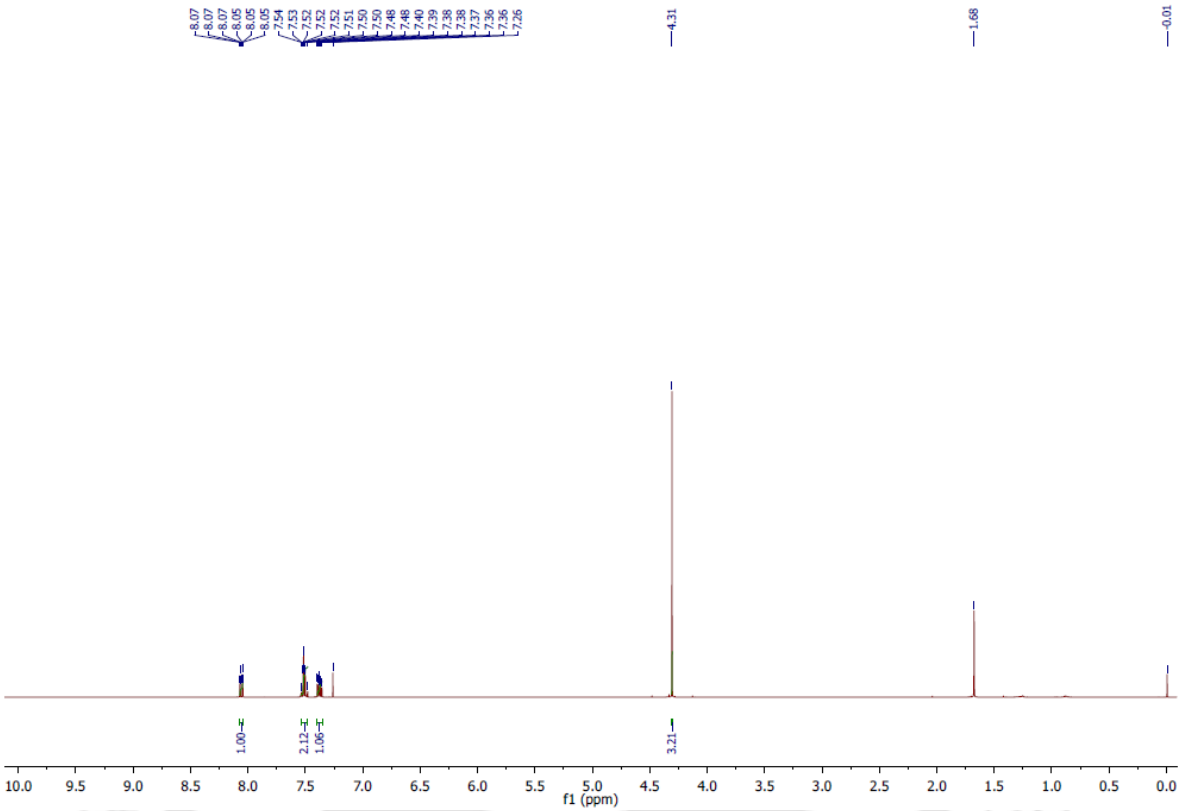

Figure A4.2 ^{1}H NMR spectrum of 1-methyl-1H-benzo[d][1,2,3]triazole.

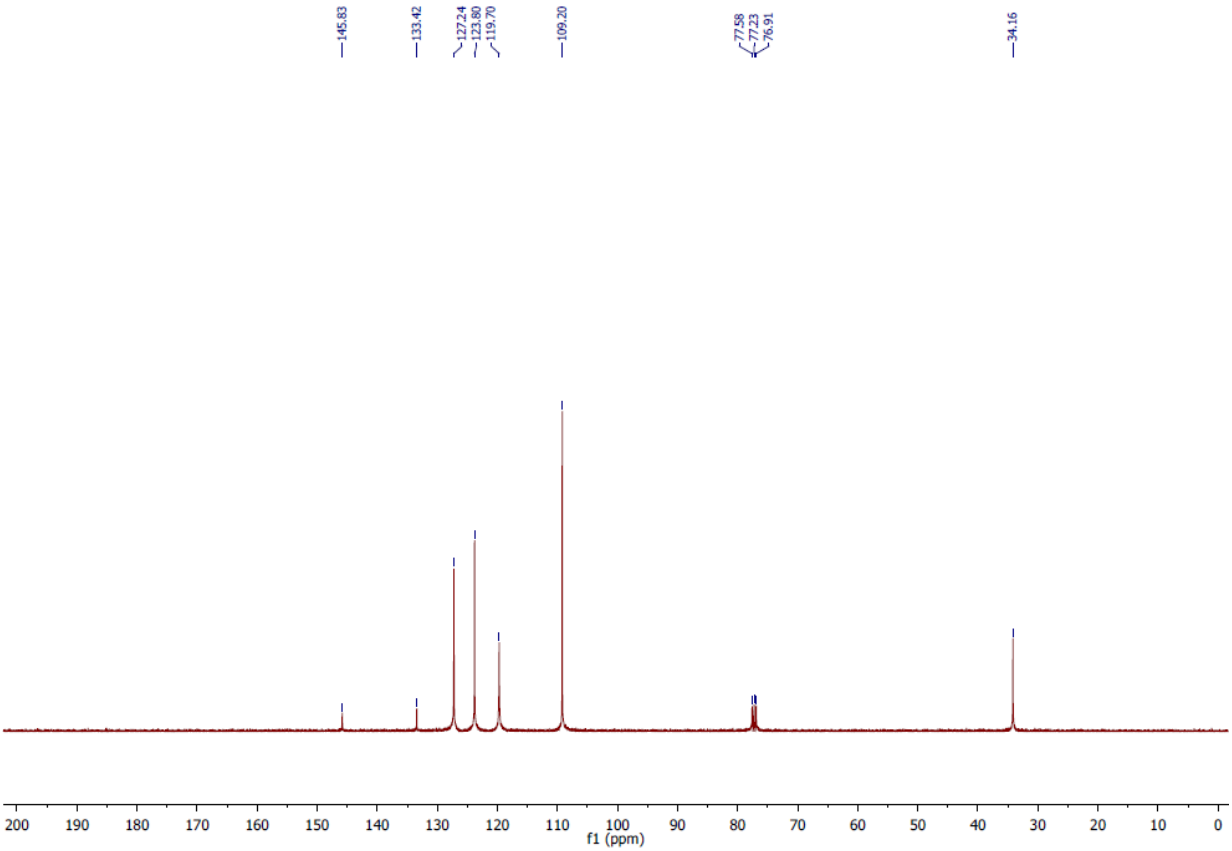

Figure A4.3 ^{13}C NMR spectrum of 1-methyl-1H-benzo[d][1,2,3]triazole.

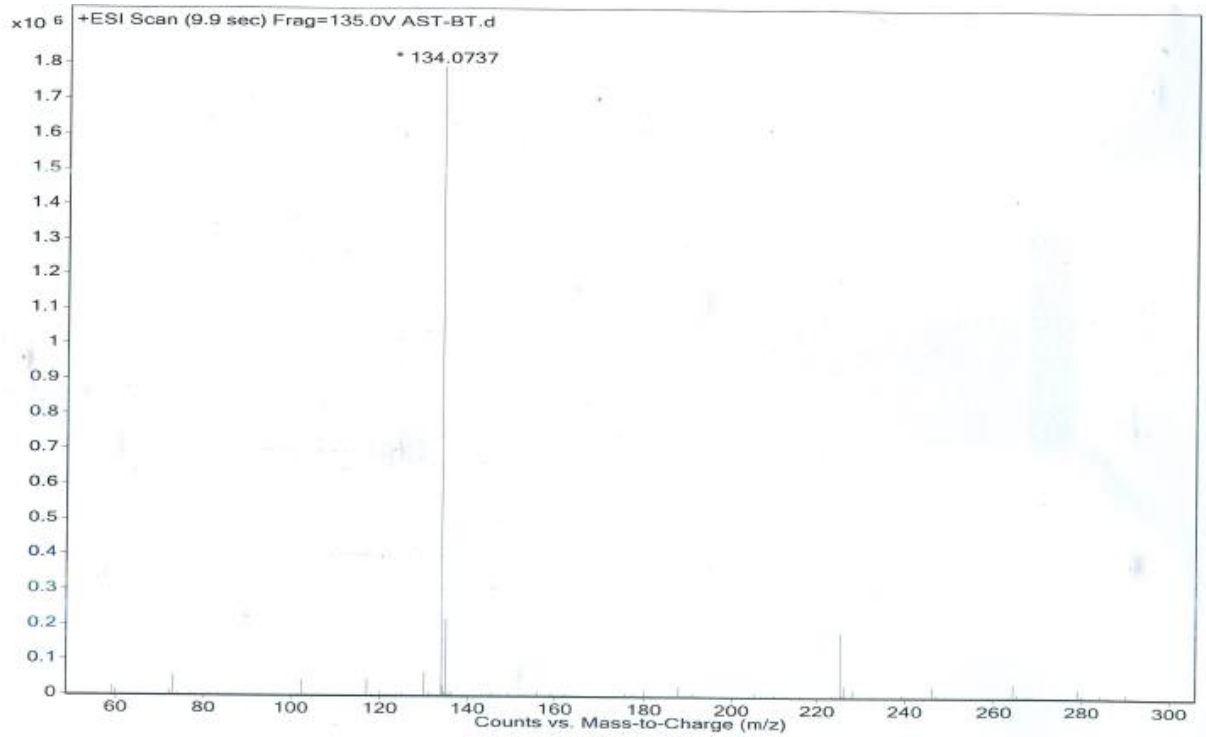

Figure A4.4 High resolution mass spectrum of monomer 1-methyl-1H-benzo[d][1,2,3]triazole.

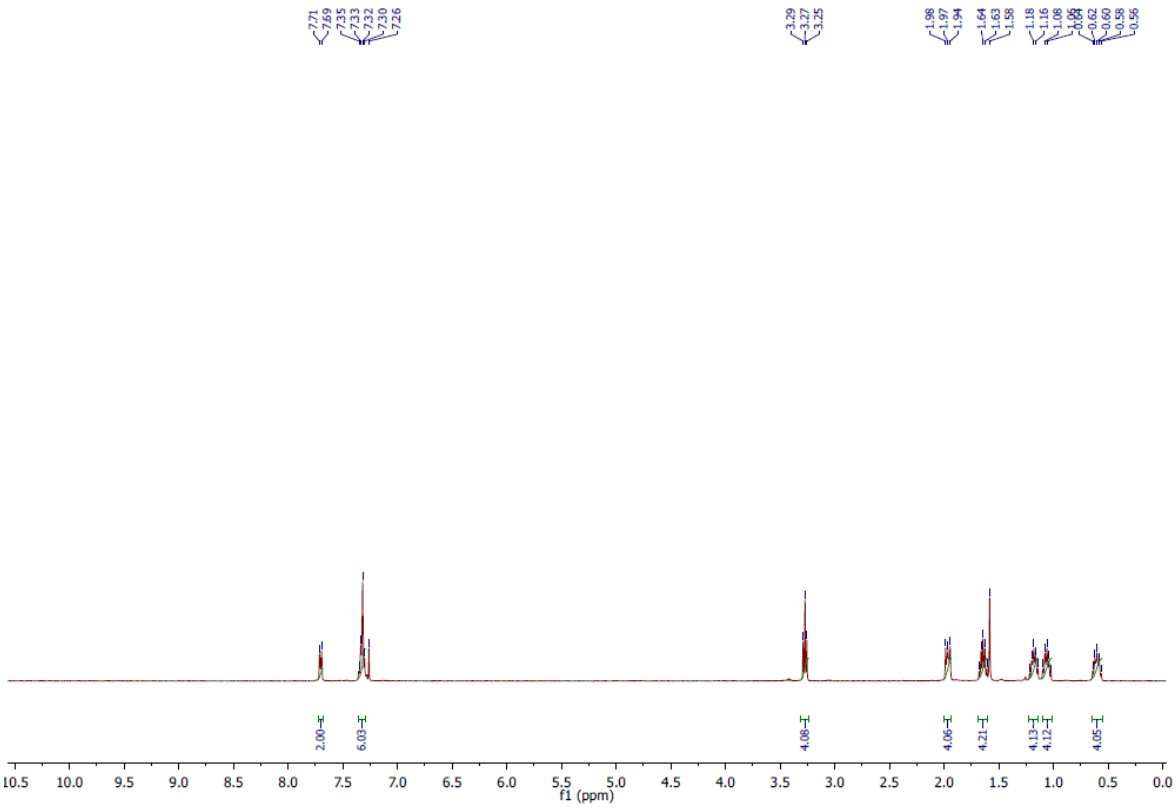

Figure A4.5 ^{1}H NMR spectrum of M2.

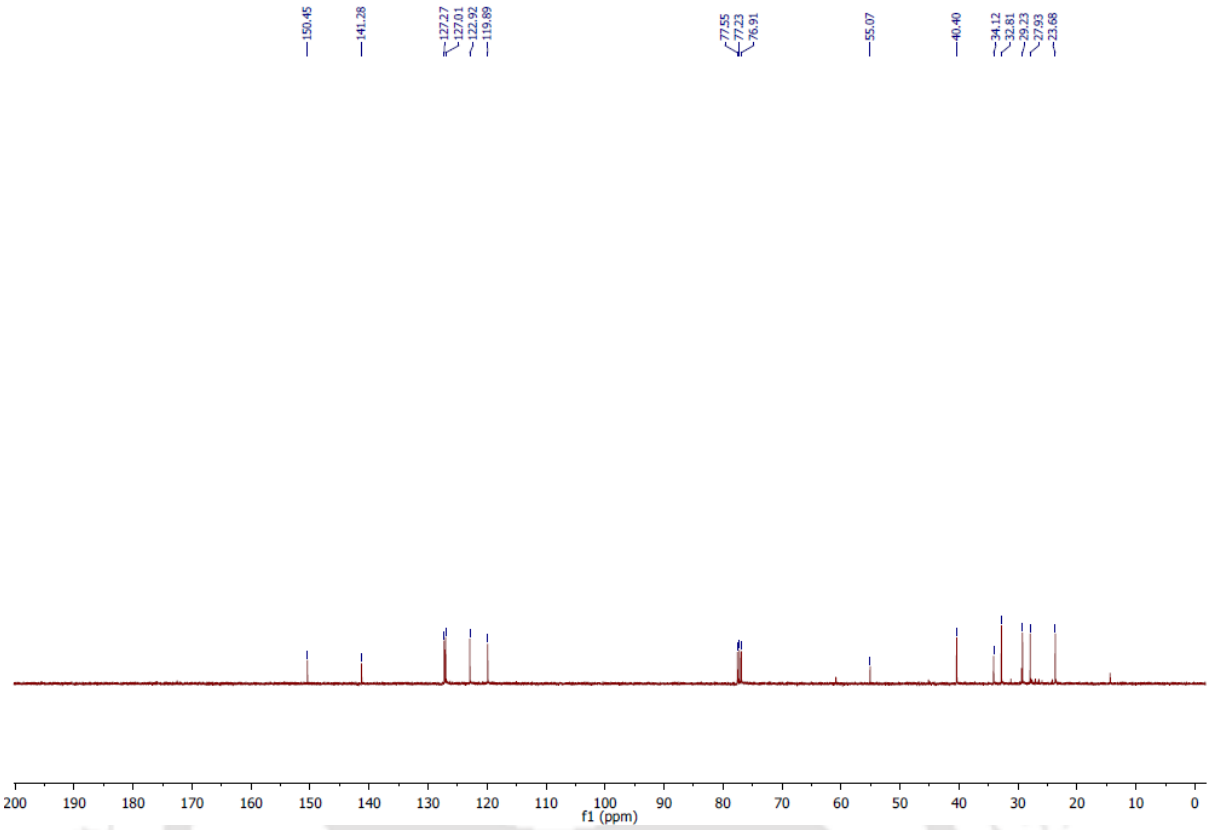

Figure A4.6 ^{13}C NMR spectrum of M2.

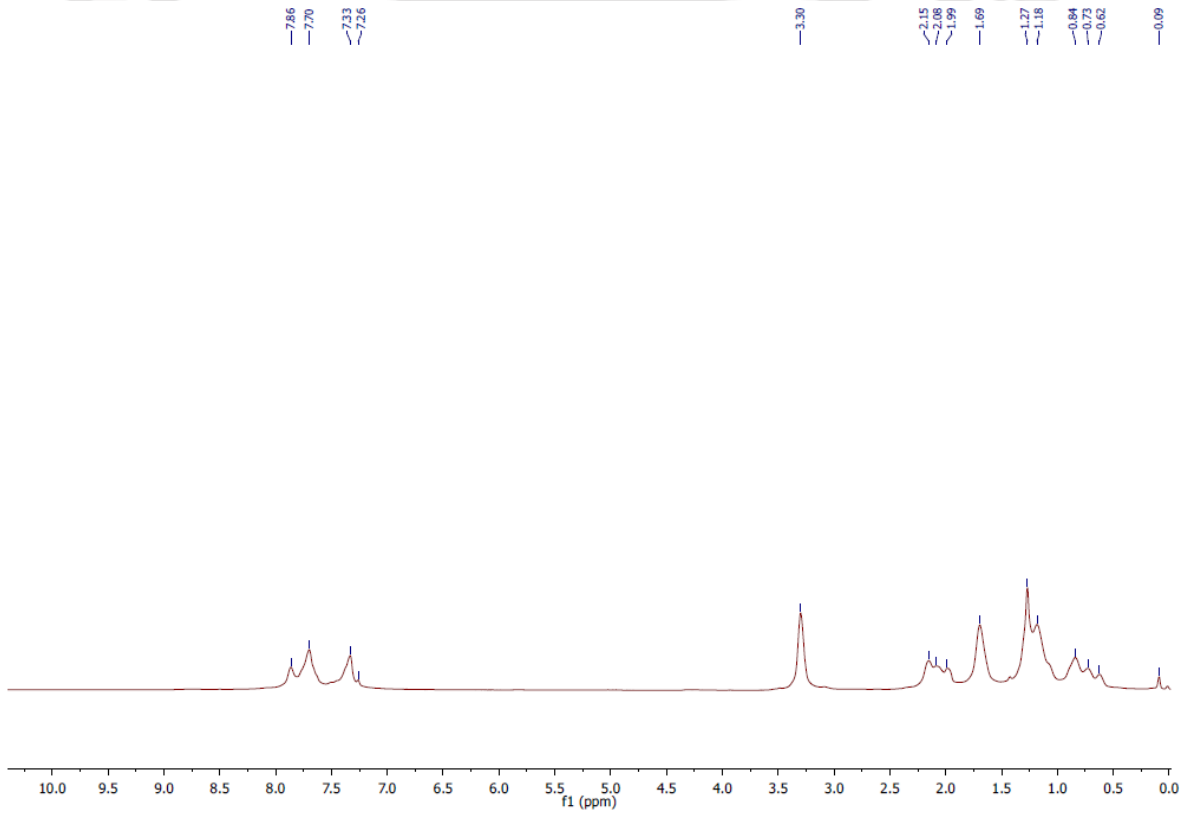

Figure A4.7 ^{1}H NMR spectrum of PF.

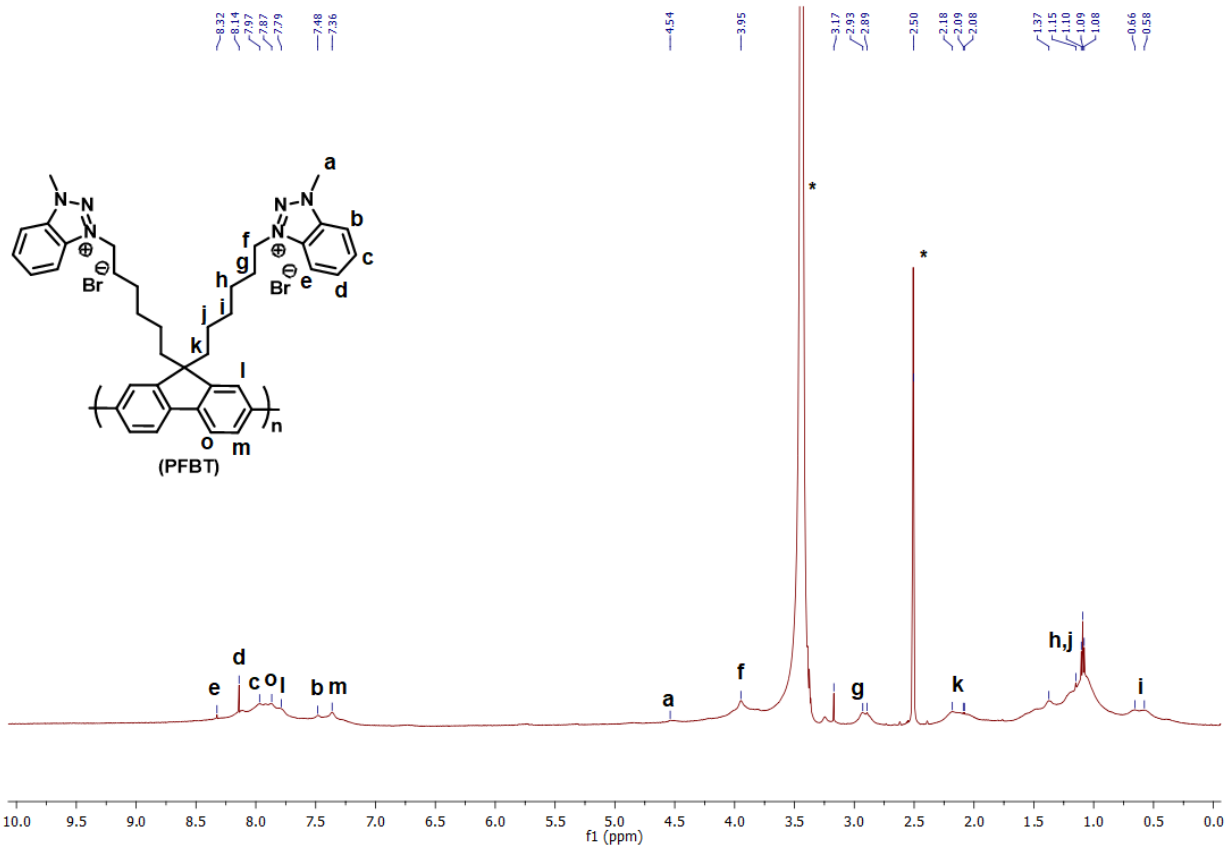

Figure A4.8 ^{1}H NMR spectrum of PFBT.

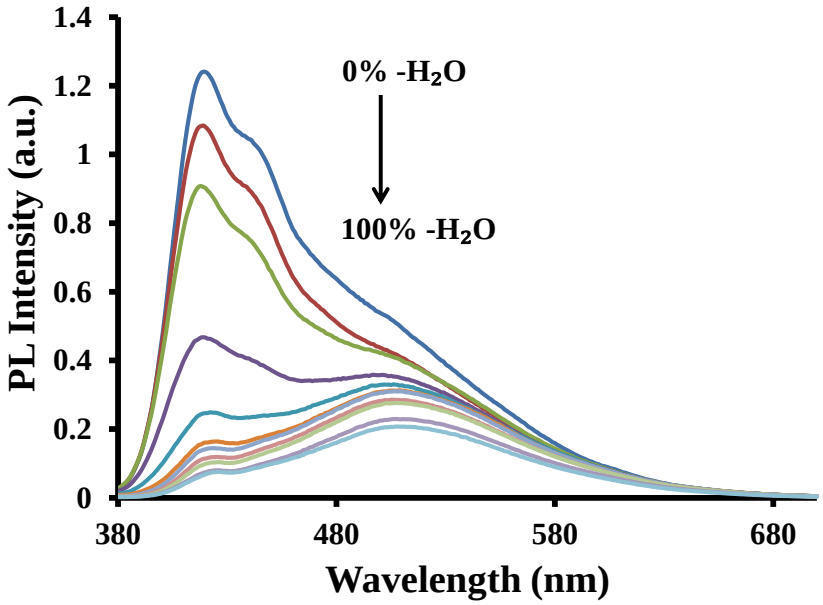

Figure A4.9 Photoluminescence spectra of PFBT (3.3×10^{-6} M) in various DMSO and Water ratios.

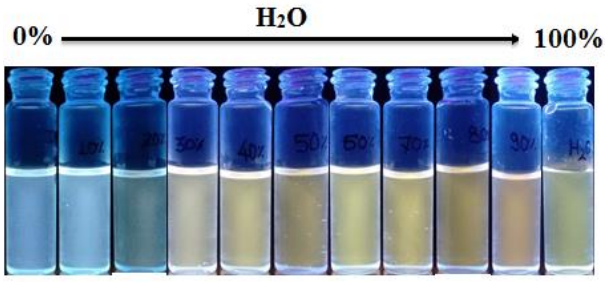

Figure A4.10 Solution of PFBT (3.3×10^{-6} M) in various DMSO and Water ratios under UV lamp (365 nm).

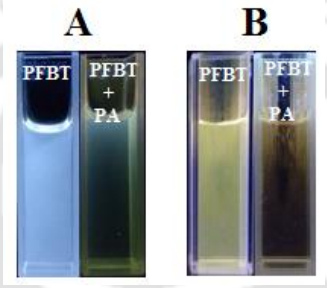

Figure A4.11 Solution of PFBT (3.3×10^{-6} M) in (A) DMSO and (B) Water buffered with HEPES (pH-7.0, 10 mM) before and after addition of PA under UV lamp (365 nm).

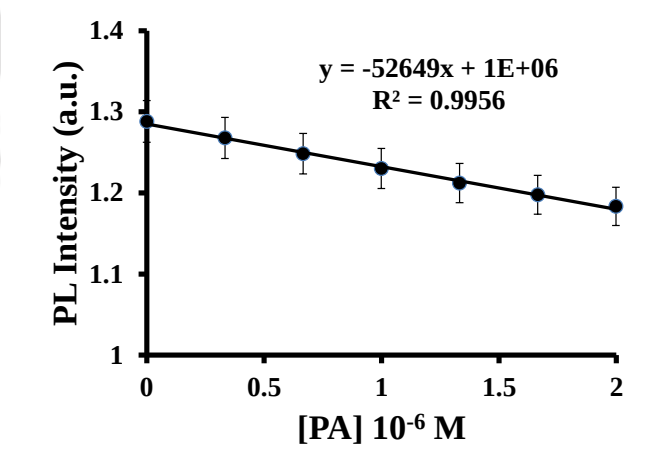

Figure A4.12 Fluorescence intensity of PFBT in DMSO *vs* PA concentration.

LOD=3 × S.D./k

LOD = 3 × 1627.68 / (52649× 10^6)

LOD= 92.7 nM

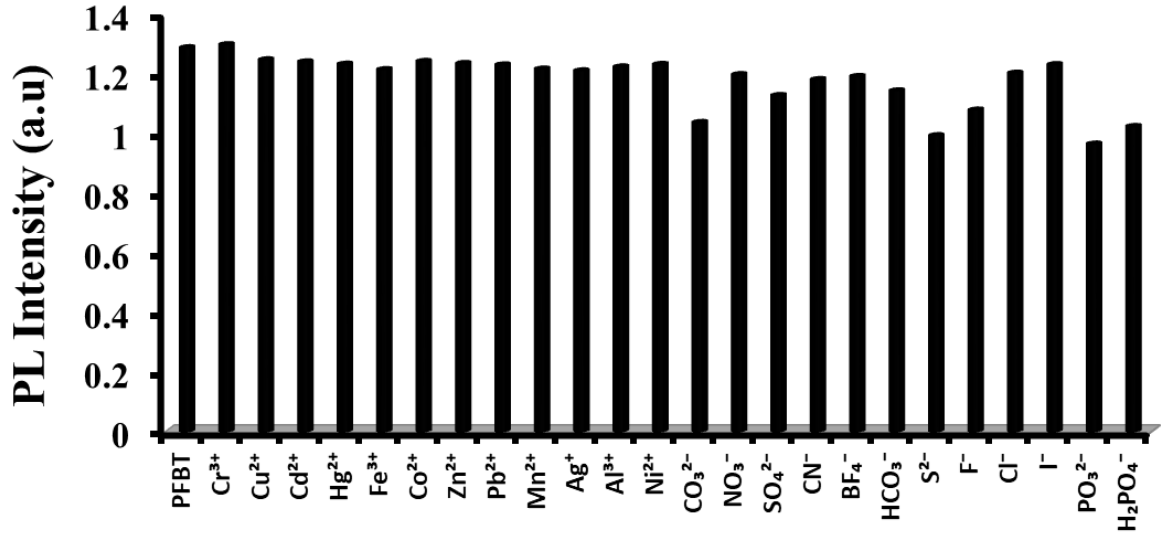

Figure A4.13 Bar diagram depicting effect of various ions (93.3×10^{-6} M) on the fluorescence intensity of PFBT (3.3×10^{-6} M) in DMSO solvent.

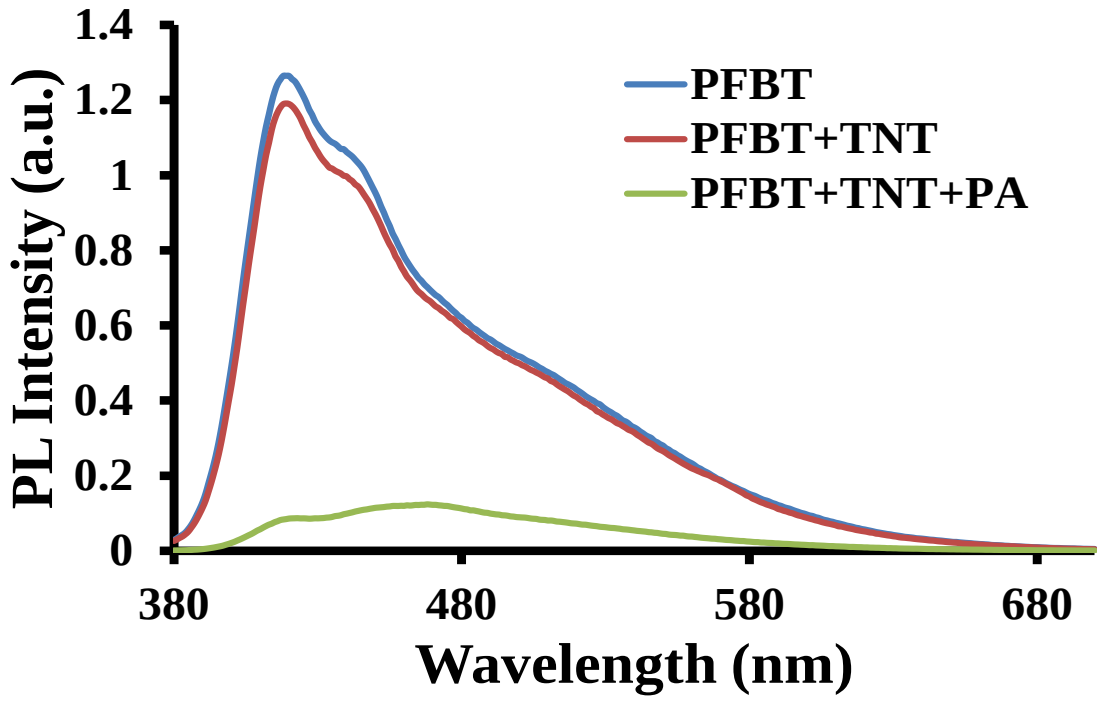

Figure A4.14 Emission spectra of PFBT (3.3×10^{-6} M) with TNT (93.3×10^{-6} M) followed by addition of PA (93.3×10^{-6} M) in DMSO.

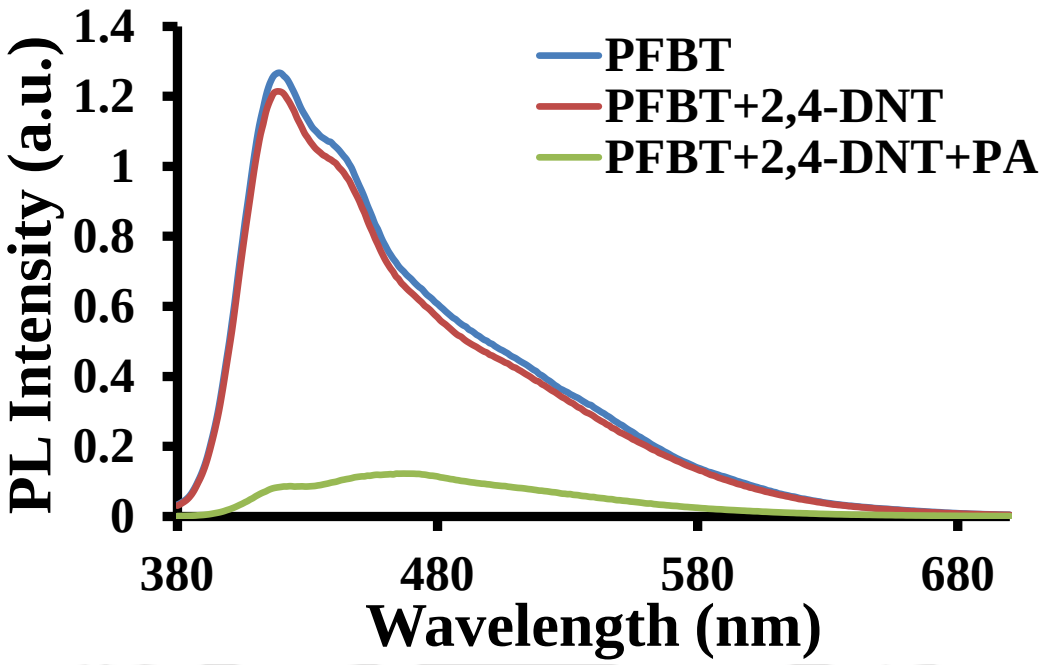

Figure A4.15 Emission spectra of PFBT (3.3×10^{-6} M) with 2,4-DNT (93.3×10^{-6} M) followed by addition of PA (93.3×10^{-6} M) in DMSO.

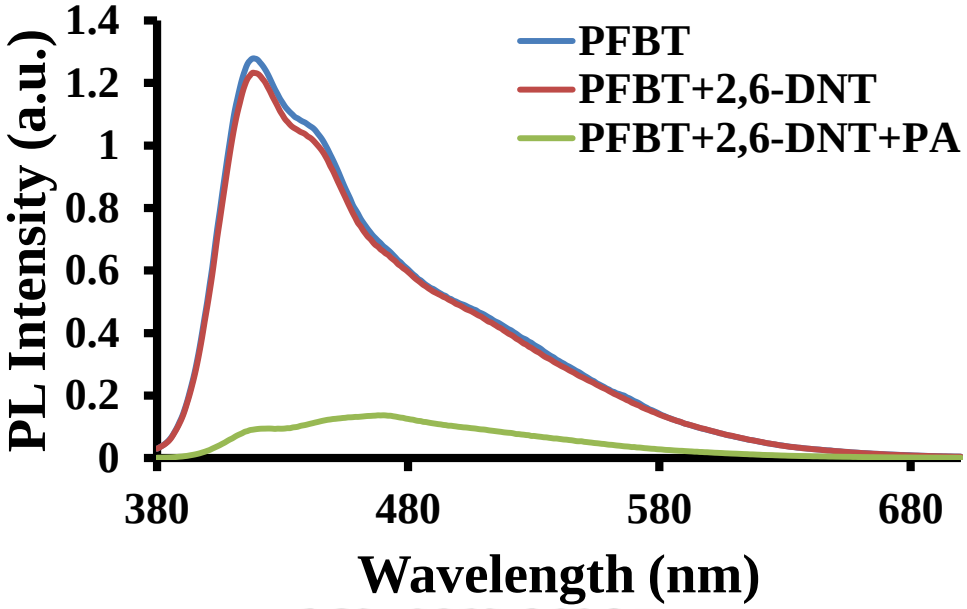

Figure A4.16 Emission spectra of PFBT (3.3×10^{-6} M) with 2,6-DNT (93.3×10^{-6} M) followed by addition of PA (93.3×10^{-6} M) in DMSO.

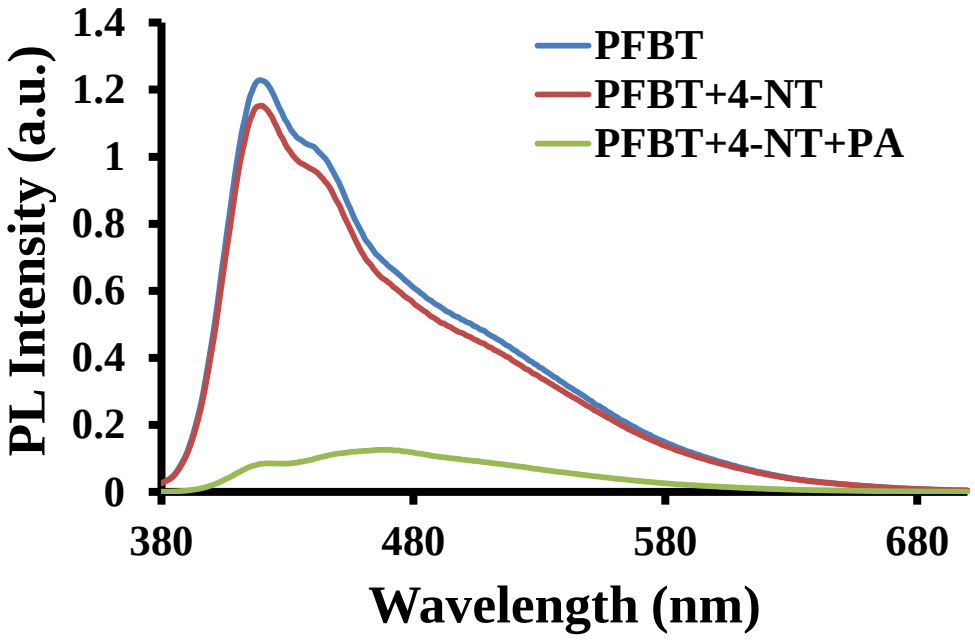

Figure A4.17 Emission spectra of PFBT (3.3×10^{-6} M) with 4-NT (93.3×10^{-6} M) followed by addition of PA (93.3×10^{-6} M) in DMSO.

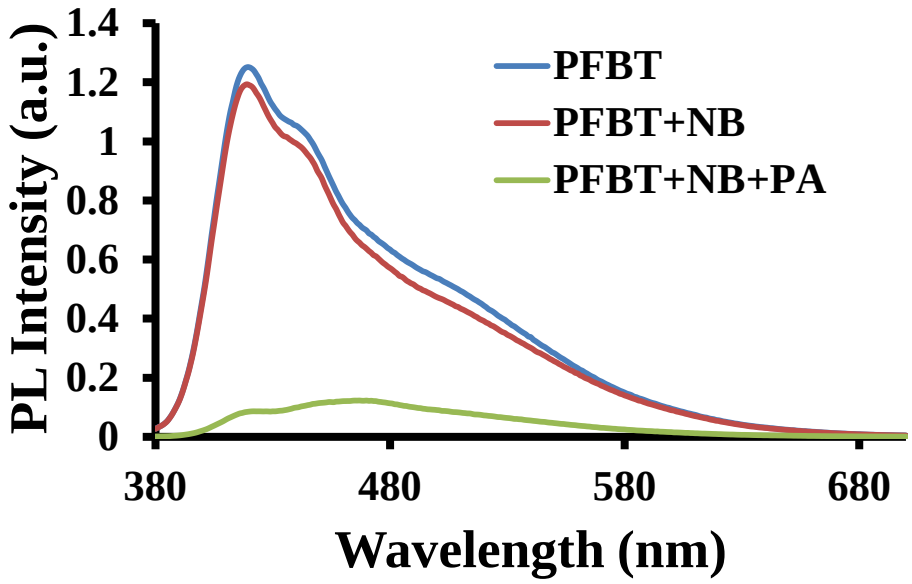

Figure A4.18 Emission spectra of PFBT (3.3×10^{-6} M) with NB (93.3×10^{-6} M) followed by addition of PA (93.3×10^{-6} M) in DMSO.

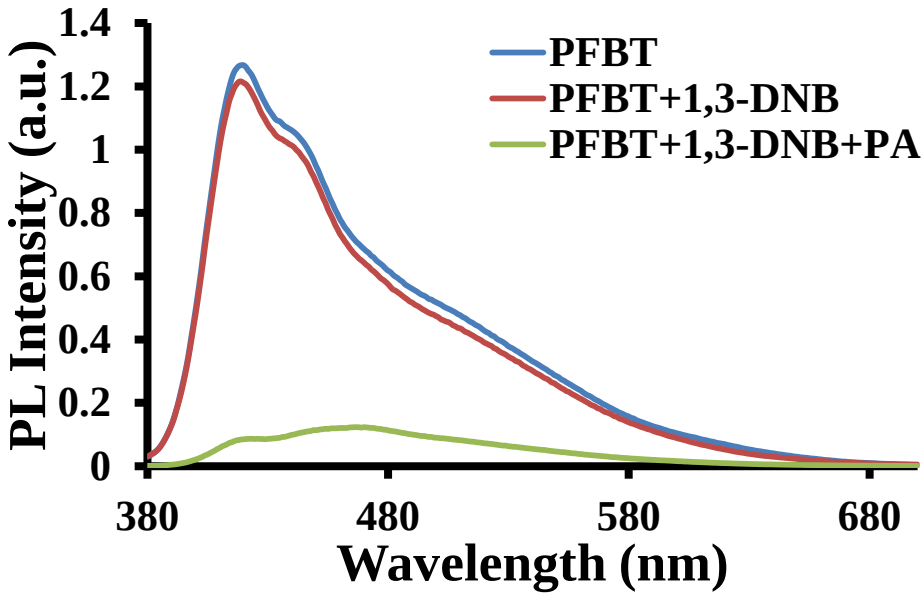

Figure A4.19 Emission spectra of PFBT (3.3×10^{-6} M) with 1,3-DNB (93.3×10^{-6} M) followed by addition of PA (93.3×10^{-6} M) in DMSO.

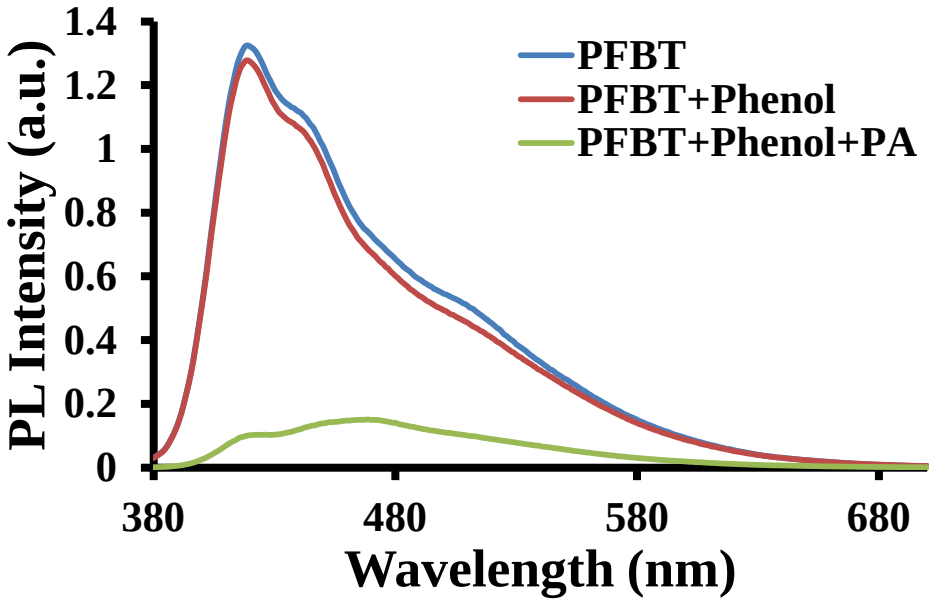

Figure A4.20 Emission spectra of PFBT (3.3×10^{-6} M) with phenol (93.3×10^{-6} M) followed by addition of PA (93.3×10^{-6} M) in DMSO.

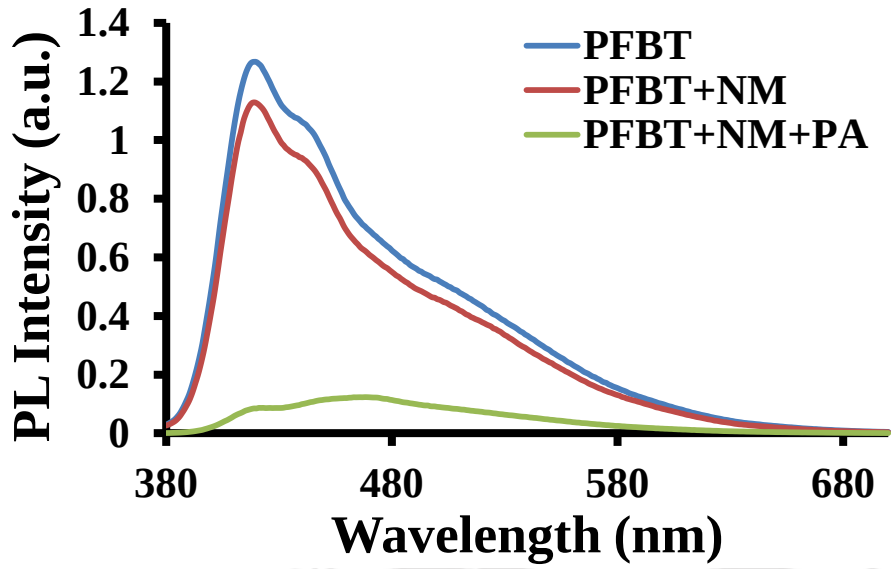

Figure A4.21 Emission spectra of PFBT (3.3×10^{-6} M) with NM (93.3×10^{-6} M) followed by addition of PA (93.3×10^{-6} M) in DMSO.

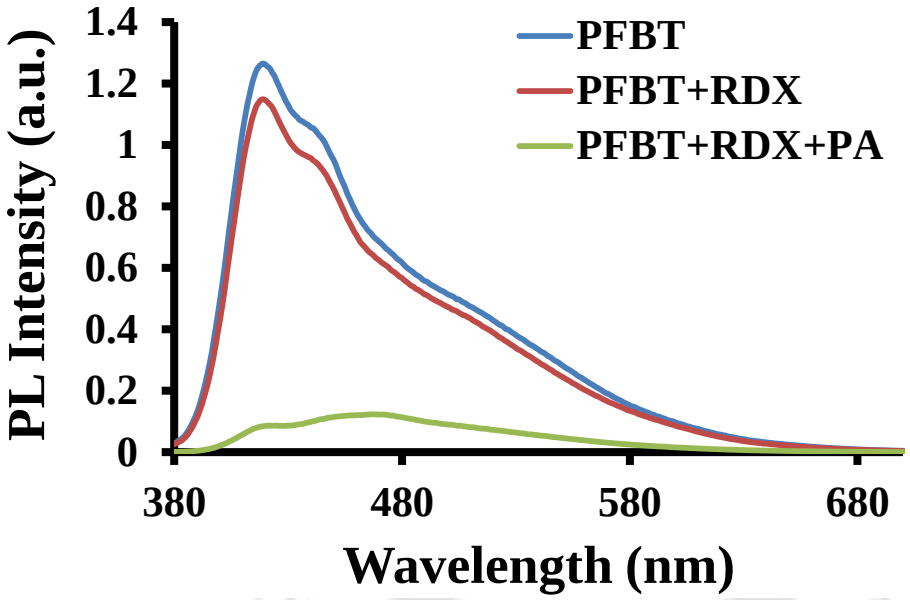

Figure A4.22 Emission spectra of PFBT (3.3×10^{-6} M) with RDX (93.3×10^{-6} M) followed by addition of PA (93.3×10^{-6} M) in DMSO.

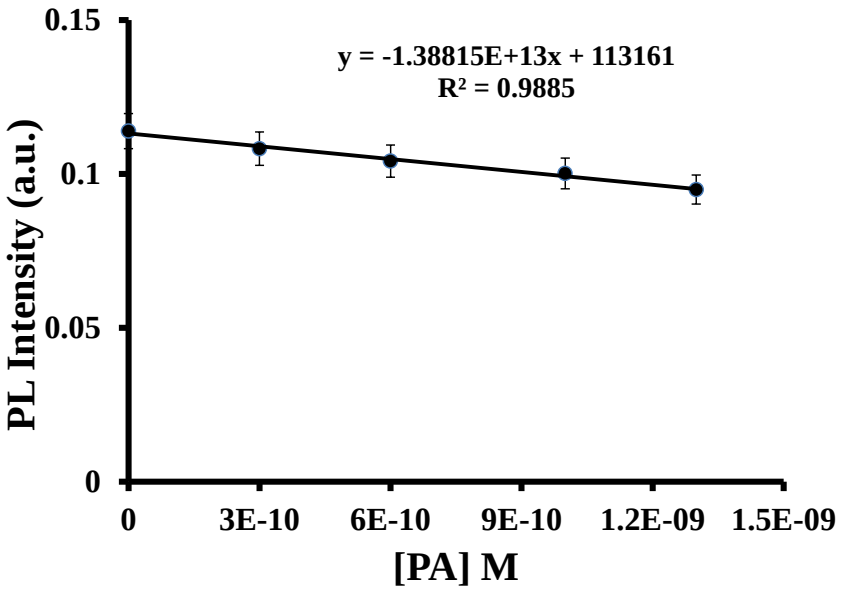

Figure A4.23 Fluorescence intensity of PFBT in water buffered with HEPES (pH=7.0, 10 mM) *vs* PA concentration.

LOD=3 × S.D./k

LOD = 3 × 922.48 / (138815× 10^8)

LOD= 0.19 nM

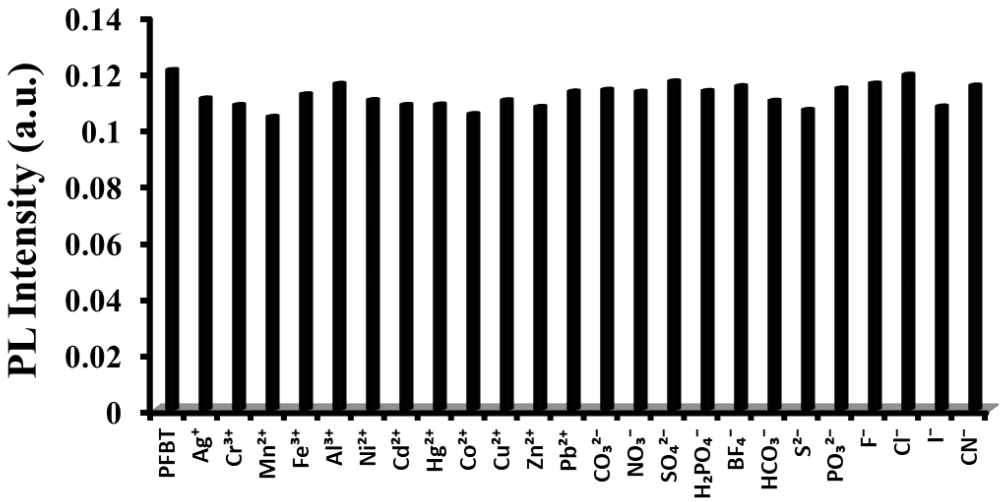

Figure A4.24 Bar diagram depicting effect of various ions (26.6 × 10^{-6} M) on the fluorescence intensity of PFBT (3.3 × 10^{-6} M) in water buffered with HEPES (pH=7.0, 10 mM).

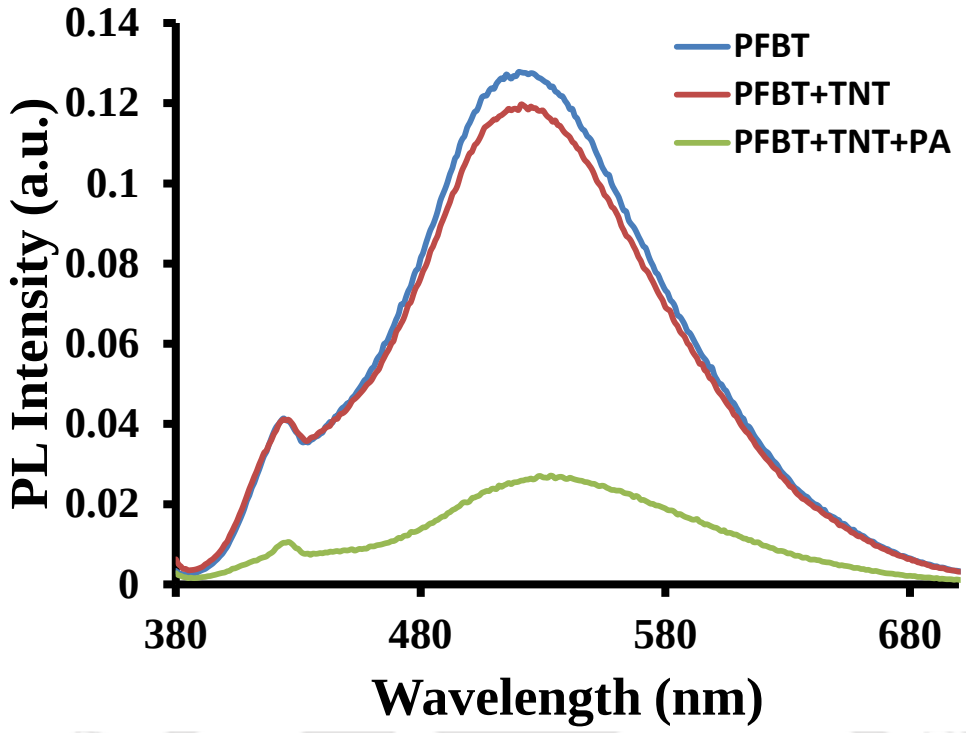

Figure A4.25 Emission spectra of PFBT (3.3×10^{-6} M) with TNT (26.6×10^{-6} M) followed by addition of PA (26.6×10^{-6} M) in water buffered with HEPES (pH=7.0, 10 mM).

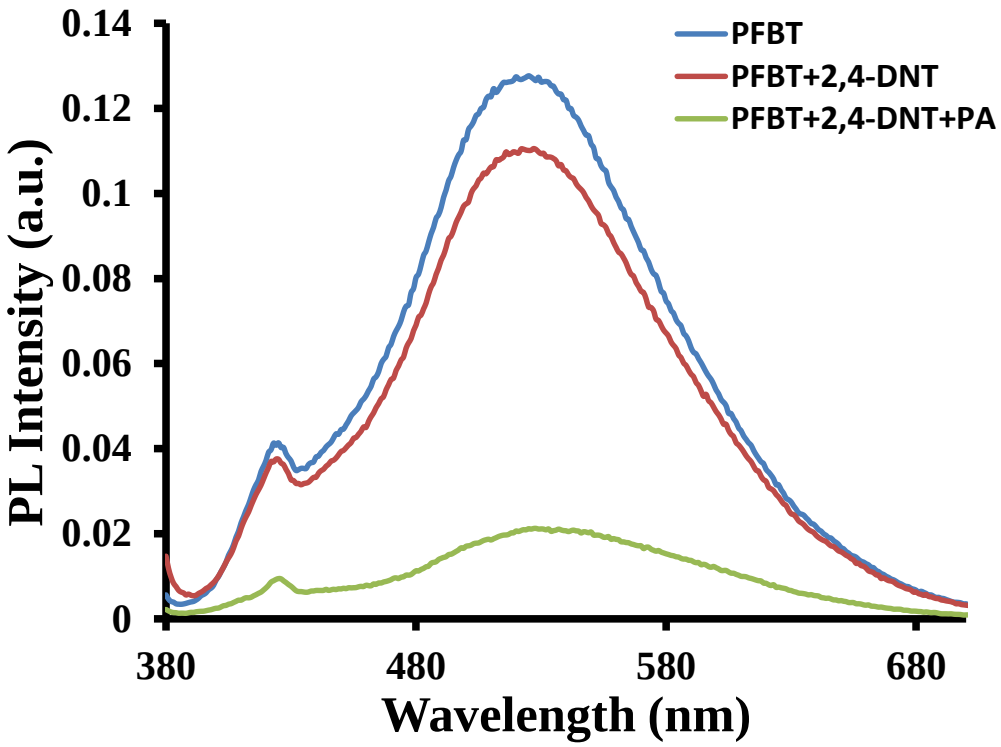

Figure A4.26 Emission spectra of PFBT (3.3×10^{-6} M) with 2,4-DNT (26.6×10^{-6} M) followed by addition of PA (26.6×10^{-6} M) in water buffered with HEPES (pH=7.0, 10 mM).

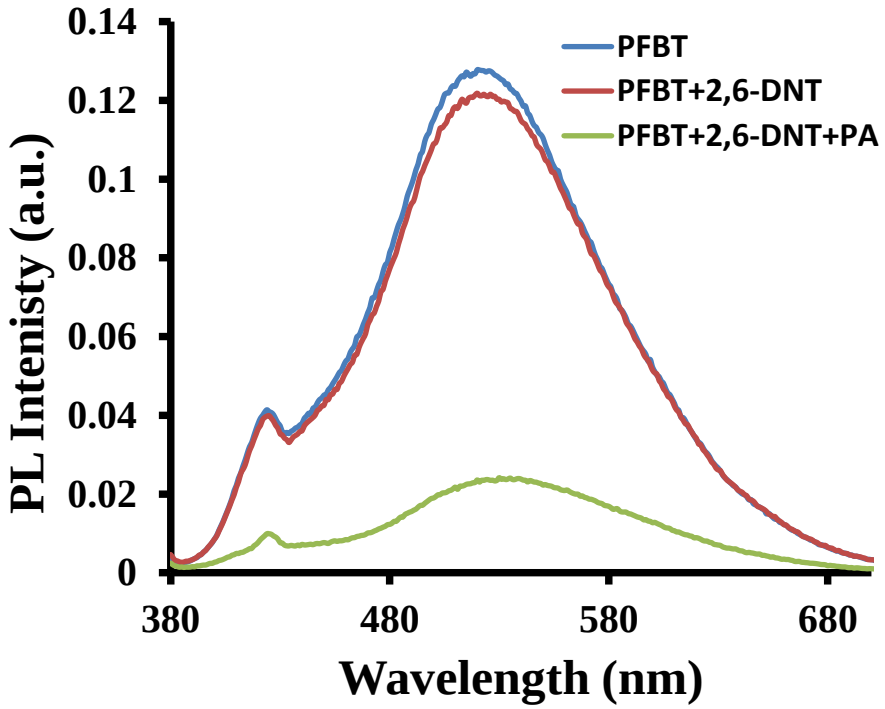

Figure A4.27 Emission spectra of PFBT (3.3×10^{-6} M) with 2,6-DNT (26.6×10^{-6} M) followed by addition of PA (26.6×10^{-6} M) in water buffered with HEPES (pH=7.0, 10 mM).

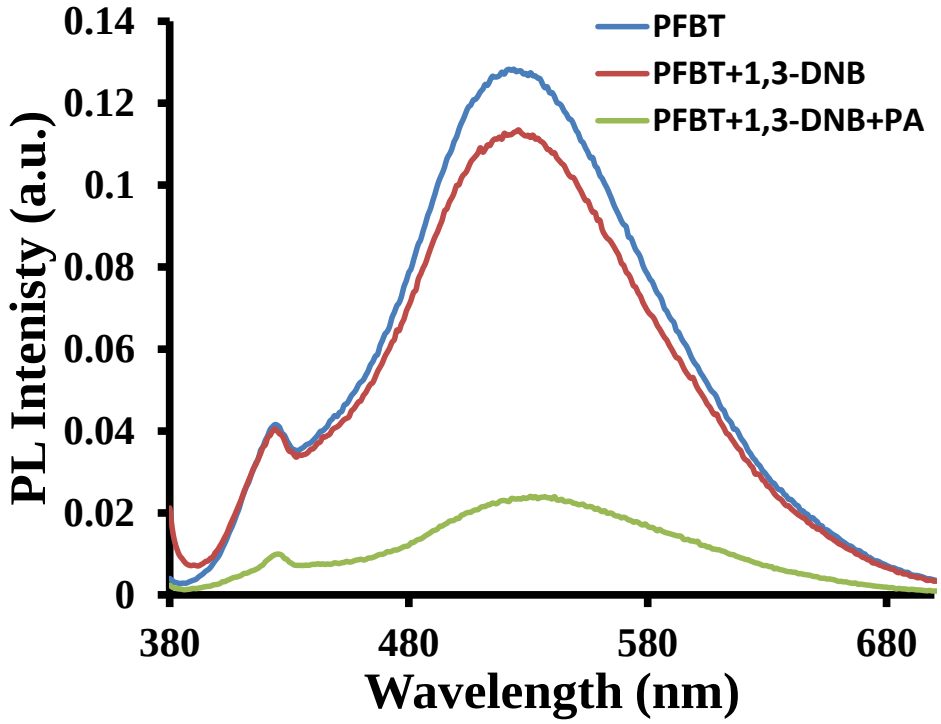

Figure A4.28 Emission spectra of PFBT (3.3×10^{-6} M) with 1,3-DNB (26.6×10^{-6} M) followed by addition of PA (26.6×10^{-6} M) in water buffered with HEPES (pH=7.0, 10 mM).

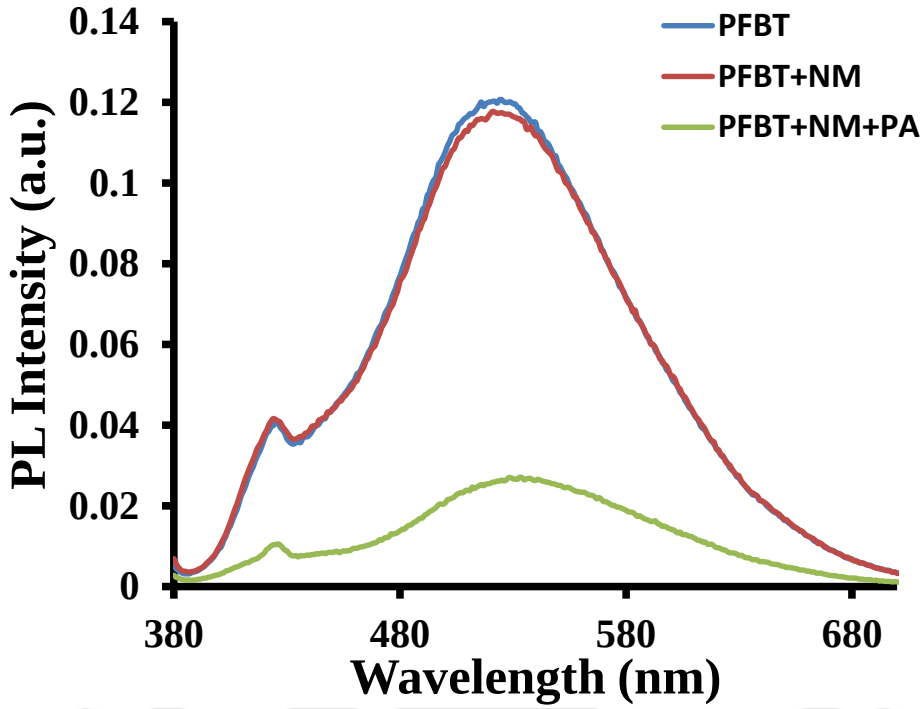

Figure A4.29 Emission spectra of PFBT (3.3×10^{-6} M) with NM (26.6×10^{-6} M) followed by addition of PA (26.6×10^{-6} M) in water buffered with HEPES (pH=7.0, 10 mM).

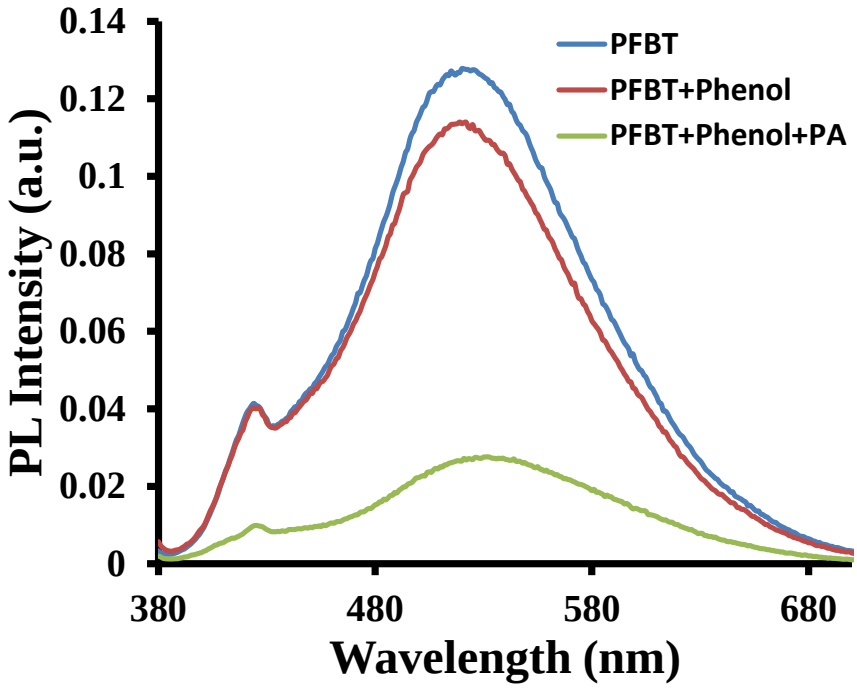

Figure A4.30 Emission spectra of PFBT (3.3×10^{-6} M) with phenol (26.6×10^{-6} M) followed by addition of PA (26.6×10^{-6} M) in water buffered with HEPES (pH=7.0, 10 mM).

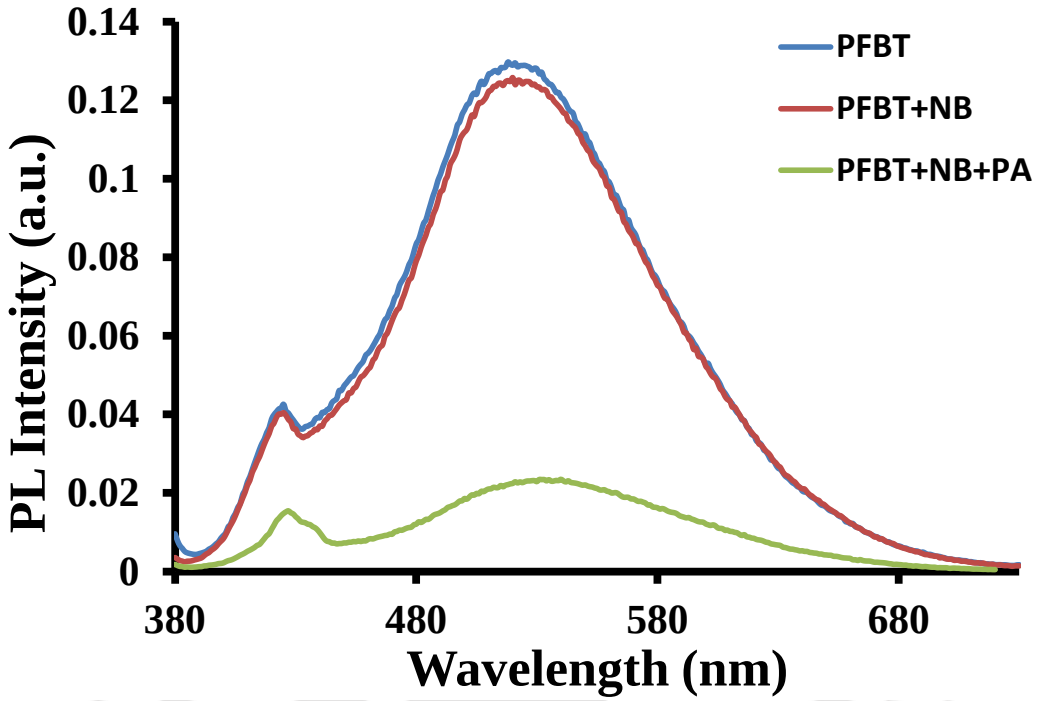

Figure A4.31 Emission spectra of PFBT (3.3×10^{-6} M) with NB (26.6×10^{-6} M) followed by addition of PA (26.6×10^{-6} M) in water buffered with HEPES (pH=7.0, 10 mM).

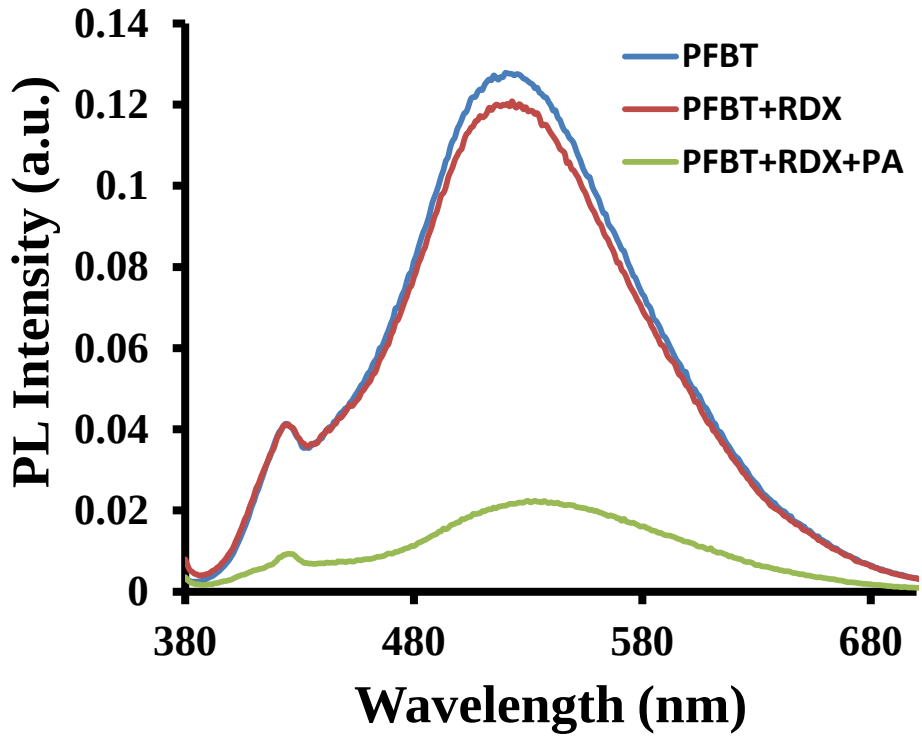

Figure A4.32 Emission spectra of PFBT (3.3×10^{-6} M) with RDX (26.6×10^{-6} M) followed by addition of PA (26.6×10^{-6} M) in water buffered with HEPES (pH=7.0, 10 mM).

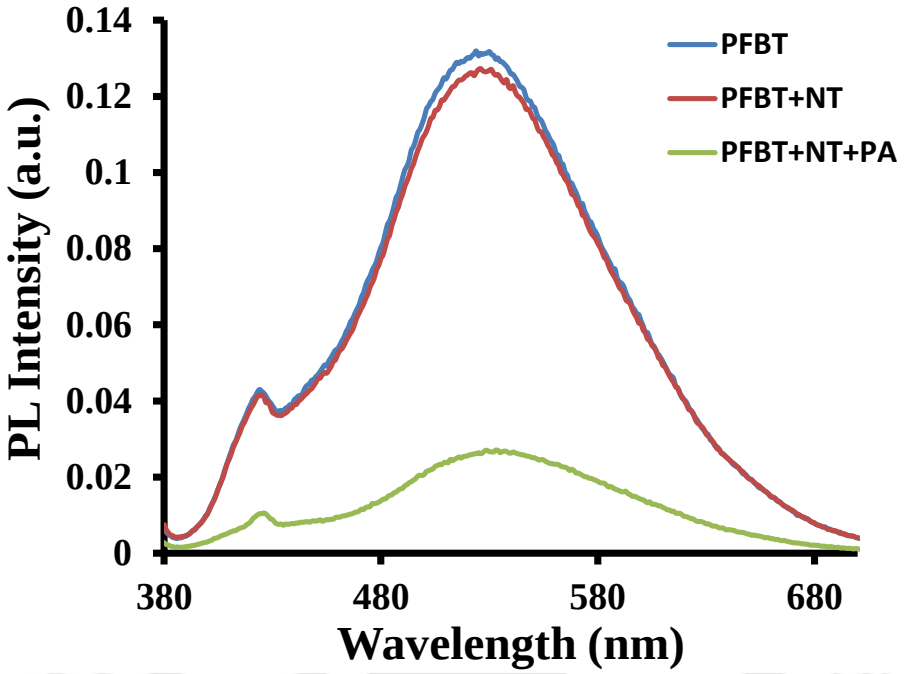

Figure A4.33 Emission spectra of PFBT (3.3×10^{-6} M) with NT (26.6×10^{-6} M) followed by addition of PA (26.6×10^{-6} M) in water buffered with HEPES (pH=7.0, 10 mM).

Table A4.3 Förster distance, Overlap integral J (λ) values and RET efficiency calculated for PA in the DMSO and water buffered with HEPES (pH=7.0, 10 mM).

Solvent	Förster distance R_0 (Å)	J (λ) values ($M^{-1}cm^{-1}nm^4$)	RET efficiency
DMSO	34.89	1.82×10^{14}	1.9
H_2O	21.32	2.67×10^{13}	52.1

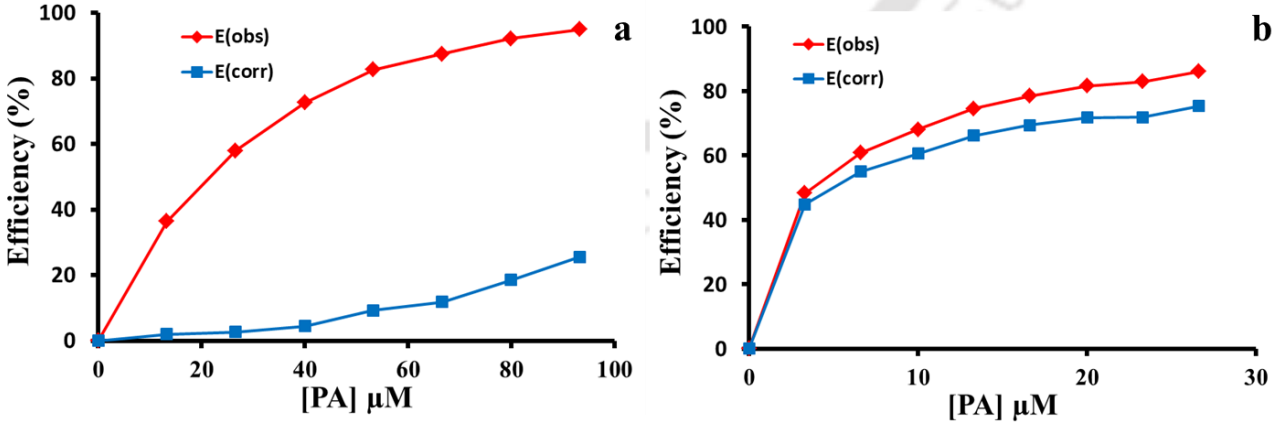

Figure A4.34 Quenching efficiency (E%= 1- I/I_0) of the corrected (blue) and observed (red) measurements for PFBT after addition of various concentration of PA in (a) DMSO and (b) Water (buffered with HEPES) solvent. Where I and I_0 are the fluorescence intensities of PFBT in presence and absence of PA.

Table A4.4. Calculations for IFE corrections for quenching in DMSO.

PA(μM)	A_{ex}	A_{em}	I_{obs}	I_{corr}	I_{corr}/I_{obs} Correction factor (CF)	$I_{corr}/I_{corr,o}$	E_{obs}	E_{corr}
0	0.039952	0.009627	1308600	1385467.734	1.05874	1	0	0
13.3	0.263665	0.161107	832044.5	1356852.255	1.630745	0.979346	36.4172	2.065402
26.6	0.477182	0.302843	549043	1347779.546	2.45478	0.972797	58.04348	2.72025
40	0.692118	0.442767	358040.4	1322435.624	3.693537	0.954505	72.63943	4.549518
53.3	0.910493	0.580956	225746.8	1257031.09	5.568324	0.907297	82.74899	9.270273
66.6	1.071489	0.677135	163034.3	1220649.146	7.487072	0.881038	87.54132	11.89624
80	1.29072	0.804451	101043.2	1127437.963	11.15798	0.81376	92.27853	18.62402
93.3	1.48138	0.909261	65712.14	1030305.738	15.67908	0.743652	94.97844	25.63481

Table A4.5. Calculations for IFE corrections for quenching in water.

PA(μM)	A_{ex}	A_{em}	I_{obs}	I_{corr}	I_{corr}/I_{obs} Correction factor (CF)	$I_{corr}/I_{corr,o}$	E_{obs}	E_{corr}
0	0.062055	0.00206	128678.1	138535.8	1.076608	1	0	0
3.3	0.117949	0.002376	66482.37	76360.54	1.148583	0.551197	48.33434	44.88028
6.6	0.180098	0.002273	50468.91	62260.04	1.233632	0.449415	60.77893	55.05851
10	0.243191	0.002539	41115.84	54559.97	1.326982	0.393833	68.04751	60.6167
13.3	0.307217	0.002785	32742.41	46785.54	1.428897	0.337714	74.55478	66.22855
16.6	0.36874	0.003023	27629.01	42388.38	1.534198	0.305974	78.52858	69.40258
20	0.431753	0.00299	23697.72	39091.12	1.649573	0.282173	81.58371	71.78266
23.3	0.495079	0.003144	21924.65	38908.47	1.774645	0.280855	82.96163	71.9145
26.6	0.557521	0.002004	17939.82	34164.93	1.904419	0.246614	86.05837	75.33855

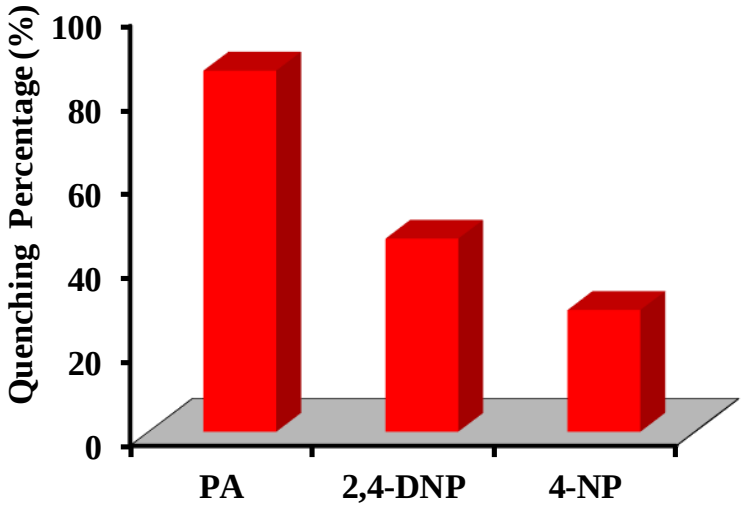

Figure A4.35 Comparison of fluorescence quenching caused by PA, 2,4-DNP and 4-NP of PFBT in water buffered with HEPES (pH-7, 10 mM).

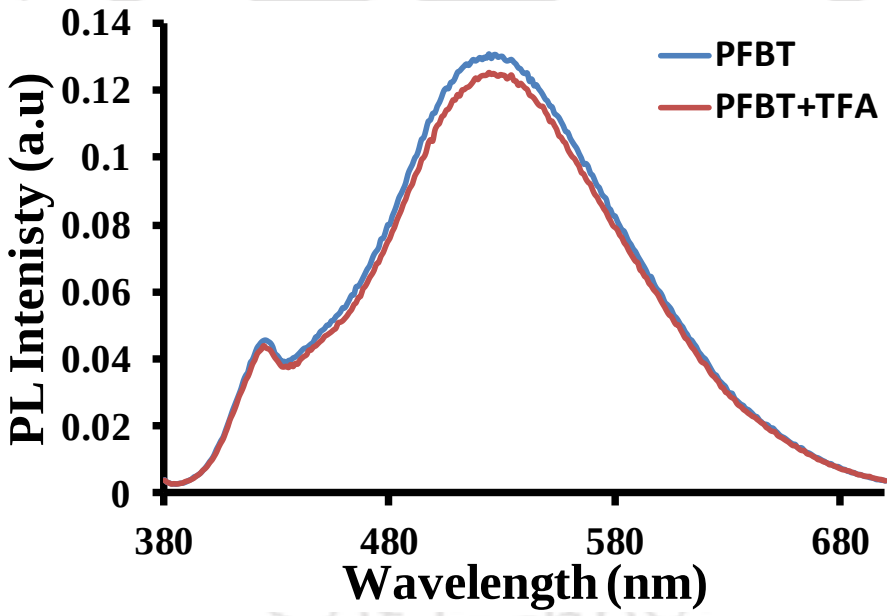

Figure A4.36 Emission spectra of PFBT (3.3×10^{-6} M) before and after adding TFA (26.6×10^{-6} M) in water buffered with HEPES (pH=7.0, 10 mM).

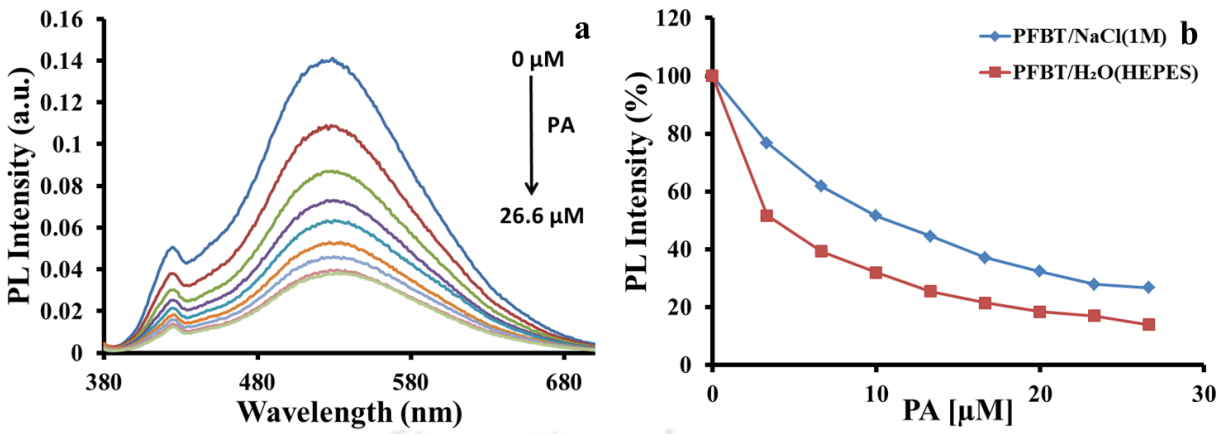

Figure A4.37 (a) PL spectra of PFBT (3.3×10^{-6} M) with various concentration of PA in water having 1 M NaCl ionic strength. (b) Comparison of PL Intensity (%) of PFBT with various concentration of PA in 1 M NaCl Solution and in water buffered with 10 mM HEPES (pH=7.0).

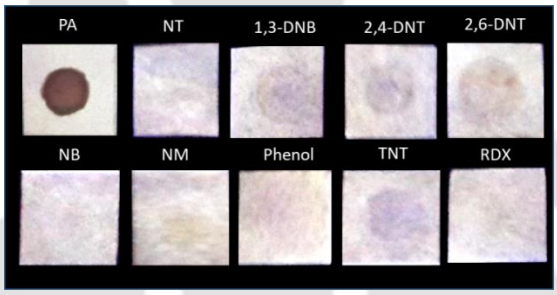

Figure A4.38 Color of PFBT coated paper strips under UV light (lamp excitation-365 nm) after addition of 10 µL of 10^{-3} M solution of various analytes.

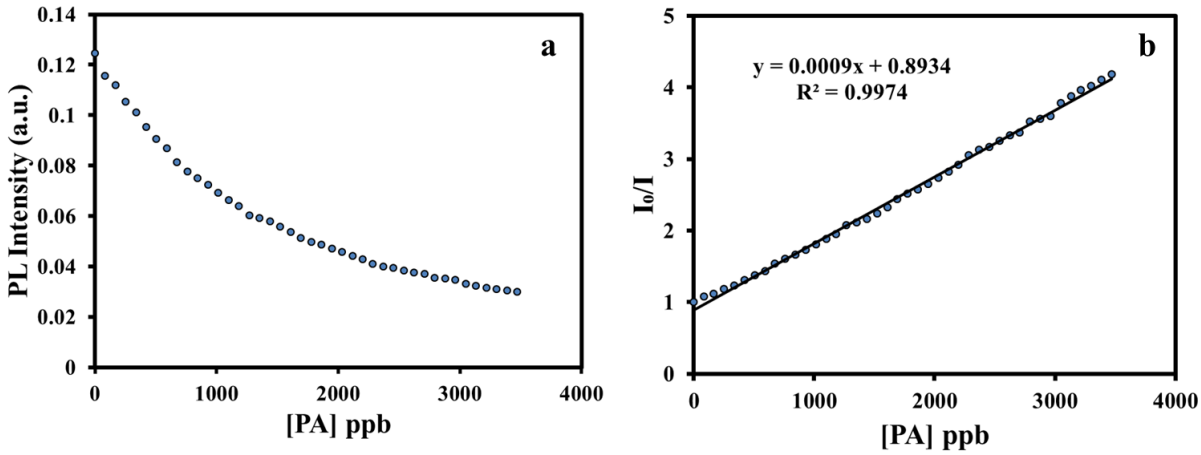

Figure A4.39 (a) PL intensity of PFBT (3.3×10^{-6} M) with increasing concentration of PA vapors in water buffered with HEPES (pH=7.0,10 mM). (b) Stern-Volmer plot obtained for the vapor sensing of PA.

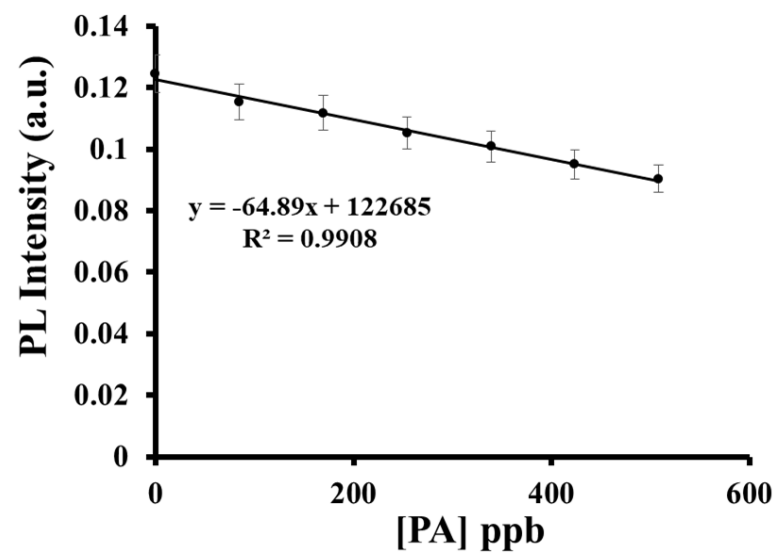

Figure A4.40 Fluorescence intensity of PFBT in water buffered with HEPES (pH=7.0, 10 mM) *vs* PA vapor concentration.

LOD = 3 × S.D./k

LOD = 3 × 922.48 / (64.89)

LOD = 42.6 ppb

Table A4.6: A comparative study of some conjugated materials based reports for picric acid detection.

Publication	Material Used	Detection Limit	Selectivity	Sensing Mechanism	Medium Used
Present Manuscript	***Conjugated Polymer***	***92.7×10^{-9} M (21.23 ppb) And 0.19×10^{-9} M (43.53 ppt)***	***Selective***	***IFE and RET***	***DMSO And Water***
J. Am. Chem. Soc. **2003**, *125*, 3821-3830	Polymetalloles	Not reported	Not selective	Electron-transfer	THF
Macromolecules **2009**, *42*, 9400-9411	Conjugated Polyelectrolyte	0.17 ppm (0.72 µM)	Not studied	-	THF:H_2O
Macromol. Rapid Commun. **2010**, *31*, 834–839	Poly(silylenevinylene)	Upto 1ppm	Not studied	-	THF:H_2O
Macromolecules **2011**, *44*, 5977–5986	Poly(silylenevinylene)s	Upto 1ppm	Not studied	Electron and/or energy transfer	THF:H_2O
Macromol. Rapid Commun. **2013**, *34*, 796−802	Polytriazole	9×10^{-8} M	Not studied	Energy transfer	THF:H_2O
RSC Adv., **2013**, *3*, 8193–8196	Poly(arylene ynonylene)	1 ppm	Not studied	-	THF:H_2O
Macromolecules **2013**, *46*, 3907−3914	Poly(aroxycarbonyltriazole)s	Upto 1µg/mL	Not studied	-	THF:H_2O
Macromolecules **2014**, *47*, 4908−4919	poly(dipropargyl amine)s	1µM	Not selective	Energy transfer	THF:H_2O
Polym. Chem., **2014**, *5*, 5628–5637	Poly(acrylate)	2.5 ppm	Not selective	Electron transfer	THF:H_2O
J. Mater. Chem. A, **2014**, *2*, 15560–15565	polydiacetylene	0.11 ppm (0.48µM)	Selective	Electron transfer	CH_3OH
Chem. Commun., **2015**, *51*, 7207–7210	*Conjugated Polyelectrolyte*	0.128 ppb	Selective	Electron and/or energy transfer	H_2O
J. Mater. Chem. A, **2015**, *3*, 92–96	*Covalent-organic polymer*	About 1 ppm	Selective	Electron transfer	CH_3OH
ACS Sens. ***2016**, 1, 1070−1077*	*Conjugated Polymer*	57.8 nM	Selective	IFE and PET	THF:H_2O
ACS Omega ***2017**, 2, 4424−4430*	*Conjugated Polyelectrolyte*	295 nM	Selective	IDA	H_2O

Chapter 5

"Receptor Free" IFE Based Detection of Nitroexplosive-Picric Acid Using Two Polyfluorene Derivatives in Solution and Solid State and IFE Correction

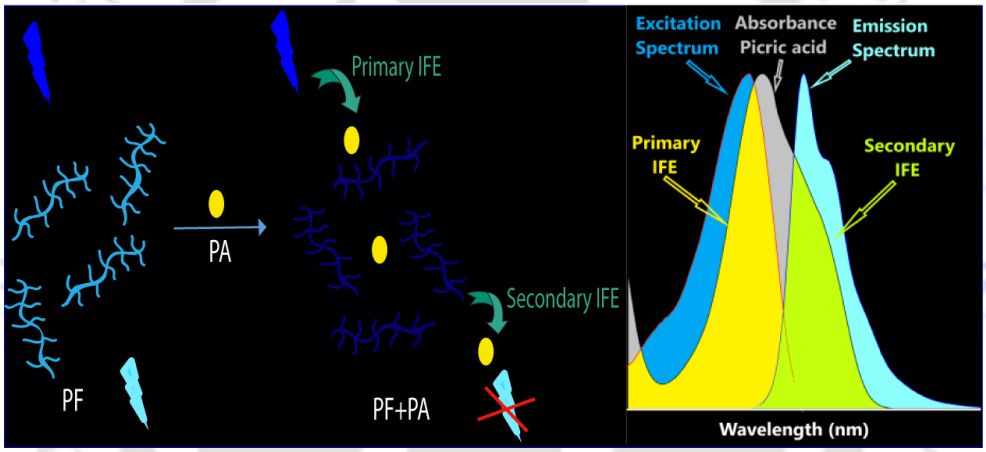

Tanwar, A. S.; Patidar, S.; Ahirwar, S.; Dehingia, S.; Iyer, P. K. (*Analyst* **2019**, *144*, 669-676.)

Abstract

Two "Receptor-free" fluorescent conjugated polymers (CPs) of fluorene namely 9,9-bis(6-bromohexyl)-2-phenyl-9H-fluorene (PF1) and 9,9-bis(6-bromohexyl)-9H-fluorene (PF2) were synthesized using Suzuki cross coupling polymerization and oxidative coupling polymerization methods in high yields and well characterized by gel permeable chromatography, NMR, UV-vis, fluorescence and time-resolved photoluminescence (TRPL) spectroscopies. Both CPs explicitly recognized nitroexplosive picric acid (PA) and displayed fluorescence quenching response in solution and on solid support via Inner Filter Effect (IFE) mechanism. Both CPs were highly selective and sensitive towards PA with a high quenching constant values (K_{sv}) of 5.1×10^4 M^{-1} and 5.0×10^4 M^{-1} and remarkably low limit of detection (LOD) values of 110 nM and 219 nM. Contact mode detection of PA was also performed using economical and transportable fluorescent paper test strips for onsite sensing, which easily detects a minimum of 22.9 femtogram level of PA. Earlier, the IFE mechanism for PA sensing has not been explored elaborately and therefore experiments for IFE correction were performed carefully for PA to observe ~77% suppression efficiency due to IFE. Such studies provide fundamentally important information to IFE based mechanism for detection of various analytes.

5.1 Introduction

Picric acid (PA) which is also known as 2,4,6-trinitrophenol, a well-known nitroexplosive possessing potent explosive nature, higher than even 2,4,6-trinitrotoluene (TNT),[1] has gained attention of many researchers in order to develop a method for its detection.[2-3] However, to date, nitroexplosive detection remains as a challenging task. Besides its explosive nature, it has been used extensively in various other application purposes such as in dye industries, pharmaceutical industries, leather, matchbox industries, etc.[4-6] Owing to its high water solubility, PA contaminates very easily land and nearby water reservoirs, making it as a potential environment pollutant which has very severe effects on health of living beings causing chronic diseases such as cancer, kidney and liver damage, sycosis as well as respiratory problems.[7-9] Moreover, it has low rate of degradation in biosystems and converts into picramic acid under metabolism, which has much more mutagenic activity as compared to PA itself.[10] Thus, keeping this in view, detection of PA is highly significant for forensic investigation, terrorist threats, abandoned military bases or war sites, homeland security as well as environment protection.

Several detection platforms are presently available for nitroexplosive sensing based on few analytical techniques namely electrochemical methods,[11] solid phase microextraction-ion mobility spectroscopy,[12] dynamic light scattering,[13] and enzyme linked immunosorbent assay (ELISA), etc.[14] However, most of these analytical methods are deficit in selectivity, expensive, suffer from portability issues and therefore possess limited on-site use. As a result, fluorescent technique based sensors came into existence and recently played a major role as a detection method in nitroexplosive sensing owing to the remarkable sensitivity, fast response time and convenient in portability.[3,15] Therefore, several reports for nitroexplosive detection based on a variety of fluorescent probes such as organic molecule dyes, metal complexes, conjugated and non-conjugated polymers, metal organic frameworks, quantum dots, carbon dots, nanoparticles etc. are reported[16-30] though many reports still bear poor sensitivity, discrimination issues, and lack selectivity in competitive environment, challenging for on-site detection due to difficulty in handling probes and their portability. Moreover, the mechanism of sensing found in these reports was either photo induced electron transfer (PET), Förster resonance energy transfer (FRET), ground state charge transfer complexation, static or dynamic quenching or indicator displacement assay (IDA) based or combination of two or more mechanism.[30-34]

Interestingly, all of the above reported mechanism tend to have interaction between the probe and the nitroexplosive, while none of the previous report involves "interaction free" or "receptor free" detection of PA in case of conjugated polymers i.e. inner filter effect (IFE) except a handful.[34] IFE is an important phenomenon in spectrofluorometry based on the non-irradiation energy conversion model, which arises when a quencher/absorber (PA) absorbs the emission and/or excitation light in the detection system, that subsequently leads to an amplified or exponential quenching of florescence of fluorophore, giving rise to low limit of detection (LOD) and enhances sensitivity of the system.[35] As compared to the other mechanisms, IFE based sensing works in a straightforward manner, devoid of any interaction between fluorophore (probe) and absorber (PA). However, in order to design IFE based systems, a desired fluorophore and a quencher combination is still quite challenging. Therefore, keeping this in view, two polyfluorenes derivatives (PF1 and PF2) based conjugated polymers (CPs) were designed as fluorophores. Notably in the last few years, CPs have gained much attention for their wide range of applications, especially in the area of sensing, owing to the efficient photophysical properties like remarkable molar absorptivity, high quantum efficiency, extraordinary amplification in signals via "molecular wire effect" and film forming property,[36-39] which encouraged us to choose CPs based fluorophore i.e. PF1 and PF2, for the "Receptor free" detection of nitroexplosive-PA, which until now remains a highly challenging analyte.

5.2 Experimental

5.2.1 Materials and Methods

Nitroexplosives namely, 2,4-dinitrotoluene (2,4-DNT), 2,6-dinitrotoluene (2,6-DNT), 1,3-dinitrobenzene (1,3-DNB) and 4-nitrotoluene (4-NT) were purchased from Sigma Aldrich. 2,4,6-trinitrotoluene (2,4,6-TNT) and RDX were purchased from AccuStandard and used as received. Picric acid (PA) was obtained from Loba Chemie Pvt. Ltd. All other chemicals and reagents were bought from Merck and Alfa-Aesar, and were used without further purification. Milli-Q water was used everywhere in titration. ^{1}H NMR (400 and 600 MHz) and ^{13}C NMR (100 and 150 MHz) spectra were recorded on Varian-AS400 NMR spectrometer and Bruker Ascend 600 spectrometer respectively. Photoluminescence spectra were taken on a Horiba Fluoromax-4 spectrofluorometer using 10 mm path length quartz cuvettes with a slit width of 3 nm at 298 K. Perkin Elmer Lambda-25 spectrophotometer was used to record absorption spectra. Edinburg Life Spec

II instrument was used for execution of time-resolved fluorescence studies. Cyclic voltammograms were recorded using CH instruments Model 700D series Electrocchemical workstation. Gel Permeable Chromatography was carried out in THF using polystyrene as standard. Paper strip test was done by using Whatman qualitative filter paper grade 1.

5.2.2 Synthetic Procedure

5.2.2a Synthesis of 2,7-Dibromo-9,9-bis(6-bromohexyl)-9H-fluorene (M2):

Monomer (M2) was synthesized by using a previously established procedure from literature.[40] As reported earlier in chapter-2, 2,7-dibromofluorene (1.0 g, 3.086 mmol) and catalytic amount of tetrabutyl ammonium iodide (TBAI) (0.24 g, 0.617 mmol) were taken in a 50 mL round bottom flask. 50% aqueous NaOH (50%, 12 mL) was added to the flask under inert condition. The flask was degassed using freeze-thaw cycles followed by addition of 1,6-dibromohexane (3.32 mL, 21.602 mmol). The reaction mixture was maintained at 70 °C and stirred for 4 h. Further, it was cooled to room temperature and extracted with dichloromethane (DCM). The DCM layer was washed with water thrice and dried over anhydrous sodium sulfate. The organic layer was concentrated using rotatory evaporator and crude compound obtained was purified via column chromatography over a silica gel pad using hexane. (Yield = 1.8 g, 90 %). ^{1}H NMR (400 MHz, $CDCl_3$, δ ppm): 7.53 (d, 2H), 7.45 (m, 4H), 3.29 (t, 4H), 1.92 (t, 4H), 1.68 (m, 4H), 1.18 (m, 4H), 1.08 (m, 4H), 0.58 (m, 4H). ^{13}C NMR (100 MHz, $CDCl_3$, δ ppm): 152.40, 139.31, 130.57, 126.33, 121.80, 121.45, 55.79, 40.26, 34.05, 32.83, 29.17, 27.97, 23.68.

5.2.2b Synthesis of poly 9,9-bis(6-bromohexyl)-2-phenyl-9H-fluorene (PF1):

A mixture of M2 (0.200 g, 0.35 mmol), benzene-1,4-bisboronic acid (0.053 g, 0.32 mmol), tetrakistriphenylphosphine palladium (0.018 g, 0.015 mmol), 3 mL of 2M aqueous solution of K_2CO_3 and THF (9 mL) were added to a two neck round bottom flask equipped with a reflux condenser. The reaction mixture was degassed thrice by freeze-thaw cycles followed by refluxing for 15 h under inert atmosphere. The reaction mixture was cooled and concentrated via rotatory evaporator then extracted with chloroform/water thrice. The chloroform layer was evaporated to get a thick solution which was further purified by precipitation in methanol thrice, to obtain a pale white solid. (Yield = 70 %, 0.140 g). ^{1}H NMR (400 MHz, $CDCl_3$, δ ppm): 7.82 (br), 7.66 (br), 7.48 (br), 7.36 (br), 3.28 (br), 2.09 (br), 1.65 (br), 1.23 (br), 1.12 (br), 0.77 (br). GPC using polystyrene as standard in THF: Mw =1.87×10^4, PDI=1.64.

5.2.2c Synthesis of 9,9-bis(6-bromohexyl)-9H-fluorene (F2):

Monomer (F2) was synthesized by using a previously established procedure from literature.[40] As reported earlier in chapter 4, fluorene (1 g, 6.016 mmol) and catalytic amount of tetrabutyl ammonium iodide (TBAI) (0.476 g, 1.203 mmol) were taken in a 50 mL round bottom flask. 50% aqueous NaOH (15 mL) was added to the flask under inert condition. The flask was degassed using freeze thaw cycles followed by addition of 1,6-dibromohexane (6.47 mL, 42.112 mmol). The reaction mixture was maintained at 70 °C and stirred for 4 h. It was further cooled to room temperature and extracted with dichloromethane (DCM). The DCM layer was washed with water thrice and dried over anhydrous sodium sulfate. The organic layer was concentrated using rotatory evaporator and 2.4 g of crude compound obtained was purified via column chromatography over a silica gel pad using hexane. (Yield = 82 %). ^{1}H NMR (400 MHz, $CDCl_3$, δ ppm): 7.72 (d, 2H), 7.32 (m, 6H), 3.27 (t, 4H), 1.97 (t, 4H), 1.65 (m, 4H), 1.18 (m, 4H), 1.06 (m, 4H), 0.60 (m, 4H). ^{13}C NMR (100 MHz, $CDCl_3$, δ ppm): 150.45, 141.28, 127.27, 127.01, 122.92, 119.89, 55.07, 40.40, 34.12, 32.81, 29.23, 27.93, 23.68.

5.2.2d Synthesis of poly(9,9-bis(6-bromohexyl)-9H-fluorene) (PF2):

As reported in chapter 4, In a 50 mL two necked round bottom flask fitted with argon inlet, ferric chloride (anhy.) (8.124 mmol, 1.4 g) was dissolved in nitrobenzene (15 mL). A solution of monomer (F2) (2.031 mmol, 1 g) in nitrobenzenze (10 mL) was added slowly to the above round bottom flask via a syringe under inert atmosphere and stirred for 36 h at room temperature. The reaction mixture was poured in methanol and stirred for 1 h to get precipitate, centrifuged and filtered. The polymer obtained was dissolved in chloroform and further precipitated with methanol. The polymer was repeatedly washed with methanol and finally dried under reduced pressure to obtain 49 mg of brown colored polymer. ^{1}H NMR (400 MHz, $CDCl_3$, δ ppm): 7.84 (br), 7.70 (br), 7.37 (br), 3.30 (br), 2.07 (br), 1.67 (br), 1.27 (br), 1.14 (br), 0.72 (br). GPC using polystyrene as standard in THF: Mw =2.41×10^4, PDI=3.6.

5.2.3 Preparation of stock solutions

Stock solution of polymer PF1 and PF2 were prepared in THF solvent at a concentration of 1×10^{-4} M. Stock solution of other nitroaromatic compounds i.e. nitromethane (NM), phenol, 4-nitrophenol (4-NP), nitrobenzene (NB), were prepared at concentrations of 1×10^{-2} M. Stock solution of 2,4- dinitrophenol (2,4-DNP) was prepared in Milli-Q water at a concentration of 1×10^{-3} M. Stock solution of other nitroaromatics namely 4-Nitrotoluene

(4-NT), 1,3-Dinitrobenzene (1,3-DNB), 2,4-Dinitrotoluene (2,4-DNT), 2,6-Dinitrotoluene (2,6-DNT), were prepared in HPLC grade THF at concentrations of 1×10^{-2} M. Stock solution of TNT and RDX were prepared at concentration of 1×10^{-2} M in 1:1 CH_3CN:MeOH. The absorption and fluorescence titrations were carried out in a quartz cuvette (1 cm × 1 cm) after preparing various solution of PF1 (1.6×10^{-7} M) and PF2 (3.3×10^{-7} M) separately in 4:1 THF:HEPES (10 mM, pH=7) each containing different concentration of nitroaromatic compounds. All the spectra were recorded at room temperature after thoroughly mixing of the resultant mixture.

5.2.4 Time-resolved decay measurements

Lifetime decay measurements of PF1 (1.6×10^{-7} M) in the absence and presence of PA (66.6×10^{-6} M) were performed via pulse excitation of 375 nm and emission at 408 nm in 4:1 THF:HEPES (10 mM, pH=7). Similarly, Lifetime decay measurements of PF2 (3.3×10^{-7} M) in the absence and presence of PA (66.6×10^{-6} M) were performed via pulse excitation of 375 nm and emission at 415 nm in 4:1 THF:HEPES (10 mM, pH=7). The curves for PF1 and PF2 were fitted mono- and bi-exponentially respectively and the average life time was considered for uniformity in results. Table A5.1 and A5.2 in the supporting information file shows amplitude, lifetime of each component and average lifetime.

5.2.5 Preparation of paper strips

Whatman filter paper (70 mm diameter) was used to prepare fluorescent paper strips by dipping it into a solution of polymer (1×10^{-4} M) in THF followed by drying in air. The dried polymer coated test strip was cut into desired size (1 cm × 1 cm) and used a portable PA detection purposes.

5.2.6 Detection limit calculations

Various solutions of PF1 (1.6×10^{-7} M) in 4:1 THF:HEPES (10 mM, pH=7) each containing PA (2.33 µM, 2.00 µM 1.66 µM, 1.33 µM, 1.0 µM, 0.66 µM, 0.33 µM, 0.0 µM) were prepared separately and emission spectrum was recorded for each sample. Similarly, Various solutions of PF2 (3.3×10^{-7} M) in 4:1 THF:HEPES (10 mM, pH=7) each containing PA (2.33 µM, 2.00 µM 1.66 µM, 1.33 µM, 1.0 µM, 0.66 µM, 0.33 µM, 0.0 µM) were prepared separately and emission spectrum was recorded for each sample. A calibration curve was obtained for both PF1 and PF2 separately, between the emission intensity maxima and the concentration of PA to get a regression curve equation. The

limit of detection (LOD) was evaluated from the equation 3σ/k, where σ is the standard deviation (SD) in the emission intensity for the blank polymer solution in the absence of PA and K is the slope of the calibration curve.

5.2.7 Calculations for photoluminescence quantum yield

The quantum yield of polymers PF1 and PF2 were determined in THF using quinine sulphate (Φ_r = 0.54 in 0.1M H_2SO_4) as reference material. The following equation[34] was employed for calculations.

$$\Phi_s = \Phi_r (A_r F_s / A_s F_r) (\eta_s^2 / \eta_r^2)$$

where, s and r represents the sample and reference, respectively, A denotes the absorbance, F is the relative integrated fluorescence intensity and η is used for refractive index of the medium used.

5.2.8 Cyclic voltammetry studies

CV measurements were performed using a CH Instruments 760D electrochemical workstation at a scan speed of 50 mV/s. A three-electrode cell with platinum wire counter electrode, glassy carbon working electrode and Ag/Ag^+ reference electrode was used. Tetrabutylammonium hexafluorophosphate (0.1 M) in acetonitrile was used as supporting electrolyte and Fc^+ /Fc was used as reference. A thin film of polymer was casted from 10 μL, 1 mM solution in DCM on the glassy carbon working electrode and the measurements were performed at room temperature under inert atmosphere.

5.3 Result and Discussion

5.3.1 Synthesis and characterization of 9,9-bis(6-bromohexyl)-2-phenyl-9H-fluorene (PF1) and 9,9-bis(6-bromohexyl)-9H-fluorene (PF2)

The highly fluorescent neutral conjugated polyfluorene derivatives PF1 and PF2 were synthesized via Suzuki cross coupling polymerization and oxidative polymerization methods, respectively as shown in scheme 5.1. Monomers (M2 and F2) were synthesized in high yields using an environmentally green methodology in aqueous media.[40] Both monomers (M2 and F2) and polymers (PF1 and PF2) were purified and characterized before further use (Figure A5.1- A5.6). The molecular weight of the Polymers PF1 and PF2 was found to be 5.68×10^3, PDI=2.7 and 2.41×10^4, PDI=3.6, respectively (Figure A5.7-A5.8). Both polymers PF1 and PF2 were found to be highly soluble in most of organic solvents with a high value of PL quantum yield (Φs) in THF i.e 0.61 and 0.40

respectively. Polymers PF1 and PF2 displayed absorption maxima at 354 nm and 373 nm, respectively and emission maxima at 408 nm (excitation at 360 nm) and 415 nm (excitation at 369 nm) respectively in THF.

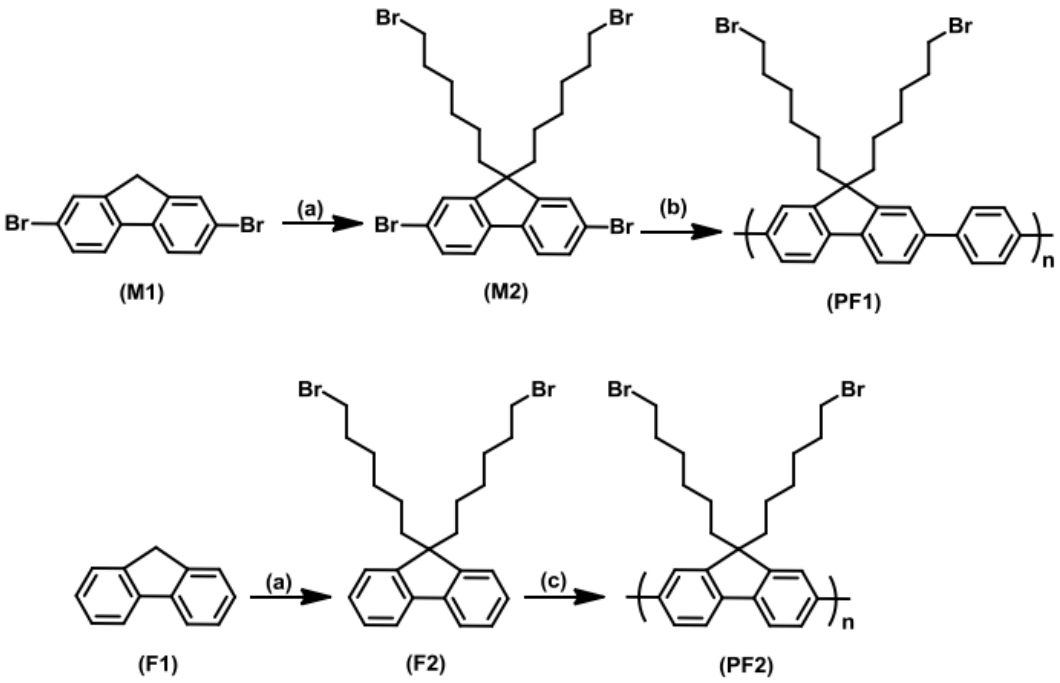

Scheme 5.1 Synthesis of the polymer-PF1 and PF2. (a) 1,6-dibromohexane, 50% NaOH(aq.), TBAI, 70°C, 4h. (b) tetrakistriphenylphosphine palladium (0), benzene-1,4-diboronic acid, 2 M aq. K_2CO_3, THF, reflux, 24 h. (c) $FeCl_3$, nitrobenzene, 36 h, rt.

5.3.2 Sensing studies

Considering environmental applications, PL sensing of PA were accomplished in 4:1-THF:Water (buffered with 10 mM HEPES at pH=7.0). Dilute solution of polymers PF1 and PF2 in 4:1-THF:HEPES buffer (10 mM, pH= 7.0) showed strong blue fluorescence under UV lamp irradiation (Figure A5.9). PL sensing of nitroexplosive-PA was performed with both polymers PF1 and PF2 by gradually increasing the amount of nitroexplosive in the respective solution of PF1 (1.6×10^{-7} M) and PF2 (3.3×10^{-7} M). It was witnessed that addition of 3.3 µM of PA solution caused instantaneous PL quenching of 9 % and 10 % in PF1 and PF2 solution respectively, which reached up to 93 % and 95 % after addition of 66.6 µM of PA concentration (Figure 5.1a and 5.2a) in the respective solutions. The fading of the blue fluorescence after addition of PA could be seen easily under UV lamp irradiation (Figure A5.9). Stern-Volmer (S-V) plot i.e. a plot of I_o/I versus

[Q] was attained for both polymers PF1 and PF2, where I_o symbolizes intensity of fluorophore without a quencher, I symbolizes intensity of fluorophore with a quencher, and [Q] symbolizes concentration of quencher i.e. [PA]. The quenching constant or S-V constant (K_{sv}) was calculated to be 5.1×10^4 M^{-1} and 5.0×10^4 M^{-1} for the both the polymers PF1 and PF2, respectively via the linear fitting of S-V plot (Figure A5.10-A5.11) signifying extraordinary sensitivity of PF1 and PF2 toward PA. LOD was evaluated to be 110 nM and 219 nM for polymers PF1 and PF2, respectively via the equation $3\sigma/k$ (Figure A5.12-A5.13),[41] Polymer PF1 showed superior results over PF2 and which is also superior to most of the sensor reported for PA detection earlier (Table A5.3).

5.3.3 Selectivity studies

To investigate the sensing behavior of PF1 and PF2 towards various interfering analytes, fluorometric titrations were done with various interfering nitroexplosive compounds such as TNT, RDX, 2,6-DNT, 2,4-DNT, 4-NT, NB, 1,3-DNB, phenol and NM in the respective solution of PF1 (1.6×10^{-7} M) and PF2 (3.3×10^{-7} M) (Figure A5.14-A5.15). Interestingly, addition of these analytes hardly affected fluorescence of both the CPs (Figure 5.1b and 5.2b). Figure 5.1c and 5.2c showed the S-V plot obtained for various analytes for PF1 and PF2 respectively, which follows a linear relationship with the concentration of various analytes added whereas in case of PA, it follows a linear relationship at low concentration and diverges from linearity at higher concentration of PA. This divergence or non-linear nature of S-V plot is an indication for an amplified quenching in CPs and could be due to efficient singlet exciton migration, or existence of either static and dynamic quenching mechanism, or self-absorption, or any other additional energy transfer process, or IFE due to higher concentration of quencher.[34] Considerably high difference in K_{sv} value was obtained for PA in comparison to various analytes, suggesting remarkably high selectivity and amplified fluorescence quenching of PF1 and PF2 via PA. Additionally, various inorganic ions (Fe^{3+}, Fe^{2+}, Cd^{2+}, Zn^{2+}, Cu^{2+}, Ni^{2+}, Ca^{2+}, Co^{2+}, Cr^{3+}, Pb^{2+}, Hg^{2+}, Ag^{+}, Mn^{2+}, I^-, F^-, Cl^-, NO_3^-, N_3^-, S^{2-}, BF_4^-, CO_3^{2-}, $H_2PO_4^-$, HPO_4^{2-}, PO_4^{3-}, SO_4^{2-}, NO_2^-, AcO^-) that could interfere with the detection of PA in natural water, did not show any significant effect on the emission of PF1 and PF2 (Figure A5.16-A5.19) suggesting exclusive selectivity of the system and signifying its further applicability in contaminated natural water bodies.

For consistent application, a sensor must be able to detect a particular analyte in presence of various competitive analytes. For this purpose, we tested PF1 and PF2 for the selective recognition of PA in presence of other nitroaromatic compounds as they hold similar electron deficient nature like PA and therefore, might affect in the detection of PA. In a typical experiment, initially fluorescence measurement of PF1 was recorded when TNT solution (66.6×10^{-6} M) was added to the polymer solution, so that TNT could interact with polymer prior to the further addition of PA (66.6×10^{-6} M). However, no significant effect of TNT was observed on the PL of CPs and no interference was observed in the detection of PA in presence of TNT (Figure A5.20). Similar sets of fluorescence titration were done with rest of the nitroaromatic compounds and similar results were obtained as in case of TNT (Figure 5.1d, A5.20-A5.28). The above competitive titrations were repeated with the polymer PF2 to obtain similar results (Figure 5.2d & Figure A5.29-A5.37). The remarkably high selectivity of these polymers is exceptional as compared to various chemosensors synthesized for PA sensing and thus provides an exceptional platform for fast, reliable and selective sensing of PA in competitive environment

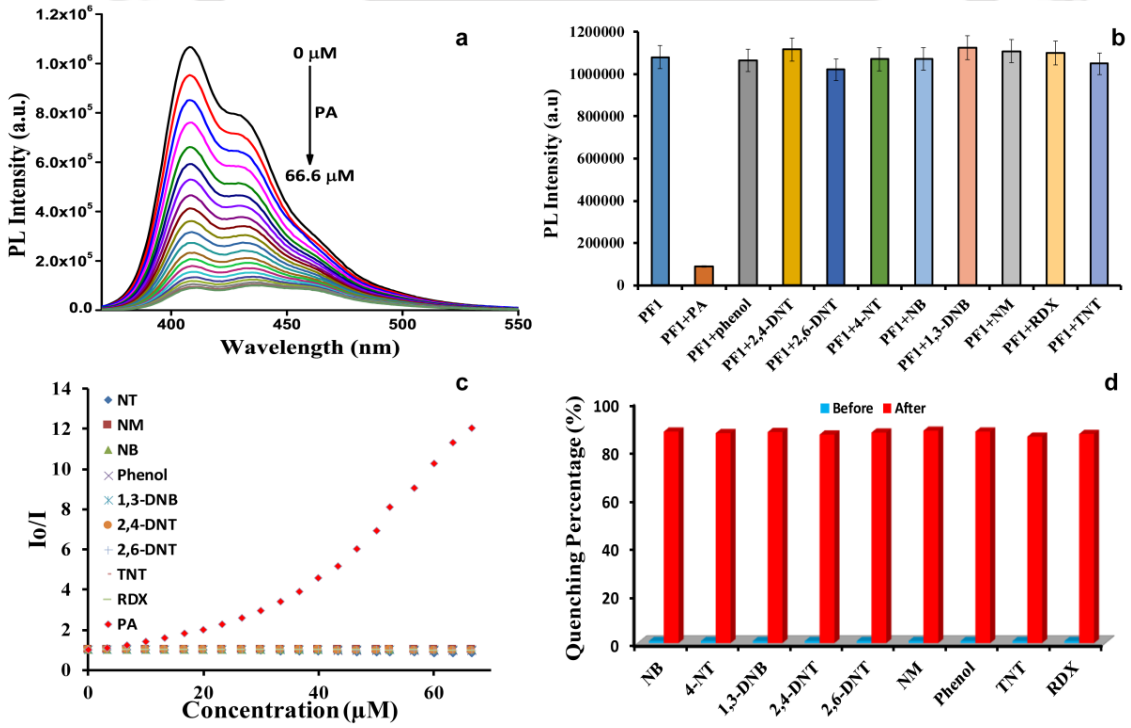

Figure 5.1 (a) Photoluminescence spectra of PF1 (1.6×10^{-7} M) with different concentrations of PA in 4:1 THF:H_2O (buffered with 10 mM of HEPES (pH= 7.0)). (b) Bar diagram showing influence of different interfering analytes (66.6×10^{-6} M) on fluorescence maximum of PF1 (1.6×10^{-7} M). (c) Stern-Volmer plots achieved for different interfering analytes. (d) Quenching percentage of emission of PF1 (1.6×10^{-7} M)

by different interfering analytes (66.6 × 10^{-6} M) before and after addition of 66.6 × 10^{-6} M PA.

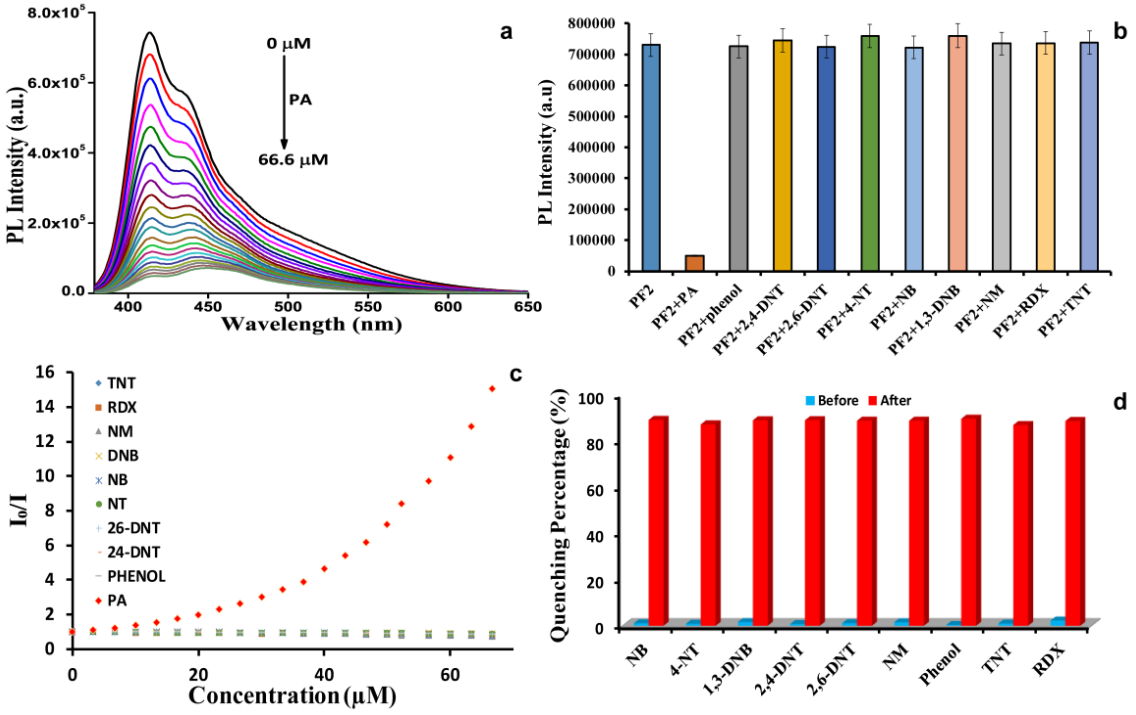

Figure 5.2 (a) Photoluminescence spectra of PF2 (3.3 × 10^{-7} M) with different concentrations of PA in 4:1 THF: H_2O (buffered with 10 mM of HEPES (pH= 7.0)). (b) Bar diagram showing influence of different interfering analytes (66.6 × 10^{-6} M) on fluorescence maximum of PF2 (3.3 × 10^{-7} M). (c) Stern-Volmer plots achieved for different interfering analytes. (d) Quenching percentage of emission of PF2 (3.3 × 10^{-7} M) by different interfering analytes (66.6 × 10^{-6} M) before and after addition of 66.6 × 10^{-6} M PA.

5.3.4 Mechanism of sensing

There are many possible ways, which can lead to the quenching of fluorescence such as static quenching (e.g. ground state donor-acceptor complexation), dynamic quenching (e.g. collisional/diffusional quenching), Förster resonance energy transfer (FRET), electrostatic interaction, aggregations caused quenching (ACQ), photoinduced electron transfer (PET) and IFE. However, to elucidate the exact reason for the quenching of fluorescence of CPs (PF1 and PF2) by PA, certain set of experiments were performed. Firstly, note that PA has a broad range of UV-vis absorption spectrum of around 280 nm to 480 nm, which almost overlaps with the excitation as well as emission spectra of both CPs (Figure 5.3a and 5.3b). This gives a clear indication for the possibility that either

FRET or IFE may occur in this system. As this condition fulfills the primary requirement for both FRET and IFE, which tends to have overlapping emission spectrum of fluorophore (CPs) with the absorption spectrum of the quencher (PA), while in addition to emission spectrum overlap, IFE may include an extra excitation spectrum overlap also. Besides, a second condition for FRET requires the optimum distance between fluorophore/donor (CPs) and quencher/acceptor (PA) in order to achieve a feasible energy transfer from donor (CPs) to acceptor (PA), which is only possible if there is some kind of strong interaction present between them. Whereas, in the present case, such kind of strong interaction was not feasible between them, hence unable to reach Förster radii for FRET to happen. Furthermore, to ascertain involvement of FRET or dynamic quenching, time resolved photoluminescence (TRPL) studies were performed. The fluorescence lifetime decay of the CPs were examined before and after the addition of PA to the solution. It can be seen from Figure 5.3c and 5.3d that lifetime of PF1 (0.551 ns) and PF2 (0.719 ns) remains unchanged even after addition of PA to their respective solution i.e. (0.548 ns and 0.717 ns respectively). This confirms that the quenching of fluorescence is static in nature and excludes possibility of the involvement of FRET or dynamic quenching in the mechanism. However, to understand the role of static quenching in the mechanism, UV-vis spectra of PF1 and PF2 were studied in the presence of PA. It was noticed that UV-vis absorption band of CPs (PF1 and PF2) after the addition of PA almost completely overlap with the CPs itself and just rise in the absorption band of CPs with no appearance of new peak or any shift in the band was observed (Figure A5.38-A5.39). This implies that the interaction between the CPs (PF1 and PF2) and PA are very weak and there is no formation of any ground state charge transfer complexation, also no aggregation of CPs occur after addition of PA. Therefore, this excludes the possibility of static quenching mechanism in the sensing process. All of the above results collectively indicate the presence of IFE in sensing process. Additionally, IFE is also supported by the Figure 5.3a and 5.3b, where efficient overlap of excitation/emission spectrum of CPs with absorption of PA leads to strong IFE while inefficient overlap in case of other nitroaromatics leads to poor IFE and results in higher selectivity of CPs toward PA. Thus, to prove the role of IFE in the suppression of the fluorescence of CPs, the observed fluorescence intensity was corrected by using the below equation.[42,43]

$$I_{corr}/I_{obs} = 10^{(Aex+Aem)/2} \qquad (1)$$

The equation (1) describes a simple correction method and has been used very rarely previously.[35,44] I_{corr} is the fluorescence intensity after the IFE correction and I_{obs} is the

fluorescence intensity before the IFE correction. A_{em} and A_{ex} are the UV-vis absorption value of the fluorophore (CPs) having analytes (PA) at fluorescence emission and excitation wavelengths, respectively. The simplified equation (1) is applicable for correcting the fluorescence IFE in a spectrum taken via a fluorescence cuvette of 1 cm × 1 cm dimension. The correction factor of fluorescence IFE (I_{corr}/I_{obs}) and the observed (E_{obs}) and corrected (E_{corr}) fluorescence quenching efficiencies at various concentration of PA was therefore calculated in Table A5.4 and A5.5. The outcomes validated that the suppression efficiency (E %) of IFE for PA to PF1 and PF2 reaches ~77% indicating the suppressed fluorescence quenching primarily was from IFE only (Figure 5.4)

To further support the involvement of IFE in detection mechanism, two model compounds such as 4-NP and 2,4-DNP were chosen, which are chemically similar to PA except the number of nitro group attached to the phenyl ring and thus possessing different absorption spectra.

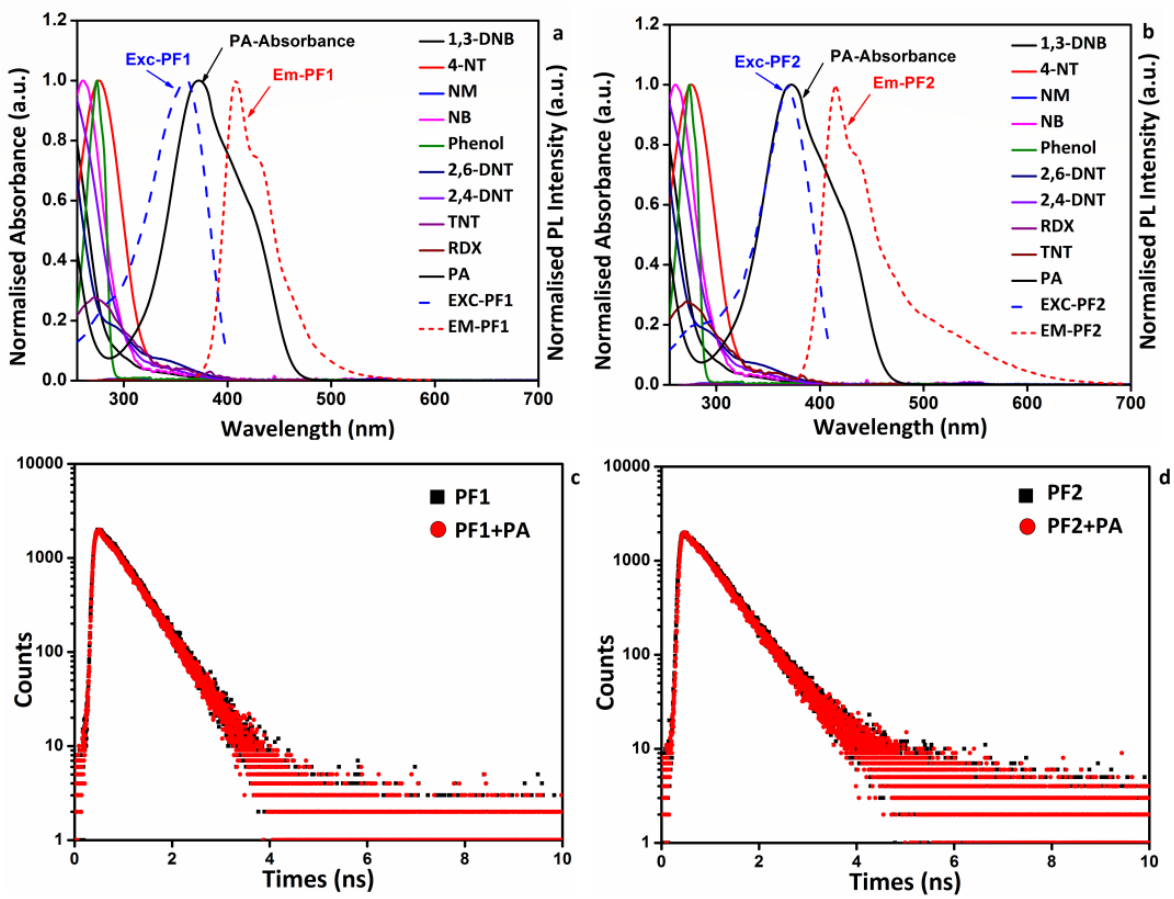

Figure 5.3 Overlapping of excitation/emission spectra of (a) PF1 and (b) PF2 with absorption spectrum of various nitroexplosive compounds. Lifetime decay of (c) PF1 (1.6×10^{-7} M) and (d) PF2 (3.3×10^{-7} M) before and after addition of PA (66.6×10^{-6} M).

As IFE does not require any interaction between fluorophore and absorber or quencher, there won't be any interaction except the IFE, which would govern the quenching of fluorescence of the polymers (PF1 and PF2) by these analytes. It was observed that the UV-Visible spectrum of these nitrophenols significantly overlaps with the excitation and emission spectrum of the PF1 and PF2 (Figure A5.40-A5.41) and the resulting quenching efficiency obtained follows a particular order i.e. PA>2,4-DNP>4-NP, indicating dominancy of IFE in case of PA (Figure A5.42-A5.43). Furthermore, the HOMO levels of the polymers PF1 (- 5.76 eV) and PF2 (- 5.80 eV) were calculated from the cyclic voltammetry (CV) (Figure A5.44-A5.45) and using the optical band gap (E_g) of the polymers PF1 (2.96 eV) and PF2 (2.81 eV) via onset of absorption band of the polymers, LUMO of both polymers PF1 (-2.79 eV) and PF2 (-2.98 eV) was obtained. It was then compared with the LUMO levels of various nitroexplosive compounds such as PA (-3.89 eV), 2,4-DNP (- 2.82 eV), 4-NP (-2.22 eV), TNT (-3.7 eV), DNT (-3.5 eV) and NT (-3.2 eV). It was observed that there could also be possible electron transfer through PET, but due to the very weak physical interaction between fluorophore and quencher tendency for PET are very low (~10%) as indicated by very high IFE (~80%). Consequently, all these studies cumulatively suggested the key role of IFE in the quenching mechanism.

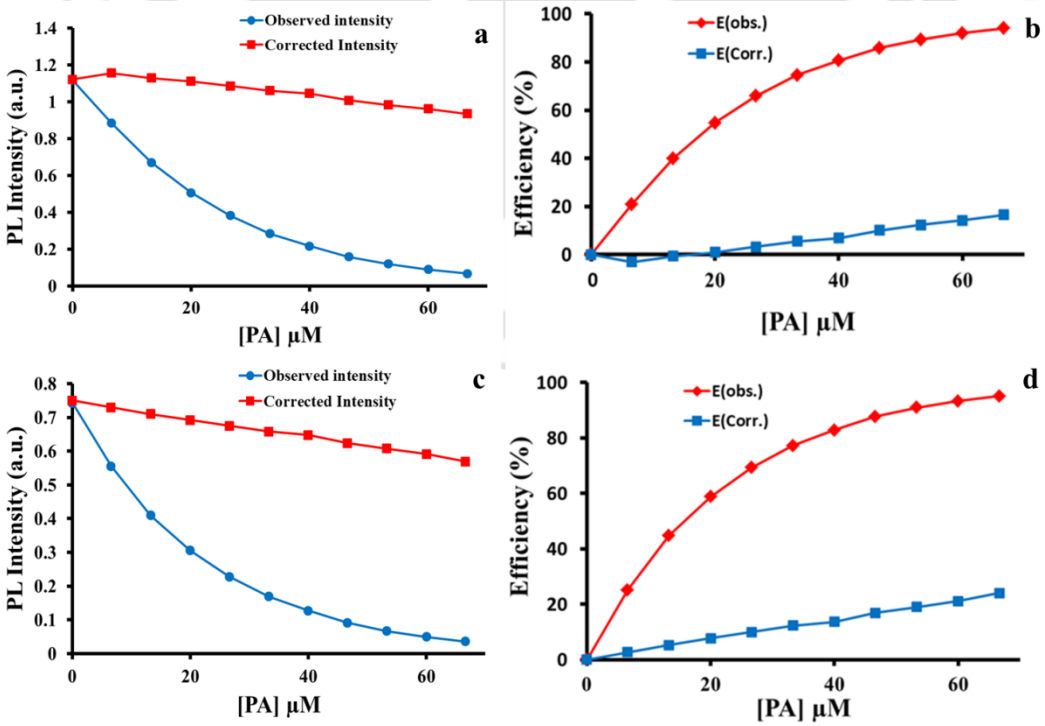

Figure 5.4 Observed (blue line, I_{obs}) and corrected (red line, I_{corr}) fluorescence intensity of the (a) PF1 and (c) PF2 under the influence of PA concentration. Suppressed

efficiency (E, %) of the corrected (blue) and observed (red) fluorescence intensity for (b) PF1 and (d) PF2 under the influence of PA concentration.

5.3.5 Analysis of PA in natural water samples

To validate the practicability of this system (polymer-PF1), natural sea water collected from Bay of Bengal and Brahmaputra river water (nearby IITG campus) were analysed. Initially, the water samples were centrifuged and filtered through 0.2 µm membrane filter and then spiked with known varying amount of PA (Table 5.1). A standard calibration curve was plotted for comparing the results obtained from the spiked natural water samples (Figure A5.46). It can be seen from the Table 5.1, that recoveries for PA was clearly found, which varied from 91 % to 99 % for both sea and river water samples, indicating feasibility of this system for efficiently sensing PA in a highly competitive environment.

Table 5.1 Determination of PA in Natural Water Samples [a]An average of three replicate measurements with standard deviation.

Sample	Added(10^{-6} M)	Found(10^{-6} M)[a]	Recovery (%)
River Water	10.00	9.16 ± 0.05	91.6
	17.00	16.82 ± 0.06	98.9
	25.00	24.88 ± 0.11	99.5
Sea Water	13.00	12.47 ± 0.11	95.9
	28.00	27.08 ± 0.02	96.7
	42.00	40.16 ± 0.14	95.6

5.3.6 Test paper strips for on-site visual detection

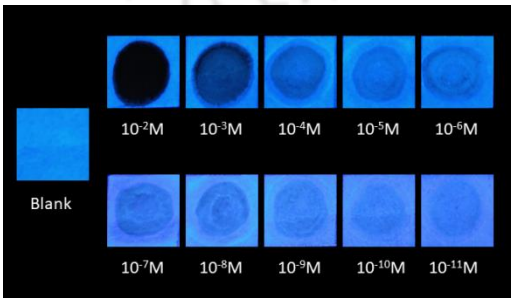

Figure 5.5 Photographs of the filter paper test strips coated with fluorescent Polymer PF1 after applying the solution of PA at various concentration under UV light (365 nm).

For economical and swift on-site detection of nitroexplosive-PA, low cost and portable fluorescent paper strips were prepared by means of Whatmann filter paper. Desired size of Whatman paper was cut into pieces (1 cm × 1 cm) and thereafter immersed into the polymer PF1 solution (1×10^{-3} M) and dried in air. Different solutions of PA (10 µL) with varying concentration was introduced into each test strip. A dark spot was seen on the position of contact as a result of quenching of the fluorescence of fluorescent CP after the introduction of the PA over it under UV light (365 nm), which can be seen easily for a minimum of 10^{-11} M of PA i.e. equivalent to 22.9 femtogram of PA (Figure 5.5). These experiments validate the potential of both the CPs for portable sensor development with the ability of rapid onsite detection of PA in natural contaminated samples.

5.4 Conclusion

In conclusion, two neutral highly fluorescent conjugated co-polymer (PF1) and homopolymer (PF2) of fluorene were synthesized via Suzuki-cross coupling polymerization and oxidative polymerization methods, respectively. These "receptor free" polymers showed blue emission and were found to be highly sensitive and remarkably selective towards nitroexplosive-PA. Polymer PF1 and PF2 can detect as low as 110 nM (25.2 ppb) and 219 nM (50.1 ppb) of PA in solution respectively, while a minimum of 22.9 femtogram of PA can be detected using portable test strips of PF1. The key mechanism of quenching was found to be exclusively IFE, which was confirmed and thoroughly explained via IFE corrections. These types of detection systems are unique and do not require any kind of interactions, and hence the chances of interference during detection are very minimum and can be further utilized in analyzing analytes of choice even in natural water samples.

References

(1) Ma, Y.; Li, H.; Peng, S.; Wang, L. *Anal. Chem.* **2012**, *84*, 8415.

(2) Shanmugaraju, S.; Mukherjee, P. S. *Chem. Commun.* **2015**, *51*, 16014.

(3) Sun, X.; Wang, Y.; Lei, Y. *Chem. Soc. Rev.* **2015**, *44*, 8019.

(4) Han, Y.; Chen, Y.; Feng, J.; Liu, J.; Ma, S.; Chen, X. *Anal. Chem.*, **2017**, *89*, 3001.

(5) Peng, Y.; Zhang, A.; Dong, M.; Wang, Y. *Chem. Commun*. **2011**, *47*, 4505.

(6) Ding, A.; Yang, L.; Zhang, Y.; Zhang, G.; Kong, L.; Zhang, X.; Tian, Y.; Tao, X.; Yang, J. *Chem. Eur. J.* **2014**, *20*, 12215.

(7) Akhavan, J. In Chemistry of Explosives, Royal Society of Chemistry, 2nd ed., **2004**.

(8) Ashbrook, P. C.; Houts, T. A. *Chem. Health Safety*, **2003**, *10*, 27.

(9) Innovative Treatment Technologies: Annual Status Report, U.S. Environmental Protection Agency: Washington, D.C., 8th ed., **1996**.

(10) Wollin, K.-M.; Dieter, H. H. *Arch. Environ. Con. Tox.* **2005**, *49*, 18.

(11) Chen, X.; Cheng, X.; Gooding, J. J. *Anal. Chem.* **2012**, *84*, 8557.

(12) Du, Y.; Wang, W.; Li, H. *Anal. Chem.* **2012**, *84*, 1725.

(13) Dasary, S. S. R.; Senapati, D.; Singh, A. K.; Anjaneyulu, Y.; Yu, H.; Ray, P. C. *ACS Appl. Mater. Inter.* **2010**, *2*, 3455.

(14) Sapsford, K. E.; Charles, P. T.; Patterson, C. H.; Ligler, F. S. *Anal. Chem.* **2002**, *74*, 1061.

(15) Hu, Z.; Deibert, B. J.; Li, J. *Chem. Soc. Rev.* **2014**, *43*, 5815.

(16) Dinda, D.; Gupta, A.; Shaw, B. K.; Sadhu, S.; Saha, S. K. *ACS Appl. Mater. Inter.* **2014**, *6*, 10722.

(17) Meher, N.; Iyer, P. K. *Nanoscale* **2017**, *9*, 7674.

(18) Bhalla, V.; Gupta, A.; Kumar, M.; Rao, D. S. S.; Prasad, S. K. *ACS Appl. Mater. Interfaces* **2013**, *5*, 672.

(19) Kaur, S.; Gupta, A.; Bhalla, V.; Kumar, M. *J. Mater. Chem. C* **2014**, *2*, 7356.

(20) Ye, J.; Zhao, L.; Bogale, R. F.; Gao, Y.; Wang, X.; Qian, X.; Guo, S.; Zhao, J.; Ning, G. *Chem. Eur. J.* **2015**, *21*, 2029.

(21) Gole, B.; Bar, A. K.; Mukherjee, P. S. *Chem. Eur. J.* **2014,** *20*, 13321.

(22) Kaur, S.; Bhalla, V.; Vij, V.; Kumar, M. *J. Mater. Chem. C* **2014**, *2*, 3936.

(23) Zhang, Y. R.; Chen, G.; Lin, Y. L.; Zhao, L. F.; Yuan, W. Z.; Lu, P.; Jim, C. K. W.; Zhang, Y. M.; Tang, B. Z. *Polym. Chem.* **2015,** *6*, 97.

(24) Li, X.-G.; Liao, Y.; Huang, M.-R.; Strong, V.; Kaner, R. B. *Chem. Sci.* **2013**, *4*, 1970.

(25) Xu, Y. Q.; Li, B. H.; Li, W. W.; Zhao, J.; Sun, S. G.; Pang, Y. *Chem. Commun.* **2013**, *49*, 4764.

(26) Wang, X.; Guo, Y.; Li, D.; Chen, H.; Sun, R.-c. *Chem. Commun.* **2012**, *48*, 5569.

(27) Martinez, H. P.; Grant, C. D.; Reynolds, J. G.; Trogler, W. C. *J. Mater. Chem.* **2012**, *22*, 2908.

(28) Dey, N.; Samanta, S. K.; Bhattacharya, S. *ACS Appl. Mater. Inter.* **2013**, *5*, 8394.

(29) Bauri, K.; Saha, B.; Mhanti, J.; De, P. *Polym. Chem.*, **2017,** *8*, 7180.

(30) Tanwar, A. S.; Iyer, P. K. *ACS Omega* **2017**, *2*, 4424.

(31) Malik, A. H.; Hussain, S.; Kalita, A.; Iyer, P. K. *ACS Appl. Mater. Inter.* **2015**, *7*, 26968.

(32) Kalita, A.; Hussain, S.; Malik, A. H.; Barman, U.; Goswami, N.; Iyer, P. K. *ACS Appl. Mater. Inter.* **2016**, *8*, 25326.

(33) Hussain, S.; Malik, A. H.; Afroz, M. A.; Iyer, P. K. *Chem. Commun.* **2015**, *51*, 7207.

(34) Tanwar, A. S.; Hussain, S.; Malik, A. H.; Afroz, M. A.; Iyer, P. K. *ACS Sensors* **2016**, *1*, 1070.

(35) S. Chen, Y.-L. Yu, J.-H. Wang, *Analytica Chimica Acta* (**2017**), doi: 10.1016/j.aca.2017.10.026

(36) Zhu, C.; Liu, L.; Yang, Q.; Lv, F.; Wang, S. *Chem. Rev.* **2012**, *112*, 4687.

(37) McQuade, D. T.; Pullen, A. E.; Swager, T. M. *Chem. Rev.* **2000**, *100*, 2537.

(38) Thomas III, S. W.; Joly, G. D.; Swager, T. M. *Chem. Rev.* **2007**, *107*, 1339.

(39) Kim, H. N.; Guo, Z.; Zhu, W.; Yoon, J.; Tian, H. *Chem. Soc. Rev.* **2011**, *40*, 79.

(40) Saikia, G.; Iyer, P. K. *J. Org. Chem.* **2010**, *75*, 2714.

(41) Hussain, S.; De, S.; Iyer, P. K. *ACS Appl. Mater. Interfaces*, **2013**, *5*, 2234.

(42) Lakowicz, J. R. *In Principles of Florescence spectroscopy*, 3rd ed; Springer: Singapore, **2010**.

(43) Kusbita, M.; Sjoback, R.; Eriksson, S.; Albinsson,B. *Analyst*, **1994**,*119*, 417.

(44) Malik, A. H.; Iyer, P. K. *ACS Appl. Mater. Interface* **2017**, *9*, 4433.

Appendix

Table A5.1: Fluorescence lifetime decay of each component and their fractions.

Sample	τ_1 (ns)	%	χ^2
PF1	0.551	100	1.093
PF1-PA	0.548	100	1.047

Table A5.2: Fluorescence lifetime decay of each component and their fractions.

Sample	τ_1 (ns)	%	τ_2 (ns)	%	χ^2	τ_{avg} (ns)
PF2	0.599	94.104	2.637	5.896	1.126	0.719
PF2-PA	0.596	94.585	2.838	5.415	1.105	0.717

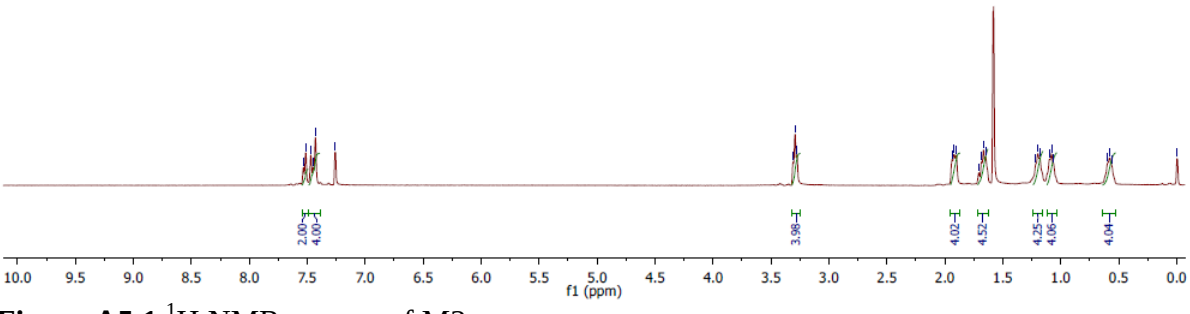

Figure A5.1 ^{1}H NMR spectra of M2.

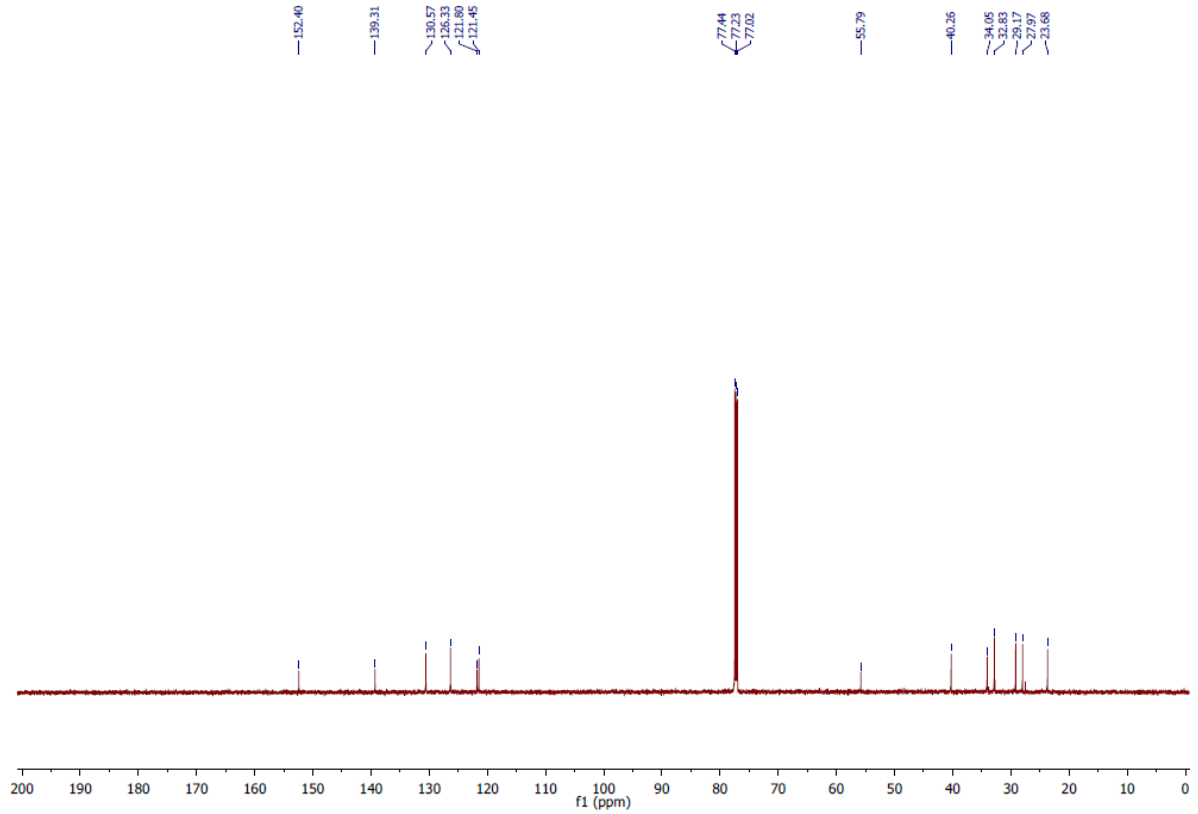

Figure A5.2 ^{13}C NMR spectra of M2.

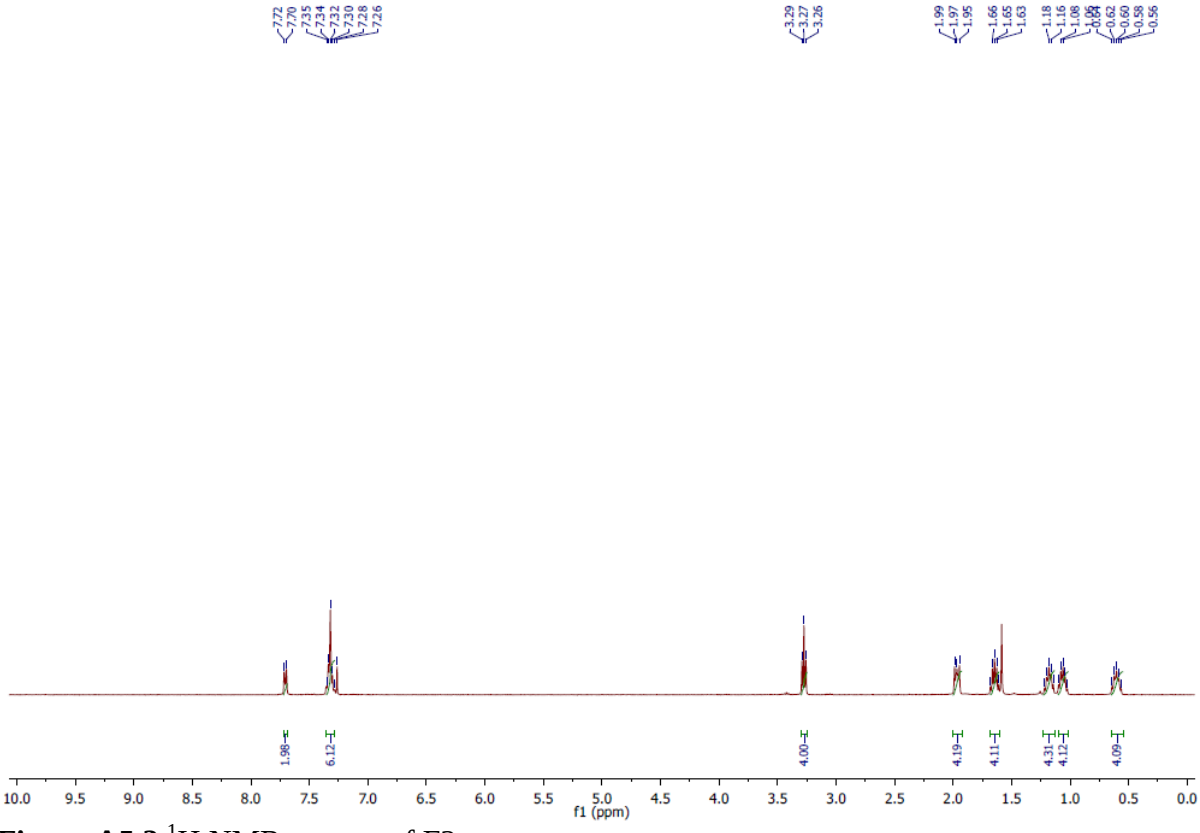

Figure A5.3 ^{1}H NMR spectra of F2.

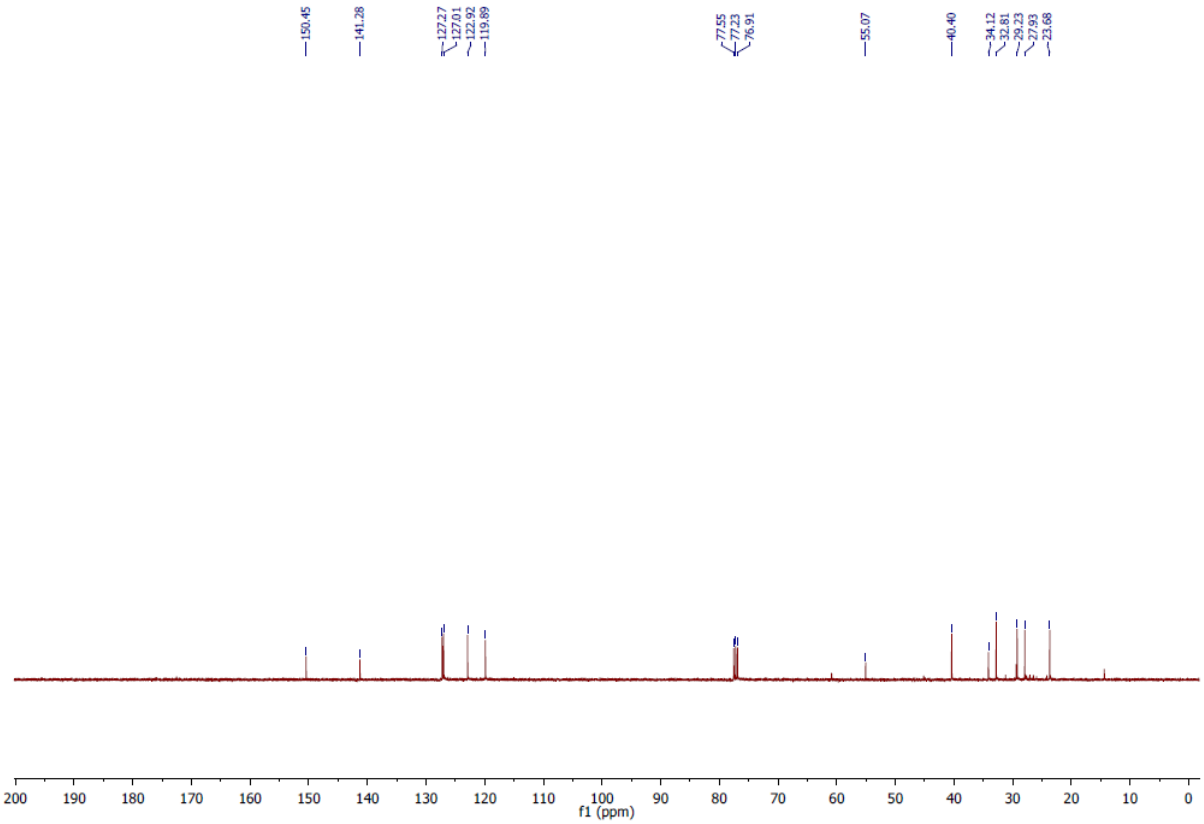

Figure A5.4 ^{13}C NMR spectra of F2.

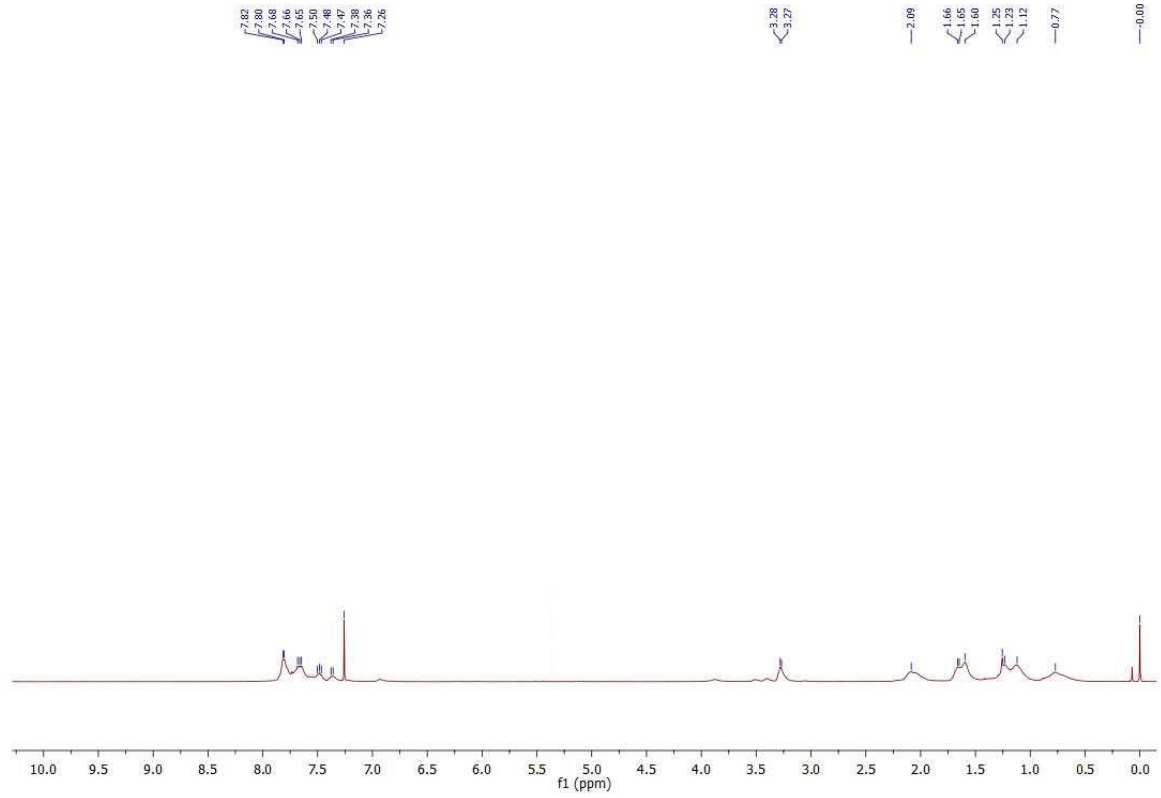

Figure A5.5 ^{1}H NMR spectra of PF1.

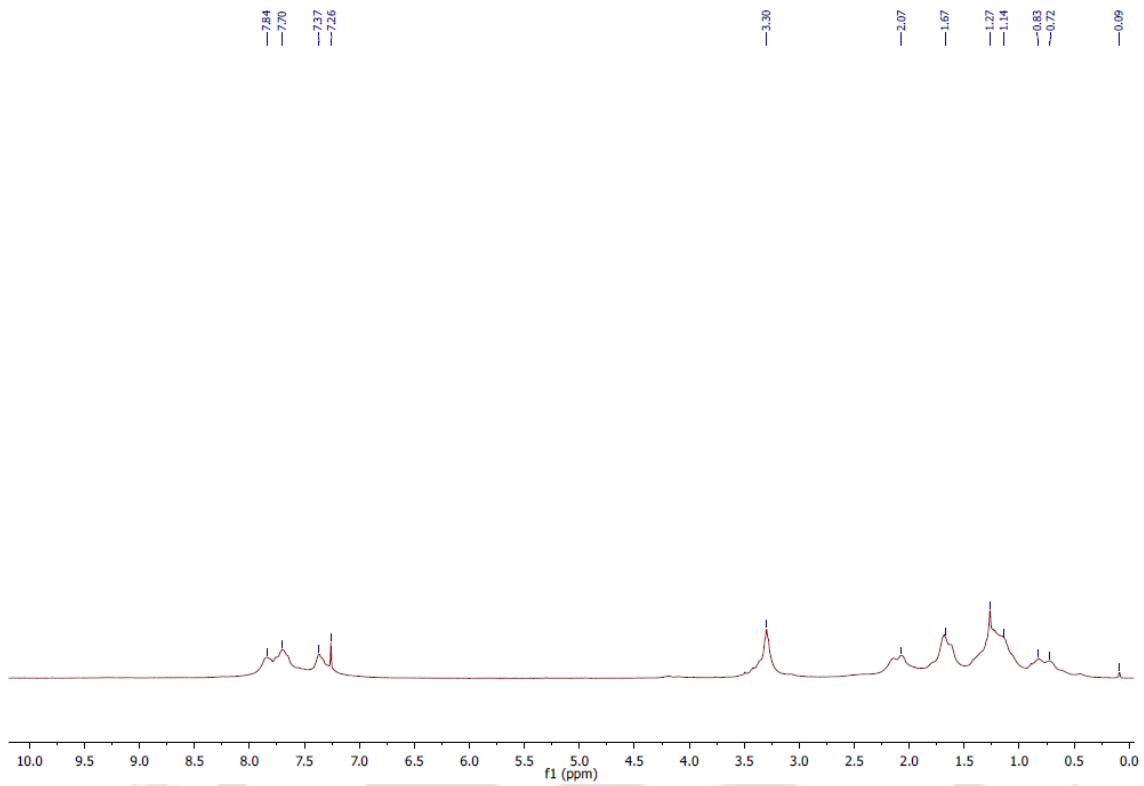

Figure A5.6 ^{1}H NMR spectra of PF2.

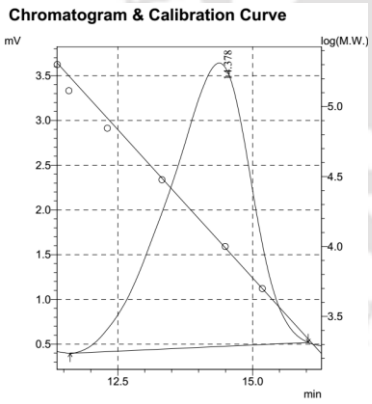

[Average Molecular Weight]

Number Average Molecular Weight(Mn	11364
Weight Average Molecular Weight(Mw	18716
Z Average Molecular Weight(Mz	32477
Z+1 Average Molecular Weight(Mz1	50981
Viscosity Average Molecular Weight(Mv	0
Mw/Mn	1.64687

Figure A5.7 GPC chromatogram of polymer PF1.

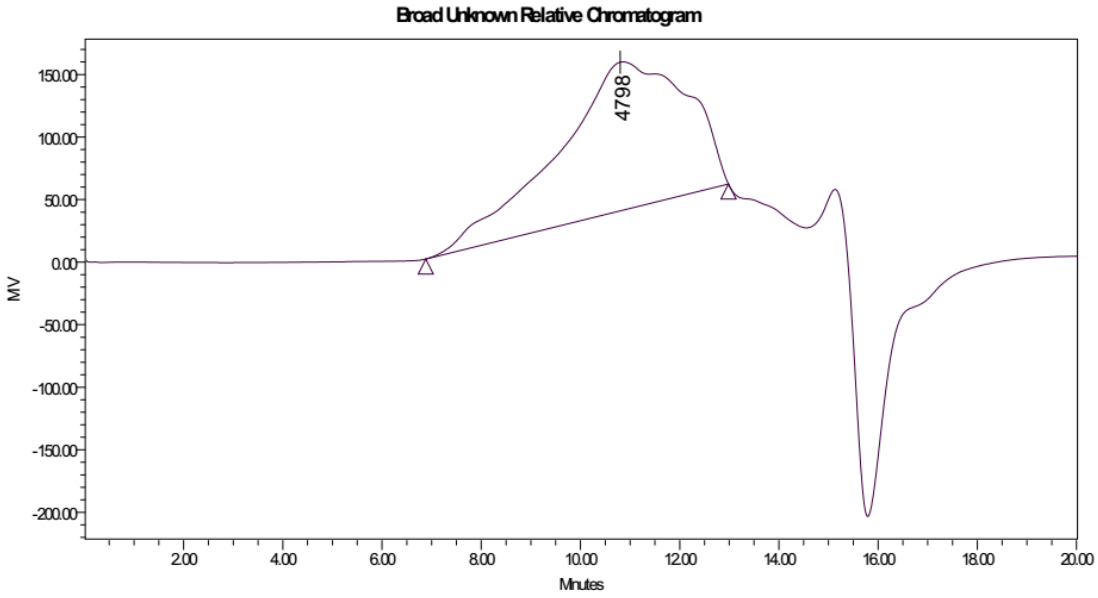

Broad Unknown Relative Peak Table

	Distribution Name	Mn (Daltons)	Mw (Daltons)	MP (Daltons)	Mz (Daltons)	Mz+1 (Daltons)	Polydispersity	Mz/Mw	Mz+1/Mw
1		6630	24199	4798	76488	118339	3.649713	3.160826	4.890288

Figure A5.8 GPC chromatogram of polymer PF2.

Figure A5.9 Image of PF1 and PF2 under UV-light before and after addition of PA.

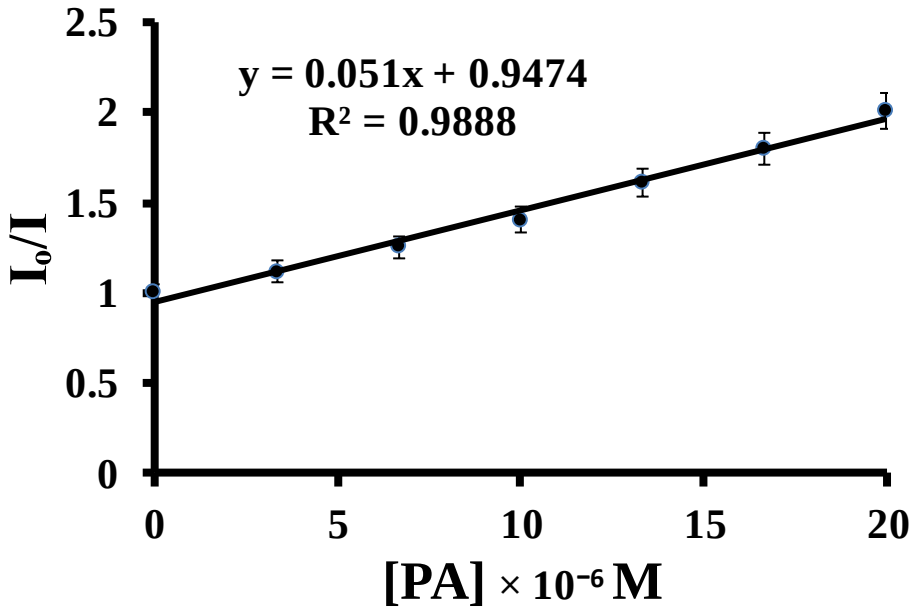

Figure A5.10 Stern-Volmer plot obtained at lower concentration of PA for PF1.

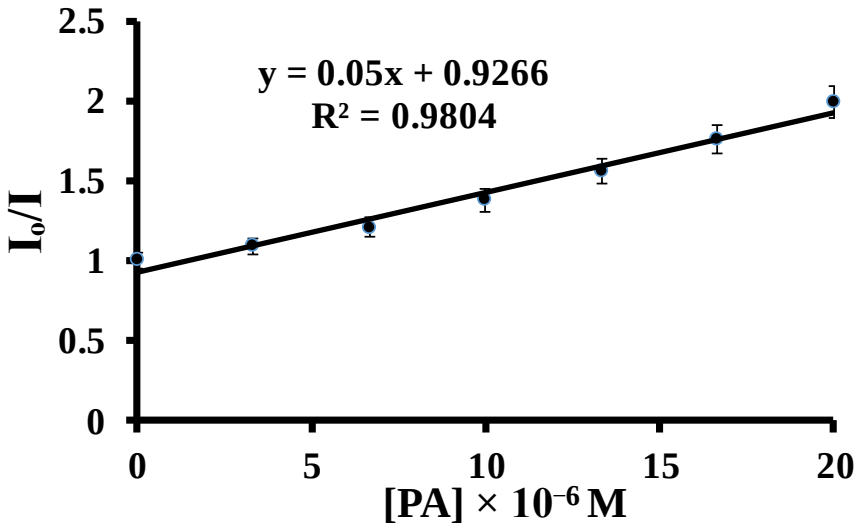

Figure A5.11 Stern-Volmer plot obtained at lower concentration of PA for PF2.

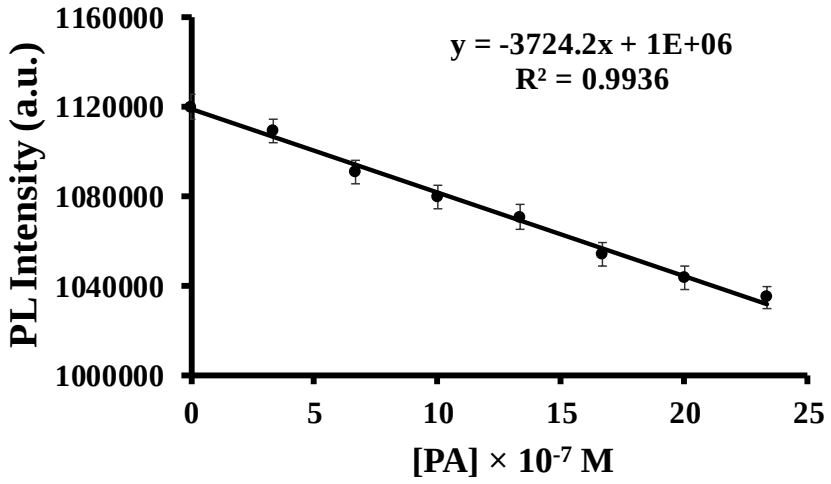

Figure A5.12 Fluorescence intensity of PF1 in 4:1/THF:HEPES buffer (pH=7, 10 mM) *vs* PA concentration.

LOD=3 × S.D./k

LOD = 3 × 1375.02/ (3724.2 ×10^7)

= 110 nM or 25.2 ppb

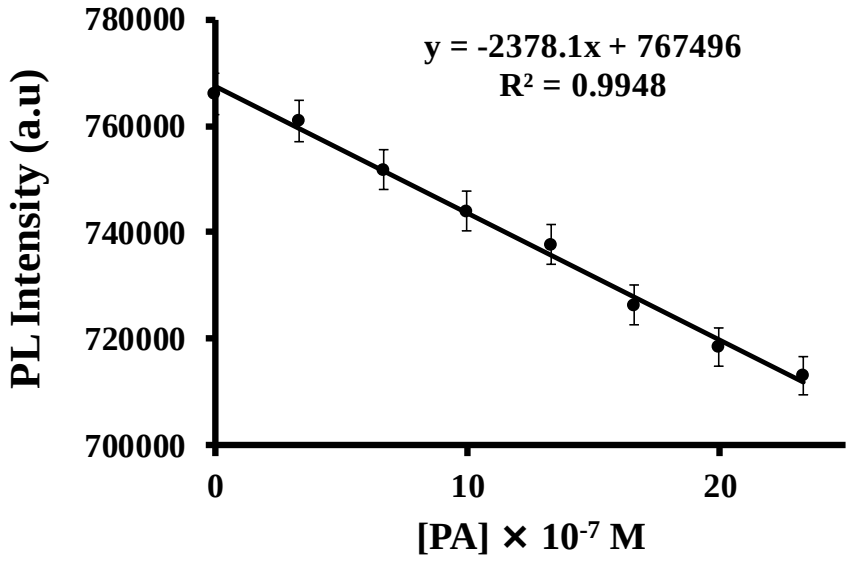

Figure A5.13 Fluorescence intensity of PF2 in 4:1/THF:HEPES buffer (pH=7, 10 mM) *vs* PA concentration.

LOD=3 × S.D./k

LOD = 3 × 1739.66/ (2378.1 ×10^7)

= 219 nM or 50.1 ppb

Table A5.3: A comparative study of some conjugated polymers based reports for picric acid detection.

Publication	Material Used	Detection Limit	Selectivity	Sensing Mechanism	Medium Used
Present Manuscript	***Conjugated Polymers***	***110 × 10^{-9} M (25.2 ppb) And 219 × 10^{-9} M (50.1 ppb)***	***Selective***	***IFE***	***THF:H_2O***
J. Am. Chem. Soc. ***2017****, 139, 5437−5443*	*Poly(β-aminoacrylate)s*	3.87 µM for P1a2d and 0.12 µM for P1b2d	Not studied	AIE	THF/water
J. Am. Chem. Soc. ***2017****, 139, 2421−2427*	*Conjugated Covalent Organic Frameworks*	-	Not Selective	-	CH_2Cl_2
ACS Appl. Mater. Interfaces ***2017****, 9, 13415−13421*	*polyimide covalent organic framework*	0.25 µM	Selective	Electron Transfer And IFE	C_2H_5OH
ACS Omega ***2017****, 2, 4424−4430*	*Conjugated Polyelectrolyte*	295 nM	Selective	IDA	H_2O
ACS Sens. ***2016****,*	*Conjugated Polymer*	57.8 nM	Selective	IFE and	THF:H_2O

1, 1070−1077				PET	
J. Mater. Chem. A, **2015**, *3*, 92–96	*Covalent-organic polymer*	About 1 ppm	Selective	Electron transfer	CH_3OH
J. Mater. Chem. A, **2014**, *2*, 15560–15565	polydiacetylene	0.11 ppm (0.48µM)	Selective	Electron transfer	CH_3OH
Macromolecules **2014**, *47*, 4908−4919	poly(dipropargyl amine)s	1µM	Not selective	Energy transfer	$THF:H_2O$
Polym. Chem., **2014**, *5*, 5628–5637	Poly(acrylate)	2.5 ppm	Not selective	Electron transfer	$THF:H_2O$
RSC Adv., **2013**, *3*, 8193–8196	Poly(arylene ynonylene)	1 ppm	Not studied	-	$THF:H_2O$
Macromolecules **2013**, *46*, 3907−3914	Poly(aroxycarbonyltriazole)s	Upto 1µg/mL	Not studied	-	$THF:H_2O$
Macromol. Rapid Commun. **2013**, *34*, 796−802	Polytriazole	9×10^{-8} M	Not studied	Energy transfer	$THF:H_2O$
Macromolecules **2011**, *44*, 5977–5986	Poly(silylenevinylene)s	Upto 1ppm	Not studied	Electron and/or energy transfer	$THF:H_2O$
Macromol. Rapid Commun. **2010**, *31*, 834–839	Poly(silylenevinylene)	Upto 1ppm	Not studied	-	$THF:H_2O$
Macromolecules **2009**, *42*, 9400-9411	Conjugated Polyelectrolyte	0.17 ppm (0.72 µM)	Not studied	-	$THF:H_2O$
J. Am. Chem. Soc. **2003**, *125*, 3821-3830	Polymetalloles	Not reported	Not selective	Electron-transfer	THF

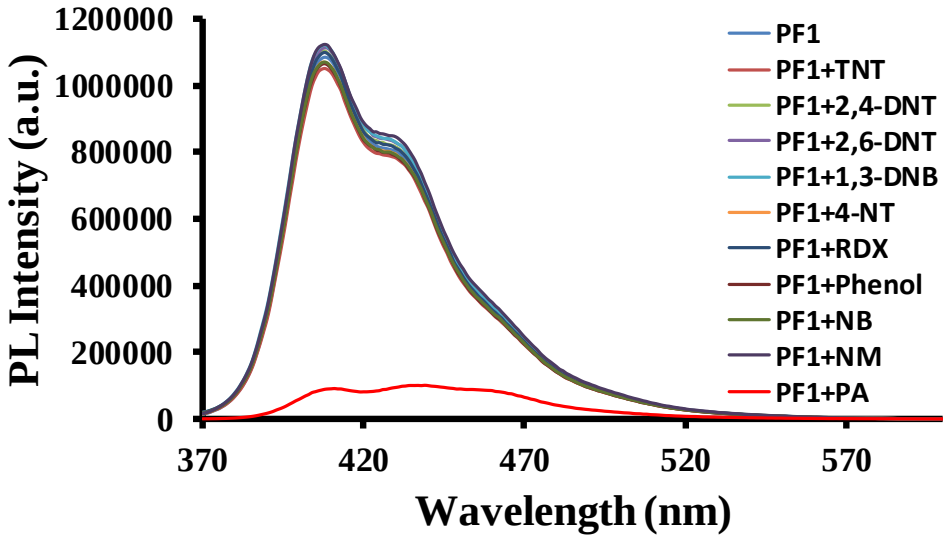

Figure A5.14. Photoluminescence spectra showing the effect of various nitro analytes (66.6×10^{-6} M) on fluorescence emission of PF1 (1.6×10^{-7} M) in 4:1/THF:water.

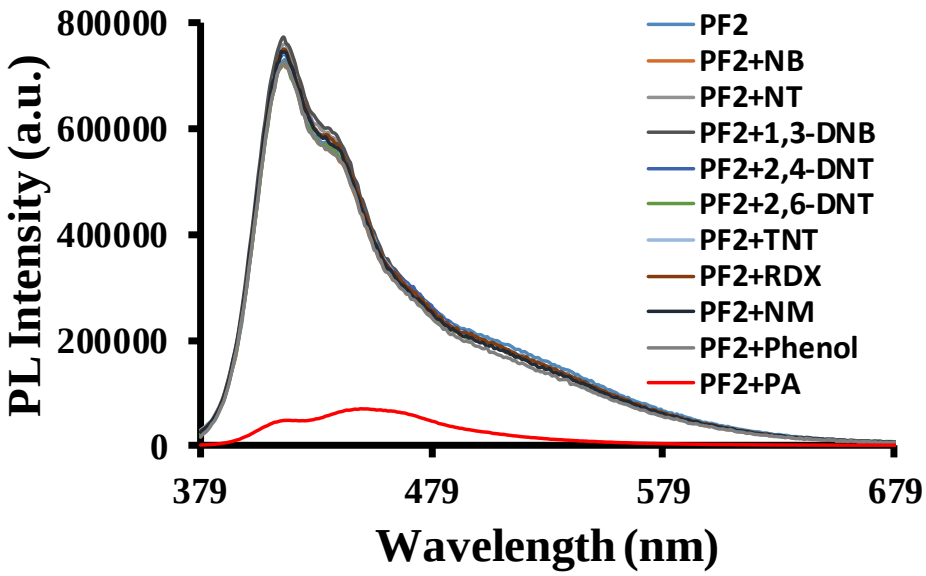

Figure A5.15. Photoluminescence spectra showing the effect of various nitro analytes (66.6×10^{-6} M) on fluorescence emission of PF2 (3.3×10^{-7} M) in 4:1/THF:water.

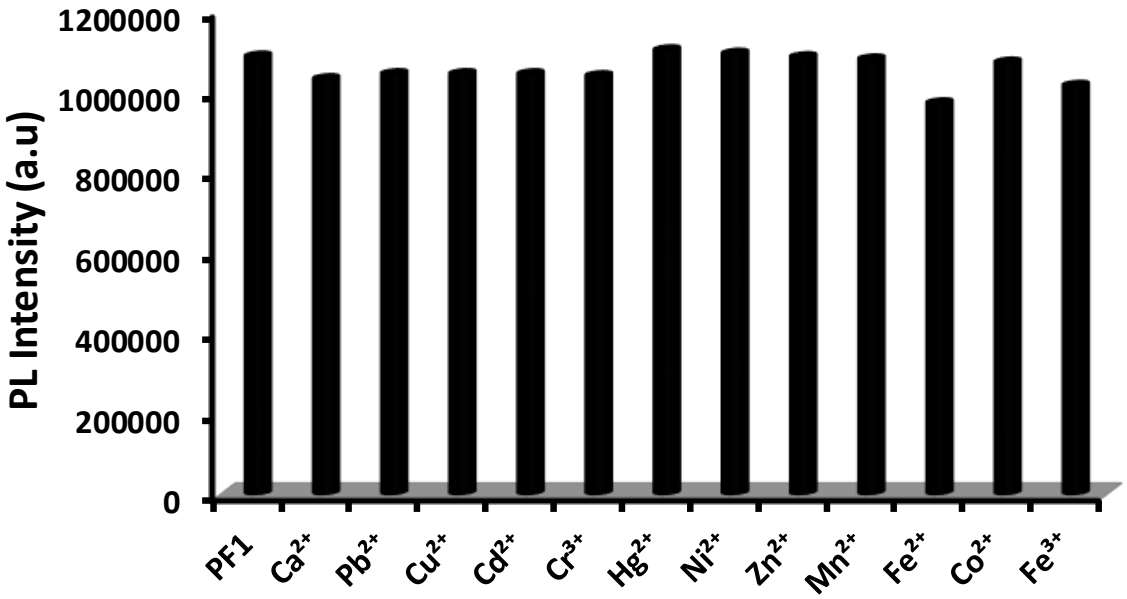

Figure A5.16 Bar diagram depicting effect of various metal ions (66.6×10^{-6} M) on the fluorescence intensity of PF1 (1.6×10^{-7} M).

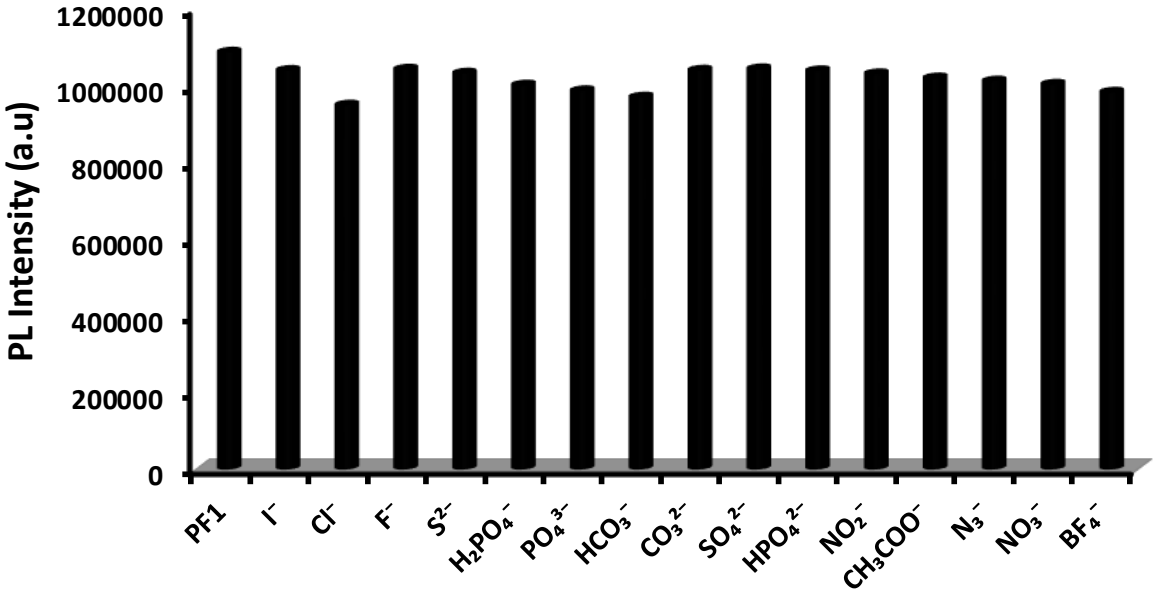

Figure A5.17 Bar diagram depicting effect of various anions (66.6×10^{-6} M) on the fluorescence intensity of PF1 (1.6×10^{-7} M).

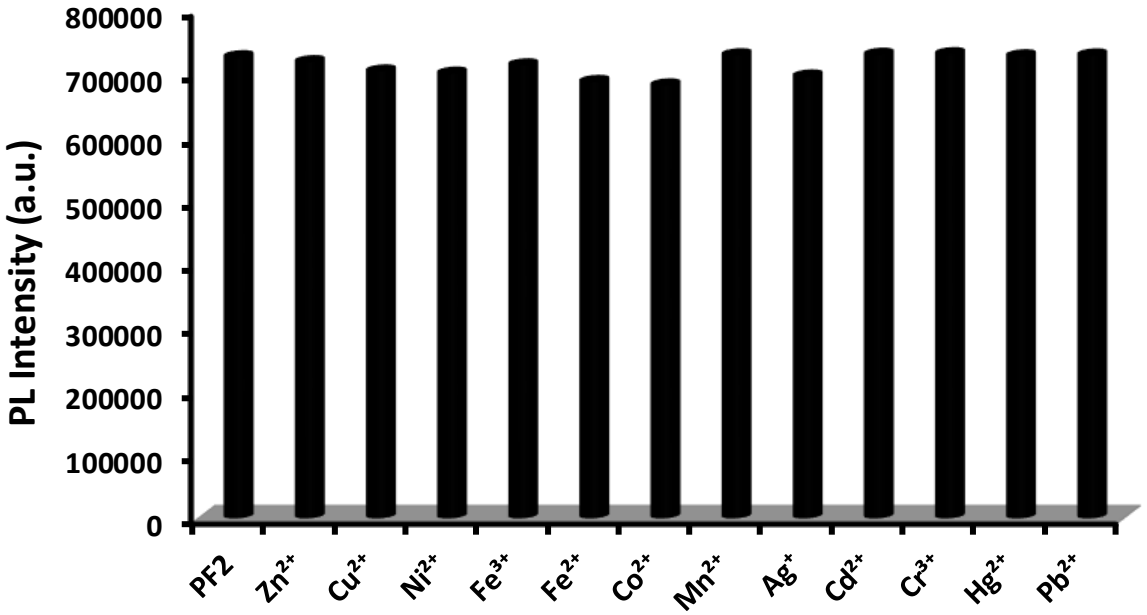

Figure A5.18 Bar diagram depicting effect of metal ions (66.6×10^{-6} M) on the fluorescence intensity of PF2 (3.3×10^{-7} M).

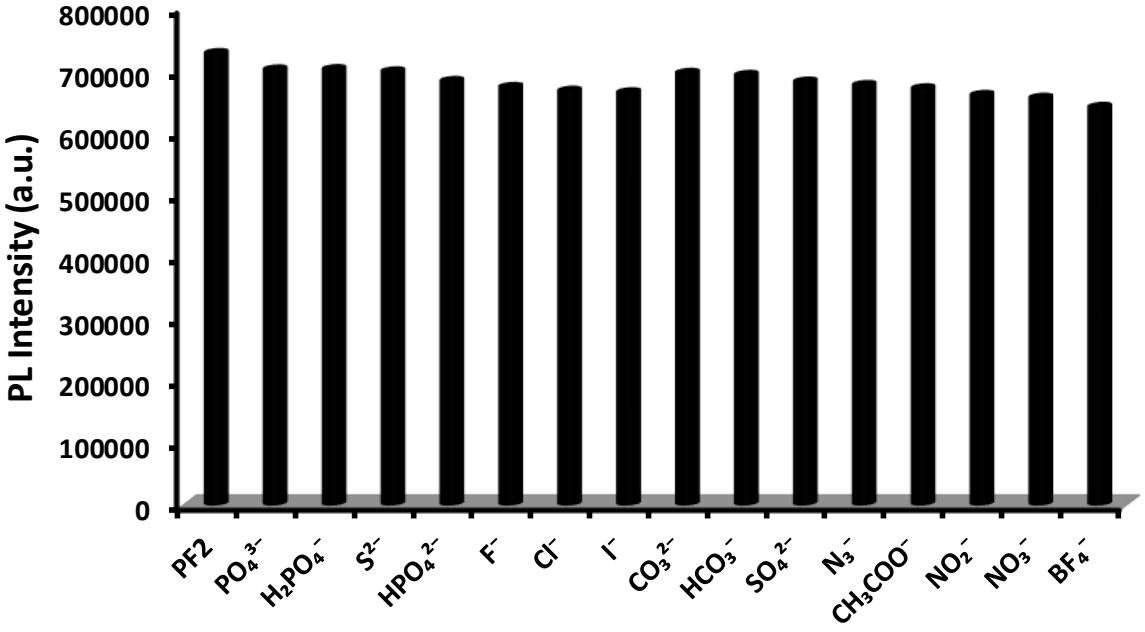

Figure A5.19 Bar diagram depicting effect of various anions (66.6×10^{-6} M) on the fluorescence intensity of PF2 (3.3×10^{-7} M).

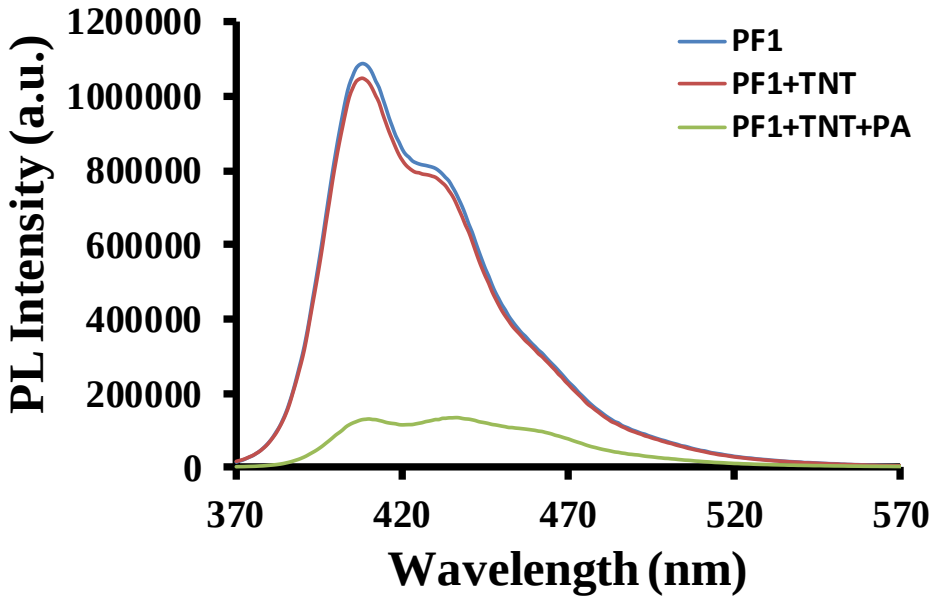

Figure A5.20 Emission spectra of PF1 (1.6×10^{-7} M) with TNT (66.6×10^{-6} M) followed by addition of PA (66.6×10^{-6} M).

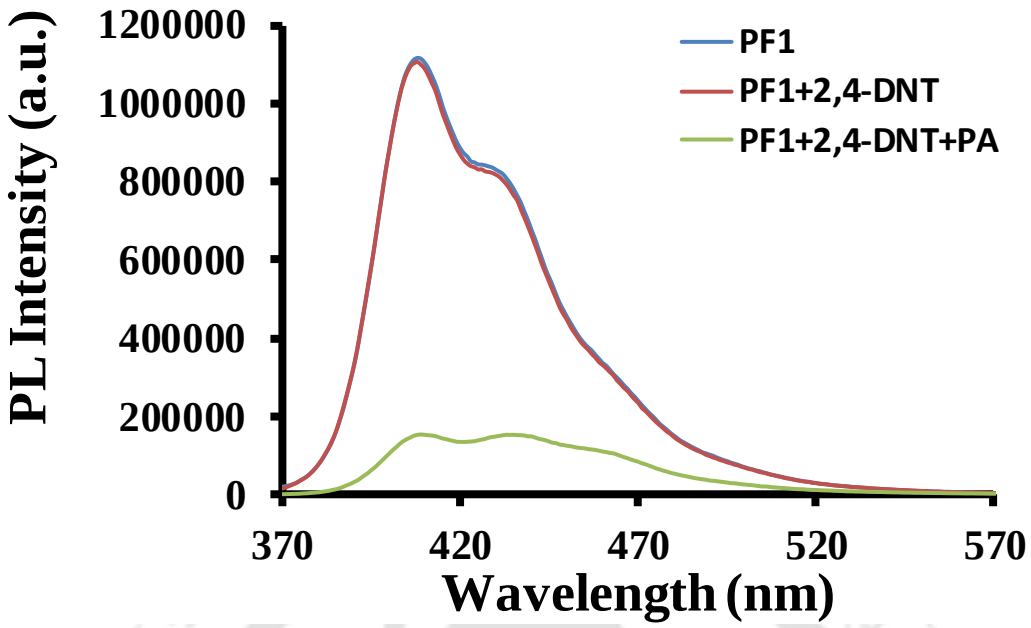

Figure A5.21 Emission spectra of PF1 (1.6×10^{-7} M) with 2,4-DNT (66.6×10^{-6} M) followed by addition of PA (66.6×10^{-6} M).

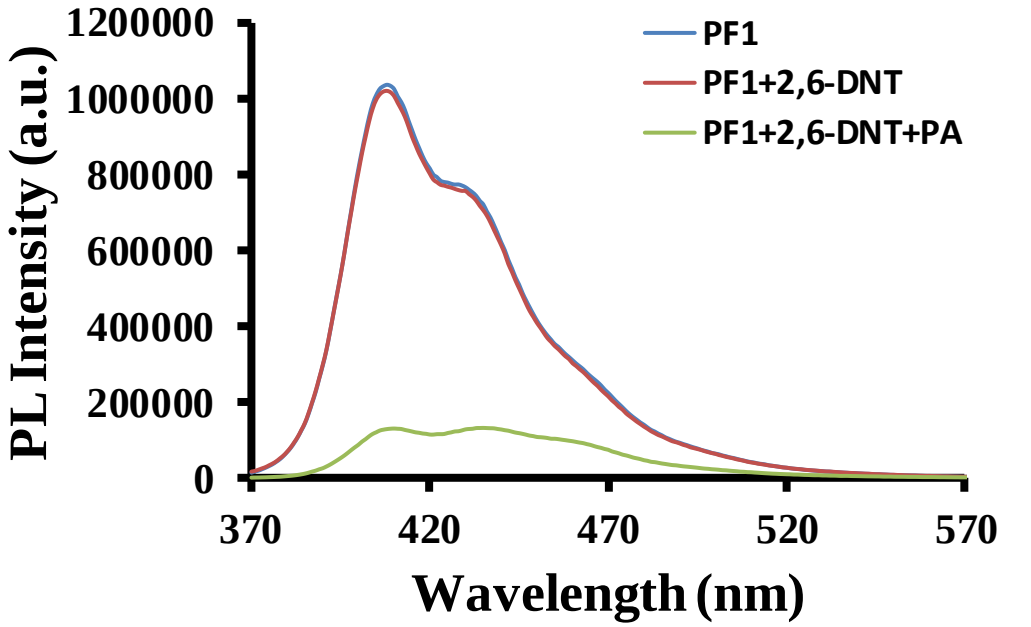

Figure A5.22 Emission spectra of PF1 (1.6×10^{-7} M) with 2,6-DNT (66.6×10^{-6} M) followed by addition of PA (66.6×10^{-6} M).

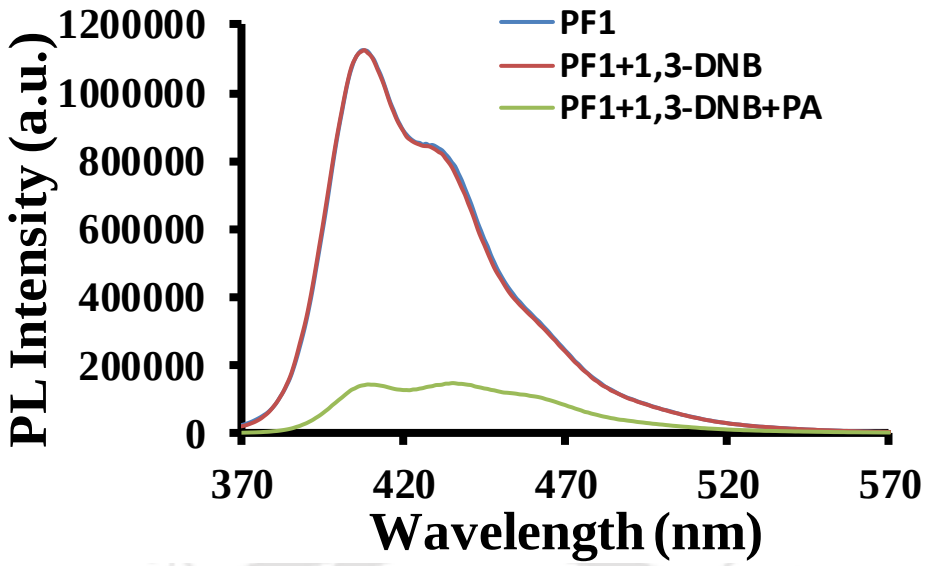

Figure A5.23 Emission spectra of PF1 (1.6×10^{-7} M) with 1,3-DNB (66.6×10^{-6} M) followed by addition of PA (66.6×10^{-6} M).

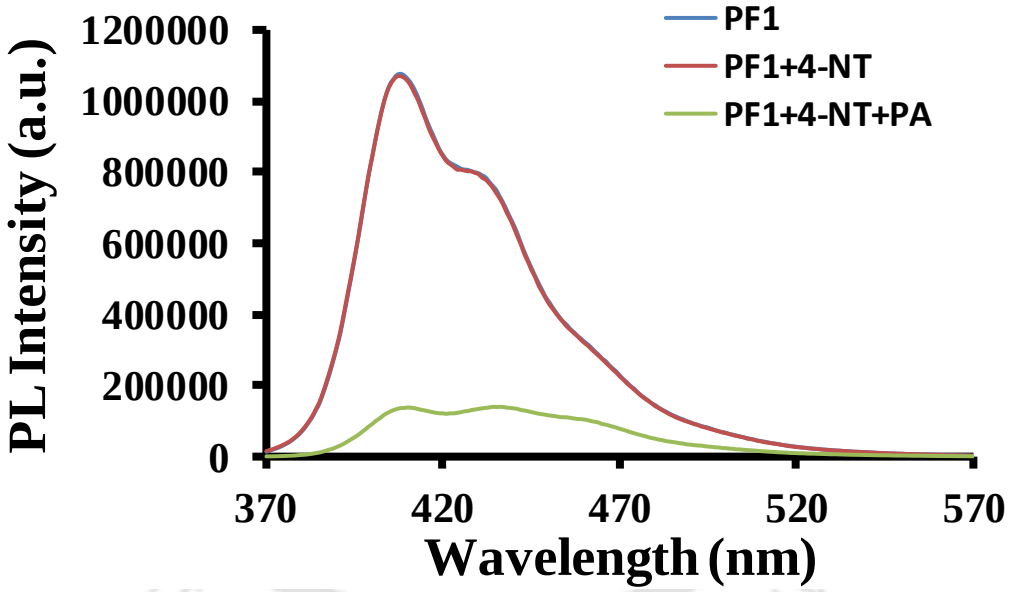

Figure A5.24 Emission spectra of PF1 (1.6×10^{-7} M) with 4-NT (66.6×10^{-6} M) followed by addition of PA (66.6×10^{-6} M).

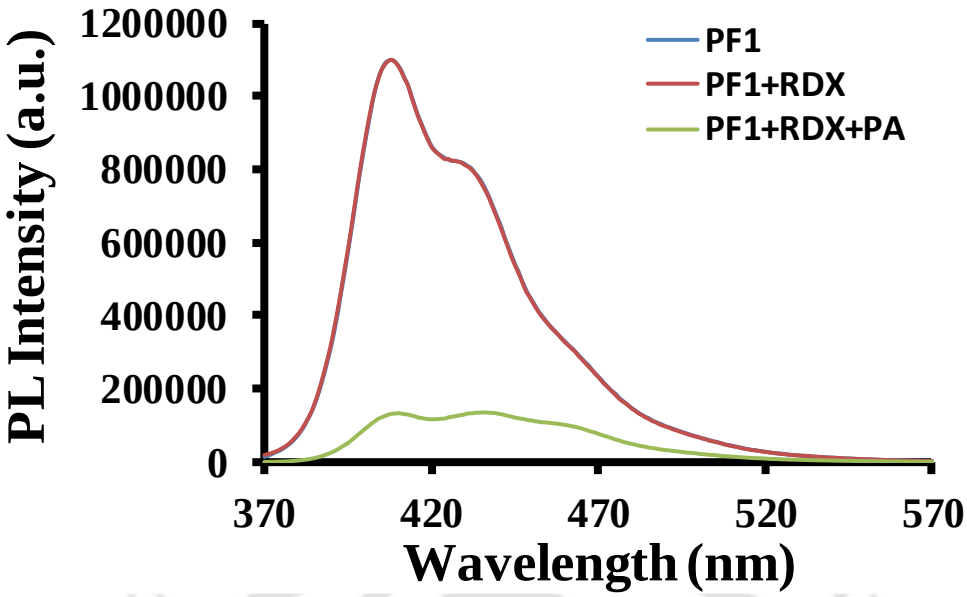

Figure A5.25 Emission spectra of PF1 (1.6×10^{-7} M) with RDX (66.6×10^{-6} M) followed by addition of PA (66.6×10^{-6} M).

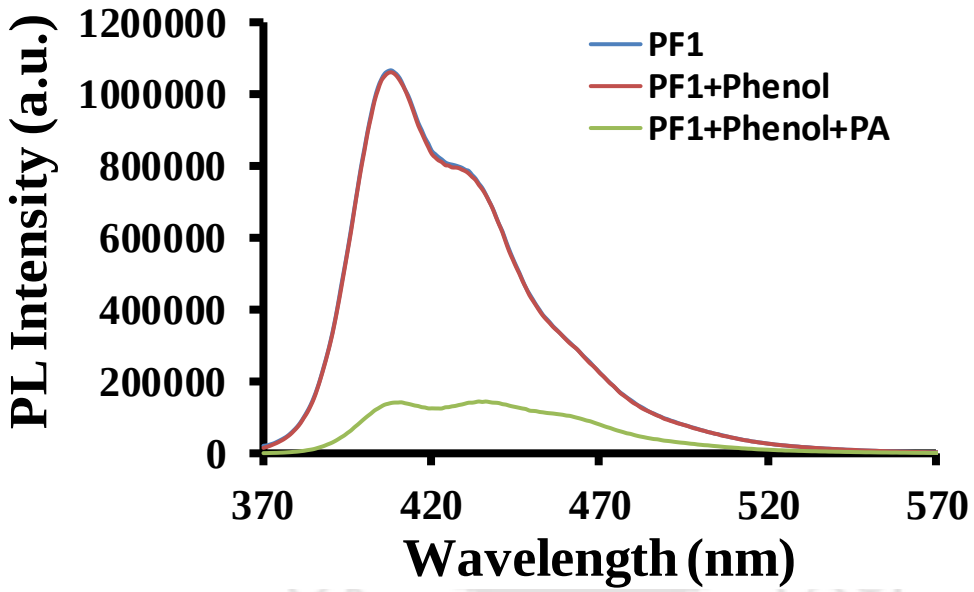

Figure A5.26 Emission spectra of PFBT (3.3×10^{-6} M) with phenol (93.3×10^{-6} M) followed by addition of PA (93.3×10^{-6} M) in DMSO.

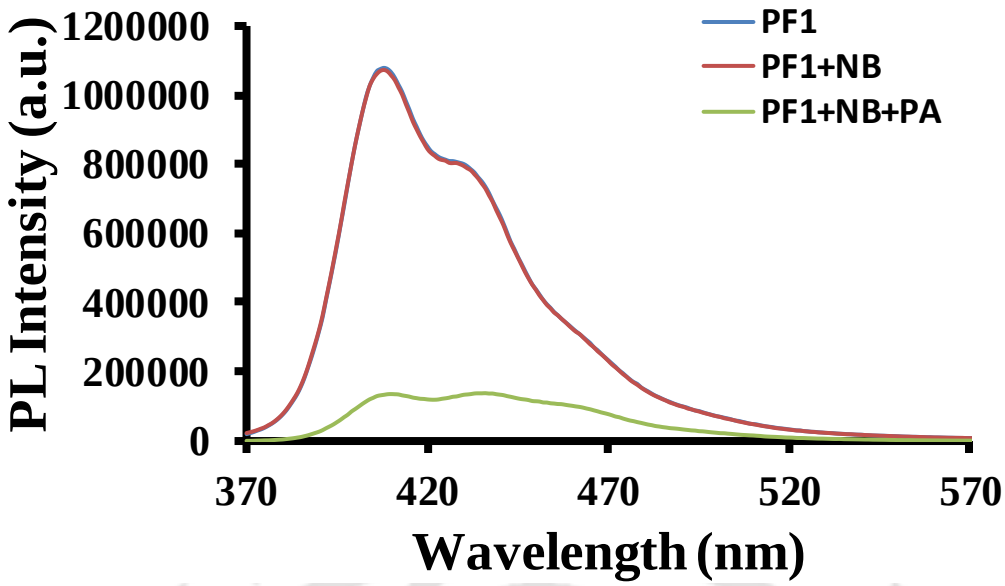

Figure A5.27 Emission spectra of PF1 (1.6×10^{-7} M) with NB (66.6×10^{-6} M) followed by addition of PA (66.6×10^{-6} M).

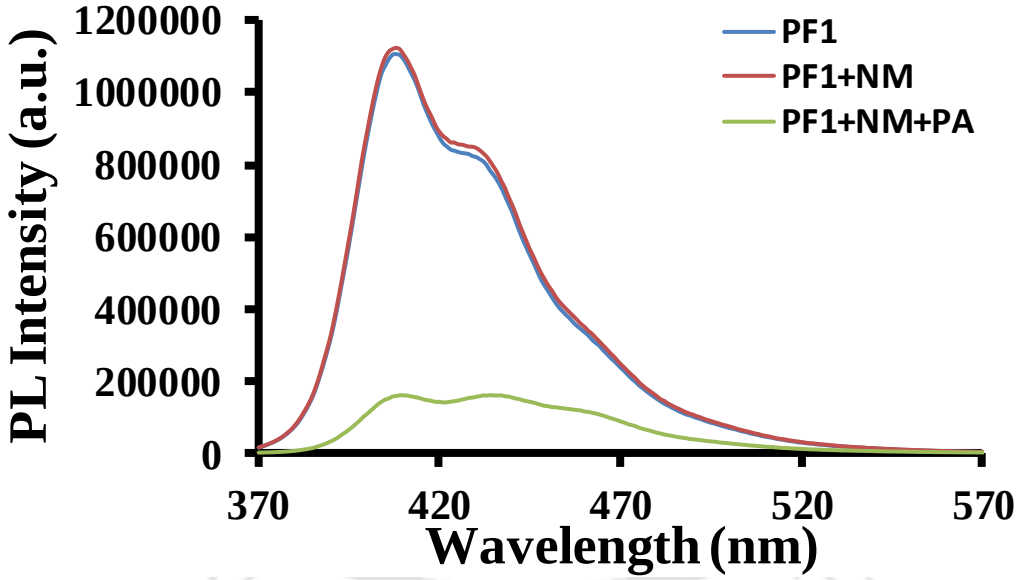

Figure A5.28 Emission spectra of PF1 (1.6×10^{-7} M) with NM (66.6×10^{-6} M) followed by addition of PA (66.6×10^{-6} M).

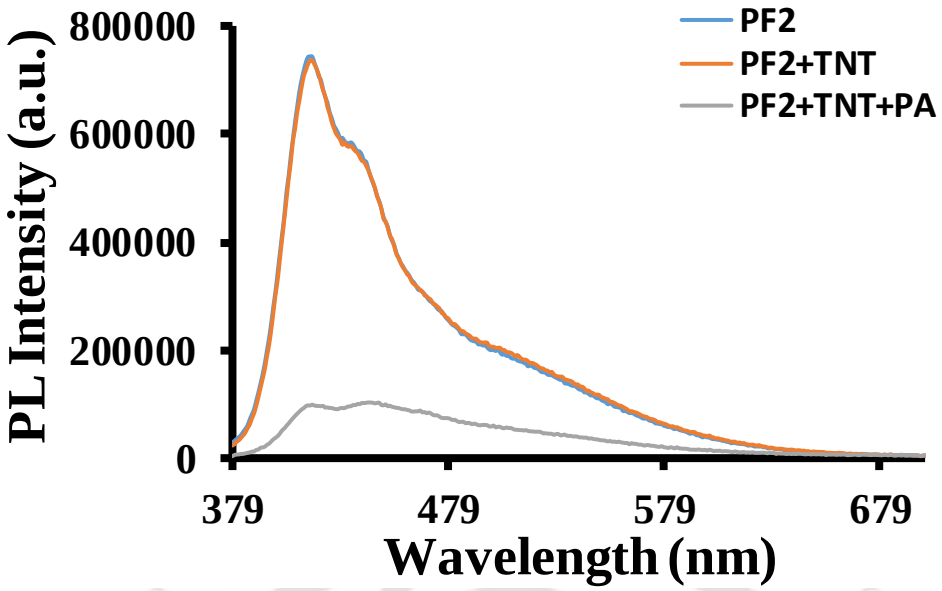

Figure A5.29 Emission spectra of PF2 (3.3×10^{-7} M) with TNT (66.6×10^{-6} M) followed by addition of PA (66.6×10^{-6} M).

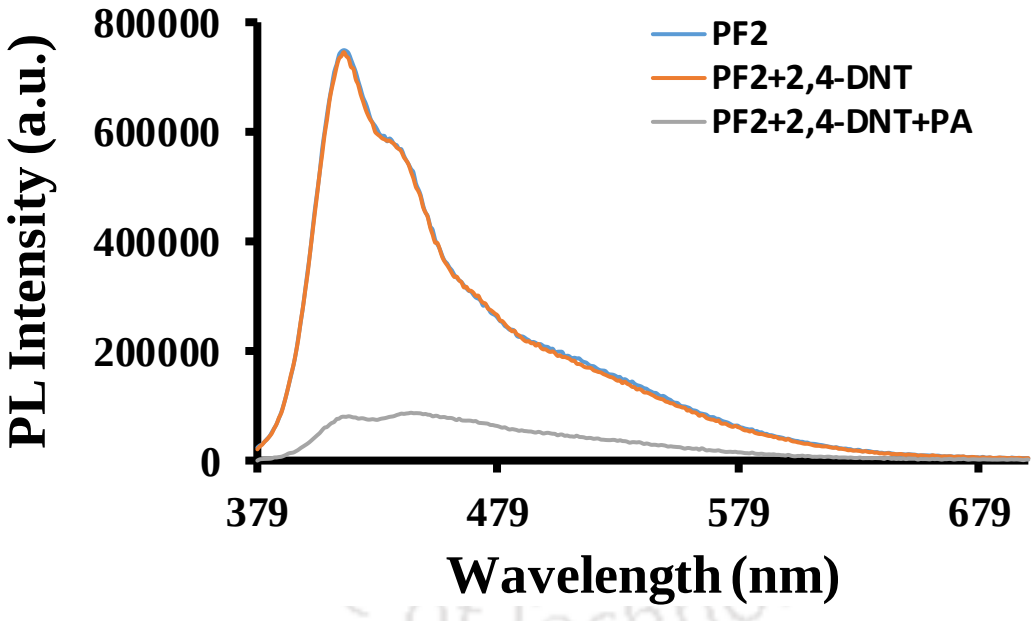

Figure A5.30 Emission spectra of PF2 (3.3×10^{-7} M) with 2,4-DNT (66.6×10^{-6} M) followed by addition of PA (66.6×10^{-6} M).

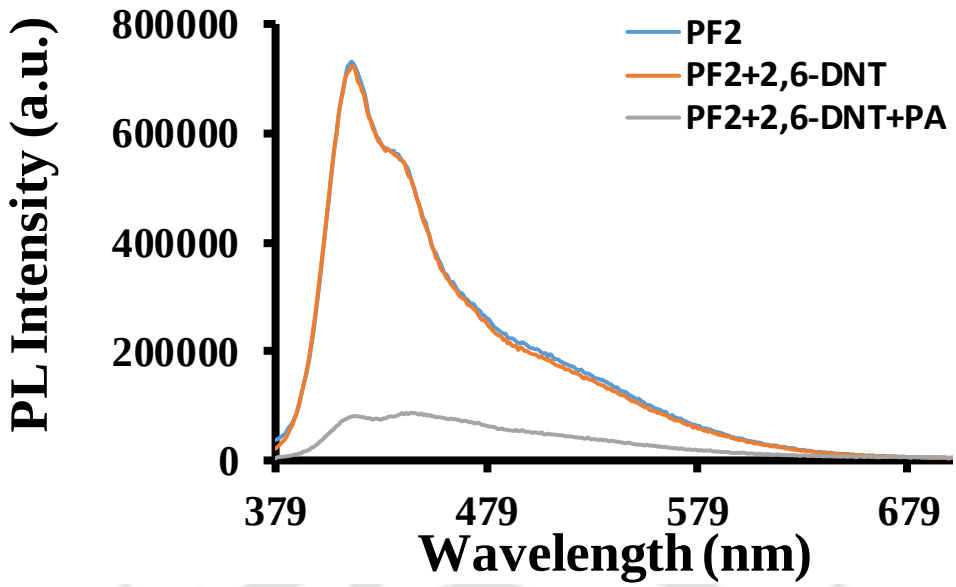

Figure A5.31 Emission spectra of PF2 (3.3×10^{-7} M) with 2,6-DNT (66.6×10^{-6} M) followed by addition of PA (66.6×10^{-6} M).

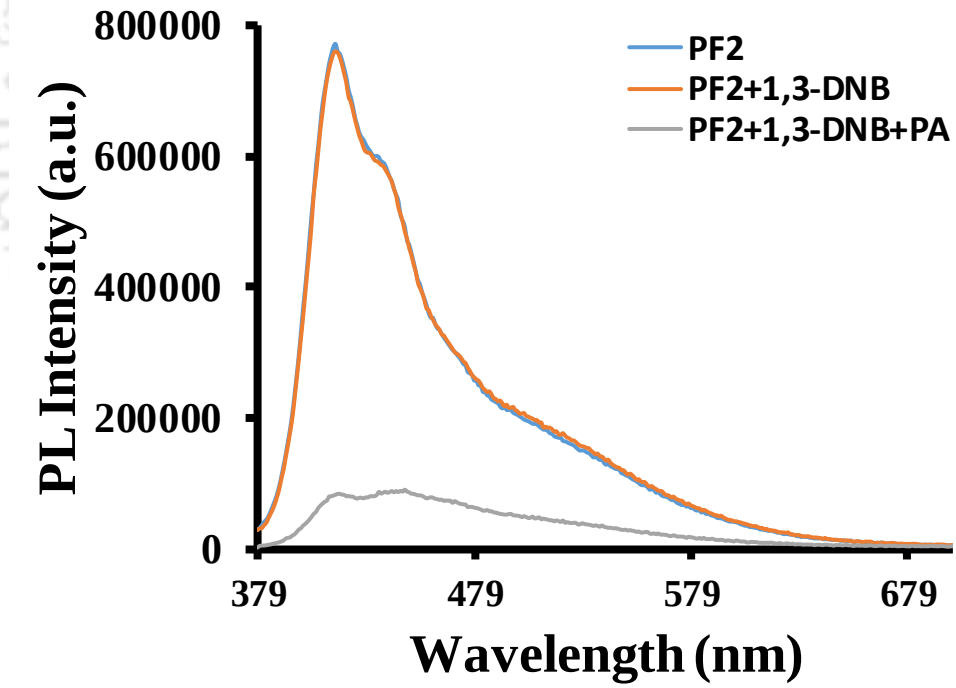

Figure A5.32 Emission spectra of PF2 (3.3×10^{-7} M) with 1,3-DNB (66.6×10^{-6} M) followed by addition of PA (66.6×10^{-6} M).

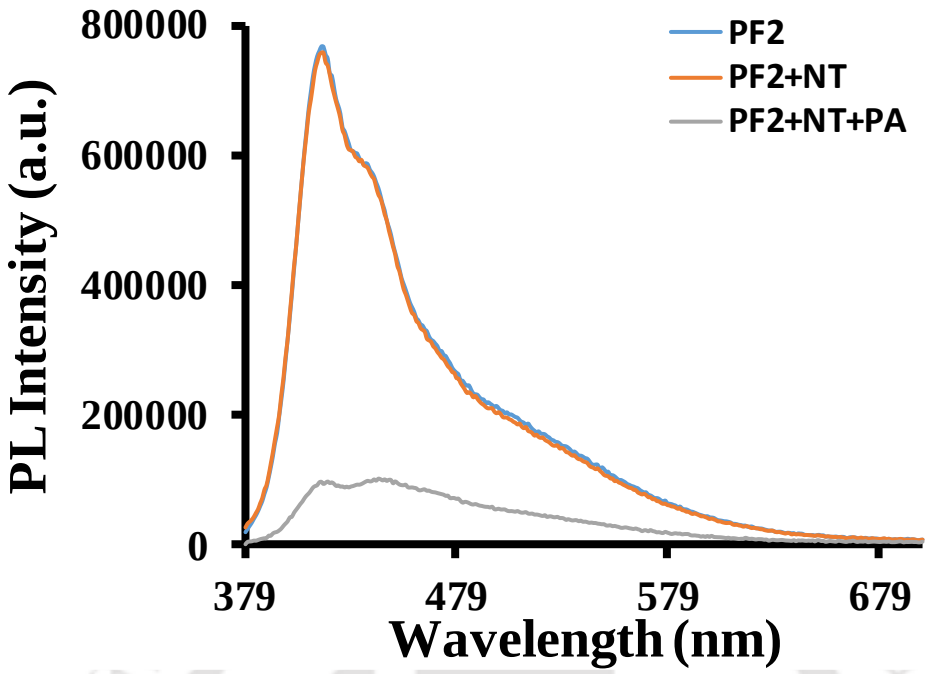

Figure A5.33 Emission spectra of PF2 (3.3×10^{-7} M) with 4-NT (66.6×10^{-6} M) followed by addition of PA (66.6×10^{-6} M).

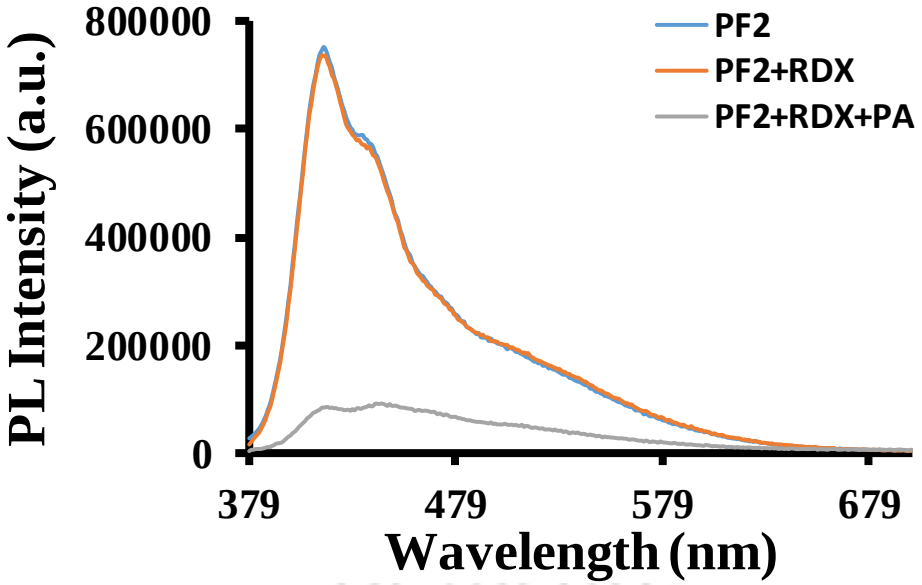

Figure A5.34 Emission spectra of PF2 (3.3×10^{-7} M) with RDX (66.6×10^{-6} M) followed by addition of PA (66.6×10^{-6} M).

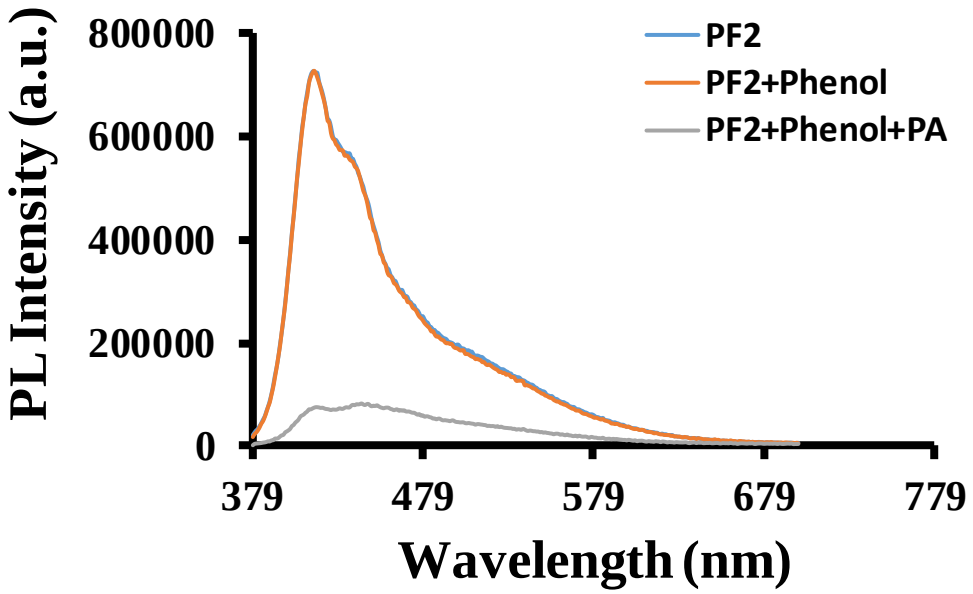

Figure A5.35 Emission spectra of PF2 (3.3×10^{-7} M) with phenol (66.6×10^{-6} M) followed by addition of PA (66.6×10^{-6} M).

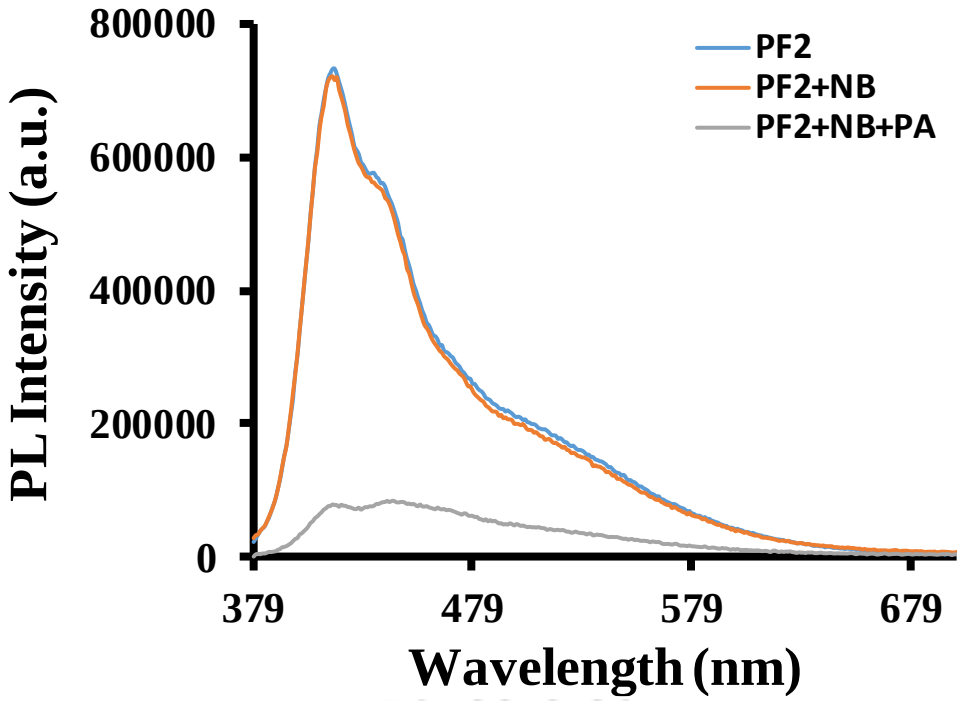

Figure A5.36 Emission spectra of PF2 (3.3×10^{-7} M) with NB (66.6×10^{-6} M) followed by addition of PA (66.6×10^{-6} M).

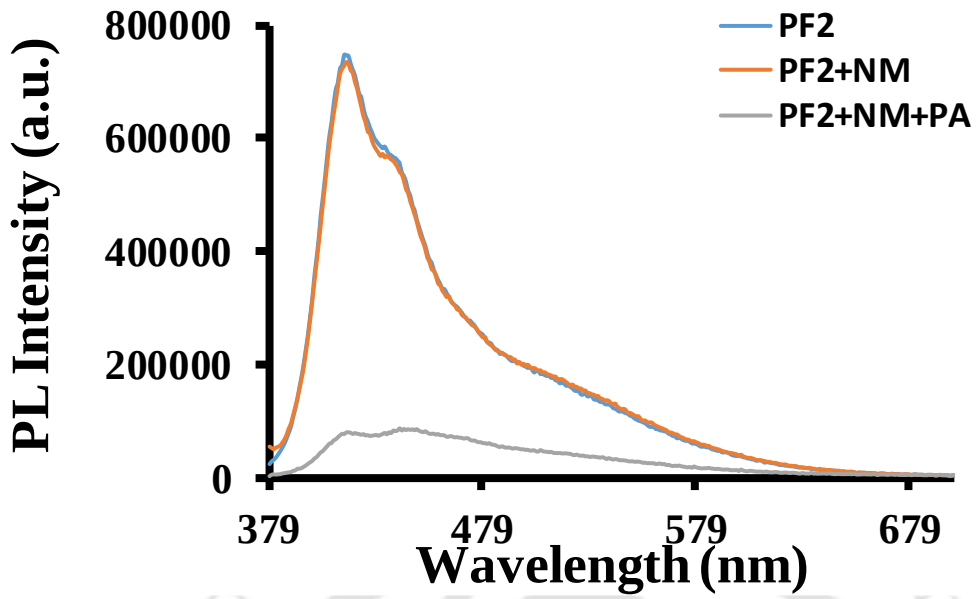

Figure A5.37 Emission spectra of PF2 (3.3×10^{-7} M) with NM (66.6×10^{-6} M) followed by addition of PA (66.6×10^{-6} M).

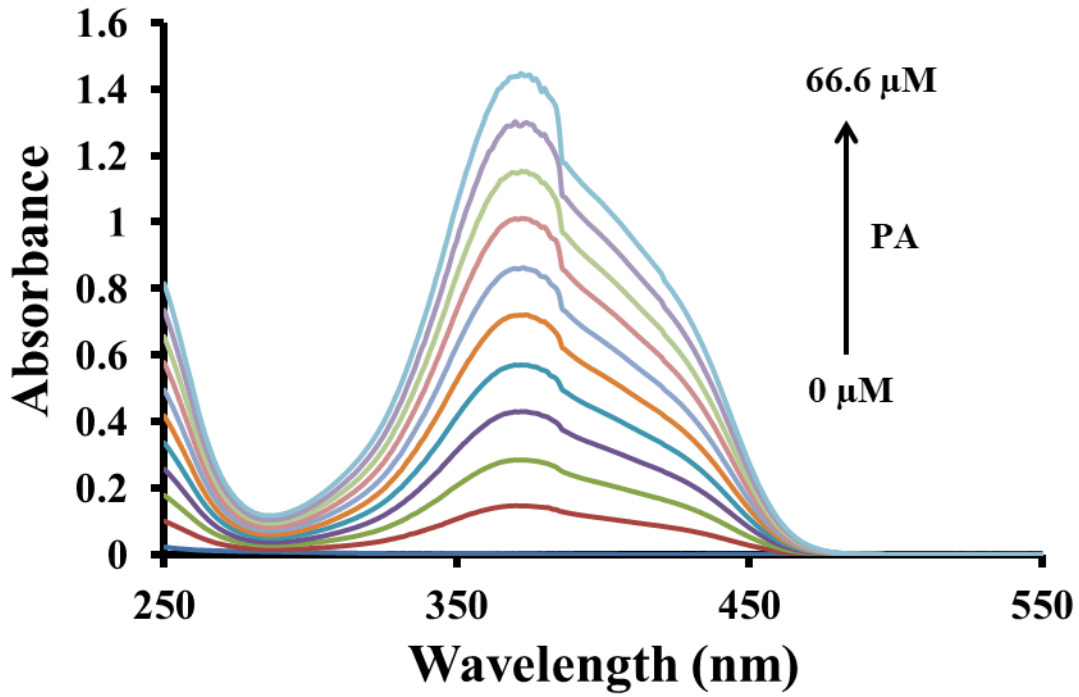

Figure A5.38 UV-Visible spectrum of PF1 (1.6×10^{-7} M) with the increasing concentration of PA.

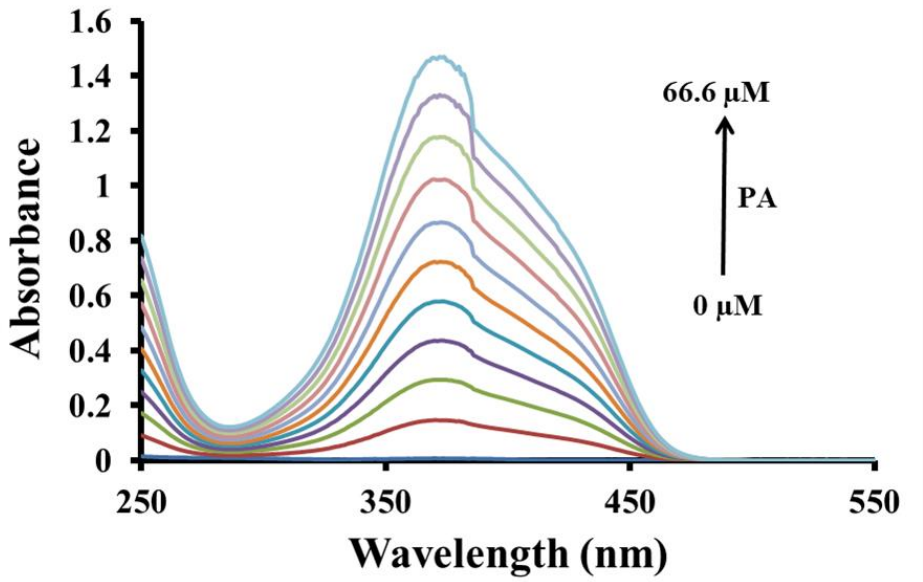

Figure A5.39 UV-Visible spectrum of PF2 (3.3×10^{-7} M) with the increasing concentration of PA.

Table A5.4. IFE of PA on the fluorescence of PF1.

PA(µM)	A_{ex}	A_{em}	I_{obs}	I_{corr}	I_{corr}/I_{obs} Correction factor (CF)	$I_{corr}/I_{corr,o}$	E_{obs} (%)	E_{corr} (%)
0.0	0.00327	-0.00035	1117560	1121318	1.003363	1	0	0
6.6	0.134571	0.098285	883766.4	1155488	1.307459	1.030473	20.92	-3.0473
13.3	0.260257	0.192205	670316	1128523	1.683569	1.006426	40.01968	-0.64258
20.0	0.392172	0.290904	505958.9	1110844	2.195523	0.99066	54.72646	0.934048
26.6	0.521551	0.385995	381816.6	1085495	2.842975	0.968053	65.8348	3.194731
33.3	0.657292	0.487313	283849.2	1060206	3.735102	0.9455	74.60099	5.450042
40.0	0.787289	0.581273	216180.1	1044953	4.833715	0.931897	80.65606	6.810312
46.6	0.924155	0.680701	158820.8	1007710	6.344947	0.898683	85.78861	10.13169
53.3	1.056392	0.774255	119473.1	983090.7	8.228554	0.876728	89.30947	12.32723
60.0	1.189109	0.870032	89895.4	962294.4	10.7046	0.858181	91.9561	14.18185
66.6	1.322754	0.962819	67334.48	935457.4	13.89269	0.834248	93.97487	16.57521

Table A5.5. IFE of PA on the fluorescence of PF2.

PA(μM)	A_{ex}	A_{em}	I_{obs}	I_{corr}	I_{corr} /I_{obs} Correction factor (CF)	$I_{corr}/I_{corr,o}$	E_{obs} (%)	E_{corr} (%)
0.0	0.006842	0.001354	742999.6	750043.7	1.009481	1	0	0
6.6	0.145425	0.091007	555744.7	729611	1.312853	0.972758	25.20255	2.724209
13.3	0.291972	0.185852	409644.4	710099.2	1.733453	0.946744	44.86613	5.325621
20.0	0.433255	0.276891	305668	692345.7	2.265025	0.923074	58.86027	7.692614
26.6	0.575615	0.368119	227674.9	674811.1	2.963924	0.899696	69.35733	10.03044
33.3	0.720185	0.459858	169103.4	657921.1	3.890644	0.877177	77.24045	12.28231
40.0	0.862995	0.550753	127194.5	647652.8	5.091831	0.863487	82.88095	13.65132
46.6	1.02185	0.649378	91055.99	623623.6	6.848792	0.83145	87.74481	16.85503
53.3	1.173185	0.745069	66709.42	607175.4	9.101794	0.80952	91.02161	19.048
60.0	1.320497	0.837099	49314.7	591254.5	11.98942	0.788293	93.36275	21.17067
66.6	1.465231	0.926808	36267.65	569559.3	15.70433	0.759368	95.11875	24.06319

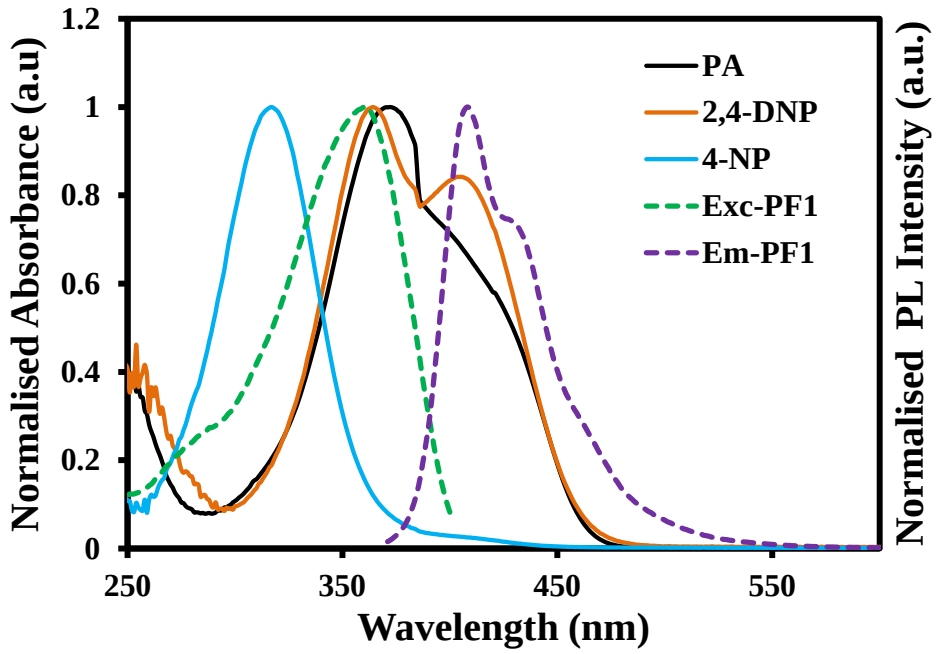

Figure A5.40 The normalised UV-Visible spectrum of PA, 2,4-DNP, 4-NP and the normalised fluorescence excitation and emission spectrum of PF1.

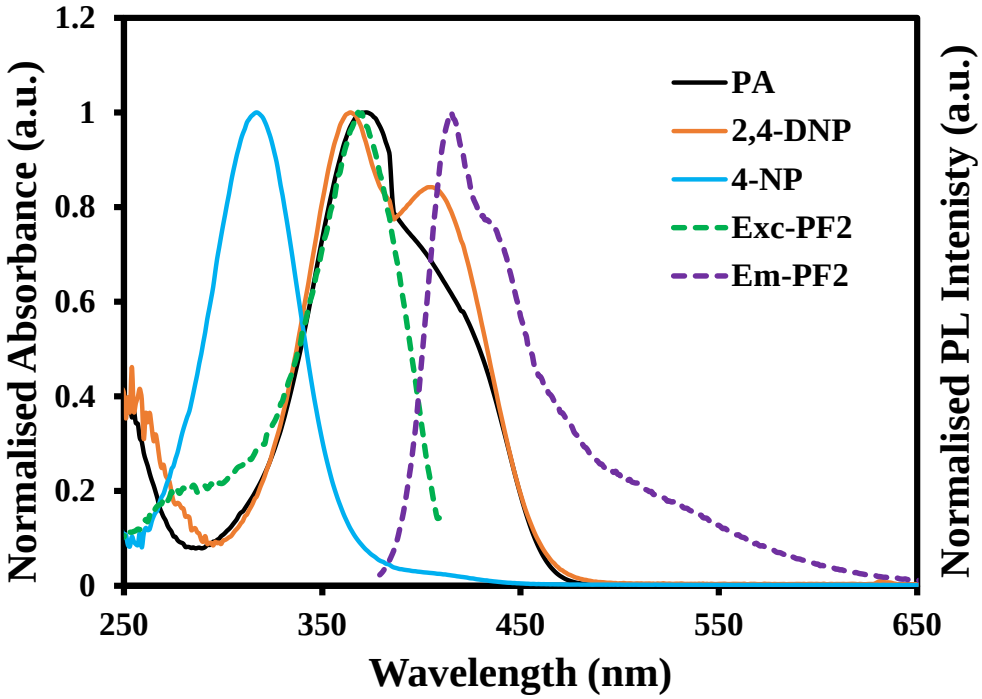

Figure A5.41 The normalised UV-Visible spectrum of PA, 2,4-DNP, 4-NP and the normalised fluorescence excitation and emission spectrum of PF2.

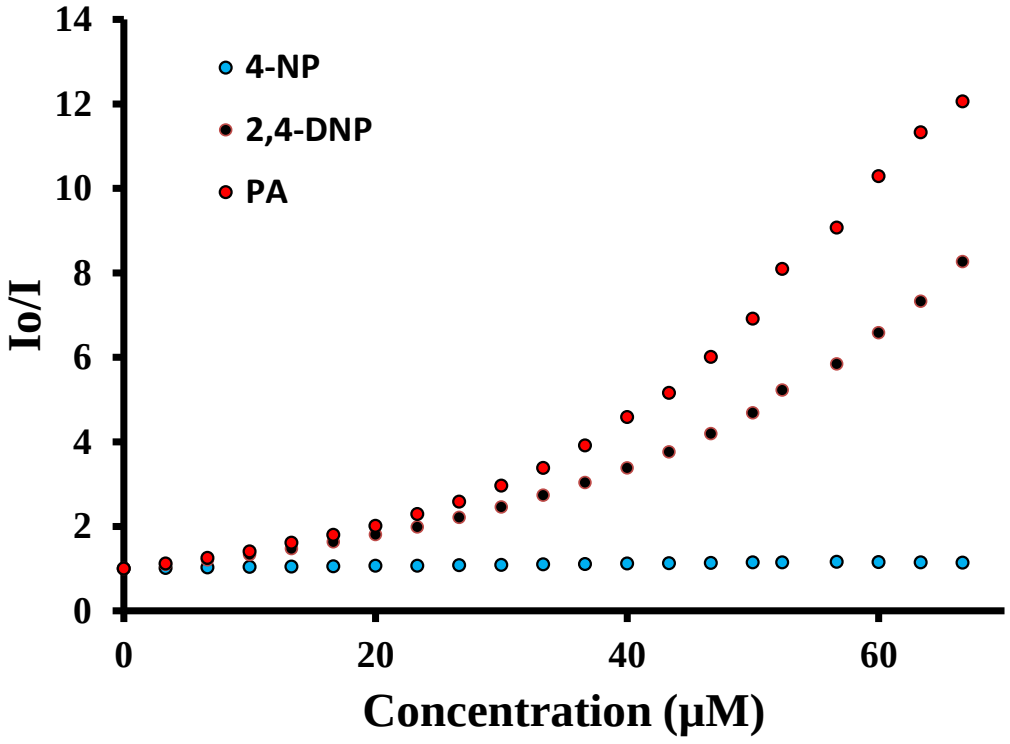

Figure A5.42 Comparison of quenching efficiency for 4-NP, 2,4-DNP and PA in 4:1-THF:HEPES (10 mM, pH=7.0) for PF1.

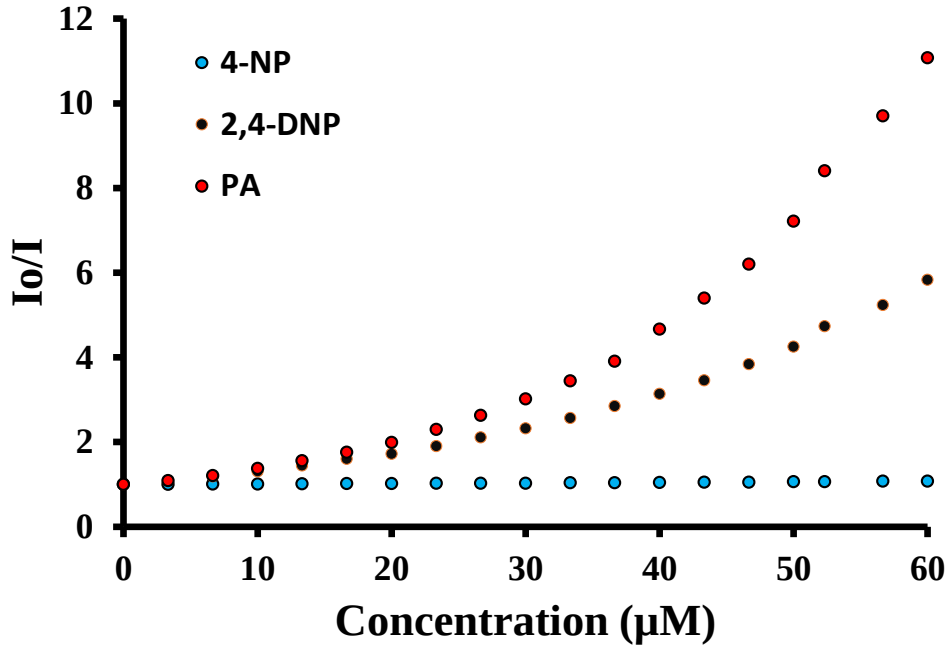

Figure A5.43 Comparison of quenching efficiency for 4-NP, 2,4-DNP and PA in 4:1-THF:HEPES (10 mM, pH=7.0) for PF2.

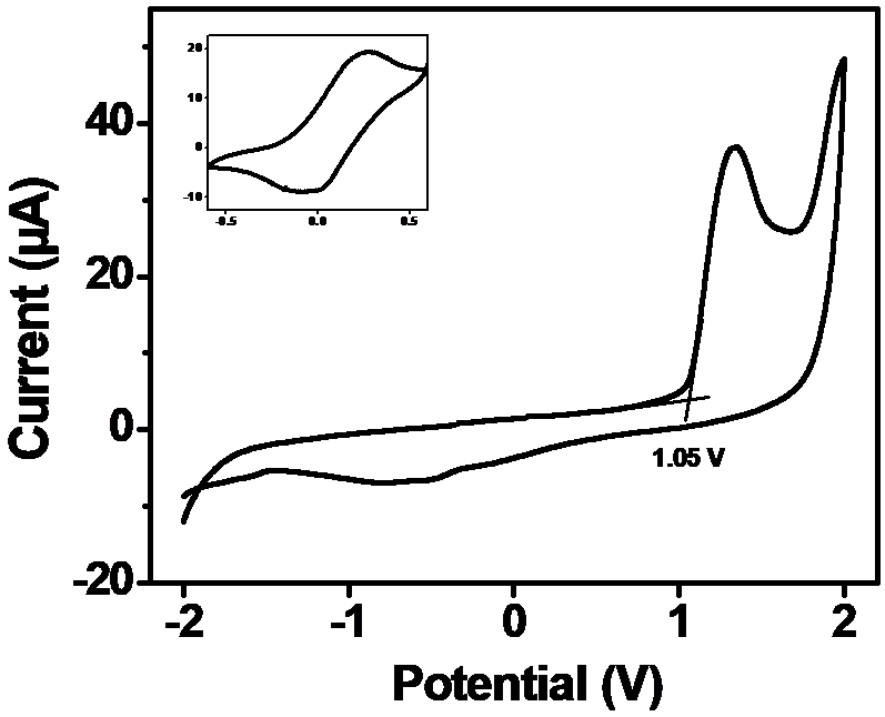

Figure A5.44 Cyclic voltammogram of PF1 (inset shows ferrocene peak).

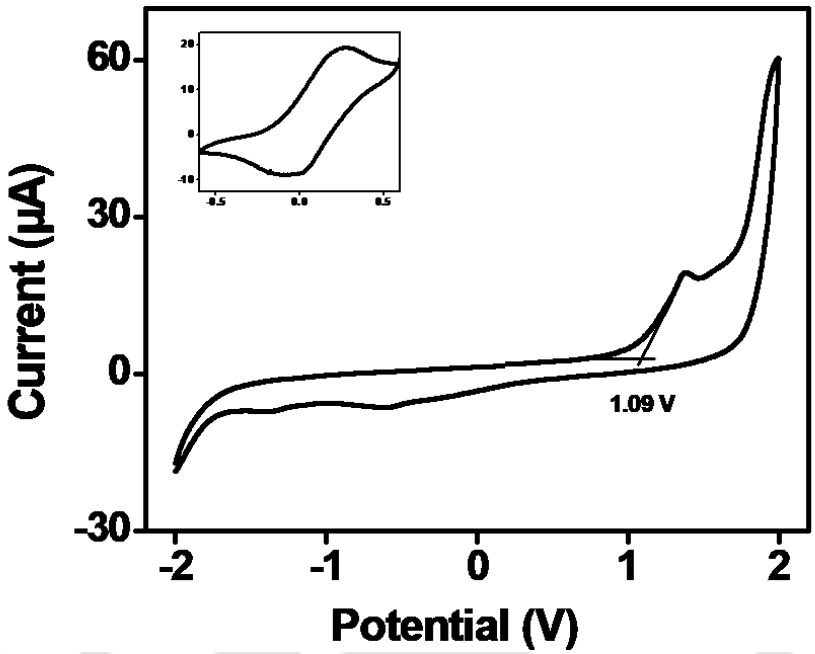

Figure A5.45 Cyclic voltammogram of PF2 (inset shows ferrocene peak).

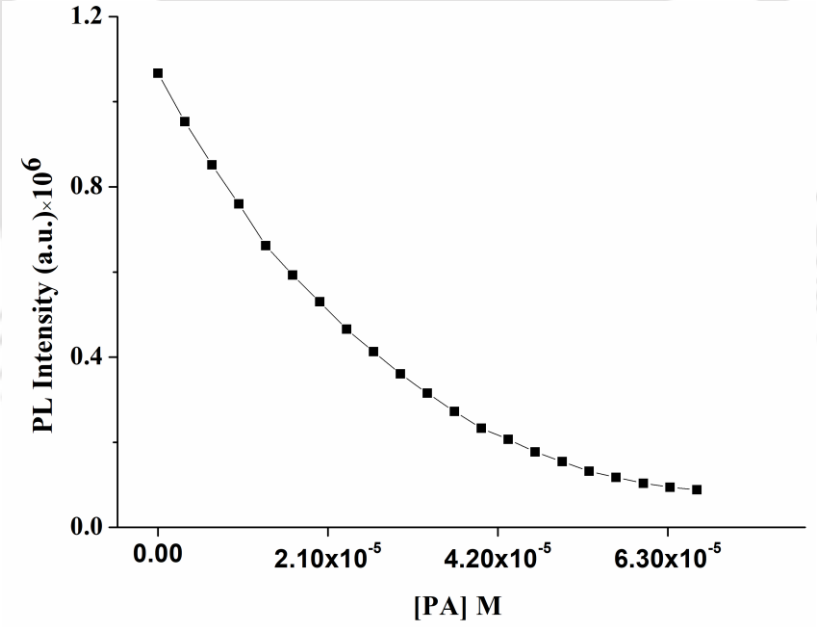

Figure A5.46 Calibration curve obtained for Polymer PF1.

Chapter 6

Thesis Overview and Future Perspectives

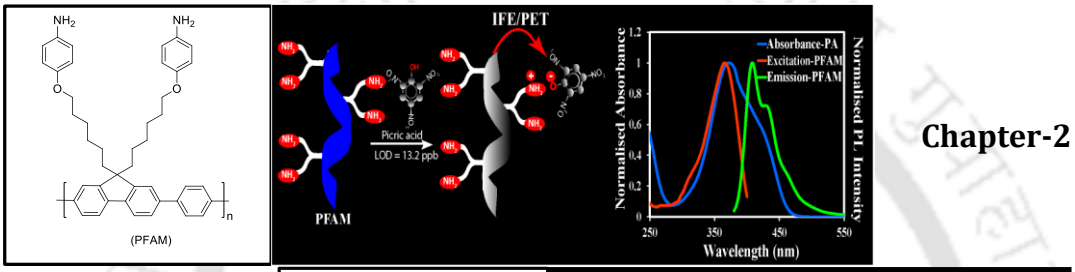

Chapter-2

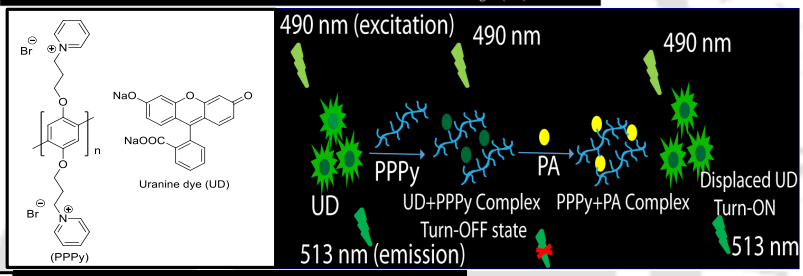

Chapter-3

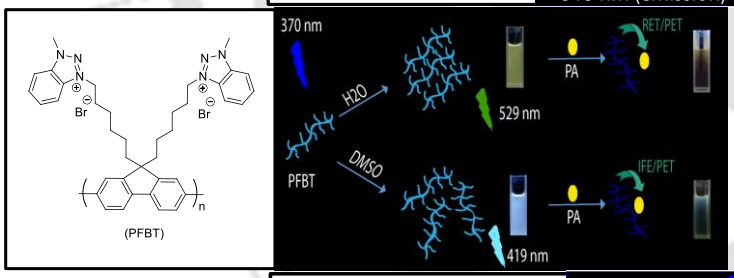

Chapter-4

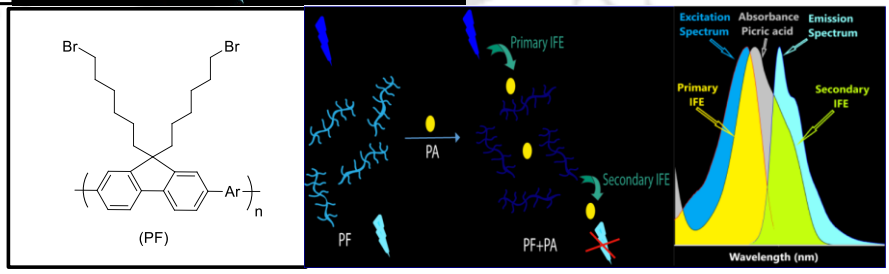

Chapter-5

6.1 Thesis overview

Due to the influential motivation and demand of recent day technology for highly efficient explosive sensing device, this thesis entitled **"Newly Developed Conjugated Polymer Systems for Nitroexplosive Detection: Insights into the Mechanistic Investigations"** mainly focuses on the development of various conjugated polymer systems for the nitroexplosive detection and its mechanism of sensing. For this purpose, different types of conjugated polymeric systems have been designed, synthesized and utilized in attaining simple, low cost and portable optical sensors capable of monitoring nitroexplosive-Picric acid (PA) at ultra-trace level. The mechanism of sensing for each of the CPs was studied in detail and explored. In Chapter-2, CP PFAM showed rapid and specific recognition toward PA on solid support and in solution based on IFE/PET mechanism. In Chapter-3, the non-fluorescent cationic conjugated polymer PPPy participates in indicator displacement assay resulting "turn-on" fluorescence selectively in presence of PA. In Chapter-4, the cationic conjugated polymer PFBT displayed substantial fluorescence quenching for PA in solution as well as solid state based on IFE and RET mechanism at attogram level of PA and utilized in making economical paper strips for on-site detection of nitroexplosive. In Chapter-5, the neutral "receptor-free" highly fluorescent conjugated polymers (PF1 and PF2) detect PA by a fluorescence turn-off response which was found as a result of mainly strong IFE and was further confirmed via IFE corrections. All the CPs systems were found to be highly sensitive and selective towards nitroexplosive-PA. The results obtained from each chapter are shown in below Table 6.1.

Chapter No.	Polymer	Stern-Volmer Constant (K_{sv})	Detection Limit (LOD)	Sensing Mechanism	Fluorescence Signal	Solvent Used
2	PFAM	$1.05 \times 10^5\ M^{-1}$	57.8 nM	IFE/PET	Turn-Off	THF:H_2O
3	PPPy	-	295 nM	IDA	Turn-On	H_2O
4	PFBT	$2.69 \times 10^4\ M^{-1}$	92.7 nM	IFE/PET	Turn-Off	DMSO
		$2.18 \times 10^5\ M^{-1}$	0.19 nM	RET/PET	Turn-Off	H_2O
5	PF1	$5.1 \times 10^4\ M^{-1}$	110 nM	IFE/PET	Turn-Off	THF:H_2O
	PF2	$5.0 \times 10^4\ M^{-1}$	219 nM	IFE/PET	Turn-Off	THF:H_2O

Table 6.1 Comparison of the sensing results of various conjugated polymers shown in thesis.

6.2 Future Perspective

Additionally, this thesis includes chemo-sensors based on fluorescence "turn-off", indicator displacement assay and "receptor-free" sensing, as shown in figure 6.2**.** To date, there are only countable reports available for the PA detection based on CPs. There is still scope for better design and exploring new sensing mechanisms, in order to achieve an ideal sensory system for nitroexplosive detection.

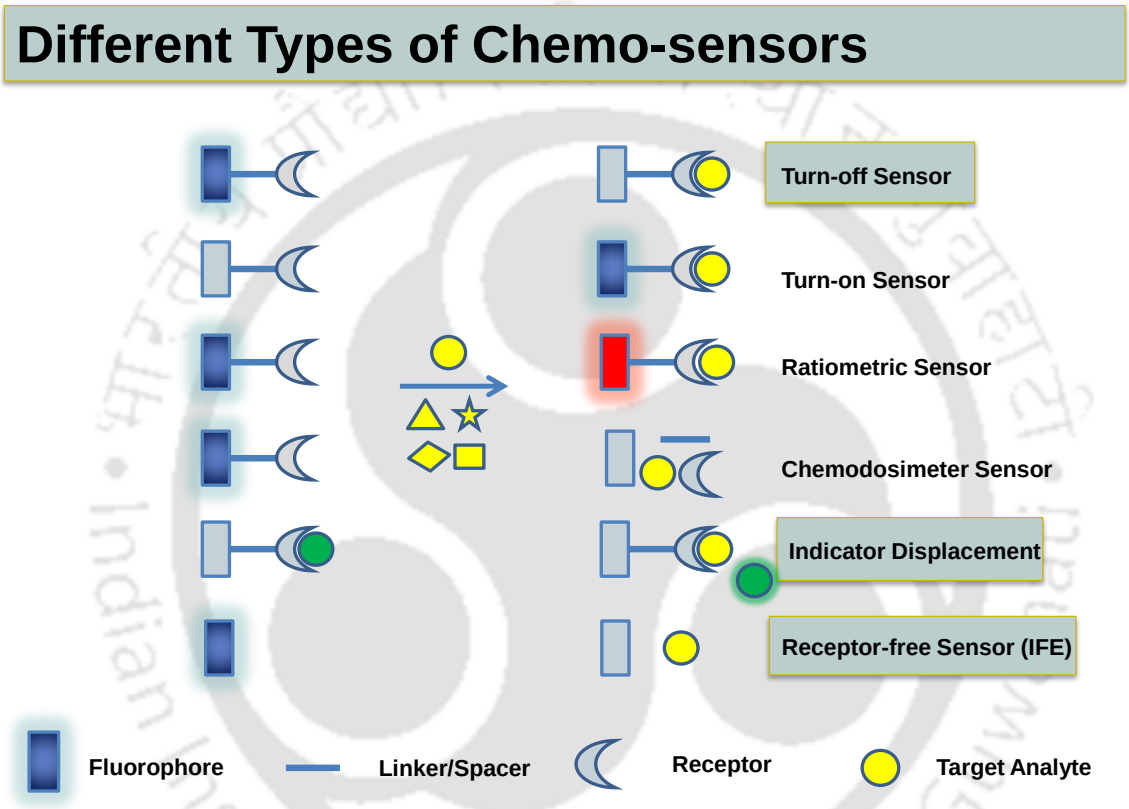

Figure 6.2 Possible types of different chemosensors.

Publications

1. **Tanwar, A. S**.; Patidar, S.; Ahirwar, S.; Dehingia. S.: Iyer, P. K. "Receptor Free" Inner Filter Effect Based Detection of Nitroexplosive-Picric Acid using two Polyfluorenes derivatives in solution and solid state and IFE corrections. *Analyst* **2019**, *144*, 669-676.

2. **Tanwar, A. S**.; Adil, L. R.; Afroz, M. A.; Iyer, P. K. Inner Filter Effect and Resonance Energy Transfer Based Attogram Level Detection of Nitroexplosive-Picric acid Using Dual Emitting Cationic conjugated Polyfluorene. *ACS Sensors* **2018**, *3*, 1451-1461. (Published authors biography on a special invitation in *ACS Sensors* **2018**, *3*, 1432–1432)

3. **Tanwar, A. S**.; Iyer, P. K. Fluorescence "Turn-On" Indicator Displacement Assay Based Selective Detection of Nitroexplosive-picric Acid in Aqueous Media via a Cationic Conjugated Polyelectrolyte and Dye Complex. *ACS Omega* **2017**, *2*, 4424-4430.

4. Meher, N.; Kalita, A.; **Tanwar, A. S**.; Adil, L. R.; Malik, A. H.; Hussain, S.; Iyer, P. K. Conjugated Smart Materials for Sensing Application on Multiple Platforms. *ISRAPS Bulletin* **2017**, 29, 21-36.

5. **Tanwar, A. S**.; Hussain, S.; Malik, A. H.; Afroz, M. A.; Iyer, P. K Inner Filter Effect Based Selective Detection of Nitroexplosive-picric Acid in Aqueous Solution and Solid Support Using Conjugated Polymer. *ACS Sensors* **2016**, *1*, 1070–1077.

6. Malik, A. H.; Hussain, S.; **Tanwar, A. S**.; Layek, S.; Trivedi, V.; Iyer, P. K. Anionic Conjugated Polymer as a Multi-Action Sensor for the Sensitive Detection of Cu^{2+}, PPi, Real-Time ALP Assaying and Cell Imaging. *Analyst* **2015**, *140*, 4388-4392.

Conferences & Seminars

1. Delivered an ***ORAL Presentation*** at the Reflux 2018 during 16-18th March 2018, Annual Symposium organized by Department of Chemical Engineering, IIT Guwahati.
2. Presented a ***POSTER*** at the Research Conclave'18 organized by Student Academic Board, IIT Guwahati during 8-11th March 2018. **(First Prize)**.
3. Delivered an ***ORAL Presentation*** talk at the Research Conclave'18 organized by Student Academic Board, IIT Guwahati during 8-11th March 2018.
4. Presented a ***POSTER*** in 5th International Conference on Advanced Nanomaterials and Nanotechnology during 18-21st December 2017 held at Centre for Nanotechnology, Indian Institute of Technology Guwahati.
5. Attended a ***WORKSHOP*** on 'Quick Look of Technologies' held at Centre for Nanotechnology, IIT Guwahati.
6. Presented a ***POSTER*** at Research Conclave'17 organized by Student Academic Board (SAB), IIT Guwahati during 16-19th March 2017. **(Department Best Poster and Institute Best Poster- Molbiogen Certificate)**
7. Presented a ***POSTER*** in the 20th CRSI National Symposium in Chemistry held from February 3-5th, 2017, organized by Department of Chemistry, Guwahati University.
8. Presented a ***POSTER*** during Reflux 2017, Annual Symposium organized by Department of Chemical Engineering, IIT Guwahati.
9. Attended the full agenda of **ACS on campus** (An initiative from the American Chemical Society) at IIT Guwahati on 16 Jan 2017.
10. Presented a **Research Paper** in the International Conference of Functional Materials (ICFM 2016) at Kharagpur organised by Material Science Centre, IIT Kharagpur. **(Best Poster)**
11. Presented a ***POSTER*** at Frontiers in Chemical Sciences (FICS 2016) conducted by Department of Chemistry, IIT Guwahati during 8-11th Dec 2016.

Conferences & Seminars

12. Presented a ***POSTER*** in 4th International Conference on Advanced Nanomaterials and Nanotechnology from 8-11 December, 2015 at Centre for Nanotechnology, IIT Guwahati.
13. **Participated** in 68th Annual Session of Indian Institute of Chemical Engineers (CHEMCON 2015) at IIT Guwahati during 27-30th December 2015.
14. Presented a ***POSTER*** in ChemConvene 2015 on 8th April, 2015 at IIT Guwahati.
15. **Participated** in the National Conference on "Recent Advances in Cancer Biology and Therapeutics-2014 (RACBT)" organized by Department of Biotechnology, IIT Guwahati held on 5th December,2014.
16. **Attended** the 3rd International Conference on Advanced Nanomaterials and Nanotechnology (ICANN) from 01-03 Dec, 2013 held at Centre for Nanotechnology, IIT Guwahati, India.
17. Participated in **WORKSHOP** on "Sensors and its Applications" on 15th November, 2013 organized by Polymer Section, Physical Sciences Division, Institute of Advanced Study in Science and Technology, Guwahati, India.